VuAB Recovery

Final Report

DSE Group 2
25-01-2018

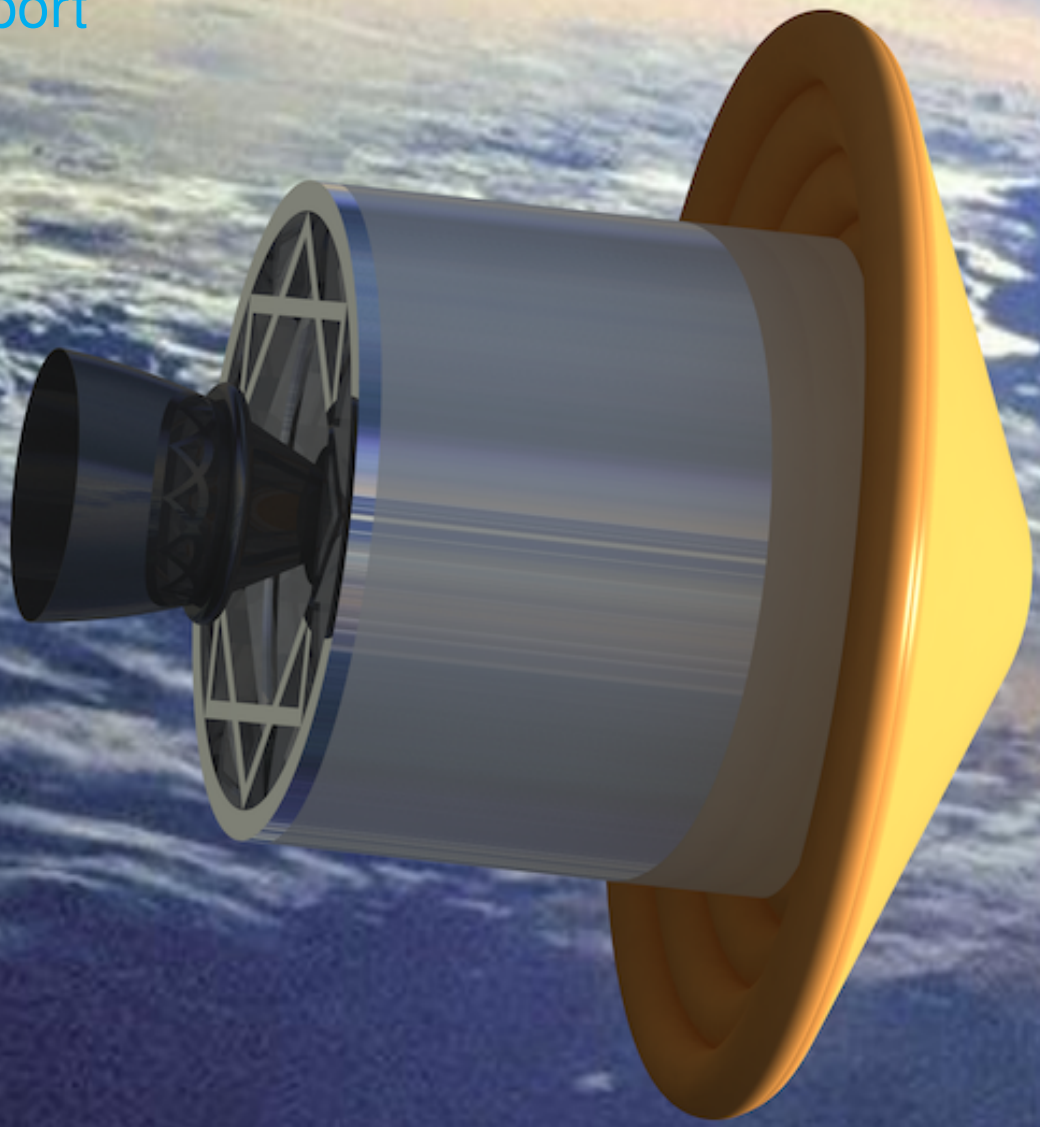

Technische Universiteit Delft

TU Delft

VuAB Recovery

Final Report

by

DSE Group 2
25-01-2018

Table 1: Version Registration

Report	Version	Date
Final Report	1.0 (Final Draft)	25-01-2018

Students:	Akke Toeter	1507958
	Casper Dek	4300653
	Jasper Slimmens	4286324
	Jean-Luc Overkamp	4350170
	Job van Zijl	4380185
	Pietro Areso Rossi	4273311
	Ricardo Machado	4392329
	Sjef Hereijgers	4274504
	Tom Hoppenbrouwer	4297628
	Veli Kilic	4093720
Project duration:	November 13, 2017 – February 2, 2018	
Tutor:	ir. M. Naeije	TU Delft
Coaches:	ir. M. Coppola	TU Delft
	dr. D. Zarouchas	TU Delft

TU Delft

Preface

Delft, 25-01-2018

Before you lies the fourth and final report of a ten week study for the Fall 2017 Design Synthesis Exercise, conducted by Group 2. The group consists of ten students Aerospace Engineering in the final phase of their Bachelor. The project came to realisation through a collaboration of the Aerospace Engineering faculty of the Delft University of Technology and Airbus Defense and Space Netherlands.

The report serves to present the final design of a feasibility study into the reusability for Airbus Defense and Space Netherlands and is available to all who are interested. Readers who are especially interested in the final design are encouraged to read Chapter 4 of the report. For those interested in the financial feasibility of the design it is advised to read Chapter 8.

We would like to thank our tutor Marc Naeije, our coaches Mario Coppola and Dimitrios Zarouchas and Erwin Mooij from the faculty of Aerospace Engineering of the Delft University of Technology for their support and feedback during the process of writing this final report. Additionally we would like to thank Jack Offerman and in particular Henk Cruijssen for their feedback, cooperation and for making this subject available for our Design Synthesis Exercise.

Design Synthesis Exercise Group 2

Summary

The first launch of the Ariane 6 launch vehicle is planned for 2020, however in its current design no significant part of the launcher will be reusable. A current trend in the global space market is decreasing the costs of spacecraft launches through recovery, retrieval and refurbishment of parts of launchers. As a first step towards this market demand, it is to be investigated whether it is cost-effective to recover, refurbish and reuse the key components of the first stage of the Ariane 6, which are contained in the Vulcain Aft Bay (VuAB). This is where the engine, fuel lines, thrust frame and electronics are attached. The team has the task to develop a cost effective way of reusing the Vulcain Aft Bay. In the preceding report, multiple concepts were analysed and one concept was selected to complete the conceptual design. This concept consists of an Inflatable Heat Shield for re-entry, a Parafoil to control the flight at lower altitudes and a Mid-Air retrieval using a helicopter to perform a soft landing.

A functional analysis was performed to define concept specific functions. This was done by means of a Functional Flow Diagram and Functional Breakdown Structure. In order to fulfil these functions, simulations were created of the most critical moments of the mission. One set of simulations analyse the trajectory of the system throughout the mission, predicting the location of landing. The other set of simulations is used to predict the critical load cases of the system.

The aforementioned simulations were used to design the individual components of the system. By integrating these simulations and managing the iteration process, the overall system characteristics and configuration were established. The system was then analysed for sustainability, reliability, risk, maintainability and safety. The requirement compliance of the system was then updated, detailing which requirements have achieved full compliance, marginal compliance, no compliance and which have not been sufficiently investigated. Proposals to make all requirements fully compliant are included in a feasibility analysis. These include different design approaches for the team and design changes to the VuAB to accommodate the recovery system.

From there strategies on future verification and validation activities was set forth together with operational, refurbishment and production plans. These plans and the design of the system were used to create an updated business model with return on investment figures, which predict a significant cost reduction on a per launch basis within five years.

Finally a set of future recommendations and plan is proposed for the continuation of the project.

List of Abbreviations & Symbols

List of Abbreviations

ADCS	Attitude Determination and Control System
CER	Cost Estimation Relationship
EPC	Cryogenic Main Stage
ESC	Cryogenic Upper Stage
GNC	Guidance, Navigation and Control
HEART	High Energy Atmospheric Reentry Test
HIAD	Hypersonic Inflatable Aerodynamic Decelerator
IAD	Inflatable Aerodynamic Decelerator
IRDT	Inflatable Re-entry and Descent Technology
IRVE	Inflatable Reentry Vehicle Experiment
LLPM	Lower Liquid Propulsion Module
MAR	Mid-Air Retrieval
PEP	Position Error Probability
TPS	Thermal Protection System
USD	United States Dollar
VuAB	Vulcain Aft Bay

List of Symbols

$\dot{q}$	Heatflux	$\frac{W}{cm^2}$
$\frac{dQ}{dt}$	Total heat rate	W
γ	Specific Heat Ratio of Air	-
μ_0	Reference viscosity coefficient	kg/(m· s)
μ_∞	Absolute viscosity coefficient	kg/(m· s)
ρ_∞	Freestream Density	$\frac{kg}{m^3}$
σ_y	Yield Strength	MPa
θ_a	half-cone angle	°
θ_{lat}	Angle formed between helicopter line and Inertial Reference Frame YZ-plane	rad
θ_{long}	Angle formed between helicopter line and Inertial Reference Frame XZ-plane	rad
a	Profile length of square parafoil attachment block	m
a_{cp}	Centripetal acceleration on the VuAB due to swinging of the VuAB.	m/s^2
b	Height of parafoil attachment	m
c	chord length	m^2
C_f	Skin Friction Coefficient	-
D_a	Catch cable elongation	m
D_o	Aeroshell Diameter	m
D_t	Toroid diameter	m
F_{ca}	Total tension force on helicopter during catch of VuAB	N
F_{cp}	Centripetal force acting on catch cable due to swinging of the VuAB.	N
$F_{d,a}$	Tension force in attenuation cable due to uniform deceleration	N
f_n	Natural frequency of a structure	Hz

$F_{Parafoil}$	Peak force during deployment of parafoil	N
$F_{T,D_{max},V}$	The maximum tension force due to the drag force on the VuAB during catch.	N
$g_{0,catch}$	Gravitational constant at height of catch	$\frac{m}{s^2}$
h_0	Total enthalpy of the freestream	$\frac{J}{kg \cdot K}$
h_w	Enthalpy of the gas at the wall	$\frac{J}{kg \cdot K}$
l_{min}	the minimum length of the cable between the helicopter and the VuAB.	m
m_{att}	Mass of the attenuation system including elongation cable	kg
M_a	Aeroshell mass	kg
$m_{h,p}$	Helicopter payload mass	kg
$m_{max,h,p}$	Maximum allowable helicopter payload mass	kg
$m_{V_{catch}}$	Mass of the VuAB at the moment of catching	kg
p_s	Static Pressure	Pa
$q_{\infty,max}$	Maximum Dynamic Pressure	Pa
q_∞	Dynamic Pressure	Pa
R_{nose}	Nose-cone radius	m
Re_c	Reynolds number over a flat plate	-
S_p	Projected Surface Area	m^2
T	Temperature	K
T_0	Reference temperature	K
V_∞	Freestream Velocity	$\frac{m}{s}$
$V_{h,V}$	Initial absolute velocity difference between helicopter and VuAB	m/s
V_{m,S_lon}	Maximum swinging velocity of the VuAB in longitudinal flight direction of the helicopter	m/s
$V_{m,S_{lat}}$	Maximum swinging velocity of the VuAB in lateral flight direction of the helicopter	m/s
C_{stage1}	First stage cost	€
$C_{Vulcain}$	Vulcain 2.1 engine cost	€
F_{ee}	Expendable rocket engine cost	€
F_{er}	Reusable rocket engine cost cost	€
F_{se}	Expendable launcher stage cost	€
F_{sr}	Reusable launcher stage cost	€
$M_reusable$	Expendable launcher stage mass	kg
$M_{expendable}$	Expendable launcher stage mass	kg
x_b	Helicopter Inertial Reference Frame	m
k	Stiffness of a structural element in a vibrational analysis	N/m
M	Mach number	-

Contents

1 Introduction

This report aims to show the results of the Design Synthesis Exercise on the Recovery of the Vulcain Aft Bay of the Ariane 6, in short: the VuAB. Over the course of 3 months several steps in the design process have been taken. First, a project planning has been made, in which a planning of all steps to be taken to come up with a design were presented. Then, a baseline has been established in which the requirements were set and all functions to be performed by the system were defined. Then, a large set of concepts was generated using design option trees for the different mission phases: space, re-entry, atmospheric flight and landing. A more detailed view on these mission phases is given in Chapter 2. From these design option trees four concepts were generated by doing a qualitative analysis. These concepts were preliminarily sized and designed in order to perform a quantitative analysis and trade-off. The first concept consisted of a Vertical Landing concept, using a rocket boost to land. The second one consisted of Mid-Air Retrieval, using a parafoil to fly and a helicopter to catch the VuAB. The third concept also uses a parafoil to fly and was designed to perform a soft landing on an airbag or in a net. The fourth one was designed to fly with wings and perform a horizontal, aircraft-like landing. In this midterm phase, the Mid-Air Retrieval was chosen due to its overall performance and low mass figures. This final report will show the results on the feasibility study and preliminary design performed on the Mid-Air Retrieval of the VuAB.

First, an overview of the background of the project, the concept, mission phases and all functions to be performed are shown in Chapter 2. Then, all models used to determine the flight trajectory and define the load cases are shown in Chapter 3, after which the approach on the design of all systems and the results of this design is shown in Chapter 4. This chapter follows the structure of the functions as defined earlier on, starting with the space phase and ending with the catch and electrical design. Furthermore, the integration of all designed elements is reported in this chapter. Then, the design is analysed for sensitivity to input parameters, sustainability, risk, reliability, maintenance, availability and safety, after which the compliance with the requirements as established in the Baseline is checked. This design analysis can be found in Chapter 5. Then, the verification and validation procedures are elaborated on in Chapter 6, showing both the procedures as applied throughout the report, as well as suggestions for validation procedures later on in the development process. The operations, refurbishment and production plan are dealt with in Chapter 7 and the business case is analysed in Chapter 8. Finally, recommendations for future design and a planning for further development, testing and production is given in Chapter 9, after which the conclusion will conclude the report in Chapter 10.

2

Mission Analysis

This chapter provides an overview of the purpose of the project, as well as an overview of the chosen concept and mission phases as defined in the midterm report [71]. This is shown in Section 2.1. Then, the functional analysis, showing all functions the system should be able to perform, is shown in Section 2.2.

2.1. Global Picture

This section will provide the motivation of Airbus Defence of Space to investigate the reuse of the Vulcain aft bay (VuAB), along with the specified mission need statement and project objective statement. Also, the concept and different mission phases will be shown.

2.1.1. Launcher Reusability in a Global Market

In recent years the market for space launch vehicles has seen significant change. Private companies started innovating, which has led to new developments that were unseen of for decades. Reusability especially has been of great interest lately as it would decrease the cost of launching objects into space drastically. The past few years the global space market has been pushing towards lowering the costs of launching spacecraft by reusing parts of the launchers [68]. As private companies have now proven that it is feasible to make a launch vehicle reusable and over time might decrease the cost per launch this is an opportunity that Airbus likes to explore in their design for the Ariane 6 Launch Vehicle. As a first step towards this market demand, Airbus Defence and Space is investigating whether it is cost-effective to recover, refurbish and reuse the key components of the first stage of the Ariane 6. The Ariane 6 (A6) is a future European space launcher which is expected to be operational by 2020.

2.1.2. Mission Need Statement and Project Objective Statement

As mentioned, the intention of Airbus Defence and Space is to accomplish an A6 launch cost reduction through the recovery, refurbishment and reuse of the key components of Ariane 6's first stage. To this purpose, the mission need statement (MNS) has been formulated and is stated below.

"Reduce the operational cost of an Ariane 6 launch by recovering, refurbishing and reusing key components of the first stage of the Ariane 6 launcher."

For the purpose of the project that is conducted, the MNS has been specified into a project objective statement (POS), which is stated as:

"Design a feasible recovery system for the Vulcain aft bay of the first stage of the Ariane 6 launcher that shall be operational by 2022, conducted by 10 students in 10 weeks."

On top of the MNS and POS, the stakeholder requirements define the scope of the project. For a complete understanding of the scope of the project, how the stakeholder requirements define the boundaries of this project and what the design process will be, it is advised to take a look at the Baseline Report [70].

2.1.3. Ariane 6 Vulcain Aft Bay

The first stage of the Ariane 6 consists of the Vulcain 2.1 engine and its components, two propellant tanks, the VuAB and the main stage skirt. Figure 2.1[1] shows a rough lay-out of the A6 and the placement of the VuAB. The VuAB encapsulates and supports the Vulcain 2.1. It has been established with Airbus Defence and Space that major additions to the first stage for recovery purposed shall be placed above the support cross, as depicted in green in the CAD drawing on the right side of the figure, but below the main propellant tank. For understanding the design choices it is necessary to have a clear understanding of the configuration of the VUAB.

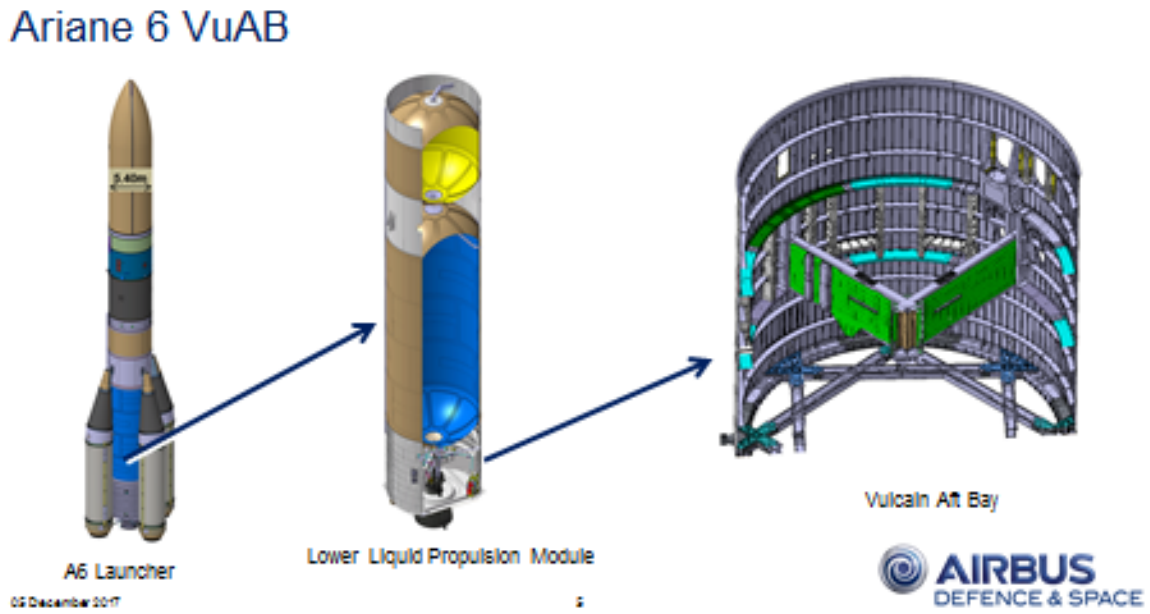

Figure 2.1: VUAB configuration in the A6 Launcher

2.1.4. Mission Profile and Concept

The mission begins with the launch of the VuAB with the rest of the Ariane 6 from the Guiana Space Centre in Kourou, French Guiana. The orbit designed for in this report is expected to be the most common launch [10], targeting a 5° inclination geosynchronous orbit. The first stage separates from the second stage before reaching orbit, at approximately 158 km altitude with a velocity of 6.9 km/s[1]. The first stage proceeds to fall down to Earth and end up in the Atlantic Ocean halfway between American and African coasts.

The recovery mission will start by separating the VuAB from the rest of the LLPM in space. Once decoupled an Attitude Determination and Control System will fire thrusters to ensure the VuAB has the right orientation when entering the atmosphere. As the VuAB travels through space an aeroshell will deploy, protecting the VuAB and Vulcain engine from the heat of re-entry.

The aeroshell will be discarded once the parafoil can be deployed. This parafoil is able to make controlled turns to change its heading and glide towards a desired end location. It employs a so called energy management control system to loiter if it reaches its destination at a greater height. During re-entry and flight its location is tracked, enabling a boat with a helicopter to approach the estimated landing location. Once close enough, the helicopter will take off and fly to the VuAB. Once the velocity vector, altitude and attitude of the helicopter and VuAB are aligned, the VuAB will be caught by the helicopter, which will carry the VuAB back to the boat. Afterwards, the VuAB will be refurbished and reused.

Figure 2.2 illustrates schematically the mission profile. Parameters of interest for each mission phase can be found on the right end of the figure.

[1]Private contact, Airbus Defence and Space (client), H. Cruijssen

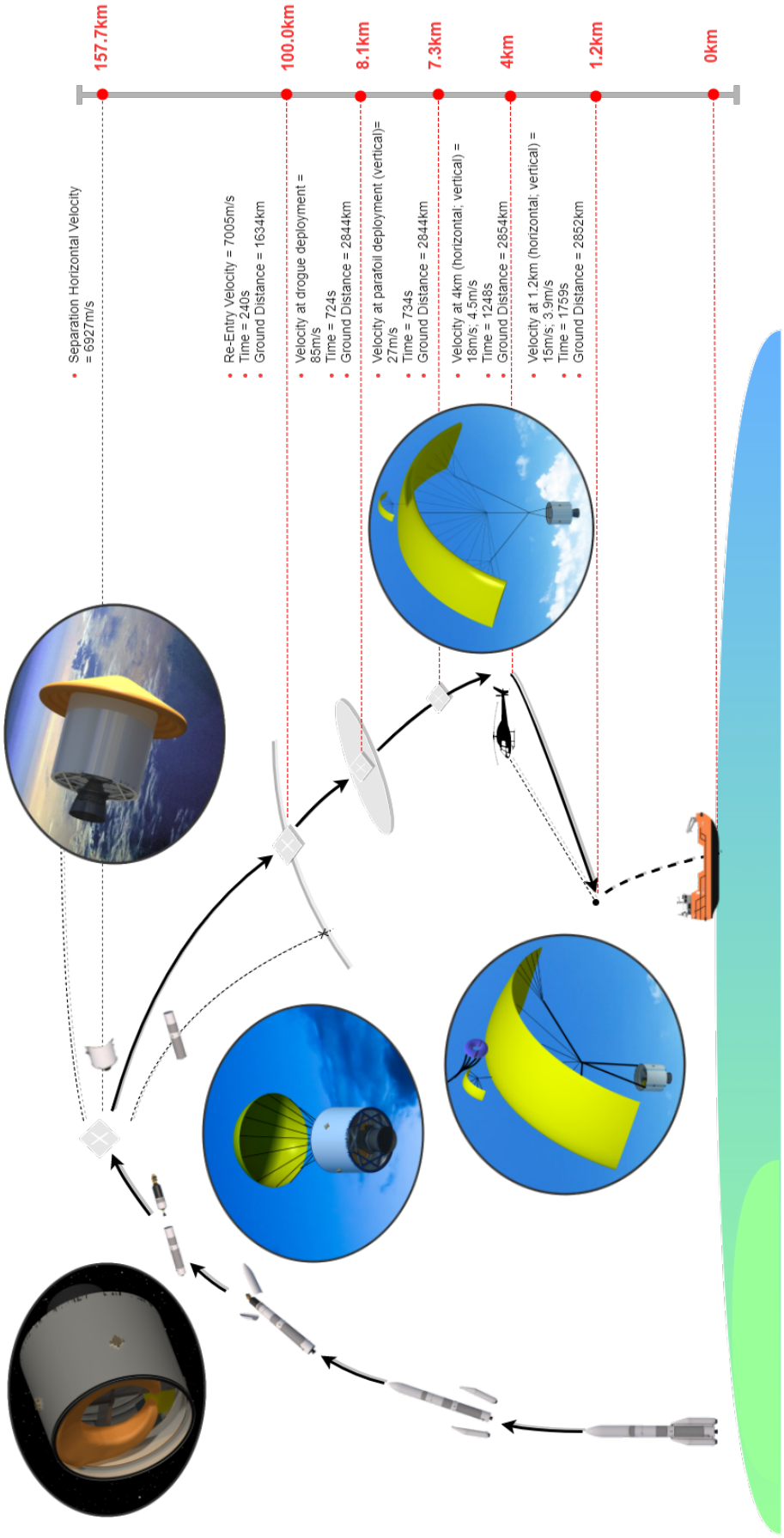

Figure 2.2: General mission profile from separation to catch

2.2. Functional Analysis

This section provides an updated version of the functional flow diagram and functional breakdown structure as presented in the baseline report [70]. This updated functional analysis is adjusted for the final concept. More detail has been added for concept specific parts, while subsystem design choices have been kept open in order to account for these choices later on in the process. The functional flow diagram can be found in Section 2.2.1 and the functional breakdown structure can be found in Section 2.2.2.

2.2.1. Functional Flow Diagram

The top level of the functional flow diagram has not been changed and is still composed of five functions: the preparations before flight, the launch, the recovery, the retrieval and the refurbishment. The top level can be found in Figure 2.3.

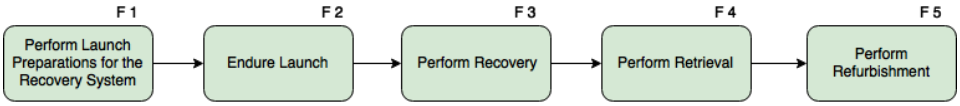

Figure 2.3: Top Level of the Functional Flow Diagram

Each of these top level functions is worked out in more detail and made specific for the final concept. The first two functions are very similar to the functional flow as defined in the Baseline report and describe the preparations for the integration of the recovery system with the already existing system and the passive phase of the mission, the launch. These functions are shown in Figure 2.4.

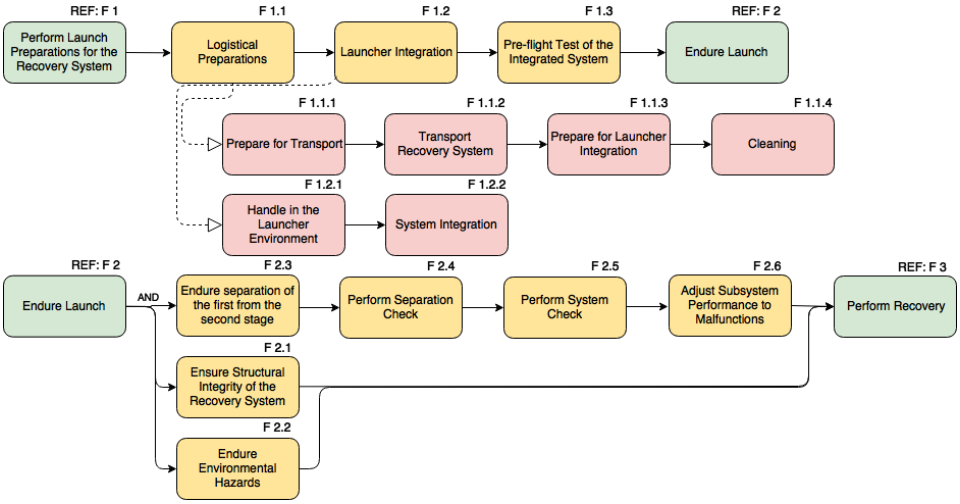

Figure 2.4: Functions one and two of the Functional Flow Diagram, showing the launch preparations and the launch

The third function is shown in Figure 2.5 and encompasses the active part of the mission for the recovery system. It shows how the power and communication functions are performed for the whole length of the active part of the mission, while the different mission phases are in a sequential order, as they are performed one after the other. These mission phases are the same as elaborated on in Section 2.1.4. The different functions of the mission phases of the recovery system during the active part are shown in more detail in figures 2.6, 2.7, 2.8 and 2.9.
During space flight, the two main functions to be performed are the separation and re-orientation, while during the re-entry the protection by means of a heat shield is shown. The atmospheric flight entails the parafoil flight and how the requirements for this parafoil flight are met, by means of a drogue parachute. The landing phase entails the functions that enable the VuAB and helicopter to couple and safely land the VuAB on the ship, while the function on helicopter operations shows the same procedures from the helicopter perspective. This function is not a part of the recovery system as installed on the VuAB, but is a part of the means of recovering as a whole. Functions four and five are shown in Figure 2.10 and show again a more passive phase of the recovery system as installed on the VuAB. It can be seen that the first part of the refurbishment will take place on the boat, in order to increase the turnaround time. Then, the actual refurbishment will take place and the order in which this is done is shown in the refurbishment function.

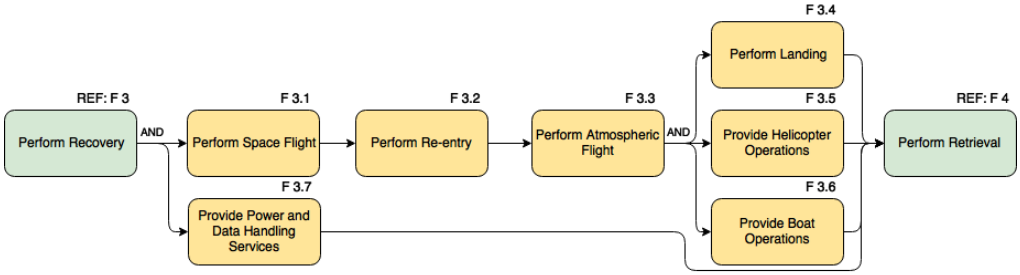

Figure 2.5: Function three of the Functional Flow Diagram, showing the recovery of the VuAB

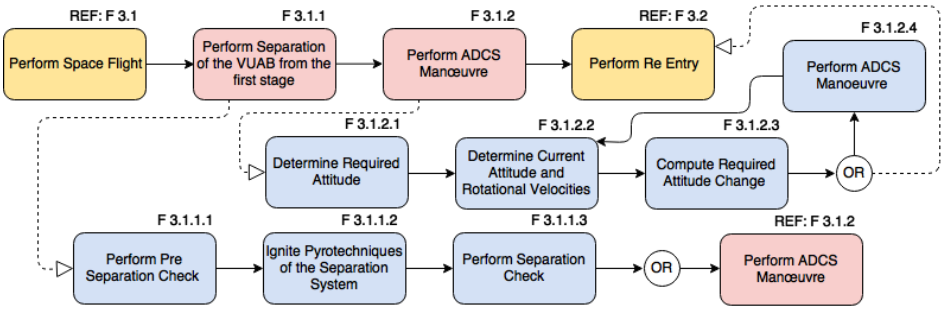

Figure 2.6: Function 3.1 of the Functional Flow Diagram, showing the space flight

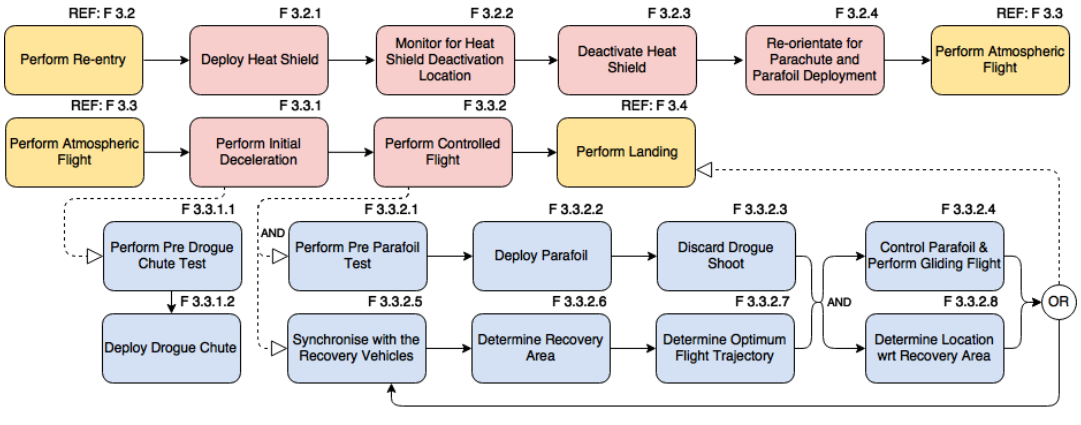

Figure 2.7: Function 3.2 and 3.3 of the Functional Flow Diagram, showing the reentry and the atmospheric flight

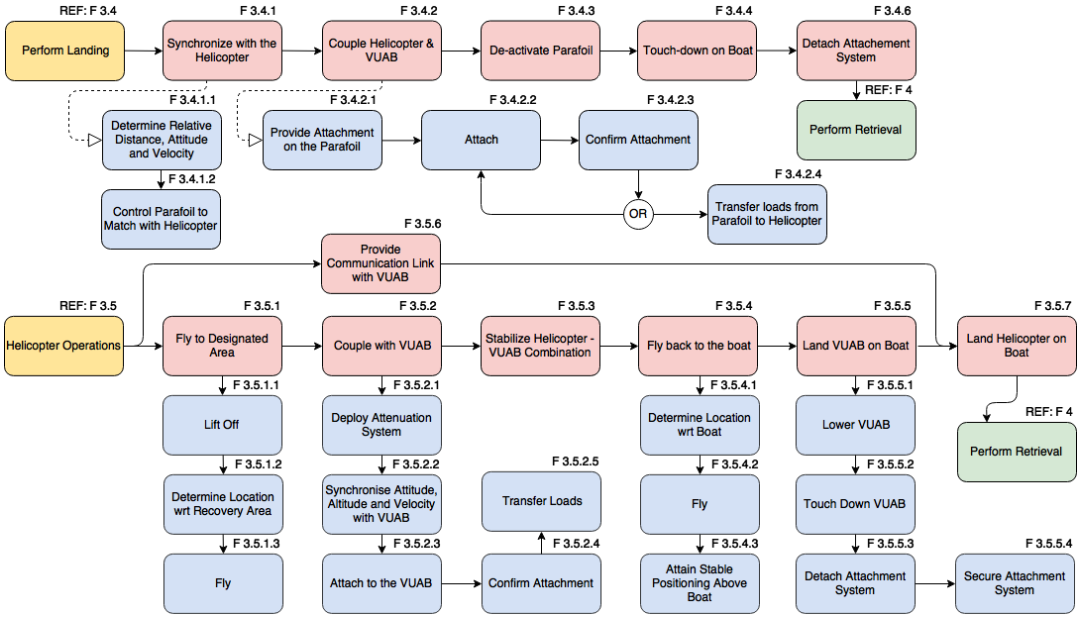

Figure 2.8: Function 3.4 and 3.5 of the Functional Flow Diagram, showing the landing and helicopter operations

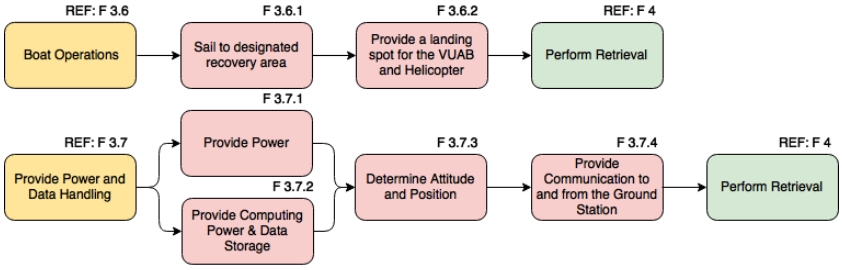

Figure 2.9: Function 3.6 and 3.7 of the Functional Flow Diagram, showing the boat operations and power- and data-handling

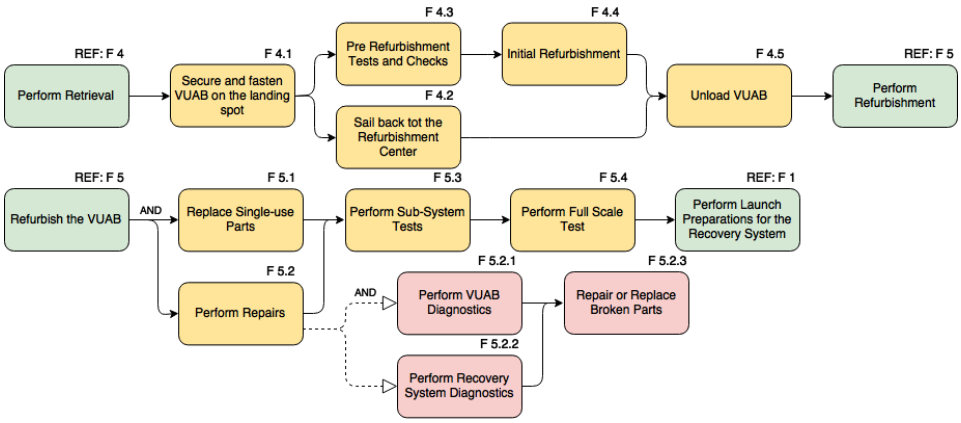

Figure 2.10: Functions four and five of the Functional Flow Diagram, showing the retrieval and refurbishment of the VuAB

2.2.2. Functional Breakdown Structure

The functional breakdown structure (FBS) gives an overview of the system's functions using a logical grouping, as opposed to the chronological order of the functional flow diagram. The FBS is largely based on the FFD and contains all of the functions that are in the FFD , with the addition of certain continuous functions that are not represented in the flow diagram. The FBS is organised in such a way that similar functions, such as position and velocity determinations or environmental protection are grouped together. This is specifically useful for subsystem design, since it gives a better overview of the functions per subsystem than the FFD does. Figure 2.11 shows the top level functions of the system, Figures 2.12, 2.13, 2.16, 2.14 and 2.15 show the lower-level functions for functions 1, 2, 3, 4 and 5.

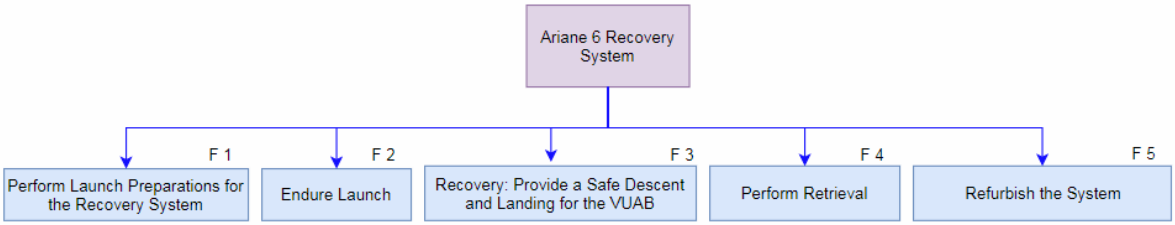

Figure 2.11: Functional Breakdown Structure Top Level

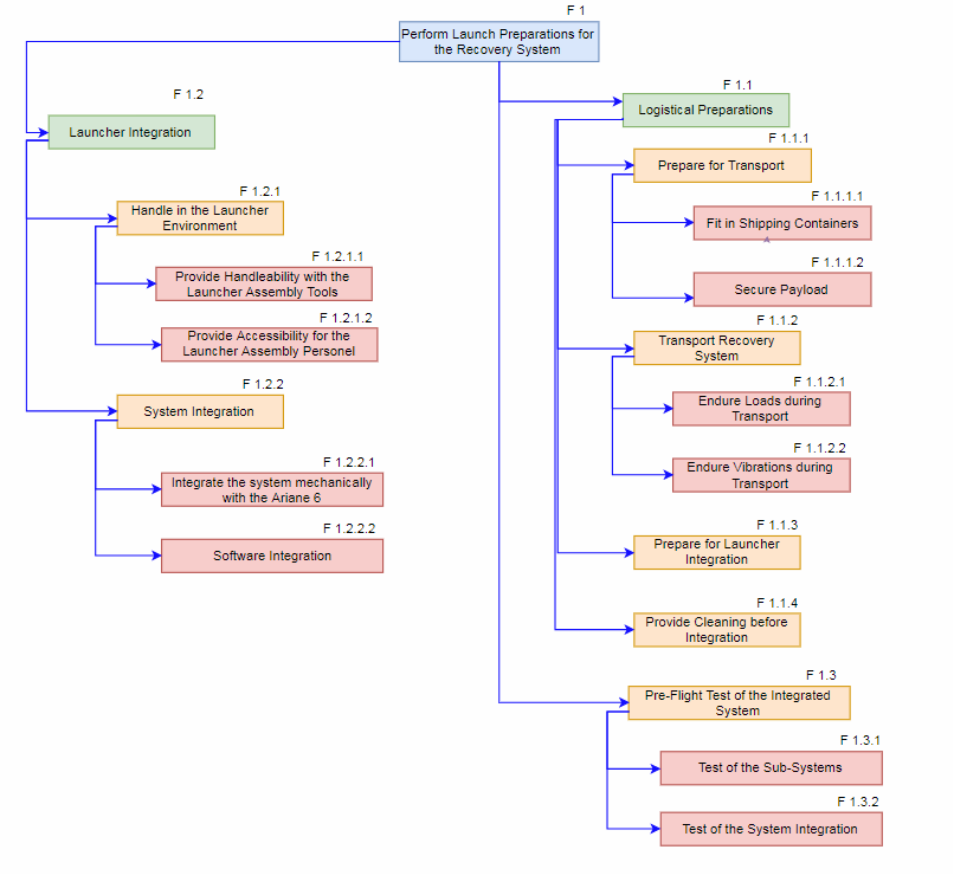

Figure 2.12: Functional Breakdown Structure, showing the launch preparations

Compared to the FBS in the baseline report [70], the top-level functions did not receive any alterations, since the functions that were drafted at that stage still accurately represent the system. The same holds for function 1, which also did not get any significant alteration, other than minor changes in names and numbering of a few lower level functions. Function 2 was slightly altered, since more information was available on the separation mechanisms available on Ariane 6.

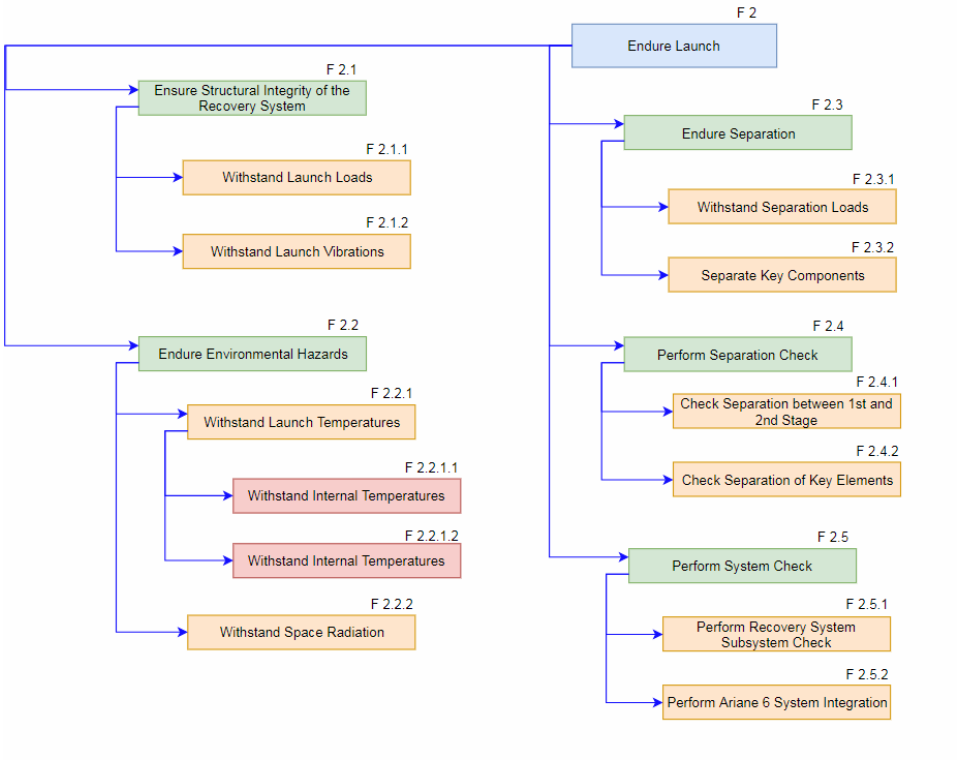

Figure 2.13: Functional Breakdown Structure, showing the launch

The most alterations as compared to the Baseline report are found in the third function, recovery, which can be seen in Figure 2.16. Since the baseline, a final concept has been selected, meaning that functions can be defined to a greater level of detail.

Certain aspects, such as structural integrity, environmental protection and large parts of providing flight trajectory are kept similar, since they still accurately represent the required functions. All the other functions such as re-entry, deceleration, atmospheric flight and landing are made significantly more detailed, as certain design choices and sub-system configurations are added. For example, the landing section has significantly been expanded with a section on the VUAB and helicopter interface, whilst in the controlled flight section, parafoil specific functions were added. Finally, boat and helicopter operations are added to the FBS, which were not present before. Similar to the first function, no alterations were made to the fourth and fifth function, which can be seen in Figure 2.14 and 2.15.

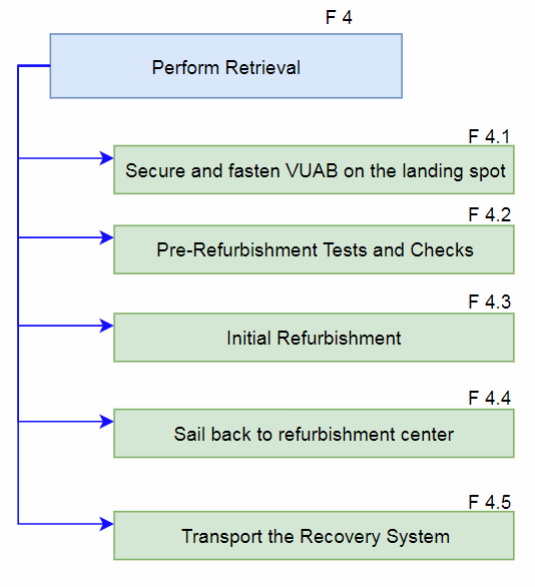

Figure 2.14: Function four in the functional breakdown structure, showing the retrieval

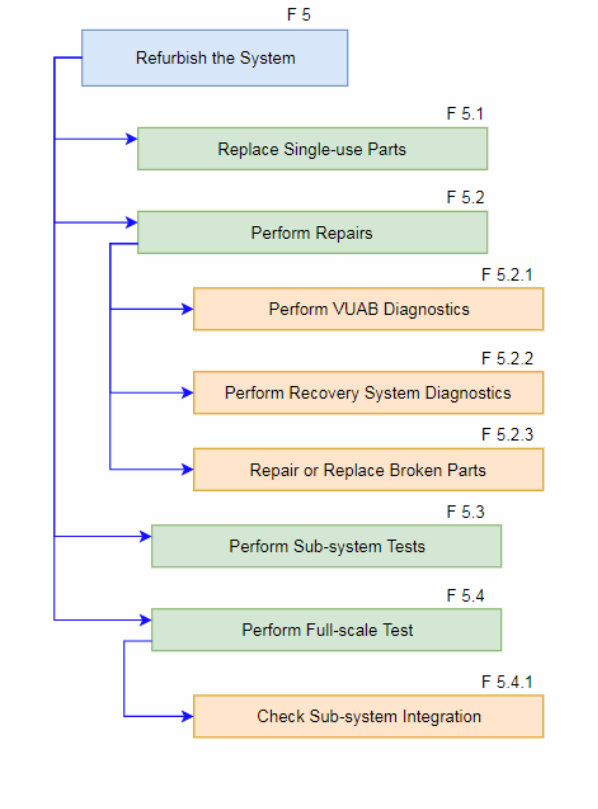

Figure 2.15: Function five in the functional breakdown structure, showing the refurbishment

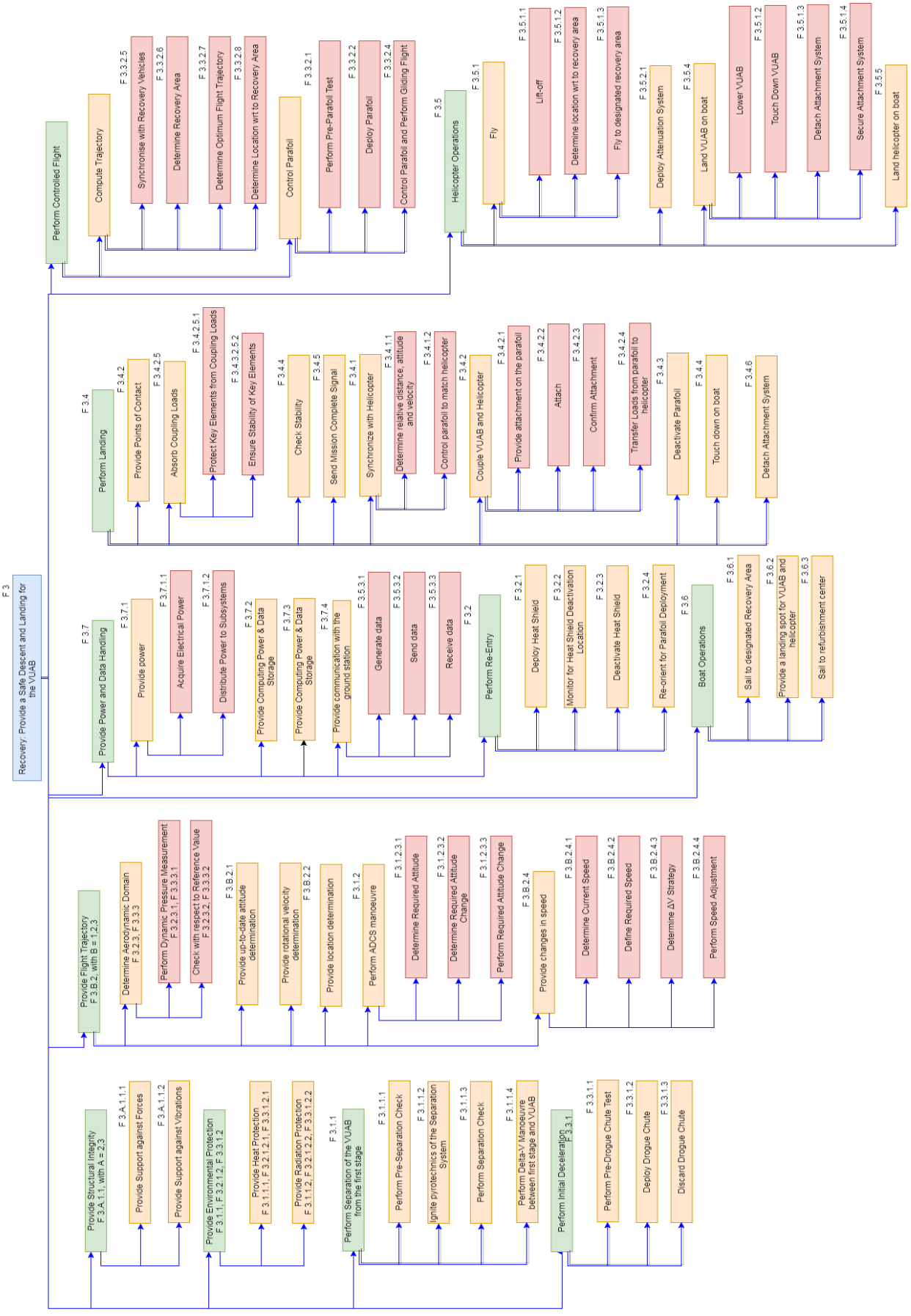

Figure 2.16: Function 3 in the functional breakdown structure

3

Simulation and Models

This chapter elaborated on all the models used throughout the design process. A model is a representation, mathematical or physical, of a system or process. This allows the understanding of a system's behavior under certain conditions. This is done by using the models for generating a simulatiion of the system behavior. The outputs of the models and simulations are used as inputs to the system design, design analysis and mission profile. First, the models describing the trajectory of the VuAB after separation will be elaborated on. This includes the space trajectory, the reentry trajectory, atmospheric flight trajectory as well as accuracy predictions. Next, several specific load cases will be dealt with. The considerd load cases are launch vibrations, parachute and parafoil deployment, catch and helicopter stability.

3.1. Trajectory Models

This section contains the models used to determine the trajectory of the VuAB. First, the space trajectory is determined using the model as stated in Section 3.1.1, after which the re-entry trajectory model is shown in Section 3.1.2. Then, the accuracy of this prediction is determined in Section 3.1.3 and the atmospheric flight trajectory model is explained in Section 3.1.4.

3.1.1. Space Trajectory

As there is no atmosphere in space, no aerodynamic forces are encountered. This means the trajectory depends only on the gravitational force and thrust forces that are introduced aboard the system. The decision was made to only use thrust for attitude control, so without any influence on the trajectory. The trajectory is then a fully ballistic one. This trajectory is visualised in Figure 3.1. The trajectory of the Ariane 6 is horizontal at the moment of first stage separation. Separation thus takes place at point C in the figure. The velocity and the height from the earth's surface at this point are 6930 m/s and 157.7 km respectively. Ariane 5 is taken as a reference in determining the separation parameters, this was confirmed and verified by Airbus Defence and Space. [1]

With these values, the angular momentum per unit mass, H, can be computed using Equation (3.1). Here V_t is the tangential velocity, which is equal to the total velocity in point C, R_e is the radius of the earth and h is the height above the earth's surface. H is constant for the whole trajectory, so the tangential velocity increases when the altitude decreases.

$$H = V_t \cdot R_a = V \cdot (R_e + h) \qquad (3.1)$$

$$p = \frac{H^2}{\mu} \qquad (3.2)$$

H is used to compute the semi-latus rectum, p, which is a parameter defining the shape of the elliptical orbit trajectory. In Equation (3.2), μ is the standard gravitational parameter for earth. Then, p and R_a are used in Equation (3.3) to compute the eccentricity of the trajectory ellipse. Using e in Equation (3.4) the ellipse radius at a certain angle θ is obtained. Rearranging Equation (3.4) gives Equation (3.13) with which the angle θ for the re-entry altitude can be determined. The beginning of reentry is defined to be at 100 km altitude from the surface of the Earth.

[1] http://spaceflight101.com/ariane-5-va226/ariane-5-va226-launch-profile/, [22-01-2018]

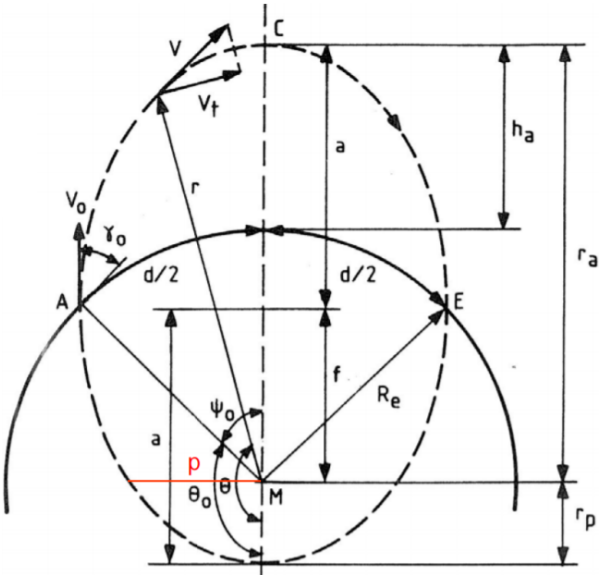

Figure 3.1: Ballistic trajectory geometry [44]

$$e = 1 - \frac{p}{R_a} \qquad (3.3) \qquad r = \frac{p}{1 + e \cdot \cos(\theta)} \qquad (3.4) \qquad \theta = \arccos\left(\frac{\frac{p}{r} - 1}{e}\right) \qquad (3.5)$$

Note that the r in both Equation (3.4) and Equation (3.13) is equal to $R_e + h$. As said the initial condition for the space flight, just after separation is at point C in Figure 3.1, for which $\theta = \pi$ rad. Reentry happens at an angle of $2\pi - \theta_r$ where θ_r is the angle for reentry altitude computed with Equation (3.13).

In the space flight model, the angle θ is varied between the above named values for separation and re-entry. For every θ, the radius r (and altitude, $h = r - R_e$) and ground distance x_g are determined using Equation (3.4) and Equation (3.6) respectively. In turn, V_t is computed using Equation (3.7). Note that V_t is not equal to the total velocity, as the flight path is not tangential to the earth surface.

$$x_g = R_e \cdot \theta \qquad (3.6) \qquad V_t = \frac{H}{r} \qquad (3.7)$$

The flightpath angle, γ_{space} with the earth's surface is determined using Equation (3.8). Here dr is the change in ellipse radius and dx_g is the change in ground distance. The pitch angle with respect to the velocity vector is then computed using Equation (3.9).

$$\gamma_{space} = \arccos\left(\frac{dr}{dx_g}\right) \qquad (3.8) \qquad \text{pitch} = \theta - \gamma_{space} \qquad (3.9)$$

In Equation (3.9), θ accounts for the angle with the earth's surface. It is assumed that the attitude of the system will not change in space, so while it turns around the earth it will pick up a pitch angle with respect to the earth's surface. To give the angle with the velocity vector the flightpath angle is subtracted. The flightpath angle is also used to give the total velocity, using Equation (3.10).

$$V_{tot} = \frac{V_t}{\cos(\gamma_{space})} \qquad (3.10)$$

Using all above mentioned equations with the given separation conditions (h=157.7 km, V = 6927 m/s) and re-entry altitude (100km) give the simulation for the space phase of the mission. Plots for the trajectory, the velocity and the pitch angle can be found in Figure 3.2, Figure 3.3 and Figure 3.4 respectively. The final conditions at 100 km altitude are used as initial conditions for the re-entry simulation.

3.1.2. Reentry Trajectory

Atmospheric entry is a critical mission phase due to the aerothermal loads (heating) and deceleration forces experienced by the VuAB when re-entering earth's atmosphere. In order to predict these extreme conditions, simulations of the atmospheric entry are performed. This simulation starts at an altitude of 100 km and runs until

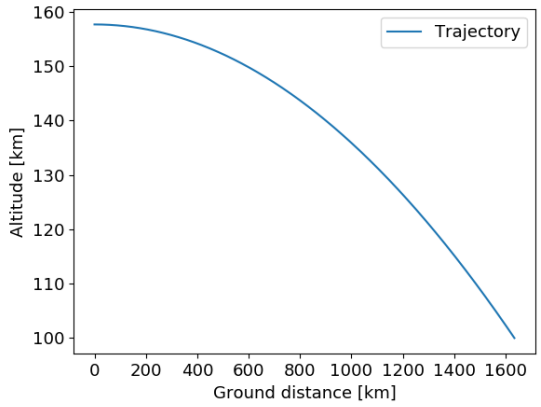

Figure 3.2: Space flight trajectory

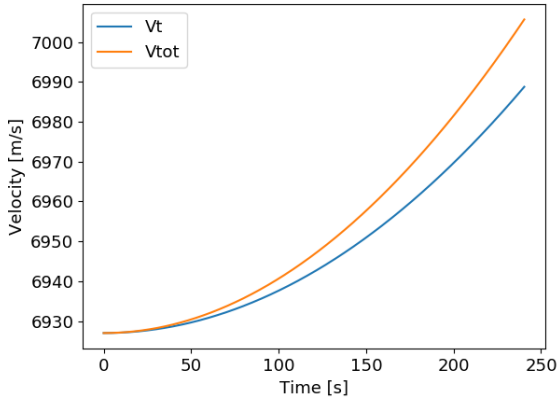

Figure 3.3: Tangential velocity and total velocity in space over time

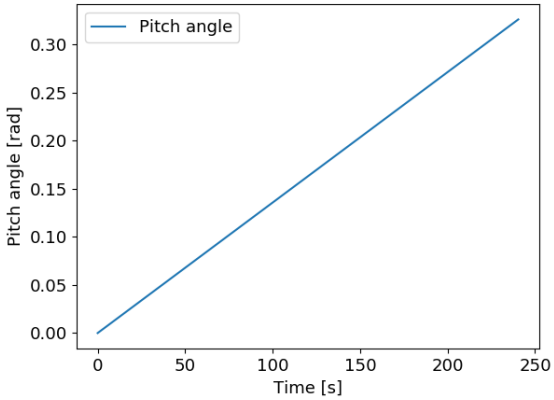

Figure 3.4: Pitch angle varying over time

an altitude of 8.1 km has been reached where the aeroshell will be discarded and the system will be decelerated further using a droguechute.

Coordinate Transformations

The order of the ground track which is covered during atmospheric entry requires earth to be modelled spherical rather than flat in order to prevent significant simulation errors. As the model is based on Newton's laws of motion which only for an inertial reference frame, use is made of axis transformations to convert the forces acting on the system during atmospheric entry in a body fixed frame to an inertial reference frame. The initial x-coordinate of the VuAB is defined to be 0. The initial y-coordinate is defined to be earth's radius plus 100 km, as 100 km is the altitude where the space trajectory model ends and the atmospheric entry model takes over. Since the re-entry model runs till a certain altitude is reached and the atmospheric properties are determined based upon the altitude of the system, the distance between the surface of earth and the VuAB is determined at every time-step using Equation (3.11) and Equation (3.12) in which r_{earth} is the radius of the earth fixed at $6371 \cdot 10^3$ m. The direction of the gravitational force is dependent on the position of the VuAB with respect to the inertial reference frame, therefore θ is updated at every time-step by using Equation (3.13). This Equation will not work when y is reduced to 0 in the case when the VuAB travels more than a quarter of Earth's circumference, which does not happen during re-entry. Finally as the lift and drag factor are transformed to the inertial reference frame using γ, defined as the angle between the velocity vector of the VuAB and the x-axis which is determined using Equation (3.14).

$$r = \sqrt{x^2 + y^2} \quad (3.11) \qquad h = r - r_{earth} \quad (3.12) \qquad \theta = \arctan(\frac{x}{y}) \quad (3.13) \qquad \gamma = \frac{V_x}{V_y} \quad (3.14)$$

Therefore the final velocity values of the space trajectory model at 100 km altitude are transferred to be the initial velocity inputs of the atmospheric entry model.

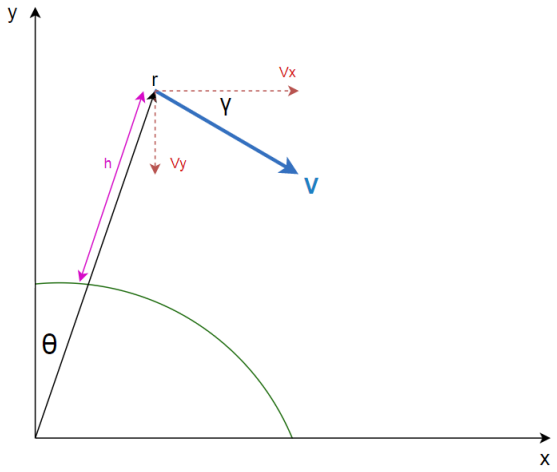

Figure 3.5: Angles and vectors used for the planar atmospheric entry model

Atmospheric Properties

During the re-entry phase, the atmospheric properties of air temperature, pressure and density surrounding the VuAB change significantly due to the changing altitude. In order to take this into account during the simulation these atmospheric properties are determined at every time-step based upon the corresponding altitude of the VuAB, making use of the International Standard Atmosphere model. The constants and equations used for this model are described in Appendix A.

Aerodynamic Coefficients

During atmospheric entry multiple aerodynamic regions are covered, ranging from the hypersonic to subsonic regime. The aerodynamic coefficients used to describe the forces acting on the system will therefore not be constant during re-entry, and are evaluated at every point in time during the simulation. The first step in this evaluation is the determination of the speed of sound using Equation (3.15) in which T is the temperature of the surrounding air at the altitude at which the aerodynamic coefficients are being evaluated. The speed of sound combined with the total velocity of the VuAB at the previous point in time gives the Mach number as illustrated in Equation (3.16).

$$a = \sqrt{\gamma RT} \qquad (3.15) \qquad\qquad M = \frac{V}{a} \qquad (3.16)$$

The drag coefficient of the aeroshell is not only dependent on Mach number, but also on the angle of attack the aeroshell has with respect to the freestream of air. The correlation between the drag coefficient and the Mach number of the aeroshell for a fixed angle of attack can be found in Figure 3.6.

This correlation was reproduced using a continuous set of linear and polynomial functions allowing the drag coefficient to be determined using any given Mach number. As can be seen in Figure 3.6 the drag coefficient is constant around 1.43 at high Mach numbers, which is the case during re-entry. This value corresponds to the angle of attack around which the aeroshell has its equilibrium with respect to the aerodynamic moment it creates. As can be seen in Figure 3.7 this angle of attack is at 20 degrees.

At this angle of attack the aeroshell will not produce an aerodynamic moment. Furthermore it can be seen that the slope of the aerodynamic moment with respect to angle of attack is linear and negative. This indicates that whenever the angle of attack of the aeroshell has an offset with respect to its equilibrium point, an aerodynamic moment will be produced in the other direction to force the aeroshell back to its equilibrium point. When the aeroshell's angle of attack deviates from this equilibrium position however, its drag coefficient will change as well, see fig. 3.7. For the simulation, this change was modelled as an offset from the drag coefficient based on the Mach number as displayed in Figure 3.6. In order to determine this offset, the drag curve as displayed in Figure 3.8 is linearised around its moment equilibrium point of 20 degrees angle of attack.

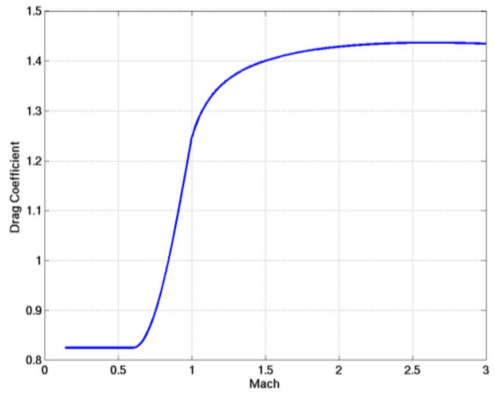

Figure 3.6: Drag coefficient of an aeroshell varying with Mach number [55]

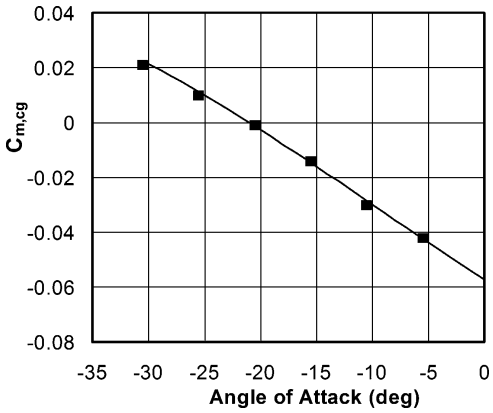

Figure 3.7: Moment coefficient of an aeroshell with respect to its angle of attack [38]

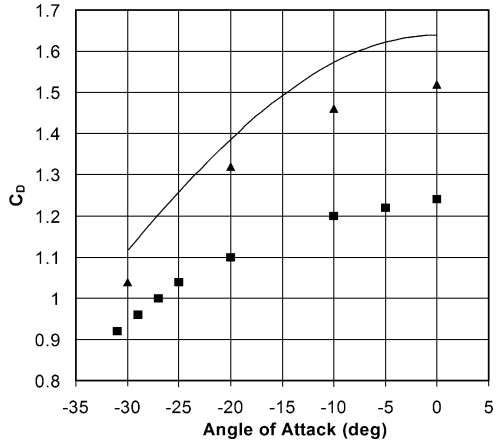

Figure 3.8: Drag coefficient of an aeroshell with respect to its angle of attack [38]

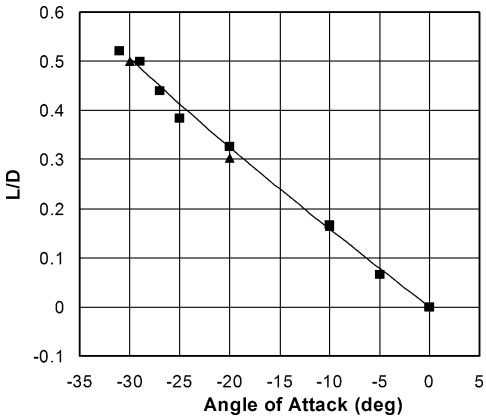

Figure 3.9: Lift to drag ratio of an aeroshell with respect to its angle of attack [38]

This offset is determined using a linear model, since the angle of attack of the aeroshell during re-entry will only change by a few degrees and hence the error of linearisation will be small. By modelling the drag coefficient based upon Mach number, and then using an offset based upon the angle of attack, the drag coefficient can be determined for any Mach number and angle of attack.

The lift coefficient can subsequently be determined by using the L/D ratio. This ratio is assumed to be invariant of Mach number. It is however heavily dependent on the angle of attack of the aeroshell. This correlation is displayed in Figure 3.9. This correlation is linearised around -20 degrees allowing the L/D ratio to be determined for any angle of attack between -30 and 0 degrees. For a given angle of attack and Mach number, first the drag coefficient is determined, which is then multiplied with the L/D factor to calculate the lift coefficient. As the drag coefficient can be determined for any angle of attack and Mach number, and the lift coefficient follows from this coefficient, also the lift coefficient can be determined for any condition during atmospheric entry. For a regular reentry simulation without random variables, a constant angle of attack of -20 degrees is used. At this angle of attack C_D is equal to 1.37 and the L/D ratio is 0.3, hence C_L is equal to 0.411.

Forces

As the aerodynamic coefficients are known, the aerodynamic forces acting on the system can be determined. The lift force is calculated using Equation (3.17) and acts perpendicular to the system's velocity vector. The drag force is determined using Equation (3.18) and acts parallel to the velocity vector. As can be seen in these Equations the forces are dependent on air density which is updated at every point in time based on the corresponding altitude at that point in time. The equations are also dependent on the total velocity of the system, of which the velocity of the system in the previous time-step is used. Finally the surface area used in these Equations is the frontal area of the aeroshell.

$$L = C_L \frac{1}{2} \rho V^2 S \qquad (3.17) \qquad\qquad D = C_D \frac{1}{2} \rho V^2 S \qquad (3.18)$$

As the total forces and accelerations of the system are calculated in the inertial reference frame, the aerodynamic forces need to be converted from the body fixed reference frame to the inertial reference frame. The lift vector is decomposed into the inertial reference frame's x-direction and y-direction as described in Equation (3.19), while the drag force is decomposed using Equation (3.20).

$$\begin{bmatrix} F_{L_X} \\ F_{L_Y} \end{bmatrix} = F_L \cdot \begin{bmatrix} \sin(\gamma) \\ \cos(\gamma) \end{bmatrix} \qquad (3.19) \qquad\qquad \begin{bmatrix} F_{D_X} \\ F_{D_Y} \end{bmatrix} = F_D \cdot \begin{bmatrix} -\cos(\gamma) \\ \sin(\gamma) \end{bmatrix} \qquad (3.20)$$

The gravitational acceleration of the system is dependent on the distance the system has with respect to the body causing the gravitational pull. Since the altitude of the system changes significantly during re-entry, the gravitational acceleration is not assumed to be constant while atmospheric entry is taking place. The relation used to describe the gravitational acceleration varying with altitude during the simulation is displayed in Equation (3.21). In this relation G is the gravitational constant of earth fixed at $6.674 \cdot 10^{-11}$, M is earth's total mass fixed at $5.972 \cdot 10^{24}$, r is the distance between the system and earth's centre, and $\hat{r}$ describes the unit vector pointing from the centre of earth to the VuAB.

$$\mathbf{g} = -\frac{GM}{r^2} \hat{\mathbf{r}} \qquad (3.21)$$

As the total forces and accelerations of the system are determined in the inertial reference frame, the vector of the gravitational force in the inertial reference frame changes during flight and is therefore updated at every time-step. The magnitude of the gravitational pull is found by multiplying the gravitational acceleration with the system mass. The components of the gravitational pull are then decomposed in the x-direction and y-direction using Equation (3.22).

$$\begin{bmatrix} F_{Z_X} \\ F_{Z_Y} \end{bmatrix} = F_Z \begin{bmatrix} -\sin(\theta) \\ \cos(\theta) \end{bmatrix} \qquad (3.22)$$

As all components of the aerodynamic and gravitational forces have been determined, the acceleration of the system due to these forces can be calculated. Therefore, at every time-step all forces expressed in the inertial reference frame are combined and divided by the system mass to determine the acceleration of the spacecraft in the x-direction and y-direction. The velocity and position of the system are then determined by integrating this acceleration over time. The altitude profile of the VuAB during reentry is displayed in Figure 3.10, and the corresponding velocities are illustrated in Figure 3.11.

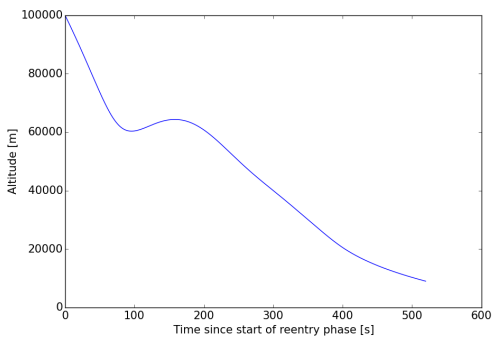

Figure 3.10: Altitude of the VuAB versus time during the reentry phase

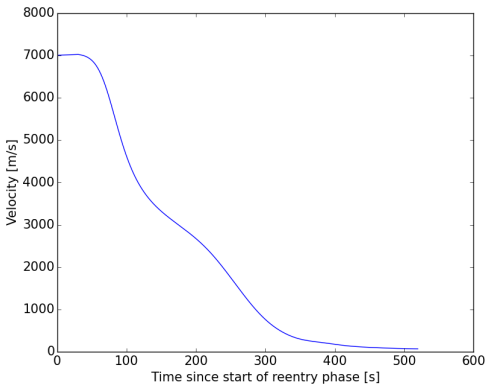

Figure 3.11: Velocity versus time of the VuAB during the reentry phase

Dynamic Pressure

Dynamic pressure is a property of a flowing gas. The aerodynamic forces acting on an object are directly related to the dynamic pressure. This will help indicate the loads introduced into the structure of the VuAB. Moreover, components such as the TPS and the drogue chute have a maximum dynamic pressure which the components can

operate at. The flow is to be modelled as a compressible flows during re-entry. The dynamic pressure is given in Equation (3.23). The specific heat ratio, γ, is taken as 1.4. Which holds for the conditions under investigation. [9]

$$q_\infty = \frac{1}{2}\gamma p_s M^2 \tag{3.23}$$

Heatflux

The heatflux, $\dot{q}$ is defined as the heat transfer rate per unit are at a given point on the body surface. Aerodynamic heating at hypersonic speeds are so severe that it will drive the aeroshell TPS design. Aerodynamic heating is a very advanced field of engineering. In 'Fundamentals of Aerodynamics', Anderson provides some engineering methods to determine aerodynamic heating for hypersonic viscous flows. Anderson argues that the aerodynamic heating at the stagnation point of a blunt body is usually the point of most severe heat transfer rate on a hypersonic vehicle, where $\dot{q} \propto \frac{1}{\sqrt{R}}$. Where R_{nose} is the nose radius at the stagnation point. This holds under the assumption that at the stagnation point the flow is laminar. Heat transfer will be determined based on laminar compressible flow theory. Anderson provides Equation (3.24) to determine the heatflux at the stagnation point of a blunt body[9]:

$$\dot{q}_w = \rho_\infty^{0.5} V_\infty^3 (1.83 \cdot 10^{-8} R_{nose}^{-0.5})(1 - \frac{h_w}{h_0}) \tag{3.24}$$

At hypersonic speeds, $h_0 \approx \frac{V_\infty^2}{2}$. The surface temperature, which relates to h_0 is very small compared to the total temperature at high Mach numbers. This leads to the following relation 3.25.

$$h_0 \gg h_w \tag{3.25}$$

To determine the wall temperature which is used to calculate h_w, the boundary layer will need to be evaluated. This can be done using the Navier-stokes equations. However, considering relation 3.25, it is much more sensible to take the the relation $(1 - \frac{h_w}{h_0})$ equal to 1. This approach leads to a marginally more conservative (thus higher) heatflux. Now all that is left is to determine the nose radius. Initial estimates are used for the model, but this is a parameter that shall be optimized as part of the aeroshell design.

It is important to note that at the stagnation point the most critical heatflux will be as determined above. For the remaining surface, the expected heatflux is much lower. A numerical method to show this is to calculate the total heat transferred to the vehicle per unit time: $\frac{dQ}{dt}$.

Total Heat Rate

The total heat rate will prove that the maximum heat flux from Equation (3.24) will not be as high for the entire surface of the heat shield.

$$\frac{dQ}{dt} = \frac{1}{4}\rho_\infty V_\infty^3 S_p C_f \tag{3.26}$$

Where S_p is the projected surface area of the heat shield and C_f the total skin friction coefficient. Considering compressible laminar boundary layer theory over a flat plate, C_f is estimated according to the following relation $C_f\sqrt{Re_c} = 0.99$. Where $Re_c = \frac{\rho_\infty V_\infty c}{\mu_\infty}$. Where c is the length of the side of the aeroshell. μ_∞ is determined according to Sutherland's law:

$$\frac{\mu_\infty}{\mu_0} = (\frac{T}{T_0})^{3/2} \frac{T_0 + 110}{T + 110} \tag{3.27}$$

The results of C_f can be verified by comparing the results to that of a plat plate for Reynolds numbers ranging between 10^6 and 10^7. [9] The total heat rate is be divided by the total surface area to show the average heating per unit area. If this average is significantly lower than the heatflux at the stagnation point in the same instant in time it shows that the surface, excluding the stagnation point, will experience much lower heat transfer rates. This can be taken into consideration for the heat shield design.

Table 3.1: Inaccuracies for the atmospheric entry with random offset used during the Monte Carlo simulation

Variable	Random deviation (2σ)	Updated every
Aeroshell surface area	2 %	Simulation
Air temperature	5 %	Timestep
Air pressure	5 %	Timestep
Air density	5 %	Timestep
Angle of attack	2.7 deg	Timestep
Sideslip angle	2.7 deg	Timestep

3.1.3. Atmospheric Entry Accuracy Prediction

The atmospheric model described so far assumes that the design parameters, atmospheric conditions and aerodynamic properties can be determined perfectly to simulate real world conditions. In reality however, these parameters will have certain inaccuracies due to, for example, turbulent conditions in the atmosphere and offsets of the aeroshell from its equilibrium point, causing a change in the lift over drag ratio. These inaccuracies might lead to significant changes in the ground track, time of the reentry phase, heatflux, and deceleration forces, driving the design of not only the aeroshell, but also other elements of the recovery system. Therefore, it is important to determine the size of the fluctuations in these parameters while designing the recovery system. This problem is tackled by making use of a Monte Carlo simulation in which 1000 atmospheric entries are simulated where the properties with uncertainties receive a random value per simulation, or even per time-step. Due to the randomness of these variables, multiple unique solutions to the same model are produced. The consequence of this Monte Carlo simulation is that a range of possible outputs are produced, rather than only one output for the perfect scenario. In this way the design can be based on the worst case scenario. For the Monte Carlo simulation it is important that the range of the random samples taken to describe the variables with inaccuracies are realistic. If the domain is too big, the worst case scenario which is produced will be worse than in reality, causing the solution to the problem to be over-designed. On the other hand, if the domain is too small, the outputs of the Monte Carlo simulation might not include the worst case scenario which might actually occur in reality. Making use of a safety factor mitigates the risk of underestimating the worst case scenario to design for example structural elements of the aeroshell, but these factors will not be able to determine the domain of possible positions of the VuAB after the atmospheric entry, showing the importance of carrying out a Monte Carlo analysis.

Probability Distribution of Random Variables

During the Monte Carlo simulation 6 variables will receive random values. The random offsets are normally distributed with a random domain based on a comparable Monte Carlo simulation to research the capabilities of planetary entry using an inflatable aeroshell [59]. The variables which are altered during the Monte Carlo simulation together with their random offset and the frequency of drawing a random value are summarised in Table 3.1. A random offset of 2% indicates that the original value of the corresponding variable will be multiplied with random sample drawn from a Gaussian distribution with a mean of 1 and a standard deviation of 0.025 (Norm(1,0.025)), causing 95% of the samples to be within 2% of the original value. The frontal surface area of the aeroshell has a 2% offset since the aerodynamic forces on the aeroshell cause it to deflect during reentry, while the atmospheric properties have a 5% deviation due to chaotic circumstances in the atmosphere.

Finally, 95% of the time the angle of attack of the aeroshell is within a 2.7 degree offset of its equilibrium point due to the deflected shape of the aeroshell during reentry, and because the aeroshell is not instantly returned to its equilibrum position after any disturbance. This 2.7 degree offset is not only altering the angle of attack, but also introduces a sideslip angle, defined as φ, causing a lateral force on the system. This means that due to to the randomness in the sideslip angle, the VuAB does not only have planar motion anymore, introducing a z-axis for lateral position in the model. The 2.7 degree offset is thus a circular angle offset, with 95% probability. Therefore, the offset of the angle of attack and sideslip angle is determined using a circular random generation where the radius and the angle are defined using Equation (3.28) and Equation (3.29) respectively. To convert these samples to sideslip and angle of attack offset, the radius of every sample was multiplied with its cosine for the sideslip, and its sine for the angle of attack offset, as displayed in Figure 3.12.

$$r = 2.7|Norm(1,0.025)| \qquad (3.28) \qquad\qquad \theta = U(0,2\pi) \qquad (3.29)$$

After the random angles have been determined, C_D will be re-evaluated using the linearisation of the drag curve as explained in Section 3.1.3 as the drag will change according to the new angle of attack. Subsequently C_L will

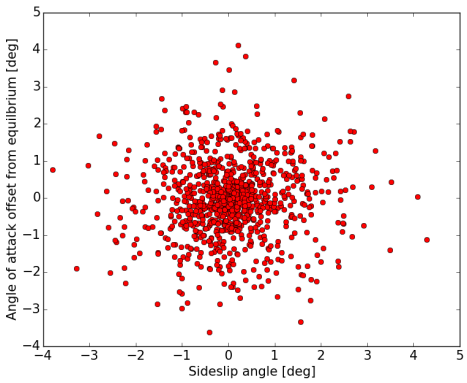

Figure 3.12: Circular random distribution of sideslip angle and angle of attack offset for 1000 samples

be determined using the L/D ratio. This lift vector will then be tilted due to the sideslip angle. The resulting relations to determine the forces due to lift in the inertial reference frame are described in Equation (3.30).

$$\begin{bmatrix} F_{L_X} \\ F_{L_Y} \\ F_{L_Z} \end{bmatrix} = F_L \begin{bmatrix} \sin(\gamma)\cos(\varphi) \\ \cos(\gamma)\cos(\varphi) \\ \sin(\varphi) \end{bmatrix} \tag{3.30}$$

The components of the drag force are calculated using the same method as the planar model, only with the updated C_D. The z-component of the drag force and gravitational pull are not included in the Monte Carlo simulation since this component is deemed to be negligible compared to the x- and y-components. After the aerodynamic and gravitational forces have been determined they are combined to determine the accelerations after which the same integration method is performed to calculate the trajectory of the VuAB. An example of an output expressed over time for a simulation including random variables is displayed in Figure 3.13. The final accuracy output including total longitudinal and lateral range covered by the 1000 reentry simulations is displayed and used for design in Section 7.1.1.

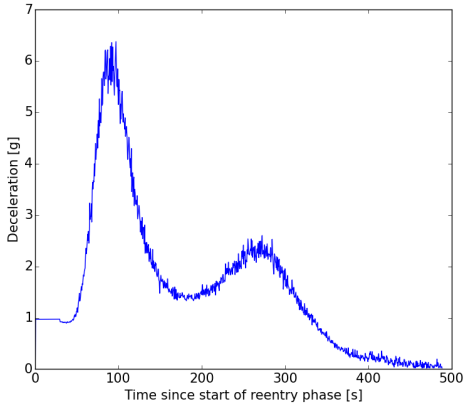

Figure 3.13: Deceleration of the VuAB versus time for one of the atmospheric entry simulations performed during the Monte Carlo analysis

Verification

In order to verify the outputs of the reentry model, the same design parameters as the High-Energy Atmospheric Reentry Test (HEART) aeroshell are used as an input to the model, after which the outputs are compared with the measurements performed during this test [22]. During this test an aeroshell with a diameter of 8.3 meters is used and the maximum payload is equal to 5500 kg. During the reentry, measurements were made of the dynamic pressure experienced by the payload, the deceleration, and the heat rate distribution over the surface. For the design of the aeroshell the maximum heat rate found at the surface is the most relevant. Therefore the

maximum heat rate of the aeroshell is plotted over time in Figure 3.14, together with the dynamic pressure and the deceleration. The same type of outputs of the model are displayed in Figure 3.15

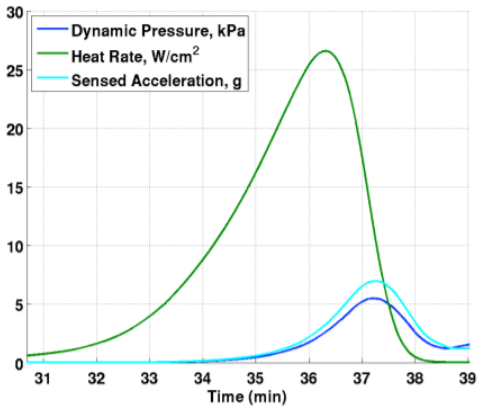

Figure 3.14: Measurements performed during the High-Energy Atmospheric Reentry Test [22]

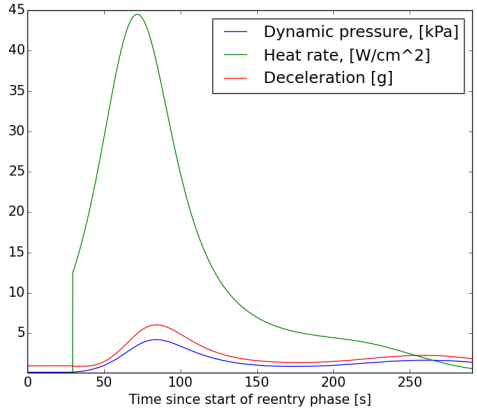

Figure 3.15: Verification of the reentry model using the same design parameters used for the High-Energy Atmospheric Reentry Test [22]

As can be seen while comparing these two Figures, the magnitude of the outputs are very comparable. The difference between maximum heat rate found at the surface is likely due to a difference in aeroshell geometry such as the nose-cone radius. The phenomenon of higher dynamic pressure and acceleration for the HEART is likely caused by a higher potential energy at the start of the atmospheric entry, as this test is being performed after separation of the International Space Station, which can be related back to the higher entry velocities.

3.1.4. Atmospheric Flight Trajectory

For the atmospheric flight model, a six degree of freedom model is developed to simulate a ram air parachute system [58, 69, 73]. This model uses three degrees of freedom for position and three for orientation. The orientation degrees of freedom use Euler angles which contain singularities at certain orientations. This problem could be avoided by using quaternions, which create a seven degree of freedom model. However, since it is assumed and validated from flight heritage data [13] that the parachute system will fly mostly straight and level, the use of Euler angles is acceptable for this application. Furthermore, this six degree of freedom model assumes that the payload will remain at a fixed orientation and location with respect to the parafoil.

Research has been performed into modelling and simulation of comparable systems using nine degrees of freedom model, which takes into account changes in relative orientation. The reason for this relative orientation arise from the fact that the physical system connects the payload and parafoil using strings. These strings can twist and stretch allowing the bodies to be at different relative positions and orientations.

This same research has shown that assuming a six degree of freedom problem is a valid assumption for systems where the payload and parafoil are close enough to each other that both experience the same wind effects. This assumption can be invalidated by high wind gusts or extreme manoeuvres.

Derivation of Rigid Body Equations

The model to be developed from here after assumes a flat earth and neglects the rotation of the earth. Both of which are valid assumptions for short flights covering small areas. To begin, let ϕ, θ, ψ represent the roll, pitch and yaw of the vehicles respectively and let P, Q and R represent the roll, pitch and yaw rates respectively.The directions follow the aerospace right hand convention. Moreover, let p_N, p_E and p_U represent the location of the rigid body in the inertial reference frame using the north, east and up convention. Let U, V, W represent the velocity of the vehicle with respect to the body fixed axis. This convention means that from a pilots perspective, U is the velocity in the forward direction, V is velocity positive in the starboard direction and W is the velocity positive in the downwards direction. With these variables the state of the system can be defined as seen in Equation (3.31).

$$x = \begin{bmatrix} p_N & p_E & p_U & \phi & \theta & \psi & U & V & W & P & Q & R \end{bmatrix}^T \tag{3.31}$$

For simplicity these variables are grouped as follows:

$$p = \begin{bmatrix} p_N \\ p_E \\ p_U \end{bmatrix} \qquad \Phi = \begin{bmatrix} \phi \\ \theta \\ \psi \end{bmatrix} \qquad \upsilon = \begin{bmatrix} U \\ V \\ W \end{bmatrix} \qquad \omega = \begin{bmatrix} P \\ Q \\ R \end{bmatrix}$$

Hence, now the state vector can be simplified to:

$$x = \begin{bmatrix} p \\ \Phi \\ \upsilon \\ \omega \end{bmatrix} \tag{3.32}$$

Additionally, let F and M represent the vector of the applied forces and moments. Let m represent the total mass of the parachute system and J represent the inertia matrix.

$$J = \begin{bmatrix} J_{xx} & -J_{xy} & -J_{xz} \\ -J_{xy} & J_{yy} & -J_{yz} \\ -J_{xz} & -J_{yz} & J_{zz} \end{bmatrix} \tag{3.33}$$

Moreover, let T_{BI} be the transformation matrix from the inertial reference frame to the body reference frame. Note that a shorthand notation for trigonometric functions is employed where sin = s, cos = c and tan = t.

$$T_{BI} = \begin{bmatrix} c_\theta c_\psi & c_\theta s_\psi & -s_\theta \\ s_\phi s_\theta c_\psi - c_\phi s_\psi & s_\phi s_\theta s_\psi + c_\phi c_\psi & s_\phi c_\theta \\ c_\phi s_\theta c_\psi + s_\phi s_\psi & c_\phi s_\theta s_\psi - s_\phi c_\psi & c_\phi c_\theta \end{bmatrix} \tag{3.34}$$

Before proceeding, its important to elaborate a bit further on the centre of mass of the system, since all the equations of motion, both forces and moments, from here after will be written with respect to this centre of mass. Figure 3.16 illustrates the canopy-payload system. Since, as was mentioned in the introduction of this section, the model being developed assumes no relative orientation or location between the payload and the canopy, this means one can compute a global centre of mass for the system as depicted in the figure as c.g. Given that this model is used to simulate a system that has a payload mass (m_p) of around 8000kg and a canopy mass (m_c) of around 410kg, it is assumed that the mass of the canopy and lines are negligible and that the centre of mass of the canopy system is located at the centre of mass of the payload. Hence, m_p is equal to m.

Furthermore, the rigid body equations to be presented hereafter use F and M to refer to the forces and moments applied to the rigid body. These forces and moments will be taken about the aerodynamic centre of the parafoil for simplicity that is assumed to be located at the quarter point of the chord. Moreover, for simplicity, the aerodynamic forces acting on the payload (lift and drag) will be neglected.

Hence, the centre of gravity will be located at a distance z_{cg} away from the aerodynamic centre along the z-axis, which as reasoned previously will be assumed to be equal to the distance between the canopy and the payload centre of masses.

Since the forces and moments are not taken about the centre of mass, and the moments and and products of inertia are taken around the centre of mass, adjustments will need to be made using parallel axis theorem. The resulting Jacobian is:

$$J = \begin{bmatrix} J_{xx} + mz_{cg}^2 & -J_{xy} & -J_{xz} \\ -J_{xy} & J_{yy} + mz_{cg}^2 & -J_{yz} \\ -J_{xz} & -J_{yz} & J_{zz} \end{bmatrix} \tag{3.35}$$

Force Equations

The force equations will be derived from basic laws of physics. To begin, let G be the vector acceleration of gravity in the body fixed frame and g be the scalar acceleration due to gravity, which is approximately 9.81 meters per second squared.

$$G = T_{BI} \begin{bmatrix} 0 \\ 0 \\ -g \end{bmatrix} = \begin{bmatrix} g s_\theta \\ -g s_\phi c_\theta \\ -g c_\phi c_\theta \end{bmatrix} \tag{3.36}$$

From Newton's second law, where the derivative is taken in the body frame:

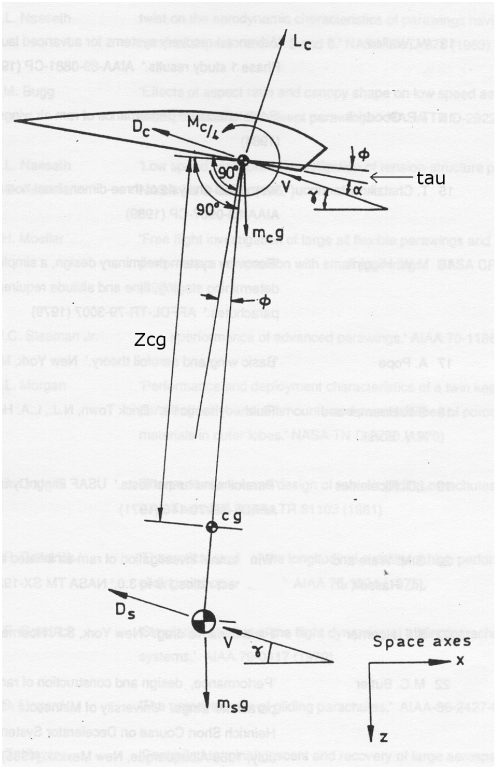

Figure 3.16: Longitudinal free body diagram of a typical ram-air parachute system [69]

$$F + mG = \frac{d}{dt} mv = m(\dot{v} + w \times v) \tag{3.37}$$

Rearranging,

$$\dot{v} = \frac{1}{m} F + G - \omega \times v \tag{3.38}$$

Where, F is the aerodynamic force and contains lift and drag.

$$F_A = \frac{1}{2} \rho S_p V C_L \begin{bmatrix} V_P(3) \\ 0 \\ -V_P(1) \end{bmatrix} - \frac{1}{2} \rho S_P V C_D \begin{bmatrix} V_P(1) \\ V_P(2) \\ V_P(3) \end{bmatrix} \tag{3.39}$$

The lift and drag coefficient C_L and C_D depend on the angle of attack $\alpha = \arctan(V_P(3), V_P(1))$.

$$C_L = C_{L0} + C_{L_\alpha} \alpha_p \tag{3.40}$$

$$C_D = C_{D_0} + C_{D_\alpha} \alpha^2 \tag{3.41}$$

Moment Equations

The moment equations can be derived in a similar method to the force equations. The state space equations for the derivative of angular velocity can be found by using Newton's second law for inertial systems.

$$M = \frac{d}{dt} J\omega \tag{3.42}$$

Note that the derivative is taken in the inertial frame which results in the following equation.

$$M = J\dot{\omega} + \omega \times J\omega \tag{3.43}$$

This equation can be rearranged to solve for the derivative of the state variables.

$$\dot{\omega} = J^{-1}(M - \omega \times J\omega) \tag{3.44}$$

Where M is the aerodynamic moment and J is the inertia matrix.

The aerodynamics generates rolling, pitching and yawing moments:

$$M = \frac{1}{2}\rho S_p V^2 \begin{bmatrix} C_l b - mgz_{cg} s_\phi c_\theta \\ C_m c - mgz_{cg} s_\theta \\ C_n b \end{bmatrix} \tag{3.45}$$

Where $C_l = 0$, $C_m = C_{m_0} + C_{m_\alpha}\alpha$ and $C_n = C_{n_r} b\frac{\omega(3)}{2V}$

Apparent Mass

When a body moves in a fluid it sets that in motion thus creating an additional field of fluid momentum and energy surrounding the body. This additional momentum is proportional to the object's acceleration and can be expressed as an increase in the object's mass m_{AM} such that Newton's second law is changed to: $F = (m + m_{AM})a$. Equation 3.38 can then be extended and re-written as:

$$\dot{v} = \frac{1}{m}F + G + F_{AM} - \omega \times v \tag{3.46}$$

The same reasoning applies to the moment equation, hence equation 3.44 can be re-written as:

$$\dot{\omega} = J^{-1}(M + M_{AM} - \Omega \times J\omega) \tag{3.47}$$

Lissaman and Brown [16] outline that the applied forces and moments due to the apparent mass terms are defined as follows:

$$F_{AM} = -M_F \dot{v} - \omega \times (M_F v) \tag{3.48}$$

$$M_{AM} = -I_F \dot{\omega} - \omega \times (I_F \omega) - v \times (M_F v) \tag{3.49}$$

The apparent mass term M_F as well as the apparent moment of inertia, can be computed using the formulae given by Lissaman and Brown [16].

$$M_F = \begin{bmatrix} A & 0 & 0 \\ 0 & B & 0 \\ 0 & 0 & C \end{bmatrix} I_F = \begin{bmatrix} I_A & 0 & 0 \\ 0 & I_B & 0 \\ 0 & 0 & I_C \end{bmatrix} \tag{3.50}$$

The terms A, B and C are computed as follows:

$$k_A = 0.848\frac{\pi}{4} \qquad A = k_A t^2 b(1 + \frac{8}{3}\overline{a}^3)$$
$$k_B = 0.339\frac{\pi}{4} \qquad B = k_B[t^2 2a^2(1 - \overline{t}^2)]c$$
$$k_C = \frac{AR}{1 + AR}\frac{\pi}{4} \qquad C = k_C c^2 b\sqrt{1 + 2\overline{a}^2(1 - \overline{t}^2)}$$

$$k_A^* = 0.055\frac{AR}{1 + AR} \qquad I_A = k_A^* c^2 b^3$$
$$k_B^* = 0.0308\frac{AR}{1 + AR} \qquad I_B = k_B^* c^2 b[1 + \frac{\pi}{6}(1 + AR)AR\overline{a}^2\overline{t}^2]$$
$$k_C^* = 0.0555 \qquad I_C = k_C^* t^2 b^3(1 + 8\overline{a}^2)$$

Where AR = $\frac{b}{c}$, a the high of the arc at the mid-point of the canopy, $\overline{a} = \frac{a}{b}$ and $\overline{t} = \frac{t}{c}$. Substituting equations 3.48 and 3.49 in equations 3.46 and 3.47 respectively and denoting F = $F_{aero} + F_{AM}$ and M = $M_{aero} + M_{AM}$ results in the following:

$$\dot{v} = (I + \frac{1}{m}M_F)^{-1}(\frac{1}{m}F + G - \omega \times (v + \frac{1}{m}(M_F v))) \tag{3.51}$$

$$\dot{\omega} = (J + I_F)^{-1}(M - \omega \times (I_F \omega) - v \times (M_F v) - \omega \times J\omega) \tag{3.52}$$

Navigation Equations

The navigation equations express a relationship between the positional derivatives $\dot{p}$ and the body fixed linear velocities v. This is done by rotating v using the transformation matrix to the inertial frame.

$$\dot{p} = [T_{IB}]^T v \tag{3.53}$$

Kinematic Equations

The kinematic equations can be easily derived by projecting into the inertial reference frame and integrating the velocity to obtain the position and by determining the derivatives of the Euler angles from the angular velocity.

$$\dot{\Omega} = \begin{bmatrix} 1 & t_\theta s_\phi & t_\theta c_\phi \\ 0 & c_\phi & -s_\phi \\ 0 & s_\phi / c_\theta & c_\phi / c_\theta \end{bmatrix} \omega \tag{3.54}$$

Control Inputs

This model assumes the parafoil contains two elevons located at the trailing edge on both sides, which is standard for parafoil architecture. Both can only be deflected to one side (down). If they are both deflected by the same angle, the parafoil will experience an increase in drag and lift, while the efficiency (glide range) decreases. This input is more commonly known as a brake, which leads to also the commonly known flare manoeuvres. If the deflection of the control surfaces is asymmetric, then there is a variation in the drag along the span of the parafoil, causing a variation in the rolling and yawing moments, which make the system turn. This input is more commonly known as the ailerons.

It's important to note that on the physical system, contrary to an airplane, when the elevons are used asymmetrically, it does not cause the system to roll, but to skid through a turn. The system may eventually roll while doing so, due to the centripetal forces it is experiencing. The effects of the ailerons of the aerodynamic moments, causing a rolling and yawing moment can be expressed as:

$$\Delta M = \frac{1}{2} \rho S_p V^2 \begin{bmatrix} 0 & 0 \\ 0 & 0 \\ C_{n_{\delta_a}} & 0 \end{bmatrix} \begin{bmatrix} \delta_a \\ \delta_b \end{bmatrix} \tag{3.55}$$

It's important to note that brake inputs and manoeuvres, will not be covered, the reason for this will be explained later in the report in Section 4.3.

Wind Disturbances

The rigid body equations presented above assume no external disturbances, such as wind. However, wind can have a significant effect on this type of systems. Let v_{wind} denote the wind velocity in the inertial frame. The rigid body equations can be modified to include wind disturbances by also solving an additional equation to relate v with the relative air velocity v_{rel} experienced by the canopy. This relationship can be expressed as follows:

$$v_{rel} = v - [T_{BI}] v_{wind} \tag{3.56}$$

Where $v_{rel} = \begin{bmatrix} U' & V' & W' \end{bmatrix}$

To determine the wind speed, v_{wind}, the wind gradient relationship is taken as a base. Equation (3.57) determines the wind on different altitudes.

$$v_w(h) = v_{10} \cdot (h / h_{10})^\alpha \tag{3.57}$$

In this equation, $v_w(h)$ is the velocity of the wind at height h and v_{10} is the velocity of the wind at a height of 10 m, which is assumed to be 2 m/s. In the formula, h represents the height in meters and h_{10} represents the height of 10 m. The α is the Hellmann exponent, which is assumed to be 0.10 for neutral air above open water surface [39]. The relation between the wind speed and altitude can also be seen in Figure 3.17 [52].

To accurately model the randomness of the wind, a random Gaussian noise was added to the magnitude of v_{wind} for the different altitudes. The vertical component of the wind is assumed to be 0 [58]. The direction of the wind was randomised by giving it a random initial direction between 0 and 2π and a change in direction between $\frac{2\pi}{100}$ and $-\frac{2\pi}{100}$ per meter. v_{wind_x} and v_{wind_y} can then be calculated using Equation (3.58) and Equation (3.59). By doing this, different values of wind speed were obtained with different directions. Every time the wind model is initiated it will provide wind velocities and directions for given altitudes.

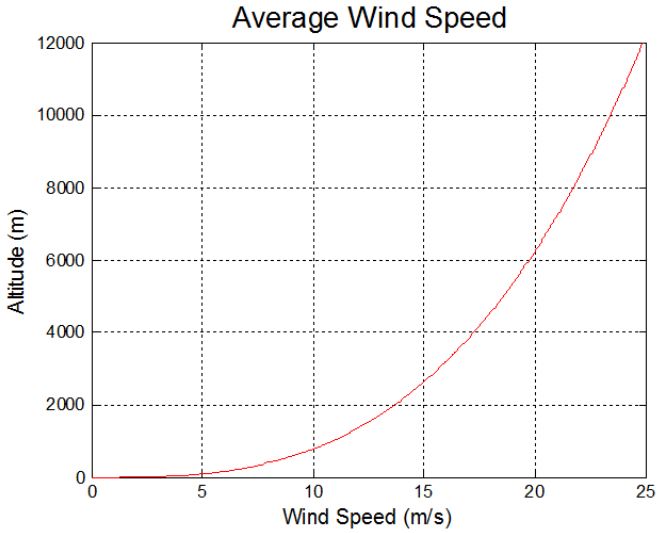

Figure 3.17: Relation of wind vs. altitude

$$v_{wind_x} = v_{wind} \cdot \cos(direction) \quad (3.58) \qquad v_{wind_y} = v_{wind} \cdot \sin(direction) \quad (3.59)$$

Sensor Dynamics

It should be noted that for the purpose of this study, sensor dynamics will not be taken into account and it will be assumed that the sensors are perfect.

Simulation

The full state matrix described above, Equation (3.31) was solved using the classical fourth order Runge-Kutta numerical method for initial valued problems. The input to the system was modelled as an aileron deflection and the output of the simulation is the systems state. The equations for a time invariant system are as follows. Note that $\dot{x} = f(x, u)$, where x is the current state and u is the input. Also, h is the time step.

$$k_1 = f(x, u) \quad (3.60)$$
$$k_2 = f(x + 0.5hk_1, u) \quad (3.61)$$
$$k_3 = f(x + 0.5hk_2, u) \quad (3.62)$$
$$k_4 = f(x + hk_3, u) \quad (3.63)$$

$$x = x + h\frac{k_1 + 2k_2 + 2k_3 + k4}{6} \quad (3.64)$$

Verification

Verification of the model was performed for both longitudinal and lateral motions. Longitudinally, the model was verified by comparing the simulation results of the model with the ones found on [69] using exactly the same parameters and initial conditions. Figure 3.18a illustrates the velocity profiles of the parafoil of the verification simulation.

The corresponding simulation result figure is Figure 4.11 in [69]. Laterally the model was verified by comparing the simulation results of the model with the ones found on [73] using exactly the same parameters and initial conditions. Figures 3.18b, 3.19a and 3.19b illustrate the roll, pitch and yaw angles time history of the parafoil, over a period of 300 s respectively, when a constant 15° aileron deflection is applied after 50 s, on the verification simulation.

Comparing Figure 3.19a and Figure 3.19b to the simplified model label given in "Modelling and motion analysis of autonomous paragliders", by C. Toglia et al. leads to some interesting findings.[73] First, the pattern and oscillations of the angles over time is very identical. The values to which each of the angles converge,

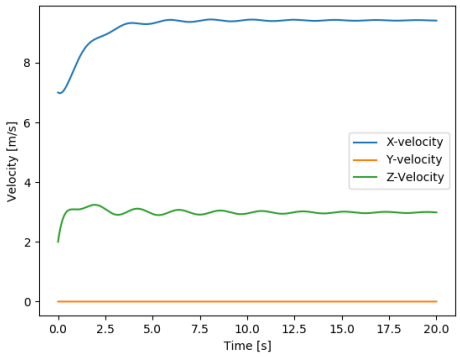

(a) Velocity profile of the verification simulation of longitudinal motion

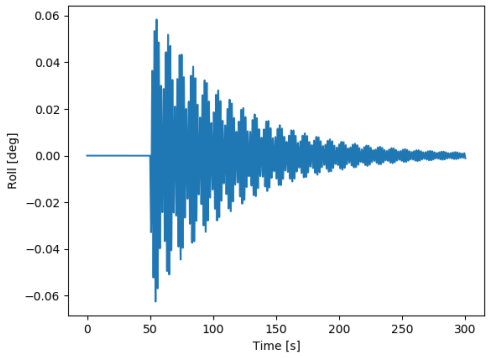

(b) Roll angle time history

Figure 3.18

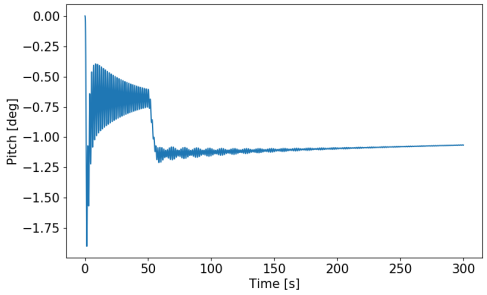

(a) Pitch angle time history

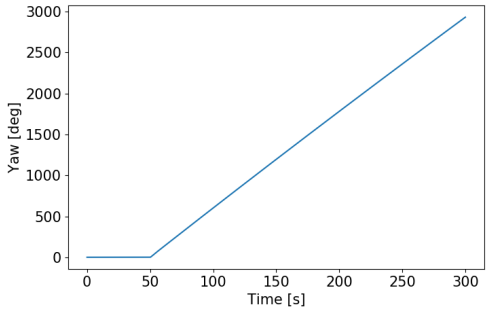

(b) Yaw rate time history

Figure 3.19

is however different, except for yaw, which is exactly the same. The reason for this discrepancy comes from the fact that when developing this model, as was stated at the start, it was assumed based on literature that the parafoil wouldn't roll in order to turn, but would rather skid around a turn. [69] The weight of this assumption becomes clear in the verification of the roll angle. C. Toglia et al. determines that the roll settles to around 10° after approximately 100s, while in Figure 3.18b the roll angle settles to zero.[73] This goes according to the assumption that was made. The same reasoning can be applied to the discrepancy between the settling pitch angle between Figure 3.19a and Figure 3.19b. The following relationship between roll and pitch shows this.

$$L\cos\phi < W$$

This equation shows that when rolling, in order to maintain the same altitude, the angle of attack needs to increase, hence an increase in pitch angle is required. Given that the parafoil in this situation is assumed not to roll, this explains the fact why the pitch angle is proportionally smaller.

Finally, comparing Figure 3.20 to the results presented by C. Toglia et al. validates the assumption made earlier of neglecting the aerodynamic effects acting on the payload.[73] The percentage error between neglecting this term and including it is of approximately 2.85% which is well within the acceptable degree of accuracy.

3.2. Load Cases

This section shows models used to analyse the different load cases occurring during the mission. First, the launch vibrations are dealt with in Section 3.2.1, after which the deployment loads of the drogue parachute and parafoil are explained in Section 3.2.2. Finally, the catch model is elaborated on in Section 3.2.3 and the model on the helicopter stability is explained in Section 3.2.4.

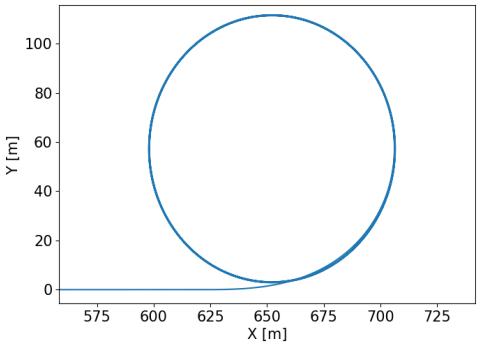

Figure 3.20: Path followed by the center of mass on the XY plane on δ_a deflection.

3.2.1. Launch Vibrations

All Recovery System components have to be checked for their natural frequency in both the x, y and z direction in order to prevent resonance during launch. This is done using an analysis based on the stiffness of the attachment of the components with the Ariane 6 and the mass of these components. z is defined as the longitudinal direction, while x and y both represent lateral vibrations.

The natural frequency is determined using Equation (3.65) [29], in which the k indicates the stiffness of the attachment and M is the mass of the component that is being analysed. k is determined using equations 3.66 and 3.67, which are found using simplifications of the structural elements as shown in Figure 3.21.

$$f_n = \frac{1}{2\pi}\sqrt{\frac{k}{M}} \tag{3.65}$$

$$k = \frac{AE}{L} \tag{3.66}$$

$$k = \frac{3EI}{L^3} \tag{3.67}$$

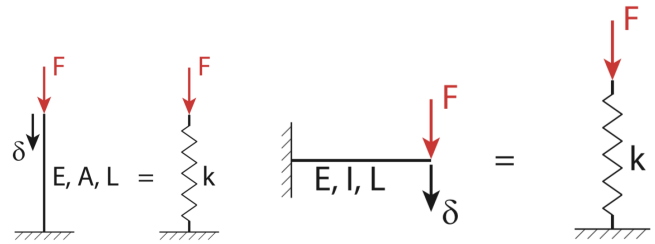

(a) (b)

Figure 3.21: This figure shows two examples of simplifications of beams in order to determine the stiffness for a frequency analysis

3.2.2. Parachute and Parafoil Deployment Loads

After the re-entry, the atmospheric flight is entered. This section describes the model used to determine the loads during this transition phase from re-entry using the heat shield to flight with the parafoil.

No components of the recovery system can be located at the bottom (close to the nozzle) of the VuAB due to the high differences in temperature during launch. Therefore, the parafoil must be deployed from the top of the VuAB, where the heat shield is located at the time of transition. The heat shield must therefore be discarded before deployment of the parafoil and the VuAB must rotate in order for the parafoil to deploy from the top side of the VuAB. Furthermore, the VuAB is probably going to need to be decelerated in order for the parafoil to be safely deploy.

The altitude and velocity during these events must be determined in order to calculate the acceleration and accompanying loads on the VuAB. First, the acceleration during each of these events are determined, after which the accelerations are integrated.

The acceleration after discarding the heat shield is estimated using Equation (3.68), in which D_{VuAB} is determined using Equation (3.69). It is assumed that the heat shield is instantly discarded, so only the drag of the VuAB and the gravity have an influence on this acceleration.

$$a = \frac{F_g - D_{VuAB}}{M_{VuAB}} \tag{3.68}$$

$$D_{VuAB} = 0.5 \cdot \rho \cdot V^2 \cdot S_{VuAB} \cdot C_{d_{VuAB}} \tag{3.69}$$

To rotate the VuAB after discarding the heat shield and to decelerate the VuAB further a drogue parachute is used. The acceleration after deployment of this parachute is determined using Equation (3.70), in which D_{chute} is determined using Equation (3.71).

$$a = \frac{F_g - D_{VuAB} - D_{chute}}{M_{VuAB}} \tag{3.70}$$

$$D_{VuAB} = 0.5 \cdot \rho \cdot V^2 \cdot S_{chute} \cdot C_{d_{VuAB}} \tag{3.71}$$

Then, the parafoil is deployed. The drogue parachute is used to deploy the parafoil. When the parafoil is released from the VuAB the drag force of the parachute becomes zero as it is pulling the parafoil instead of exciting a force on the VuAB. The acceleration in this phase is again determined using Equation (3.68). Then, the parafoil deploys in three different phases. First, the middle part of the parafoil deploys, after which the second and third parts deploy and finally the two outer parts. These different parts can be seen in Figure 3.22. The acceleration in this phase is determined using Equation (3.72), in which $D_{parafoil}$ is determined using Equation (3.73). In this equation $S_{parafoil}$ is increased when the next parts are deployed.

$$a = \frac{F_g - D_{VuAB} - D_{parafoil}}{M_{VuAB}} \tag{3.72}$$

$$D_{parafoil} = 0.5 \cdot \rho \cdot V^2 \cdot S_{parafoil} \cdot C_{d_{parafoil}} \tag{3.73}$$

Figure 3.22: Picture of the MegaFly, showing the five different sections of the total surface area

These accelerations are used in a model to determine the maximum g-forces experienced by the VuAB and the loads on the cabling induced by these g-forces. This model uses the height, velocity and acceleration at the moment of discarding the heat shield as an input, and determines the acceleration at each point in time. The change in altitude is determined by integrating the velocity over time, while the change in velocity is determined by integrating the acceleration, as shown in equations 3.74 and 3.75. ρ is continuously updated using the atmospheric model with the altitude as input.

$$h_{new} = h_{old} + \int_0^t V \delta t \tag{3.74}$$

$$V_{new} = V_{old} + \int_0^t a \delta t \tag{3.75}$$

Finally, the forces on the cabling of both the parachute and the parafoil are then determined using Equation (3.76).

$$F_{max} = a_{max} \cdot M_{VuAB} \tag{3.76}$$

The deployment of the drogue parachute is verified with the flight trajectory of the Orion [2], using the characteristics of the Orion. It is stated that after deploying the parachutes at 7620 m altitude and a velocity of 137 m/s it decelerates to 58 m/s at 2895 m altitude. As shown in Figure 3.23 the model simulates this deceleration accurately, finishing at 3000 m altitude with a velocity around 60 m/s.

[2] https://www.nasa.gov/sites/default/files/atoms/files/orion_parachutes.pdf

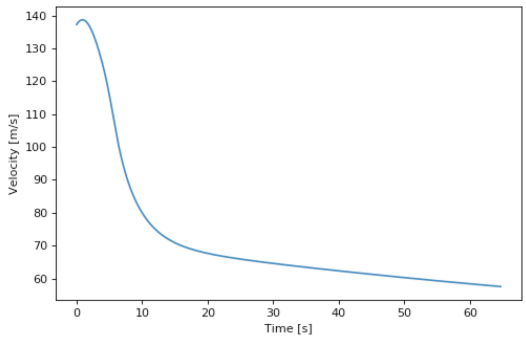

(a) Velocity vs. Time diagram of the Orion re-entry capsule after parachute deployment

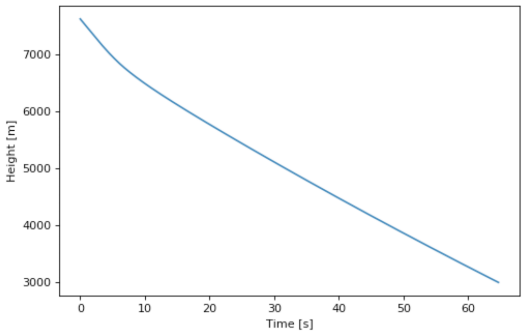

(b) Altitude vs. Time diagram of the Orion re-entry capsule after parachute deployment

Figure 3.23

3.2.3. Catch Loads

This section explains how the forces on the helicopter during the catch are computed. The results of this section serve as an input for the System Design.

First, all the different loads on the helicopter are determined, then the contribution to the load force on the helicopter and occurrence of these loads are discussed. These loads and conditions are then converted into a model representing the worst case scenario of the combination of the moment of catch and most critical seconds right after the catch.

Further transportation of the caught VuAB is then described in Section 3.2.4. The output of the model described in this section consists of the tension force on the helicopter (F_{ca}) versus the attenuation distance (D_a) and the initial absolute velocity difference between the helicopter and the VuAB at the moment of the catch ($V_{h,V}$). The output is combined with the selection of the helicopter in an iterative process, so that the allowable load force on the helicopter is larger than F_{ca}. This is done by estimating $V_{h,V}$, selecting a helicopter and determining the required attenuation length D_a.

The following parameters are used as inputs for the model:

- The absolute velocity difference between the helicopter and VuAB, $V_{h,V}$;
- The maximum swinging velocity of the VuAB in longitudinal and lateral flight direction of the helicopter, $V_{m,S_{lon}}$,$V_{m,S_{lat}}$;
- The VuAB mass at the moment of catching $m_{V_{catch}}$;
- The mass of the attenuation system, including catching cable, M_{att};
- The maximum tension force due to the drag force on the VuAB during catch, $F_{T,D_{max},V}$;
- The maximum allowable helicopter payload mass, $m_{max,h,p}$.

To model the dynamics of the catch, the worst case scenarios of the dynamics are summed. For each scenario, the worst case is taken as a static force:

- Swinging motions in both longitudinal and lateral direction hit their lowest point simultaneously;
- The drag force that could maintain a constant angle between the cable and the direction of gravity, is added at the same moment as a safety factor;
- The maximum individual forces of $F_{D_m,V}$ and F_{cp} summed simultaneously as a static force;
- The attenuation distance provides a constant force, yielding a uniform deceleration of the absolute velocity difference between the helicopter and the VuAB.

To compute the total tension force on the helicopter, the deceleration force and the static forces on the helicopter, are summed as follows:

$$F_{ca} = F_{d,a} + F_{cp} + F_{T,D_{max},V} + (m_{att} + m_{V_{catch}}) \cdot g_{0,catch} \tag{3.77}$$

Starting with the first term of the total tension force on the helicopter, Equation (3.78) can be rewritten for a uniform deceleration, with the attenuation distance $S = D_a$, $t = \frac{D_a}{V_{avg}} = \frac{D_a}{\frac{V_{h,V}}{2}}$. The average attenuation deceleration d_a is expressed as a function of initial absolute velocity difference between the helicopter and the VuAB $V_{h,V}^2$

and attenuation distance D_a in Equation (3.79).

$$S = \frac{1}{2} \cdot a \cdot t^2 \tag{3.78}$$

$$d_a = \frac{V_{h,V}^2}{2 \cdot D_a} \tag{3.79}$$

This deceleration is substituted in Equation (3.77) according to $F_{d,a} = m_{V_{catch}} \cdot d_a$. The second term is computed by substituting the centriputal acceleration of Equation (3.80) into Equation (3.81). The former is computed by squaring the magnitude of the lateral and longitudinal swing velocities and dividing it by the length of the cable from the helicopter to the VuAB. The input of the swing velocities is the output of the stability model in Section 3.2.4 and the minimum cable length is used as a safety factor since a shorter cable length yields a larger acceleration and hence a larger total load force on the helicopter.

$$a_{cp} = \frac{\sqrt{{V_{m,S_{lon}}}^2 + V_{m,S_{lon}}^2}}{l_{min}} \tag{3.80}$$

$$F_{cp} = a_{cp} \cdot m_{V_{catch}} \tag{3.81}$$

In the model in section Section 3.2.4 the drag force on the VuAB is calculated to compute the damping of the swinging motion by the orthogonal component of the drag force with respect to the catching cable. The perpendicular component of the maximum drag force on the VuAB is used as the input for Equation (3.77)

Furthermore, gravity acts as a constant force on the helicopter as the sum of $m_{V_{catch}}$ and m_{att} multiplied with the gravitational constant at the catching altitude. Filling these forces in into Equation (3.77) yields Equation (3.82):

$$F_{ca} = m_{V_{catch}} \cdot \frac{V_{h,V}^2}{2 \cdot D_a} + \frac{\sqrt{{V_{m,S_lon}}^2 + V_{m,S_lon}^2}}{l_{min}} \cdot m_{V_{catch}} + F_{T,D_{max},V} + (m_{att} + m_{V_{catch}}) \cdot g_{0,catch} \tag{3.82}$$

The total force computed in Equation (3.82) is the output where $V_{h,V}$ and D_a are variable parameters presented in figure Figure 4.31. These parameters are modified in an iterative process until a helicopter is found which has a load capability at the catching altitude that is larger than F_{ca}.

3.2.4. Helicopter Stability

Once the helicopter has caught the VuAB, the helicopter must be able to maintain stable flight back to the boat for the landing. To show this the stability of the helicopter is investigated. A helicopter dynamic model was updated to include a force input from the suspended mass.

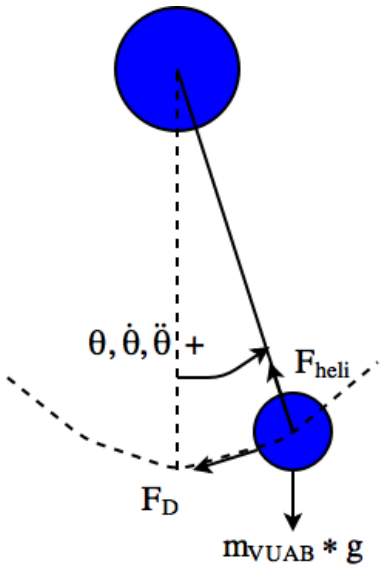

Figure 3.24: 2-D Free Body Diagram, used for determination of θ_{long} and θ_{lat}. F_D is shown for a positive velocity oriented to the right

The force the suspended mass exerts on the helicopter is decomposed along the helicopters inertial reference frame (x_b) using two angles. θ_{long}, the angle the suspension line forms with the XZ plane of x_b. θ_{lat} is similarly the angle the suspension forms with the YZ plane of x_b. Assuming the suspension line behaves as a rigid body without mass of length l, the angles can be modelled by simple pendulum motion as shown in Figure 3.24. The two swinging motions are analysed separately to be able to apply 2-dimensional dynamic relations. Summing moments about the cable attachment on the helicopter:

$$\Sigma M_{hinge} = I \cdot \ddot{\theta} = F_{tan} \cdot l \tag{3.83}$$

$$m_{VuAB} \cdot l^2 \cdot \ddot{\theta} = (-m_{VuAB} \cdot g_0 \cdot sin(\theta) \pm \frac{1}{2} \cdot \rho_0 \cdot S_{VuAB} \cdot c_d \cdot v^2) \cdot l \tag{3.84}$$

Simplifying yields the following differential equation:

$$\ddot{\theta} = -\frac{g_0}{l} \cdot sin(\theta) - \frac{\rho_0 \cdot c_d \cdot S_{VuAB}}{2 \cdot m_{VuAB}} \cdot (v_{heli} + \dot{\theta} \cdot l)^2 \tag{3.85}$$

Equation (3.85) can be applied for both $\dot{\theta_{long}}$ and $\dot{\theta_{lat}}$ using appropriate initial conditions for θ and its derivatives. Knowing the angle formed by the 2 2-D pendulums as a function of time, the tension force on the suspension line can be calculated from:

$$F_{Heli} = m_{VuAB} \cdot \dot{\theta}^2 \cdot l + m_{VuAB} \cdot g_0 \cdot cos(\theta) \tag{3.86}$$

The force derived in Equation (3.86) enters the helicopter through an attachment point placed underneath its centre of gravity so as to minimise introduction of moments to the helicopter. The only moments induced are rolling moments from lateral swinging and pitching moments from longitudinal swinging, because of a vertical distance to the centre of gravity. An LTI dynamic model from [27] for helicopters travelling with a velocity under 80 knots was adapted to model the response to the suspension line forces. As the helicopter only attempts a catch after matching velocity vectors with the VuAB for some time, it is assumed that the inertial frame and helicopter body frame are one and the same. 55

$$\dot{x} = Ax + Bu \tag{3.87}$$

$$A = \begin{bmatrix} X_u & 0 & 0 & -g_0 & 0 & 0 & 0 & 0 \\ 0 & Z_w & U_0 & 0 & 0 & 0 & 0 & 0 \\ 0 & 0 & M_q & M_\theta & 0 & M_p & 0 & 0 \\ 0 & 0 & 1 & 0 & 0 & 0 & 0 & 0 \\ 0 & 0 & 0 & 0 & Y_v & 0 & -U_0 & g_0 \\ 0 & 0 & L_q & 0 & 0 & L_p & 0 & L_\phi \\ 0 & 0 & 0 & 0 & 0 & 0 & N_r & 0 \\ 0 & 0 & 0 & 0 & 0 & 1 & 0 & 0 \end{bmatrix} \quad x = \begin{bmatrix} u \\ w \\ q \\ \theta \\ v \\ p \\ r \\ \phi \end{bmatrix} \quad B = \begin{bmatrix} 1 & 0 & 0 \\ 0 & 0 & 1 \\ \frac{m_{heli} \cdot d}{I_{yy}} & 0 & 0 \\ 0 & 0 & 0 \\ 0 & 1 & 0 \\ 0 & \frac{m_{heli} \cdot d}{I_{xx}} & 0 \\ 0 & 0 & 0 \\ 0 & 0 & 0 \end{bmatrix} \quad u = \begin{bmatrix} a_x \\ a_y \\ a_z \end{bmatrix}$$

The A and x matrices describe the aircraft response and states, these have been taken from [27]. The input matrix, u, has been adapted to include the decomposed accelerations the suspension line tension force causes on the helicopter. The B matrix has been adapted to include the influence of the tension force on $\dot{u}$, $\dot{v}$, $\dot{w}$ and $\dot{p}$.

The initial angular rates, angles and Y axis velocity entered into the system may be assumed to be 0 as the helicopter is engaged in straight steady flight before the catch. The intial X and Z velocity require outputs from the atmospheric flight model. Using the horizontal and vertical velocities of the parafoil before catch, the helicopter velocity can be deducted to have the same rate of descent and a horizontal delta-V of 3 m/s.
The system constructed in Equation (3.87) is going to output the uncontrolled reaction of the helicopter to the catch. After inputting boundary conditions for the swinging motion and helicopter parameters, the dynamic stability of the system can be evaluated.

If one of the states shows instability to the inputs, the B matrix can be extended to include the pilots controls on the helicopter from [27]. The extended B matrix looks as follows

Table 3.2: Stability and control derivatives of a Scout/attack helicopter hovering with a velocity less than 80 knots

Stability Derivative	Value	Unit
X_u	-0.01	1/s
Z_w	-1.0	1/s
M_q	-3.0	1/s
M_θ	0	1/(rad s)2
M_p	0	1/s
Y_v	-0.4	1/s
L_q	0	1/s
L_ϕ	0	1/(rads)2
N_R	-2.2	1/(rad s)2
$Z_{\delta C}$	-7.0	1/(rads)2
$M_{\delta B}$	-0.7	1/(rad s)2
$M_{\delta A}$	0	1/(rad s)2
$L_{\delta B}$	0	1/(rad s)2
$L_{\delta A}$	2.0	1/(rad s)2
$N_{\delta P}$	-3.0	1/(rad s)2

$$Bu = \begin{bmatrix} 1 & 0 & 0 & 0 & 0 & 0 & 0 \\ 0 & 0 & 1 & 0 & Z_{\delta c} & 0 & 0 \\ \frac{m_{heli} \cdot d}{I_{yy}} & 0 & 0 & M_{\delta B} & 0 & M_{\delta A} & 0 \\ 0 & 0 & 0 & 0 & 0 & 0 & 0 \\ 0 & 1 & 0 & 0 & 0 & 0 & 0 \\ 0 & \frac{m_{heli} \cdot d}{I_{xx}} & 0 & L_{\delta B} & 0 & L_{\delta A} & 0 \\ 0 & 0 & 0 & 0 & 0 & 0 & N_{\delta P} \\ 0 & 0 & 0 & 0 & 0 & 0 & 0 \end{bmatrix} \begin{bmatrix} a_x \\ a_y \\ a_x \\ \delta_B \\ \delta_C \\ \delta_A \\ \delta_P \end{bmatrix} \tag{3.88}$$

The values in the matrices from [27] are shown in Table 3.2

4

System Design

In this chapter, the models as explained in the previous chapter are applied in order to determine the flight trajectory and the critical load cases. From these parameters, all components are sized. The chapter follows the same flow as the functional flow diagram, as shown in Section 2.2. First, the systems needed for the space phase will be designed in Section 4.1, after which the re-entry will be dealt with in Section 4.2 and the atmospheric flight in Section 4.3. Then, the systems concerning the catch will be designed in Section 4.4. Afterwards, the electrical system will be designed in order to support all mission phases, as shown in Section 4.5. Finally, an overview will be given in Section 4.6.

All the different components were designed with a design philosophy based on ease of integration. The system shall be integrated in an existing design, so every element was designed such that it would not impede nominal operations of the launcher and no changes would have to be made to the current design of the VuAB or the launcher itself.

Throughout this chapter, every section will start by indicating which function from the functional analysis provided in Section 2.2 is being fulfilled.

4.1. Space Flight Characteristics

This section focuses on the design of the subsystems necessary for the space flight. First, the separation mechanism will be designed in Section 4.1.1, after which the thrusters necessary to cope with the rotational accelerations resulting from this separation are sized in Section 4.1.2. Then, the radiation in space is elaborated on in Section 4.1.3 and the thermal effects in Section 4.1.4. This section covers functions F.3.1.1 and F.3.1.2 from Figure 2.6

4.1.1. Separation Mechanism

The recovery system is designed to recover only the aft bay of the Ariane 6, for this reason a separation mechanism is investigated to ensure jettisoning of the remainder of the 1st stage. Since the Ariane 6 is a multi-stage rocket, it already uses a separation mechanism for the first stage second stage separation. The natural choice was made to use the same separation mechanism for the VuAB-first stage separation.

The separation mechanism is completely expendable and so not refurbishable. It is composed of 2 Aluminium L-rings, one attached to the VuAB and one attached to the rest of the first stage. Between the L-rings an electrically controlled pyrotechnic separation chord is placed, containing 4 charges separated 90°. When activated, the charges will detonate within milliseconds of one another separating the VuAB and first stage skirts to minimize rotations. Upon separation a delta-V under 5 m/s will be applied by the ADCS thrusters sized in Section 4.1.2 acting as retro-rockets. This will avoid unwanted contact between separated sections. The entire system once mounted onto the VuAB has a height of 3 cm. To accommodate the separation mechanism the VuAB must lose 3 cm in its height. This way the overall dimensions of the launcher will not change and not introduce large changes to the fuel line geometry.

The VuAB is also attached to the Ariane 6 through fuel lines running to LOX and LH2 tanks. The LOX fuel line runs through the outside of the launcher and into the Vulcain via a small opening in the VuAB. The LH2 fuel line runs directly from the bottom of the tank to the engine underneath it. These fuel lines must also be separated in a controlled fashion.

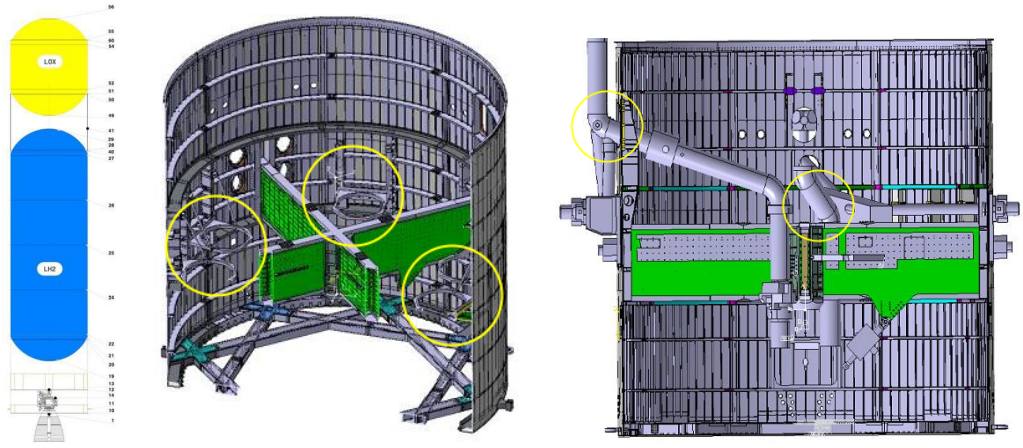

(a) (b) (c)

Figure 4.1: (a): Fuel tank configuration of the Ariane 6 (b): Location of Helium tanks in VUAB (c): Proposed locations for fuel line separation

The main challenge in cutting the fuel lines is ensuring the fuel is flushed out downstream of the separation point. By adding valves slightly upstream of the separation mechanism, the fuel flow can be stopped. The VUAB carries multiple Helium tanks on board to pressurize the fuel tanks. If this connection is closed off with a valve, the Helium can be redirected to flush out the fuel. Adding a junction from the Helium tanks to the fuel lines, connecting downstream of the fuel line separation point, allows for the Helium to flush out the fuel lines. This junction needs a valve at the helium tank and another at the fuel line. Once the fuel line valve upstream is shut off and the Helium Tank valve shuts off, the valves on the junction can open. A flushed fuel line can be separated using the same concept as the skirt separation sized appropriately. The concept choice must allow the fuel lines to perform up to standard. Validation must be conducted to prove that the fuel lines do not fail under operational pressures at the locations of the separation mechanisms and the junction.

The mass of the skirt separation mechanism was estimated at 128 kg [1]. A factor of 1.2 is applied to include the fuel line separation as they are made to separate a much smaller structure. This makes the total separation mechanism weight come out to 153 kg.

After separation a sharp edge will remain on the skirt due to the violent nature of the pyrotechnics. In order to ensure a safe deployment of the aeroshell, parachute and parafoil, a mechanism is designed to cover these sharp edges. A trade-off has been performed between several options, among which an inflatable cover. Eventually a cover made out of aluminium is chosen as the final concept for covering the sharp edges. This cover will be placed around the entire skirt ring of the VuAB. It is a curved plate of aluminium with a radius of 0.15 m and is positioned at the bottom of the separation ring, covering the lower L-shaped section. To prevent the cover from interfering with the flow of air around the VuAB during re-entry, it should not bend further than the outside of the skirt of the VuAB. Using the 0.15 m radius this is not the case. The thickness of the cover is chosen to be the same as the skirt thickness to ensure that it will properly protect all components from the sharp edges. With the cover located along the complete circumference, a radius of 0.15 m and a thickness of 0.005 m, it is estimated to be 55.8 kg. In the detailed design phase, the cover will have to be checked for its natural frequencies, in order to prevent vibrational coupling with the Vulcain engine.

4.1.2. Thruster Sizing

Due to the separation forces of the VuAB with the 1^{st} stage, the VuAB has a rotation around its longitudinal axis. To be able to deploy the aeroshell in a safe way, this rotation needs to be damped. Additionally, the system should enter the atmosphere the most optimal angle for aerodynamic purposes during re-entry. To ensure the required attitude is achieved, the system uses attitude control thrusters. The choice for thrusters was made because a control moment gyroscope would be too heavy and too slow to achieve the required attitude in the limited timespan. Also attitude control thrusters are widely available, relatively inexpensive, reliable and lightweight. This is due to the fact that these thrusters are used have been in used in many other spacecraft.

[1] Private contact, Airbus Defence and Space (client), H. Cruijssen

The aim was to design the thrusters in such a fashion that the attitude of the system could be changed in all directions desired. But when doing this, only moment couples should be used, so that no drifting occurred in space. For this reason, the system is equipped with 4 thruster clusters, each containing 4 thrusters in the same plane. These clusters were placed at an angle of 90^o with respect to each other, since this would smooth the integration with the existing design of the Ariane 6. This means that for adjustment of the roll angle a total of 4 thrusters can be used. For the pitch and yaw angle 2 thrusters in couple are used to control. Knowing the number of thrusters, one can start sizing them. To make an estimation on the needed thrust to damp the spinning motion the following equation is used:

$$F_{T,roll} = \frac{I_{roll} \cdot \omega}{L_{T,roll} \cdot t_{burn} \cdot N_{T,roll}} \tag{4.1}$$

This equation gives the thrust force, $F_{T,roll}$, needed to provide or damp a slew rate of ω. The I_{roll} stands for the moment of inertia of the whole system in the roll axis. The moment arm $L_{T,roll}$ is multiplied with the time t_{burn} and the number of thrusters needed for roll, $N_{T,roll}$.

To find the required $F_{T,roll}$, one has to know the slew rate caused by the separation. This value is taken as 8.6 deg/s. [10] Also a time in seconds is assumed, knowing that the total space flight takes about 4 minutes. By doing so the force needed by the thrusters to damp the spinning was obtained and the same thruster force was used to calculate the impulse time of the thrusters to give the system its required pitch angle before entering the atmosphere. The value for this angle is calculated in Section 3.1.2 to be 20^o. For this the following relationship is used:

$$F_{T,pitch} = \frac{\theta_{req} \cdot I_{pitch}}{L_{T,pitch} \cdot t_{pulse} \cdot (t_{total} - t_{pulse}) \cdot N_{T,pitch}} \tag{4.2}$$

with:

- $F_{T,pitch}$, the force needed for the required pitch;
- θ_{req}, the required pitch angle, which is $\theta_{req} = RequiredReentryAngle - OwnPitchAngle$;
- I_{pitch}, the moment of inertia on the pitch axis;
- $L_{T,pitch}$, the length of the moment arm of the thrusters for pitch;
- t_{pulse}, the impulse time;
- t_{total}, the total time in space;
- $N_{T,pitch}$, the amount of thrusters used for pitch.

Now an appropriate thruster could be selected. The chosen thruster is the DST-13 from MOOG [2]. This thruster has a force of 22 N. With this new force an optimization can be carried out to find a new burn and impulse time. These are $t_{burn} = 25$ s and $t_{pulse} = 0.565$ s for a total pitch correction manoeuvre time of 10 s. To finalize the thruster sizing, the mass of the propellant needed has to be determined. The total amount of propellant needed to damp the spinning and to pitch the system can be calculated using the following equations:

$$M_{prop,roll} = \frac{F_{T,roll} \cdot t_{burn} \cdot N_{T,roll}}{I_{sp} \cdot g} \tag{4.3}$$

$$M_{prop.pitch} = \frac{F_{T,pitch} \cdot (2 \cdot t_{pulse}) \cdot N_{T,pitch}}{I_{sp} \cdot g} \tag{4.4}$$

With I_{sp} being the specific impulse, which is 300 s for the DST-13. This gives a $M_{prop,roll} = 0.68$ kg and $M_{prop.pitch} = 0.02$ kg. Adding these up, the total mass of propellant can be found, which is $M_{prop,tot} = 0.7$ kg.

To see how sensitive the thruster sizing is, a sensitivity analysis is performed. This is done by changing the spinning rate caused by the separation. The spinning rate was changed from 80% to 120% to see how it effected the burn time and the propellant mass. The results can be seen in Figure 4.2a and Figure 4.2b. Also the angle that the system needs to pitch is changed from 80% to 120% to see the effects of disturbances in that axis on the propellant mass and impulse time. This is shown in Figure 4.2c and Figure 4.2d.

[2] `http://www.moog.com/content/dam/moog/literature/Space_Defense/Spacecraft/Propulsion/bipropellant_thrusters_rev_071717.pdf`, last accessed 22-01-2018

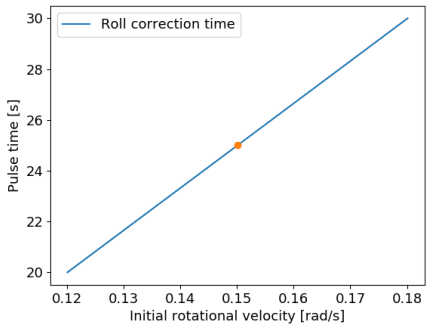

(a) The spinning rate of the VuAB after separation, against the burn time of the thrusters to damp this spinning.

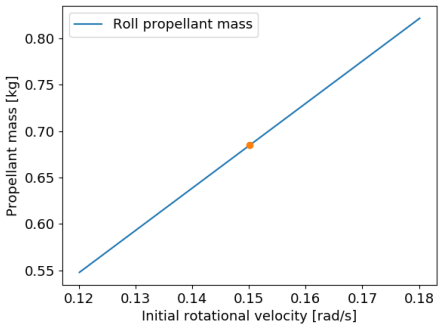

(b) The spinning rate of the VuAB after separation, against the propellant mass of the thrusters to damp this spinning.

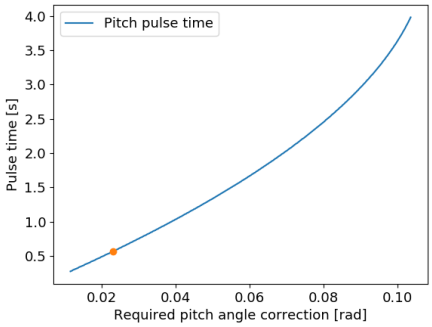

(c) The needed pitch angle of the VuAB, against the impulse time of the thrusters to provide this angle.

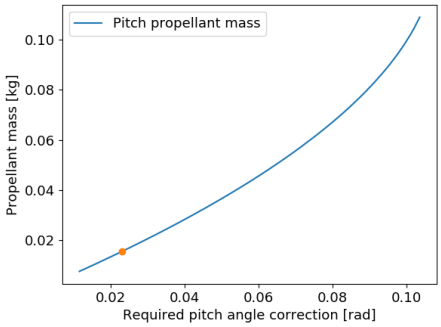

(d) The needed pitch angle of the VuAB, against the propellant mass of the thrusters to provide this angle.

Figure 4.2: Sensitivity Analysis on the thruster sizing.

4.1.3. Radiation Effects

During the space phase the VuAB and recovery system will be in a hostile environment with large temperature differences and different radiation than experienced on earth as it will be outside of the atmosphere. Using the model for space trajectory Section 3.1.1 it is determined that the duration of the space phase, from separation to re-entry will take 240 s. From literature, it is concluded that radiation can have a major effect on the performance of materials and components of space vehicles [**?**] after a long time of exposure (multiple months). As these longer periods of time will only be achieved after a very large number of launches using the same components this will have no impact on the design of the recovery system. However, in order to ensure proper functioning of the whole system during a mission, all components and materials (such as the sensors) used are chosen to be space-graded components.

It is recommended to perform an analysis on the recovered components in order to determine the effect of repeated, short duration, exposure to radiation as no statistical data is available at this point in time. Furthermore, it should be investigated whether the VuAB, after returning from space, can pose any harm to the people working on the boat and in the refurbishment teams. This could pose a problem because of radiation from the VuAB and poisonous materials and gasses on for example the aeroshell after recovering it from sea.

4.1.4. Thermal Effects

There are three significant thermal effects working on the VuAB system. First, the thermal effects coming from the engine. The cross structure supporting the Vulcain engine is set as a constraint as the lowest point of design due to the high temperature effects of the engine [3]. Above that threshold no thermal complications should occur.

[3]Private contact, Airbus Defense and Space (client), H. Cruijssen

Because no elements of the recovery system design are located below the cross structure this constraint is dealt with. The second thermal effect is that of the exposure to space for 240 s. While this is a short period, the effects can be significant. While the average temperature is 283.32 K, the temperature can vary between 173.5 and 393.15 K[4], depending on the amount of exposure to solar radiation. Systems such as the parachute system and the electrical system are designed using reference data, including the thermal protection components of those reference systems. Therefore the systems account for a certain level of thermal protection, however, that does not take into account all elements encountered during these specific parts of the mission. The third thermal effect is that of the re-entry. The heat shield is designed to mitigate the thermal effects of re-entry to such an extent that the systems inside of the VuAB do not experience any temperature fluctuations due to the re-entry. This is elaborated upon in Section 4.2.

As the second thermal effect is not investigated in enough detail the thermal effects of a period of 240 seconds of exposure to space on all systems will have to be investigated in the future, including possible mitigation strategies.

4.2. Aeroshell

After separation, the interior of the VUAB is entirely exposed to the space environment. The shape, practically an open cylinder, will give rise to extremely adverse aerodynamic effects during re-entry if it is not protected. The other end of the VUAB, on which the Vulcain engine is mounted, is covered in TPS material. However, as indicated by Airbus themselves, this TPS is expected to be 'used-up' after launch. Moreover, the shape will give rise to extreme adverse aerodynamic effects which the Vulcain engine and the aft portion of the VUAB are not designed for. As a result, the maximum dynamic pressure and heatflux experienced during re-entry give rise to the need for a protection system. The preliminary feasibility study in the Midterm Report has resulted in the thermal protection system (TPS) and the required aerodynamic performance being provided by an inflatable aeroshell. The stakeholder requirements and size and configuration of the VUAB make this the most feasible design solution. This section will discuss the design process and present the design of the aeroshell. This section will cover function F 3.2.1 to function F 3.2.4 from Figure 2.7.

4.2.1. Existing aeroshells

Multiple institution have done research into inflatable aeroshells, also called Inflatable Aerodynamic Decelerators (IADs). The progress of IAD development is in the TRL 7 phase. The technology has been demonstrated and scaled to fit the intended purposes. Currently, mission specific aeroshell design is being conducted[49]. Three primary existing and comparable aeroshells are summarized below.

- **Inflatable Re-entry and Descent Technology(IRDT)** ESA has developed and tested the IRDT. The proposed applications of the IRDT are to return samples from the ISS, deliver payload to Mars and onboard reusable launch vehicles. The technology is composed of two inflatables, one for re-entry deceleration and the second cascade for atmospheric deceleration down to landing velocities in the order of 13-15 m/s. It is being developed for payloads up to 200 kg. This application does not relate to that of the VUAB recovery. However, the first stage of the IRDT shows insights into the TPS material used, packaging, weight factors and sensor package of the first stage inflatable decelerator[74].
- **Inflatable Re-entry Vehicle Experiment(IRVE)** The IRVE is a project concerning a type of Hypersonic Inflatable Aerodynamic Decelerator(HIAD) developed by NASA. In fact, it composed of 4 flight tests involving HIAD structures. The purpose of the missions was to overcome the following main challenges: "Surviving the heat pulse during re-entry, demonstrating system performance at relevant scales and demonstrating controllability in the atmosphere" [21]. The end-goal of the HIAD program is to deliver large payloads to Mars and return large payloads to Earth. The IRVE program gives in-depth insight into several design aspects such as the inflation system, controls, telemetry, TPS and structural analysis. Though the scale of the experiments are not within the scope of the VUAB recovery, the applications show much resemblance.
- **High Energy Atmospheric Re-entry Test(HEART)** After the great success of IRVE-4, NASA has scaled up the HIAD program. The HEART aims to "demonstrate system performance at relevant scales and environments" [22]. The test parameters are as follows: entry mass of 3500-5500 kg, peak heatflux of 30 W/cm^2 and re-entry speeds of 7.6 km/s. The HEART has not been validated by means of an experiment but the resemblance with the mission characteristics of the VUAB recovery are very significant. This is very promising for future applications.

[4] `https://sciencing.com/temperatures-outer-space-around-earth-20254.html`, [21-01-2018]

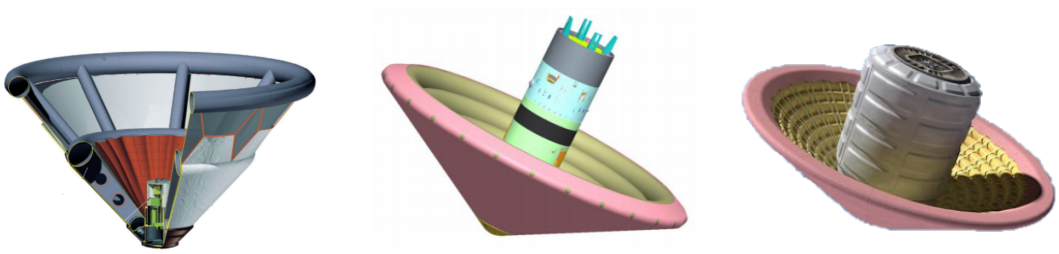

(a) Fully deployed IRDT [47] (b) Deployed IRVE-3 vehicle [21] (c) The HEART [22]

Figure 4.3

On top of the existing architecture, NASA has conducted an in-depth analysis of entry, descent and landing systems for a large payload Mars landing in which a lifting HIAD was one of the studied concepts [77]. In the initial stages of this study, it was concluded that the design case and expected entry conditions of this HIAD are very comparable to that of the VUAB recovery. This particular design case was used in the initial aeroshell sizing. However, at a later stage in the design process it became apparent that the HEART design case actually is very similar to that of the VUAB recovery. To maintain objective in the design, the HEART results shall therefore be used in the verification and validation of the aeroshell design and not in the design.

4.2.2. Sizing

The initial shape and mass breakdown of the aeroshell is based on the Lifting HIAD as suggested by Dwyer Cianciolo et al.[77]. The shape is a sphere-cone aeroshell with stacked toroids wrapped in a blanket of TPS material. The nose-cone of the aeroshell is a semi-sphere. The parameters that shall serve as an output to the aeroshell sizing are as follows:

- **Aeroshell Diameter, D_o:** The diameter of the aeroshell has major effects on its performance. The diameter relates back to the reference area, which in turn is used to compute the average heat transfer rates, lift and drag generation and the dynamic pressure.
- **half-cone angle, θ_a:** The angle of the cone is defined as the angle between the centreline and the edge of the aeroshell. It has major influences on the total TPS mass as well as the average heatflux experienced by the aeroshell. Based on existing aeroshells, the angle shall be between 60° and 70°. The reason for this is that at this stage, the effects on aerodynamic performance as well as heat transfer properties are not well-known. Therefore, the angle shall fall within the range of angles of aeroshells currently under investigation.
- **Nose-cone radius, R_{nose}:** The aeroshell has a blunt nose. The radius of the nose-cone is directly related to the maximum heatflux experienced at the stagnation point.
- **Aeroshell mass, M_a:** A very important parameter which, for space engineering, has to be minimized.
- **Toroid inflated diameter, D_t:** This is the cross-sectional diameter of the toroids when inflated. In the current design, all toroids have the same diameter.

The design process of the aeroshell is an iterative one. The general flow of information and steps of the iteration shall be discussed. Following this discussion the final results shall be presented. The initial design consists of a trajectory analysis which will output the aerodynamic and thermal characteristics. This will serve as an input to the aeroshell design. The aeroshell design will in turn serve as an input in the re-entry trajectory model, which will cause trajectory changes. This circular iterative process is illustrated in Figure 4.4.

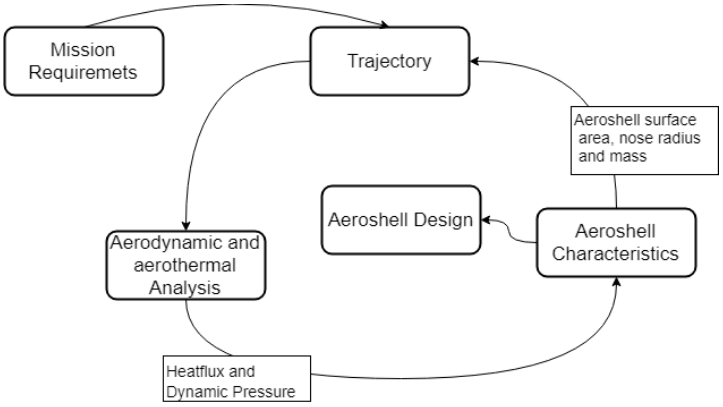

Figure 4.4: Information flow aeroshell design

The steps taken to determine the aeroshell characteristics are given below:

1. Determine diameter, spherical-cone angle, and nose-radius.
2. Compute the maximum heatflux, average heatflux, maximum dynamic pressure and toroid diameter.
3. Determine optimal TPS material.
4. Determine the mass breakdown.
5. Iterate between the above mentioned steps to optimize for mass.

As a first iteration, an initial diameter estimation was made of 10 meters, based on the results of the Mid-term report [71]. The assumed half-cone angle is 60°, and the nose radius 1 meter. This is used for the first iteration of the aeroshell.

The maximum heatflux, average heatflux and dynamic pressure are determined with the re-entry model as presented in Section 3.1.2. A summary of the results of the above mentioned parameters for different aeroshell diameters is presented at the end of this section.

In the paper "Estimating Mass of Inflatable Aerodynamic Decelerators Using Dimensionless Parameters", J. Samareh has given a method to determine the diameter of the toroid[54]:

$$D_t = \frac{D_o - D_i}{(2N-1)\sin(\theta_a) + 1 - \cos(\theta_a)} \tag{4.5}$$

Where D_i is equal to the diameter of the nose-cone. N is defined as the number of stacked toroids. A schematic representation is given in Figure 4.5a. Based on reference aeroshells, this number was estimated to be between 6 and 8. Therefore, for the initial design 7 toroids are used to be safe. The initial size estimate with the mentioned parameters is 574 mm. This method suggested by Samareh was verified by generating a CAD drawing of the aeroshell with the given dimensions. See section 4.2.5 for the aeroshell configuration.

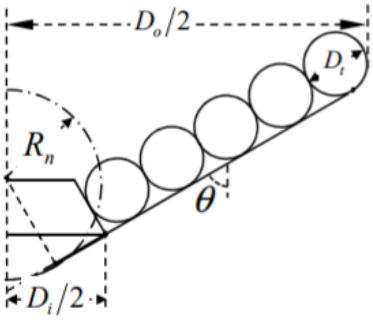

(a) Stacked toroid IAD geometry[54]

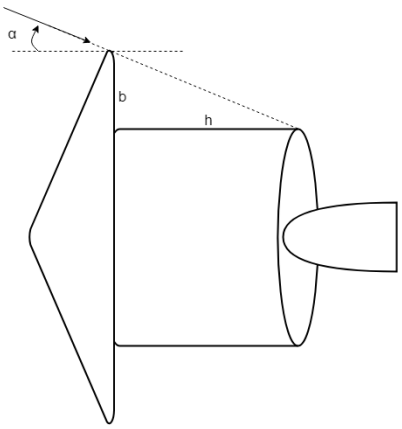

(b) Simplified representation of potential flow impingements

Figure 4.5

The purpose of the aeroshell is to protect the VuAB from the oncoming flow. So it is quite natural to argue that there shall be no flow impingements with the exposed structure of the VuAB. Since the aeroshell will have a nominal angle of attack of 20°, there is a minimum diameter constraint on the aeroshell. This is depicted in Figure 4.5b. Length h is the height of the VuAB that is protruding outside the edge of the aeroshell. Length b is the length of the aeroshell that extends beyond the diameter of the VuAB. α is the angle of attack. Simple trigonometric relations show that when h is equal to the length of the VuAB (5.134 m) and the angle of attack is 20°, the minimum length of b is 1.87 m. This leads to a minimum aeroshell diameter of 9.14 m. This length, however, is computed for the case the VuAB does not extend into the aeroshell. After each iteration, the CAD model is updated and it is evaluated if the VuAB can fit 'inside' the aeroshell. This is done with at least a 10 percent safety margin. For this reason the final diameter of the aeroshell may be smaller than the above computed 9.14 m.

4.2.3. Thermal Protection System

To protect the structure of the inflatable aeroshell and the entire VuAB, the TPS must withstand the thermal loads experienced by the aeroshell during re-entry. "This TPS must be capable of surviving the heat pulse, and the rigors of fabrication handling, high density packing, deployment, and aerodynamic loading." Del Corso et al [18].

The suitable TPS materials can be categorised into two different types: ablators and insulators. An ablator is a consumable, meaning it dissipates heat by charring and recession of the top TPS layer. An insulator absorbs the heat transfers by conduction and radiation. All flexible TPS materials have sufficient technical maturity and a TRL above 5. The insulator TPS was developed at NASA's Langley Research Center and is used and validated on the IRVE-3 and IRVE-4 tests. It consists of an double layer of outer fabric (Nextel 440), a double layer of insulator (Pyrogel 3350), and a triple laminated structural/gas barrier (Kapton-Kevlar-Kapton) [21].

The insulator peak heatflux limit is $\approx$ 60 W/cm^2. The density is 0.162 g/cm^3 and the thickness 2.76 cm [1] [18] [22]. The two suitable ablators are developed at NASA's Ames Research Center and consist of a substrate (flexible felt) plus a matrix (resin): Silicone Impregnated Reusable Ceramic Ablator (SIRCA-flex), which is a flexible Q-felt plus silicone matrix and Phenolic Impregnated Ceramic Ablator(PICA-flex) which is a flexible Q-felt plus phenolic matrix [51].

SIRCA-flex has a density of 0.24 g/cm^3, a thickness of 3.8 cm and can operate in environments with heat rates up to 115 W/cm^2 [77]. PICA-flex has a density of 0.27 g/cm^3, a thickness of 3.8 cm and can operate in environments with heat rates up to 300 W/cm^2 and dynamic pressures up to 14 kPa [43].
At each iteration, it is evaluated whether the maximum heatflux falls within the range for the suitable TPS materials. The feasible TPS material is then taken into consideration for the mass model. As established in Section 3.1.2, the heatflux is the highest at the stagnation point, which is, for zero angle of attack flight, expected to be on the nose-cone. The average heatflux is much lower. This might suggest that it is possible to use a combination of TPS materials on the surface of the aeroshell to minimize the mass of the TPS material needed. However, the aeroshell will pass through the atmosphere at an angle of attack of 20°. It has been shown that the pressure distribution over an aeroshell significantly changes at an angle of attack of 10° [74]. The peak heatflux over the surface of the aeroshell will not be constant, and at this stage of the design it is not within the scope to simulate the heatflux distribution over the surface with CFD. For that reason, a conservative approach is taken and the peak heatflux will be used for the choice of the TPS material over the entire surface of the aeroshell.

4.2.4. Mass Model and Structure

The mass model for the aeroshell is based on the lifting HIAD mass model suggested by Dwyer Cianciolo et al.[77]. However, since the configuration is not identical, some changes are made to the model which are summarised below.

The lifting HIAD has heatshield which is defined as a rigid payload containment structure to house the subsystems and provide structural support adequate to survive launch and re-entry loads. The lifting HIAD has to cope with the introduced aerodynamic loads of an aerocapture, which are higher than the direct entry and has a much higher diameter (thus induced moments). The percentage mass of the heatshield is reduced by a factor 2, this percentage is added to the TPS because the expected relative thermal loads are worse than the Lifting HIAD. Also, avionics (communication systems, guidance control systems and power) is already onboard the VuAB and thus not part of the aeroshell mass model. Additional subsystems include a compressed gas subsystem to deploy and inflate the inflatable structure, a separation system, and a payload adaptor, which is the link between the support beam and the aeroshell. The mass model that will be used is given in Table 4.1.

The structure of the aeroshell is composed of 7 stacked-toroids filled with nitrogen. The aeroshell components

for structural integrity are: radial straps that hold the toroids together and carry radial loads, gores that carry pressure loads, axial straps that carry buckling loads, reinforcing fabric wrapped around the toroids that counter hoop stress and a gas barrier. The straps and reinforcing fabrics are made of Kevlar-49 and the gores and gas barrier are made of Upilex. The gas barrier is an overwrap that prevents the nitrogen from leaking outside the toroid. This structure is largely based on the Lifting HIAD concept [77].

The IRVE-4 and testing models of the HEART are manufactured by Airborne Systems. Airborne Systems has a facility in Toulouse, France. This is advantageous for operational reasons. Therefore, Airborne Systems will be involved in the manufacturing of the aeroshell [5].

4.2.5. Sizing Results

The aeroshell sizing steps are iterated to determine the optimal shape and size. With the determined aeroshell diameter and half-cone angle, the total surface area of the aeroshell can be easily computed. This surface area is simply multiplied by the suitable TPS material thickness and density to determine the mass of the TPS material. The results are used to compute the remaining component and total aeroshell mass.

Figure 4.8a shows that for a range of aeroshell diameters, the the maximum heatflux at the stagnation point falls well within the range of all available TPS materials. Therefore, it was possible to minimize the aeroshell size. Following the CAD model integration, the minimum heatshield diameter regarding flow impingements was 8.8 meters. The VuAB in this case would extend 4.567 meters (without nozzle) from the trailing edge of the aeroshell. The toroid diameter of 57.4 cm is not changed, this means that for lay-out purposes, the nose-cone radius is changed to 1.8 meters. An increase of the half-cone angle leads to a smaller surface area, and in turn a lower TPS and aeroshell mass. Because the aerodynamic and aerothermal effects of a change in the half-cone radius are largely unknown, it was decided that the half-cone angle was increased by 5° to θ_{cone} = 65°.

It can be seen in Figure 4.8a that for the diameter of D_0 = 8.8 m and with R_{nose} = 1.8m, the maximum heatflux at the stagnation point is 55.2 W/cm^2 and occurs at 60.1 km altitude at 77.5 seconds after the beginning of re-entry. This means that both SIRCA-flex and the insulator are suitable TPS choices. However, since a full aerothermodynamic analysis is complex and difficult to predict, the conservative choice was made to use SIRCA-flex. This will be elaborated on in the sensitivity analysis. This led to a to a TPS mass of 614.3 kg. The distribution of dynamic pressure as seen in Figure 4.8c shows that the maximum dynamic pressure during re-entry is 6514 Pa at 90 seconds. This corresponds to an altitude of 56.9 km. The dynamic pressure is well within the bounds that the TPS can operate and similar to the reference aeroshell models.

Table 4.1: Aeroshell component mass breakdown

Components	%	Mass [kg]
Adapter	22.1	311.4
Heatshield (support stucture)	5.1	71.9
Inflatable	16.8	236.7
Separation	12.4	174.7
TPS	43.6	614.3
Total	100	1409

Sensitivity

A sensitivity analysis on the aeroshell sizing results gives insight into the contribution factor of each parameter. Thus, if further design iterations are performed, it will help select which parameters are to be optimised. Regarding the aeroshell sizing the following parameters are compared: diameter and half-cone angle versus mass. The two parameters are the only factors that have influence on the mass for a chosen TPS material. The selection of TPS material can also be subjected to a sensitivity study. It is conducted by comparing nose-cone radius and diameter versus maximum heatflux. With a conservative approach and considering TRLs, it can be decided that in order to use an insulator TPS, the maximum heatflux must be below 45 W/cm^2.

It can be seen in Figure 4.8a that the diameter should then be 12 meters for a nose-cone radius of 1.8 meters. This would also significantly lower the peak dynamic pressure (Figure 4.8c), but this does not matter as all types of TPS can operate in the full range of expected dynamic pressures. However, lower dynamic pressure will lead to lower aerodynamic forces, which is advantageous for structural integrity. The weight, as seen in Figure 4.7a

[5] https://airborne-sys.com/experience/space-parachutes-inflatable-military/#experience1, 24-01-2018

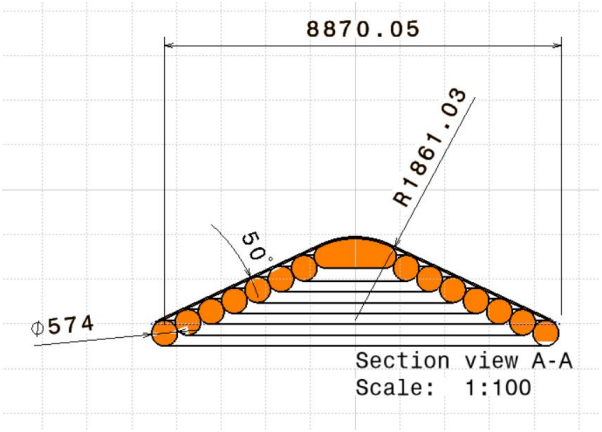

Figure 4.6: Configuration of the inflatable aeroshell

for the insulating TPS would then be lower than the current weight. So in theory, this option is more optimal. The main concern is that the packaging volume is seriously limited in the VuAB. Increasing the diameter could pose a packaging conflict. Thus, the design choices made are optimal for the current TPS materials available. A highly valuable recommendations for future design would be to improve the insulator performance and/or slightly increase the packaging volume limit, as this can potentially save very much weight.

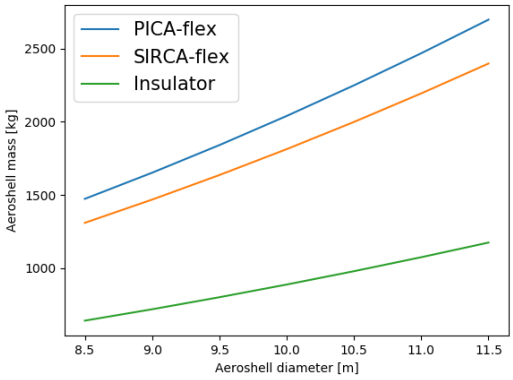

(a) Aeroshell mass vs diameter for the different TPS materials

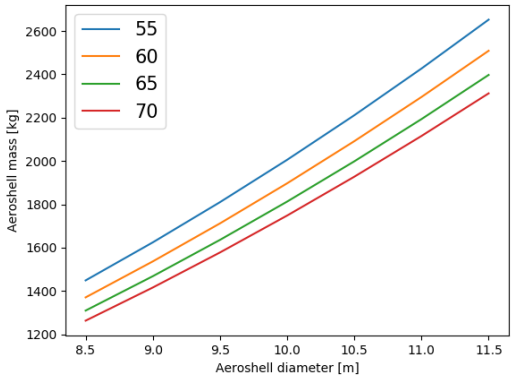

(b) Aeroshell mass vs diameter for various half-cone angles

Figure 4.7

Verification

The entry model has been verified in Section 3.1.2. This implies that the aeroshell sizing, which is an integral part of the heatlfux and dynamic pressure features, in the re-entry model is in turn verified. This leaves the mass estimation to be verified. This is done in two ways. Firstly, the inputs to the mass model can be adjusted to that of the Lifting HIAD. The results of the adjusted mass model can be compared to that of the Lifting HIAD. If the percentage difference is within 15%, it is considered verified. The percentage difference is chosen as such because the used mass model of the Lifting HIAD analysis is different, thus a low accuracy is expected. Note that because of this, it is a weak verification. The execution of this verification leads to a percentage difference of 13.9%.

The second method to verify the heatshield sizing is by compliance with the requirements. There are no direct system requirements imposed on the heatshield. However, when considering the function of the aeroshell one can easily derive the primary requirements. First and foremost, it must protect the VuAB from the aerodynamic and thermal loads. This is complied with. Next, the heatshield must be designed such that it minimises mass. This is verified and shown by the sensitivity analysis. However, there are a few limitations to this method. The

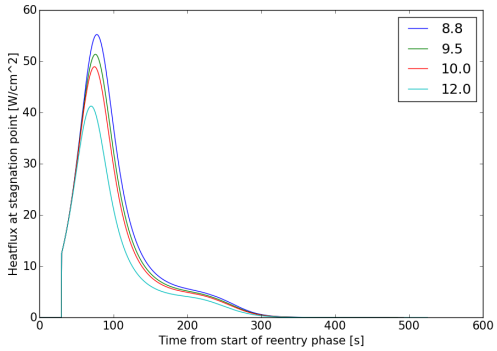

(a) Heatflux during re-entry for various aeroshell diameters

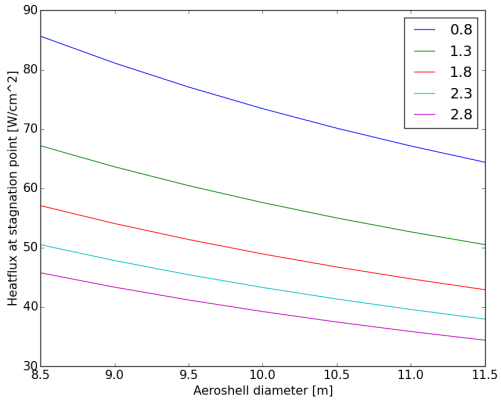

(b) Aeroshell diameter vs heatflux for varying nose cone radii

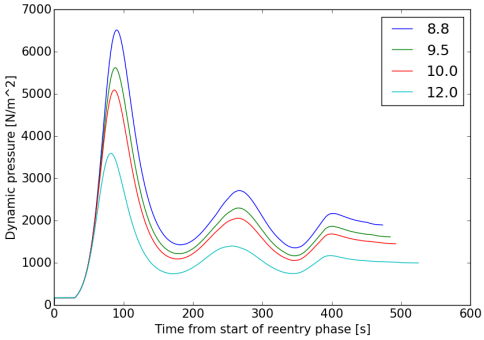

(c) Dynamic pressure during re-entry for various aeroshell diameters

Figure 4.8

design of the aeroshell can be subjected to more in depth analysis. This analysis may result in a change in the design. The recommendations for further design analysis are given in Chapter 9.

One last sanity check is to compare the aeroshell to the existing HEART. The HEART will be subjected to slightly lower thermal loading as well as dynamic pressure. This is expected as the entry mass is almost a factor 2 smaller. The entry speed is slightly higher with 7.6 km/s. The peak deceleration of the HEART is 7 g's, compared to 6 g's for the aeroshell. The HEART HIAD parameters are: 8.3 meter diameter, 1312 kg total HIAD mass, nose cone raidus of 1 meter and 55° half-angle. The smaller diameter and mass are expected as the peak heatflux is slightly lower. To conclude, the design similarities are astounding. This will serve as a verification of the design and functional feasibility of the aeroshell. It is suggested that the future detailed design is done in collaboration with the HEART research group at NASA Langley.

4.2.6. Aeroshell Packaging

This section explains why and how the aeroshell is packaged in the VuAB. First the requirements and constraints imposed on the aeroshell are discussed. This is followed by the approach to yield a solution allowing the aeroshell to fold inside the VuAB, leaving enough space for other subsystems, deploying, providing structural integrity whilst shielding the rest of the VuAB during re-entry and discarding after re-entry.

The requirements and constraints on the packaging and deployment of the aeroshell can be separated into 4 main categories:

1. Volume
   - The aeroshell needs to fit into the VuAB between the VuAB's cross structure and the fuel tank, leaving enough space for the other subsystems.
   - The ablative material is assumed to have a minimum folding radius of r_{fold} = 152 mm based on a

thickness of $t_{abl} = 38$ mm for the ablative material and a thickness of $t_{tor} = 20$ mm for the supporting inflatable toroids without minimal folding radius since the inflatable toroids are more flexible and a lot thinner [76].

2. Deployment
   - The aeroshell must deploy with minimal complexity to minimize risk of deployment failure since it is a critical part in the mission.
   - For the deployment it needs to overcome the separation height of the VuAB wall.
   - The tubes need to inflate from the edge of the aeroshell towards the center, to prevent it from inflating like an overextended umbrella.
   - The sharp cut off edges should not damage the inside of the aeroshell when it is deployed.
3. Load transfer
   - The mounting and deployment mechanism need to be located at the inside of the VuAB during launch to prevent interference with the nominal operation of the Ariane 6 rocket.
   - After deployment the aeroshell has to transfer large loads to the structural elements of the VuAB.
4. Discarding aeroshell
   - The aeroshell needs to be discarded after re-entry without damaging the VuAB.

The approach to the solution is started by stating the assumptions that are made for the aeroshell packaging. Since the complete layout is an iterative process a compromise between an optimal packing factor (the amount of mass per volume for the folded aeroshell) and ideal 3D positioning of the aeroshell with respect to the other subsystems is desired. This design space is approached by exploration of various options. This serves two purposes, it allows for a better understanding of certain design choices and the creativity yields a broader range of solutions, improving the chance of an optimal packing factor and/or 3D positioning inside the VuAB.

After the exploration of the design options of the VuAB packaging and deployment, the infeasible options are discarded. Once the design is fixed, the shape will be approximated in a model that evaluates the critical folding parameters, such as the volume occupied by the folding procedure and deployment translation freedom. The different design options are discussed below.

- The aeroshell would preferably be folded in the outer radius of the VuAB just below the tank, and then folding inwards. Since it is unlikely the narrow edges between the tank and the VuAB skirt will provide spacing to other subsystems throughout the entire VuAB circumference.
  However, this would require the merger of to open flaps of the aeroshell once it is deployed since the fuel pipes and fuel tank cut through any closed circular surface of the aeroshell. Such a merger would significantly increase complexity and risk, as it would introduce a weakness into the structure that requires reinforcement much like the way aircraft windows do in an aircraft.
- A uniform and point symmetric attachment at the outer radius of the VuAB would be an efficient way to handle any moments that will act on the aeroshell since the large radius induces a large moment of inertia of the load transferring structure at the attachment points between the VuAB and the aeroshell.
  The same counter argument as for the first design option holds.
- The aeroshell could be mounted across a line of mounting points on the side of the VuAB skirt and unfold once the fuel tank is separated.
  Besides the asymmetric attachment, the aeroshell must be mounted at least 1.5 meters from its deployment edge. Combined with the fact that the mount between the aeroshell and VuAB has to be located on the inside of the aeroshell, it entails a double fold like an overextended umbrella, which is difficult to unfold properly, increasing complexity of this choice.
- An off centre L-shaped beam with a hinge in the corner could rotate the near-horizontal part of the beam to translate the vertical part over the centre whilst extending it over the separation edge that remains of the VuAB skirt after fuel tank separation.

The last of these mention options is chosen to be further developed in the rest of this section. From this point the aeroshell, sketched in Figure 4.9a needs to be folded. The first fold (fold 1) is from a 3D cone with the ablative material on the outside, to a near 2D piece of pie. The fold line 1 is indicated in Figure 4.9b with the two solid thick green lines. The front flap is left out to show the folding radius of fold 1 and the two layers being folded flat against each other.

Once it is folded flat, it will be placed around the centre of the VuAB as shown in Figure 4.9c, with the centre of the vertical part of the deployment beam at $r = 2100$ [mm]. This is determined through an iterative process, where the lower flaps in Figure 4.9b are folded over the dashed lines. The top view of those fold lines is visualized in Figure 4.9c. The iteration starts to from the L-beam towards the outer radius, to see how far to the centre the peak of the aeroshell can be located, to fit the outer flaps between the beam and the VuAB. This process is modelled

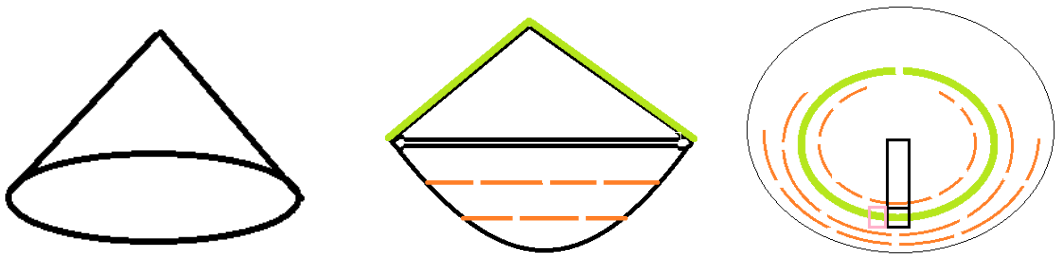

(a) Deployed Aeroshell Sketch (b) Deployed Aeroshell Sketch (c) First Fold Aeroshell

Figure 4.9

using the following input parameters:

- $r_{depl} = D_{depl}/2 = 4.40$ [m]
- $t_{abl} = 3.8$ [mm]
- $t_{tor} = 2$ [mm]
- $r_{fold} = 152$ [mm]
- $\theta_{cone} = 65°$
- $r_{skirt} = 2.70$ [m]

The most critical section is where the deployment beam is in the middle of the shield, since it increases the radial thickness of the aeroshell fold. That cross section is sketched in Figure 4.10.

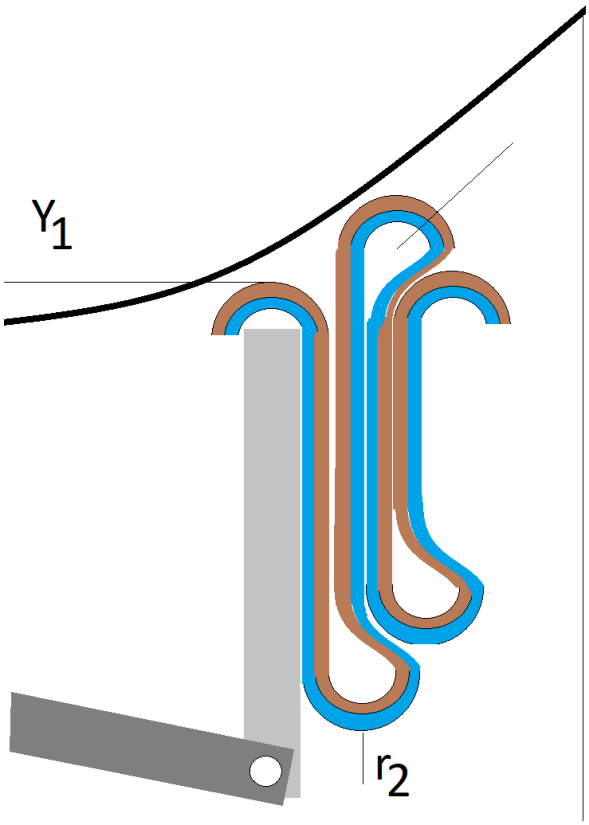

Figure 4.10: The folding pattern of the aeroshell below the fuel tank, from the L-beam outwards to the VuAB skirt on the right.

The folds are numbered from centre to the right starting at 0 over the deployment beam. To compute the length of the folds, the fuel tank height in mm from the cross to the fuel tank is interpolated at:

$$y[r] = 6.438 \cdot 10^{-7} \cdot x^{2.73} + 790 \tag{4.6}$$

Based on the size of the VuAB models provided by the client, the margin between the folds and the tank is set at 10 mm where as the bottom folds rest on the cross. The length of the shielding material in Figure 4.10 should equal the length of the shielding material $l_{s,m}$ from the centre to the edge, once it is deployed. This is computed by:

$$r_{mat} = \frac{r_{depl}}{\sin(65°)} = 4.85m \tag{4.7}$$

All folds are shifted as far to the inner radius as possible, at the expense of height per vertical flap between the folds. Fold 1 goes straight down, and fold 2 goes up to the fuel tank, after that the folds are bounded by their previous folds, as is shown for the last two folds in Figure 4.10.

The coordinates of these folds are computed. The first length computation is based on the vertical difference between the peaks of the fold, that led to $l_{s,m} = 4.94m$ at fold 4 is computed. That means fold 4 is not necessary any more, since the outer flap can go straight down next to fold 2. The outer edge of fold 3 is located at r_{outer} = 2.65 m. The same algorithm is applied but then for the folds to the inside with the adapted fuel tank height. This leads to an inner radius of: r_{inner} = 1.43 m. With the folding pattern known, the length of the folds is calculated. These are fed into the deployment, load transfer and aeroshell discarding evaluation.

Looking into the deployment this option consists of two hinges which are activated by a single piston mounted on the side of the structural cross, which has a relatively low complexity. To overcome the separation height, lower part of the L-beam rotates around the hinge at the centre until it stands vertical, at that moment a spring loaded sleeve slides over the corner hinge, fixating the straight bar.

This rotation of the lower part of the L-beam also means the folded centre of the aeroshell translates from r = 210 cm to r = 0 cm. To prevent it from touching the wall during this translation, the aeroshell is folded inwards from an angle of 81.5◦ with respect to each side of the lower part of the L-beam in the perspective of Figure 4.9c.

After L-beam deployment, the aeroshell needs to inflate from the outer toroid inwards, to prevent 1 of the folds constricting the complete aeroshell deployment like an overextended umbrella. The nitrogen tank that contains the gas that inflates the toroids is positioned on the side of the upper part of the L-beam below the inflation system, visualized in Figure 4.9c with the pink square on the side of the L-beam. During re-entry the inflation system needs to gradually increase the mass of nitrogen in the toroids as the pressure will increase, which would deflate the toroids if they would be left at a constant pressure.

4.2.7. Aeroshell Load Introduction

The loads introduced by the aeroshell during re-entry as determined with the re-entry model and the aeroshell sizing are 350 kN in lateral direction and 470 kN in longitudinal direction. As the centre of pressure is not known at this point in the design the forces are assumed to act on the nose cone and a preliminary structural analysis is performed on the beam supporting the heat shield to obtain a preliminary sizing.

First of all, the material chosen is the same for all structural elements in the recovery system and the Ariane 6, Aluminium 7075-T6, for compatibility and production purposes. The aeroshell is folded during launch with a folding radius of 0.15 m, so this is taken as the maximum value of the radius for the supporting beam. Then, the total length of the beam is determined to be 3.63 m in Section 4.2.6. The thickness of the beam will be determined using the structural analysis.

As it is expected that the moment induced by the lateral force will be critical for this beam, a hollow beam is chosen for the design. Furthermore, as is it not known in which direction the lateral force will act, a circular design is chosen with the same stiffness around the cross-section. The direction is not known as the VuAB - aeroshell combination can rotate along its longitudinal axis.

First, the moment induced by the lateral force will be determined using Equation (4.8), the moment of inertia of a hollow beam using Equation (4.24), and these are used to rewrite Equation (4.10) into Equation (4.11) [31] to determine the thickness required to handle these loads. y is constant over the cross section and is equal to R_0.

$$M = F_{lateral} \cdot L_{beam} \tag{4.8}$$

$$I_{beam} = \pi \cdot R_0^3 \cdot t \tag{4.9}$$

$$\sigma_{yield} = \frac{-M \cdot y}{I_{beam}} \tag{4.10}$$

$$t = \frac{M}{\sigma_y \cdot R_0^2 \cdot \pi} \tag{4.11}$$

Using the σ_y and density of Aluminium 7075-T6 (480 MPa, 2801 kg/m^3) the design of the beam is optimized for weight. This is done by using the largest R_0 possible, which is 0.15 m. Then, using the equations stated above

the minimum thickness is determined to be 0.040 m, with a resulting weight of 383.4 kg. A safety margin of 10% is taken into account in these calculations.

This beam is then checked for the axial load of 460 kN, using Equation (4.12). This results in a required area of 0.001054 m^2, while an area of 0.037 m^2 is obtained using the calculated thickness and radius.

$$A_{beam} = F_{longitudinal} \cdot \sigma_{yield} \tag{4.12}$$

Finally, the packed aeroshell should be checked for its natural frequencies during launch. As defined by the client, the frequencies in all directions should not be lower than 50 Hz in order to prevent vibrational coupling with the Vulcain engine during launch. As the beam has a homogeneous cross section the moment of inertia is equal in all directions. Therefore, the the lateral frequency in y direction is the same as the longitudinal (z-direction) frequency. The lateral frequency in x-direction, however, will be different as this is the axial frequency from the perspective of the beam.

Using the vibrational analysis as stated in Section 3.2.1 and using the values as stated above, the longitudinal frequency of the packed aeroshell would be 23.8 Hz. Therefore, it chosen to fix the beam at the hinge at 2.2 m from the centre, assuming that it is infinitely rigid. In this configuration, the beam consists of two different parts. The horizontal part, which is essentially fixed between two points, and the vertical part, with the package of the aeroshell on top.

For the horizontal part of the beam, which has fixed ends, Equation (4.13) [17] is used to determine the longitudinal (z) f_n, which is the same as the lateral f_n in y direction. As the beam is fixed at both ends with infinitely rigid attachments the lateral frequencies are neglected. K_n is a constant and is defined as 22.4[17] for the first mode and w is the weight of the beam per unit length. From this equation it is determined that the z & y natural frequency of the fixed beam is 1238 Hz, which meets the requirement.

$$f_n = \frac{K_n}{2 \cdot \pi} \sqrt{\frac{E \cdot I \cdot g}{w \cdot L^4}} \tag{4.13}$$

The vertical part of the beam is now analysed for both longitudinal (z) as lateral vibrations (x & y) using equations 3.65, 3.66 and 3.67. The natural frequency in longitudinal direction is calculated to be 231 Hz, while the natural frequency in lateral direction is 59.4 Hz. This meets the requirement but is close, so a good look should be given to this component in further design.

The last check to be performed are the loads during launch. As the maximum acceleration during launch is 6 g and the mass of the heat shield is 1409 kg, a maximum force of 76.8 kN is applied on the beam, which is lower than the 460 kN acting during re-entry.

4.2.8. Aeroshell Discarding

The discarding of the aeroshell should not damage the VuAB. At the moment of discarding, the VuAB has a stable angle of attack of 20 degrees, with a flight path angle of 83 degrees. Since the c.o.g. is located near the bottom of the cross, an aerodynamic stabilizing moment acting on the VuAB due to the aeroshell. If the aerodynamic stabilizing moment is removed, the low centre of gravity will cause the VuAB to increase its angle of attack, much like a near upside down float would. This is used to orient the VuAB for aeroshell discardment, by means of aeroshell deflation. Once the erected corner hinge of the L-beam experiences a threshold strain and the VuAB orientation is within the discardment range the corner hinge will release, discarding the aeroshell. Additional design challenges include the deflation mechanism, a spring mechanism to increase the separation velocity of the aeroshell, lowering the probability of the aeroshell damaging the VuAB, the aerodynamics of the deflation orientation.

4.3. Parafoil System

This section will cover the design of the parafoil, a key element is the design of the VUAB Recovery system. The parafoil, once deployed, will fly and guide the VUAB towards its rendezvous point with the helicopter all the way up to the point the VUAB is retrieved. Section 4.3.1 will cover the parafoil sizing, including elements such as the canopy. Section 4.3.2 will cover the parafoil flight control system, including the flight software on board, and the controllers used to steer and guide the parafoil. Section 4.3.3 will cover the sizing of the Air Guidance Unit (AGU) where the flight control actuators will be housed. Section 4.3.4 will cover the drogue parachute design, responsible for preparing the VuAB for full parafoil deployment. Section 4.3.5 will cover all the design choices made regarding all the supplementary systems of the parafoil and parachute system. Following this, in

section 4.3.6 the full parachute system load introduction is analysed. Finally, in section 4.3.7 the detachment is sized. This section will cover function F 3.3.1 to function F.3.3.2 from Figure 2.7 as well as function F 3.4.1 from Figure 2.8.

4.3.1. Parafoil Sizing

Sizing and optimisation of the parafoil is an iterative process. As a starting point, the Megafly from Airborne Systems is used as reference.

Canopy Dimensions

The values for the size of the main canopy of the Megafly system can be found on Table 4.2. Figure 4.12 defines some of the geometrical parameters used in the Table 4.2.

Table 4.2: Megafly physical parameters [58]

Parameter	Megafly	Units
a	14.8	m
d	30	m
Λ	120	deg
b	51.8	m
c	16.3	m
t	3	m
mass	410	kg

a is the high of the arc at the mid-point of the canopy (Figure 4.11). No data was found on this value so an approximation for curvilinear parafoils presented by Barrows [14] was used.

$$\epsilon_0 = \arcsin\frac{b/2}{R} \tag{4.14}$$

$$\overline{a} = \frac{R(1-\cos\epsilon_0)}{b} \tag{4.15}$$

From Equation 4.15, $\overline{a}$ can be approximated to be equal to 14.8m.

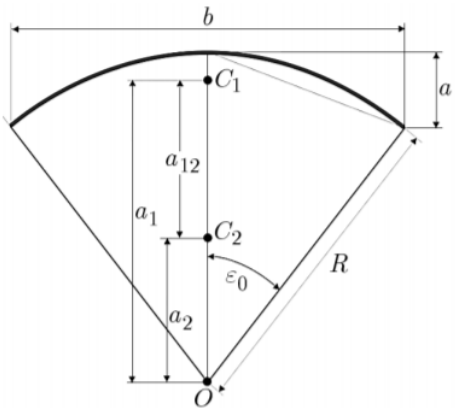

Figure 4.11: Location of characteristic points for general curvilinear parafoils [16]

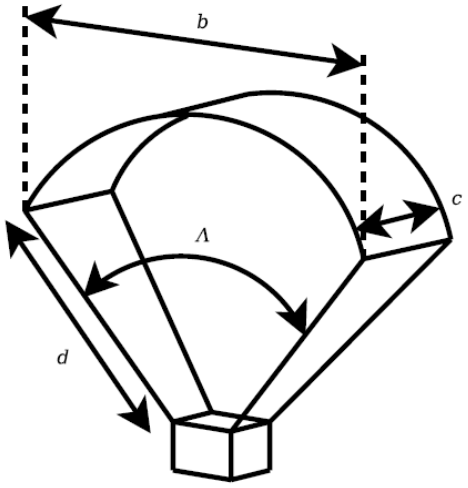

Figure 4.12: Parafoil geometry parameters [58]

Next to the main canopy, the parafoil as stated in Section 3.1.4, makes use of two elevons located at the trailing edge of the canopy. Section 4.3.1 illustrates a schematic of the canopy of a parafoil. More specifically, the two elevons span the outer section, 1, 2, 4 and 5. Each elevon has a span of 20.7m and a chord of approximately 3.5m.

Even though the parafoil possesses two elevons, these control surfaces will only be used asymmetrically during the parafoil flight. In other words, they will only be used as ailerons and not as brakes. The reason behind this will become evident in Section 4.3.2. Nevertheless, due to the discarding of the parafoil to be discussed in section 4.3.7, brakes may still be used.

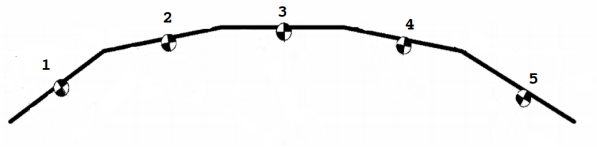

Figure 4.13: Parafoil canopy geometry

The control sensitivities of the ailerons has been modelled such that they are normalized to produce a 5°/s turn rate for a control input of 1.0. The range of the aileron is:

$$-1.0 \leq \delta_a \leq 1.0$$

Aerodynamic Coefficients

The airfoil used by the Megafly system was not found on literature, however, it was found that the X-38 Program used the Clarke Y airfoil [69], which is one of the most widely used airfoils for parafoils. Furthermore, the X-38 parafoil system was able to carry payloads up to close to 11 tons [62]. Given that the weight of the payload at the atmospheric flight mission phase where the parafoil is going to be used is close to 8 tons, its safe to assume the Clarke Y airfoil is a feasible choice. The aerodynamic coefficients of this airfoil are presented in Table 4.3.

Table 4.3: Approximate non-dimensional aerodynamic coefficients for the parafoil [69]

Coefficient	Clarke Y	Units
C_{L_0}	0.45	-
C_{L_α}	0.0384	rad
C_{D_0}	0.15	-
C_{D_α}	0.15	rad
C_{m_0}	-0.07	-
C_{m_α}	-0.004	rad
C_{n_r}	-0.0936	-
$C_{n_{\delta a}}$	0.15	-

System Parameters

Once the main parameters of the parafoil have been set, together with the known parameters of the payload the parafoil is going to be carrying, the main parameters of the parafoil system, comprised of the parafoil-payload components can now be devised.

Table 4.4 presents the parafoil system Moments of Inertia. Its important to note that these values are from a parafoil system, where the Megafly parafoil was used to carry a payload of close to 13 tons. Given that the payload the VuAB parafoil system will be carrying of close to 8 tons, the values for MoI are not exact. The reason for such a discrepancy is that no data was found on literature on the MoI of the parafoil alone. Nevertheless, its important to keep in mind that as mentioned in Section 3.1.4, the mass and the centre of mass of the system can be approximated to be located at the centre of mass of the payload and equal to the mass of the payload respectively. This means that for the I_{xx} and I_{yy} MoI an approximate value for the VuAB parafoil system can be computed using the known MoI of the VuAB plus the Steiner term from the parafoil.

$$I_{xx} = I_{xx_{VuAB}} + m_{parafoil} dz^2 = 28293 + 410 \cdot 30^2 = 397923 kgm^2 \tag{4.16}$$

The percentage difference between the result obtained with Equation (4.16) and the value of I_{xx} presented in Table 4.4 is around 9% which is within an acceptable degree of accuracy at this stage of the design. The reason why this approximation was not performed for all the MoI terms is because for instance the I_{zz} steiner term can't be computed. Hence, for consistency purposes, the values used are the ones in Table 4.4.

Finally, the value for the rigging angle, denoted by τ in Figure 3.16 is assumed to be 10deg, which is consistent with historic values found on literature of parafoil systems having an aspect ratio, AR, of close to 3 [69]. All the values presented in the subsection will be used from hereafter for simulation purposes.

Table 4.4: Moments of inertia of the parafoil-payload system

MoI	kg m^2
I_{xx}	361,650
I_{yy}	328,200
I_{zz}	131,400
I_{xz}	-2,283

4.3.2. Parafoil Flight Control

Having completed the atmospheric flight model and parafoil sizing, a controller is designed to navigate and guide the parafoil towards a given desired location. This system will then be used in sizing the Aerial Guidance Unit (AGU) and the trajectory determination. There are two distinct mission profiles for the atmospheric flight mission phase. One in conditions of little to no wind and another one for conditions with above the average wind conditions.

In the first case, after re-entry and deceleration through use of the drogue shoot, the system will compute its location relative to the retrieval ship and helicopter through use of GPS and data from the recovery vehicles. The controller will then guide the parafoil onto a trajectory towards the desired retrieval location near the recovery vessel. Upon reaching this location at sufficient altitude of 4km the parafoil will perform an energy management manoeuvre that will allow it to lose sufficient altitude, until the helicopter can retrieve the VuAB.

The second case, again after re-entry and deceleration, the system will engage in a energy management manoeuvre, from 8 to 4km. At 4km it will compute its location relative to the retrieval ship and helicopter through use of GPS and data from the recovery vehicles. The controller will then guide the parafoil onto a trajectory towards the desired retrieval location near the recovery vessel. The reason for this is that, is energy management mode, the parafoil flight trajectory is less affected by wind conditions, since by constantly moving around in squares cancels out the wind effects.

To perform these functions, three controllers were designed, being the guidance controller, the energy management controller and the pre-catch controller. For the purpose of elaborating on the controllers, case one will be used. However, for the rest of the report and the entire system has been designed for the second case, since this is the worst-case scenario as will be shown in the subsequent sections, especially the one involving operations.

Guidance Controller

After re-entry, the C&DH system will determine the location and heading of the VuAB relative to the recovery vehicles. The guidance controller is subsequently tasked with steering the parafoil in the desired direction.

For the creation of this controller, both the desired output and the controllable inputs have to be determined. In this case, even though the model has two controllable inputs, the ailerons were deemed to be the only input that should be controlled during the guided flight to the designated recovery area. Use of brakes would only increase the descent rate and would therefore not significantly aid in the guidance of the parafoil.

To keep the system simple, the output of the control system would be the heading angle with respect to the recovery vehicles. The system shall compute the desired heading angle with respect to the recovery vehicles as the reference value and shall compute the error by comparing it to the current heading of the system, as can be seen in Equation (4.17) to Equation (4.20).

$$\Psi_{actual} = \Psi_b + \arctan\frac{V_y}{V_x} \tag{4.17}$$

$$\Psi_{ref} = arctan\frac{\Delta y}{\Delta x} \tag{4.18}$$

$$e_{heading} = \Psi_{actual} - \Psi_{desired} \tag{4.19}$$

$$\delta = \begin{bmatrix}0\\1\end{bmatrix} K_p * e_{heading} = \begin{bmatrix}0\\1\end{bmatrix} K_p * (\Psi_{ref} - \Psi_{actual}) \tag{4.20}$$

Given the reference value and the error, a controller is developed that corrects the error. Given the current stage

in the design process and the aim of simplicity, a PID-controller architecture was chosen due to its incomplexity.

The strategy that is chosen is to initially tune the controller using a proportional gain only, and analyse whether the system responds as desired. In case the proportional gain only does not provide the desired response and instead has a long settling or rise time, an integral or differential controller can still be added. The block diagram of the proportional controller can be found in Figure 4.16.

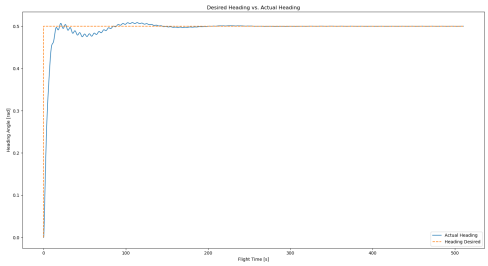

Figure 4.14: Heading response to a step input

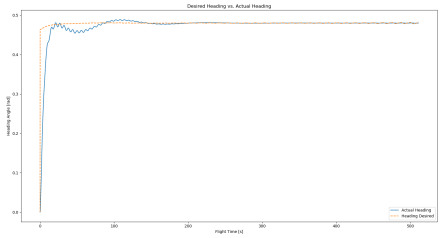

Figure 4.15: Heading response for a given target location

Following the creation of the controller, its response to inputs is evaluated. A trial and error strategy was employed to find the optimum gain for this manoeuvre, with the purpose of limiting overshoot, oscillations and retaining accuracy, whilst still keeping the turning rate at a safe level.

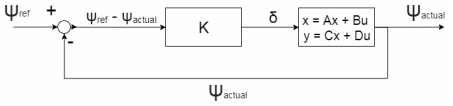

Figure 4.16: Block diagram for a proportional controller

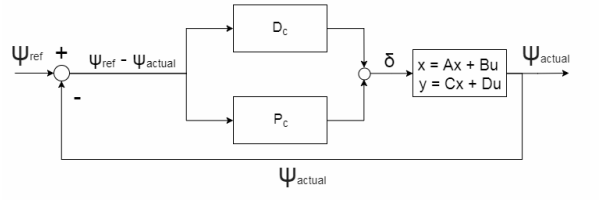

Figure 4.17: Block diagram for a differential controller

$$C = \begin{bmatrix} 0 & 0 & 0 & 0 & 0 & 1 & 0 & 0 & 0 & 0 & 0 & 0 \end{bmatrix} \tag{4.21}$$

$$D = \begin{bmatrix} 0 \end{bmatrix} \tag{4.22}$$

After a few iterations, a K_p value of 0.1 was found to produce the most optimum results. This system's response to a reference heading step input of 0.5 radians is shown in Figure 4.14. The response has a rise time of 6.60 seconds, which corresponds to a turn rate of 2.60 deg/s, which is assumed to be within the parafoil's operational limits. The settling time of the response was found to be 13.24 seconds, after which oscillations with frequencies of 0.017 and 0.17 Hz remain.

$$\delta = \begin{bmatrix} 0 \\ 1 \end{bmatrix} \left(K_p \cdot e_{heading} + K_d \cdot \frac{de}{dt} \right) \tag{4.23}$$

Figure 4.18 and Figure 4.19 show the response of the velocity components after a heading step input and a target location input, respectively. It is visible that there are still oscillations present for all velocities, shortly after deployment, which is mainly due to the fact that the system still needs to achieve its steady state. After reaching the steady state, the system does experience oscillations in y-velocity, which were initially difficult to counteract. A limiter on the y-velocity component, however, was able to solve this problem within 100 seconds after deployment.

Figure 4.15 shows the response of the proportionally controlled system when the system is given a target location at x,y = [10 000, 5000] in the earth fixed axis, after which the system computed its own desired reference heading and used this as input to the controller. Since the heading is not initially at its steady state value, the rise time and settling time of the response are slightly higher at 6.75 seconds and 13.7 seconds, respectively. Since this difference is so minor, it is deemed that the system is fully capable of determining its own trajectory and guiding the parafoil towards the target location.

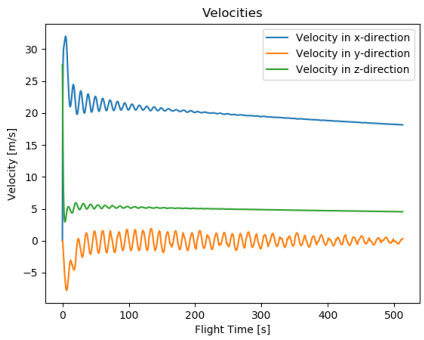

Figure 4.18: x,y and z- velocity components when given a heading step input

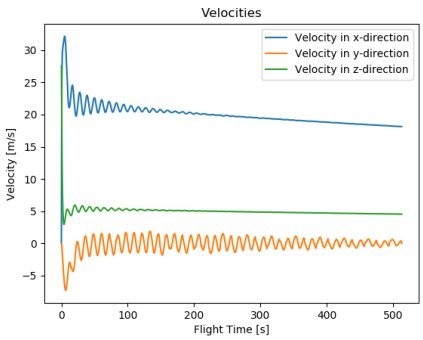

Figure 4.19: x,y and z- velocity components for a given target location at x =10000 m and y = 5000 m

To counteract the oscillations, a differential controller was devised using the same trial and error strategy, for which the aileron input equation is given in Equation (4.23) . Given a differential gain, K_d, of -10, only oscillations with an amplitude of 0.02 radians and a frequency of 0.01 Hz remained. The response to a step input by the system can be seen in Figure 4.20.

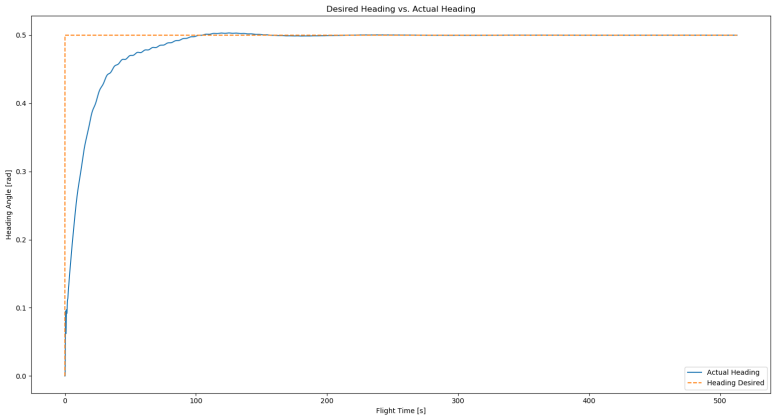

Figure 4.20: Response of the PD-controller to a step input of 0.5

Figure 4.21 Figure 4.22 shows the trajectories with x, y and z locations in the earth fixed axis system for both the step input and the response to a given target location, which demonstrates the guidance capabilities of the system. The system was put through the test with different target locations and larger reference headings, to analyse the sensitivity to large inputs. It was found that up until reference headings larger than $\frac{\pi}{2}$, the system will perform normally. Exceeding these angles, however, leads to unpredictable behaviour and instability due to excessive aileron input. This is countered by limiting the reference heading to $\frac{\pi}{2}$, which leads to predictable and stable turns to the desired heading.

Energy Management Controller

As soon as the parafoil comes within 200 m of its target location, the system will enter an energy management mode, that will send it into a 1500 m wide square loitering trajectory above its target location. This is in part done to keep it near its target and partly due to the fact that the sudden change in reference heading due to a target overshoot will command such large control inputs that it leads to an unstable remainder of the flight. The square trajectory is chosen purposely as opposed to a spiralling flight for both stability and logistical reasons. First of all the squared flight trajectory negates the stability issues associated with longer turning flight, whilst additionally limiting the altitude loss, compared to spiralling flight. Finally, the straight segments allow for an easier transition into the recovery mode, that shall be explained in the following paragraph.
The energy management controller becomes active 200 m in the xy-plane from its target location, and will

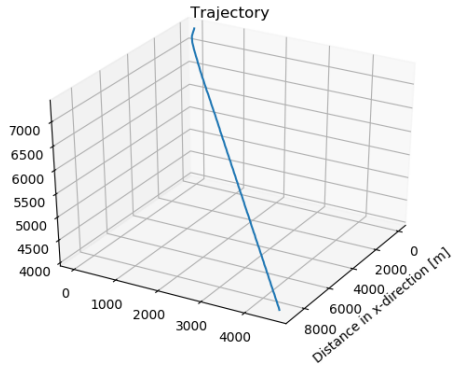

Figure 4.21: Trajectory when given a heading step input

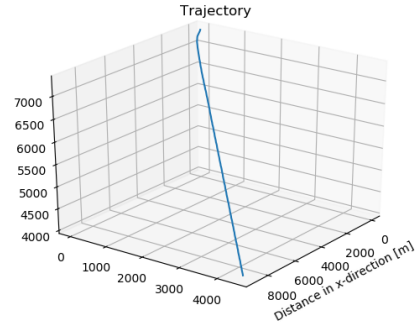

Figure 4.22: Trajectory for a given target location at x =10000 m and y = 5000 m

automatically disengage the guidance controller. Upon activation, it adds exactly $\frac{\pi}{2}$ rad to the reference heading and picks a point 1500 m away along that heading. When the system arrives within 100 m from that point, this process repeats itself, up until the point that the helicopter pilot signals the system to go into recovery mode, which is only possible when in stable straight segments of the flight. Apart from this repeating process, the controller has the exact specifications as the trajectory controller. The trajectory can be seen in Figure 4.23.

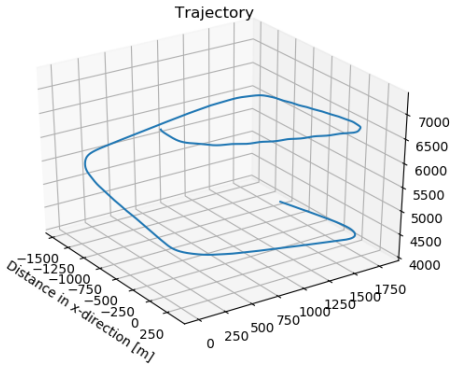

Figure 4.23: Energy Management Trajectory

Recovery Mode

As soon as the helicopter comes within recovery range, the pilot signals the VRS to go into recovery mode. Upon entering this mode, it will retain its current heading and perform straight flight until recovery is complete. It will remain in constant communication with the helicopter, outputting its current state vector to simplify the catch.

Sensitivity analysis

The sensitivity of the control system to a few different parameters is of interest. Firstly the influence of a change on the z_{cg} parameter, which is the vertical distance between the parafoil and the centre of gravity of the VuAB, on the control stability is looked into. In Figure 4.24 a plot for the roll angle over time is shown during and after a turn for different values of z_{cg}.

All three simulations are in the energy management mode and show the system's response during and after the first turn. It can be seen that the system responds quicker for a lower z_{cg}. The roll amplitude during the turn is slightly larger, but after the turn it converges faster for a similar control input. It makes sense that the system is more manoeuvrable when the centre of gravity is closer to the parafoil, as this lowers the moments of inertia. Likewise the moment of inertia will be larger if the z_{cg} is increased. This causes the system to respond slower to

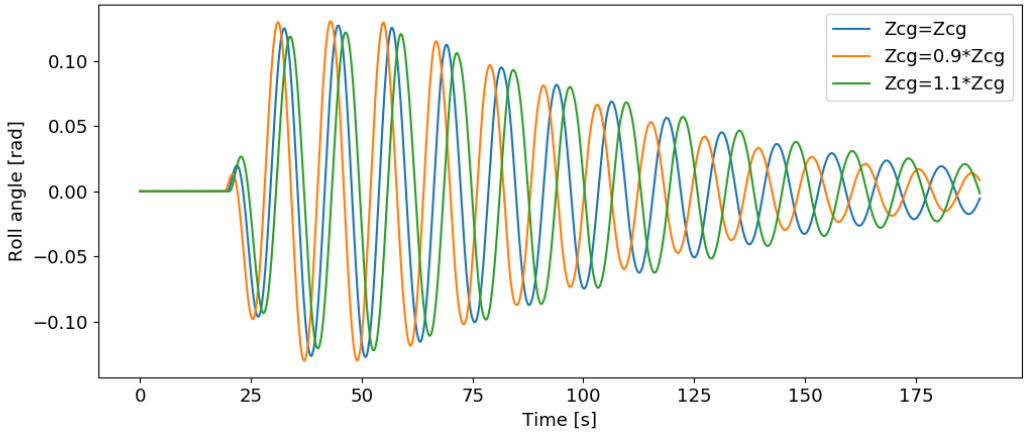

Figure 4.24: Roll angle plots during and after a turn for different values for z_{cg}

input, gives a lower roll angle during the turn and takes more time to converge to a steady state. It can however be seen that a 10% increase or decrease does not make a large difference in the system response. So although a decrease in z_{cg} would in theory be favourable, a decrease on a scale that would be feasible would not increase the performance noticeably.

Secondly, the influence of wind on the control system and the final position are of interest. Wind will be a certain factor in the real life mission profile, so it is important to get an estimate on it's influence on the systems performance. In Figure 4.25 a plot is shown for the final location of 100 simulations with randomised wind as provided by the wind model discussed in 3.1.4.

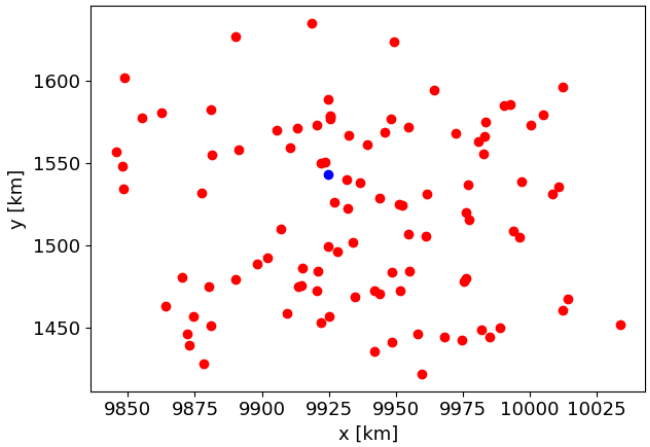

Figure 4.25: Plot of final position descending from 7367 m to 4000 m aiming at target location x = 13000 m, y = 2000 m with random wind for 100 simulations. The blue dot marks the final position without wind

This plot was made with the maximum allowable wind (using a Hellmann exponent of 0.2 in the wind model (3.1.4). With more wind the parafoil would not be able to function properly. It can be seen that over a glide distance of more than 10 km nearly all of the points are within 100 m of the position without wind. Considering the helicopter range and mobility this is a very small spread, also the expected final position of the VuAB can be continuously updated along the way becoming more accurate over time. With less wind the spread becomes slightly smaller, but not significantly, until the wind is completely gone which will yield the exact same result for every simulation.

In conclusion, wind conditions with a Hellman exponent larger than 0.2, lead to a mission reliability lower than the required one.

4.3.3. Parafoil AGU Sizing

The Air Guidance Unit, commonly denoted as the AGU, is a box usually found suspending between the parafoil and the payload that contains all the control actuators, their batteries, on-board computer, sensors, within others. The AGU is what gives the parafoil its ability to steer and navigate towards its designated point. As was done in Section 4.3.1, the Megafly's AGU is used as a reference to start off with.

The AGU of the Megafly has a total mass of around 163kg [65]. This includes all the items that were listed in the introduction paragraph of this section. Due to efficiency purposes, batteries, sensors and the on-board computer will be removed from the AGU and will be merged into bigger single components that is used by the entire recovery system.

Furthermore, from the simulations ran in Section 4.3.2, it was concluded that their is in fact no need for the use of the brake inputs. The use of brakes, is commonly used for flare manoeuvres, which require an extremely large amount of energy. Moreover, simulation results show that the average amount of aileron control input and the average degree of deflection over the entire atmospheric flight is very little when compared with the power specifications of the servo motors used by the Megafly's AGU. Table 4.5 presents the power values of the parachute system. This leads to the conclusion, that smaller and less powerful servo motors are required to fullfill the manuring characteristics of the VuAB-parafoil system mission profile. Off the shelf servos capable of satisfying the power requirements were found to weight around 2.5kg a unit, with dimensions of a cube of 100mm. A problem arises however when considering the operational temperatures of the such servos, which vary between 0 and 40 degrees celcius. At approximately 8km altitude, when the parafoil flight mission phase starts, the atmospheric temperature is on average around -37 degrees celcius. In other words, from 8km to around 2.5km (when average temperatures are around 0 degrees celcius, the parafoil-VuAB system won't be controllable. A work around is to either go for larger and heavier motors with larger operating temperature range or include a thermal control system on the AGU. The absence of flare manoeuvres alone, reduces the weight of the AGU to only 10% [6] of the initial value. Please note, that in this context the use of brakes is used to refer to the use of brakes while in parafoil flight. As mentioned in 4.3.1 the brakes will still be used for parafoil discarding, however at this point, the brakes are only applied to the mass of the parafoil and not the entire parafoil-VuAB system. For conservative purposes, and also to take into account the operational temperature factor the AGU is assumed to weigh 20% of the Megafly's AGU, hence having a mass equal to: 32.36kg.

Table 4.5: Average and peak power values required by the VuAB-parafoil flight control system for nominal manoeuvring capabilities.

Condition	Average Power (W)	Peak Power (W)
No wind	26.0	750
Wind	26.5	775

Given that at this point the AGU only houses the servo motors that actuate the control surfaces, the option to discard the box all together and just integrating the servos directly in the VuAB is considered. However, due to the angle between the two outer steering lines of 120°, the diameter of the VuAB is not large enough. The lines would be in constant contact with the outer shell of the VuAB which is deemed to be dangerous and hence this option is discarded. Therefore, an AGU box is required, and a raiser will be used to suspend it above the VuAB at a high enough distance that the steering lines are not impeded, as discussed in 4.3.5.

4.3.4. Drogue Parachute Design

The drogue parachute, from now on called the parachute, is sized using to the model described in Section 3.2.2. This model describes the motion of the VuAB after discarding the heat shield. To model the parachute behavior, also the general performance and deployment mechanism of the parafoil has to be know. First, some assumptions have to be made about both the parafoil and the parachute and some parameters defined to use this model:

- It is assumed that the VuAB is moving in a purely vertical direction after discarding the heat shield;
- It is assumed that the time between the moment of discarding the heat shield and deployment of the parachute is 2 seconds. Similarly, when the drogue parachute pulls the parafoil out, it is assumed that it takes 1 second to deploy the parafoil, during which the drag of the parachute does no longer act on the VuAB;
- The parafoil is able to deploy from an altitude of 7567 m [7] and in order to maximize the gliding flight it is

[6] Private contact, Airbus Defense and Space (client), J. Offerman

[7] `http://www.militarysystems-tech.com/files/militarysystems/supplier_docs/Airborne-Products-Brochure.pdf`, [15-01-2017]

chosen to optimize for deployment at this altitude;
- The parachute is assumed to have a C_d value of 1.4, similar to the Orion[Section 3.2.2]. The parafoil is modelled as a flat plate while moving vertically at the moment of deployment, so a C_d value of 1.28 is used [8]. The drag coefficient is estimated at 1.1 using Figure 4.26;
- The parafoil is sized at 836 m^2, as described in section Section 4.3.1, and is able to handle an opening shock of maximum 4.5 g [9]. However, a safety margin of 30% is taken into account, so the drogue parachute will be designed in such a way that maximum 3 g's will act on the parafoil;
- As stated in Section 3.2.2, the parafoil is split into five sections which deploy outwards (so-called reefing), in order to reduce the forces acting on the parafoil. The percentages of deployment per phase are found to be 23%, 36 % and 41% [26]. It is estimated that the deployment of the second part happens after 5 seconds and the deployment of the third segment after 8 seconds.

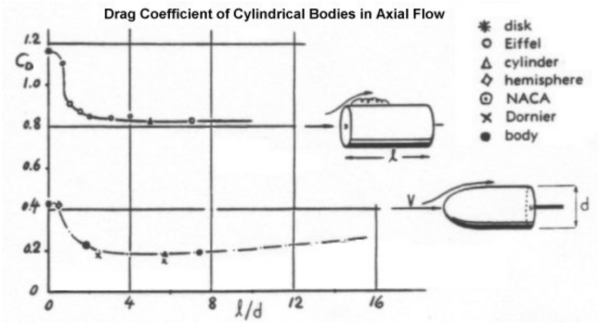

Figure 4.26: Drag coefficient for a cylinder, [28]

Using the model, assumptions and input parameters as stated above, the drogue parachute is sized for optimal parafoil performance. This means the parafoil is deployed at 7567 m altitude while not exceeding the 3 g limit. Furthermore, it is chosen to limit the amount of time the drogue parachute is deployed to the time during which the parachute still decelerates the VuAB. This is chosen as a parachute at low speed will have a lower accuracy than the heat shield at a high velocity due to for example the drift by wind. This results in a parachute deployment altitude of 8080 m, with a size of 47 m^2. The resulting acceleration of the VuAB, the velocity profile and flight path is shown in Figure 4.27. It can be seen that the maximum amount of deceleration for the parafoil is obtained with less than 3 g. The maximum forces induced by these accelerations are 180.7 kN during the deployment of the parachute and 212.8 kN during the deployment of the parafoil.

4.3.5. Parachute and Parafoil Systems Design

This section discusses the design choices and sizing made regarding the the supplementary systems of the parafoil and the parachute. The systems include the canopy, deployment device and control system of the parafoils and parachute. The system sizing includes system mass as well as packed volume sizing.

Canopy

Due to space constraints it is essential that the entire parachute system, including the parafoil, drogue chute, deployment system and control system are packed as efficiently as possible. Airborne Systems, the company producing the MegaFly parafoil system could not share packing data [10]. Using a literature study a value of 720.7 kg/m^3 was found for the packing density, using a pressure packing technique which applies a pressure of approximately 6.89 bar [34] [48]. Using this value an estimation is made on the entire parachute system packing size.
- Drogue parachute: the drogue parachute is 47 m^2. Using historical data it is estimated that the mass for this drogue chute is 47 kg, including everything but its deployment mechanism [3]. Packing this in the same manner as the parafoil would amount to 0.0652 m^3;
- Main parafoil: an estimation on the combined mass of the parafoil system is 435.45 kg, which is comprised of the canopy itself, spectra suspension lines, spectra composite slider and a suspension line confluence

[8] https://www.grc.nasa.gov/www/k-12/airplane/shaped.html, [15-01-2017]
[9] Private contact, E-mail, Airborne Systems, K. Hempe
[10] Private contact, E-mail, Airborne Systems, K.Hempe

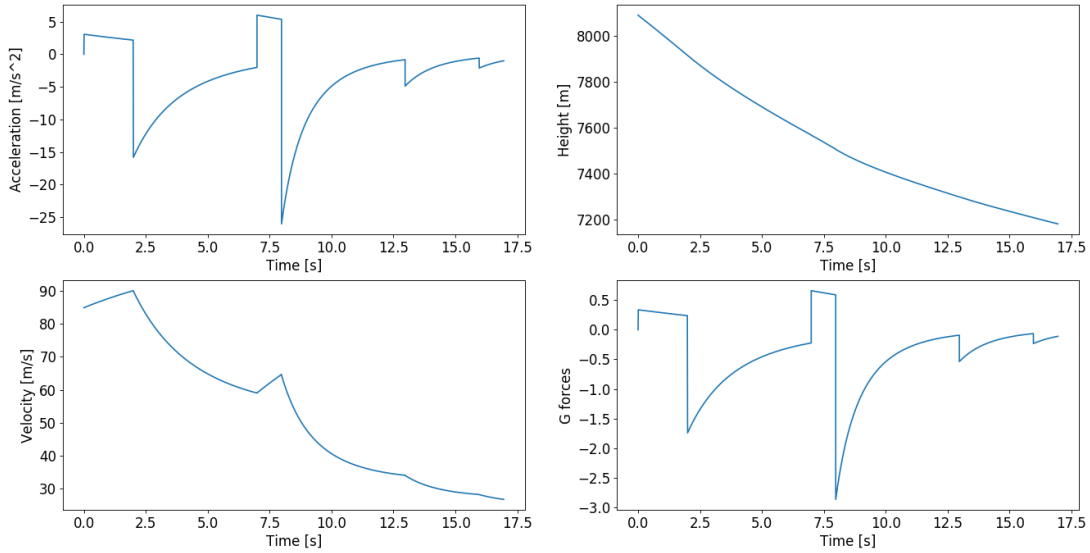

Figure 4.27: The acceleration, altitude, velocity and g-forces throughout the deployment phase of the drogue parachute and parafoil

hardware assembly [15]. Packing this using the aforementioned packing method would result in a packing size of 0.604 m^3;

– Secondary parafoil: the secondary parafoil has an area of 18.71 m^2. Using historical data [3] and the required estimated secondary parafoil line mass it is estimated that the mass for these systems is 75.67 kg including the parafoil and cable. Packing this in the same manner as the parafoil would amount to 0.105 m^3.

Deployment Device

Controlled parachute deployment starts with the forced ejection of a parachute compartment cover or a drogue gun slug that, in turn, pulls a pilot chute, or first-stage drogue chute, away from the air vehicle and into good airflow behind the vehicle. Mortar ejection or rocket extraction may also be used for forced deployment of pilot or drogue chutes [33]. A positive ejection of the pilot chute or first-stage drogue chute, as provided by a drogue gun, mortar, or extraction rocket, is mandatory whenever the parachute must be deployed from a spinning or tumbling vehicle or through the wake of a large forebody, the latter of which is the case for the VuAB recovery system. [33]

In the case of the VuAB this technique is used as follows: the drogue parachute is ejected using a forced ejection. The parafoil is attached to the drogue parachute. When the dynamic pressure is low enough for the parafoil to deploy it is deployed. During deployment a riser also deploys, which facilitates that the steering and load carrying lines of the parafoil do not make contact with the outer skirt. If this riser would not be present this would be the case. This is called a controlled deployment [33]. Below a sizing is done on the drogue parachute ejection method.

Several deployment methods exist:

– Drogue gun;
– Mortar deployment;
– Rocket extraction.

Drogue gun deployment is limited to a load of 0.91 kg and is therefore discarded as an option. The mortar gun is the most widely used system for parachute deployment. The advantages of mortar gun deployment are its low complexity, wide application due to its high success rate and its proven capabilities for deploying systems of more than 50 kg [33]. The drogue chute has a mass of 60 kg, which is a 20% higher than this. It is assumed that this mass can still be launched using a mortar. Disadvantages of the mortar deployment method are its large mortar body and the possibly large reaction force it exerts on the system. At this point this reaction force is neglected as it will have a minimal effect due to the high mass and momentum of the VuAB. The rocket extraction method has

the main advantage that its reaction force on the system it launches from is minimal. A disadvantage is its higher complexity when compared to the mortar gun deployment. Because of the fact that the reaction force effect of the mortar is neglected and its proven capabilities, the mortar deployment method is chosen as the system for deployment of the drogue parachute.

Due to a lack of data on mortar deployment systems sizing a comparison is made using a system used for deployment on Mars. The mass of this system is 26 kg, which is used to deploy a 50-60 kg drogue parachute into Mars atmosphere at supersonic velocities [2]. While Mars' density and gravity are lower, the mortar system in the VuAB deploys the drogue parachute in the low subsonic regime and thus it is assumed that this requires reduced forces compared to a supersonic ejection and thus the system of 26 kg is also applicable to the VuAB. Actual dimensions of such a system are not found.

Control system

The control system of the MegaFly system suited for the purpose of the VuAB recovery has a mass of 32.66 kg, 20% of that of the AGU of the MegaFly [65] (as talked about in Section 4.3.3). This lower mass is due to the fact that the required capabilities of the system are lower than what the standard AGU offers[11]. As sizing on this did not deliver sufficiently accurate results it is assumed that for this also the parachute density approach can be used. Due to the AGU consisting out of materials with mostly higher densities than that of the parafoil the estimated value of 0.0453 m^3 is a conservative one.

Final sizing

Adding the masses of the sized packing values of all the aforementioned elements leads to the following: a total mass of the parachute recovery system of 740.1 and a total packing size of 1.028 m^3. A safety margin of 20% is taken into account for estimation errors and system elements not yet taken into account properly. For example, as can be seen in Figure 4.28 there are multiple elements such as a riser and deployment bags that are not taken into account in the initial mass and packing density estimations. The systems, their masses and their volumes are shown together in Table 4.6.

Table 4.6: Parachute system masses and their respective volumes

System	Mass [kg]	Volume [kg/m^3]
Drogue parachute	47.00	0.065
Main parafoil	435.5	0.604
Secondary parafoil	75.67	0.105
Mortar	26.00	0.036
Control system	32.66	0.045
Margin	123.4	0.171
Total	740.1	1.028

4.3.6. Parachute system Load Introduction

Both the packed and deployed configurations of the parachute and parafoil are subjected to various types loading. This is evaluated for structural integrity. This section summarizes the types and magnitude of the expected loads on the support structure as well as the sizing of the structural components.

Packaging Configuration

As the package containing the parafoil, parachute, AGU and other components will be located within the cross, a supporting structure has to be sized to carry this package. The total mass of this package is determined to be 740.1 kg in Section 4.3.5 and the size a bit more than 1 m^3. During launch, with a maximum acceleration of 6 g, the maximum load will be 38.7 kN. In order to support the package during launch and absorb these loads, a beam will be used. During re-entry the maximum deceleration will also be about 6 g, so the beam should be designed for these loads. As a preliminary estimation for mass and natural frequencies, an I-beam is used, which will be attached to the structural cross of the VuAB. With the size of 1 m^3, it is assumed that the centre of gravity of the package will be located 0.5 m away from the cross. Furthermore, a margin is taken into account in order to prevent the package from hitting the cross while vibrating of 0.1 m.

[11] Private contact, Airbus Defense and Space (client), J. Offerman

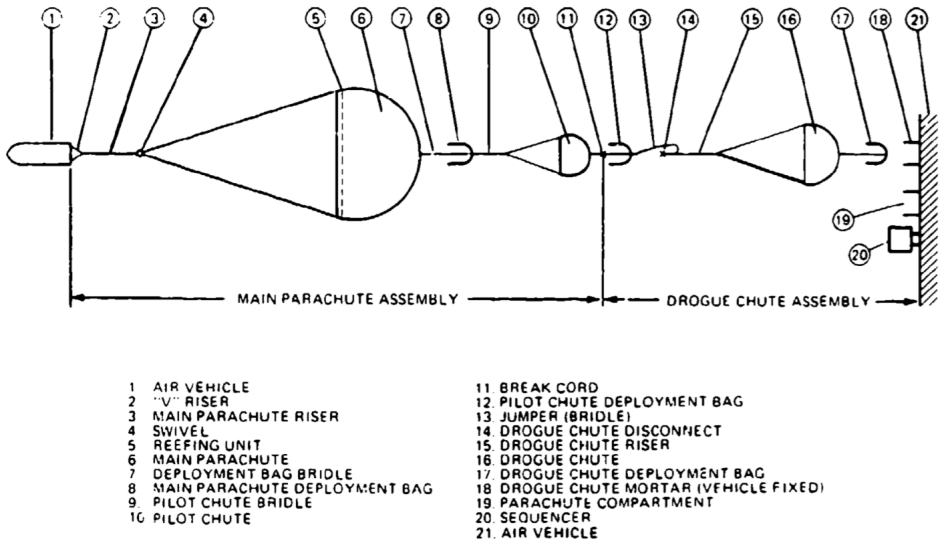

Figure 4.28: A typical parachute recovery system that consists of a drogue-chute assembly and a main parachute assembly [34]

This moment arm of 0.6 m and the maximum force of 38.7 kN results in a maximum moment on the root of the beam of 23.2 kNm. In this preliminary sizing the I beam is assumed to have a constant thickness and flanges of the same size, resulting in a moment of inertia as determined with Equation (4.24),'b' being the size of a flange. Like all structural elements, aluminium 7075-T6 is used for the sizing, with a density of 2801 kg/m^3. Using Equation (4.25) and the resulting weight of the beam, 'b' and 't' are sized by optimizing for the resulting mass. As a safety factor is already taken into account in the mass estimation, none will be used in this calculation.

$$I_y = \frac{t^3 \cdot b}{12} + \frac{b^3 \cdot t}{6} \qquad (4.24) \qquad \sigma_y = \frac{-M \cdot y}{I_y} \qquad (4.25) \qquad I_x = \frac{t \cdot b^3}{12} + \frac{b \cdot (2 \cdot t)^3}{12} \qquad (4.26)$$

This results in a b of 0.07 m and a thickness of 0.03 m. Using these values, the natural frequencies in x, y and z direction are determined. For this purpose, the equations and simplifications as described in Section 3.2 are used, with the values as described above. From this analysis, it is concluded that the the natural frequency in axial (x) direction exceeds the requirement, while the natural frequency in z direction is 51 Hz, and in y direction 54.5 Hz. Therefore, it is chosen to slightly increase the flange size of the beam to 0.08 m, resulting in a mass of the beam of 12.1 kg, while the requirement for moment is met with a maximum stress of 338.7 MPa (σ_y = 480 MPa). The natural frequencies with this design are f_{n_z} = 62.0 Hz, f_{n_x} = 1101 Hz and f_{n_y} = 61.8 Hz, which meets the requirements.

Deployed Stage Load Introduction

For the drogue chute and parafoil to decelerate and steer the VuAB during atmospheric flight the loads must be introduced into the VuAB. The loads must be introduced symmetrically about the longitudinal axis of the VUAB to avoid swinging motion of the payload. The attachment points are placed onto the ends of the VUAB's cross shaped structural element. This choice is natural as this element is made to introduce the Vulcain engine loads into the Ariane 6. The cross is extremely stiff and strong so it is well equipped to handle the deployment loads. The parafoil and drogue chute will be packaged elsewhere in the VuAB, both connected to the same attachments by separate lines. The attachments are placed at equal distances from the longitudinal axis of the VuAB so that the parafoil and drogue chute loads do not create moments, this is favourable for parafoil performance and controllability.

A single attachment does not account for redundancy. Two attachments placed opposite one another allow for swinging about the axis the attachments are placed on. As the cross has internal angles of 90 degrees, three attachments can not work symmetrically. So four parafoil attachments are chosen. For the sizing, it is assumed that the loads are introduced exclusively to one of the attachments. The driving load case for the attachment is the deployment of the parafoil as determined in Section 4.3.4: $F_{Parafoil}$ of 212 kN . The drogue parachute load case is lower, so the attachment will be oversized for it.

To reduce the structural mass, the loads are introduced into the attachment vertically. This can be achieved by having a square constraint attached to the 4 ropes constricting the ropes above the attachments.
For a square profiled attachment of sides a and height b, the maximum stress is shown in Equation (4.27).

$$\sigma = \frac{F_{Parafoil}}{a^2} \tag{4.27}$$

The attachment will be sized for this case and made out Aluminium 7075-T6 with yield strength σ_y of 480 MPa and a load safety factor of 1.1. Rearranging to solve for a:

$$a = \sqrt{\frac{212 * 1.1 * 10^3}{480 * 10^6}} = 22 \text{ mm} \tag{4.28}$$

As the stresses are independent of the height of the attachment b, it can be set at 20 mm to reduce weight. The mass of the attachment assuming a density of 3000 $\frac{kg}{m^3}$ yields a weight of 30 gram per attachment and 120 gram in total. During a detailed design the design of the attachment will evolve into a bracket to accommodate fasteners and so the weight of these attachments will increase. Regardless, the parafoil attachments will not play a significant role in the systems overall mass.

4.3.7. Detachment Sizing

While attachment of the drogue chute and parafoil is an important factor, detachment is as well. As can be seen in Section 4.4.1, both the drogue parachute and parafoil are detached. Both are attached to the attachments sized in Section 4.3.6. Detachment can be done using multiple systems. The disconnect may be of mechanical, pyrotechnical, or combined designs. [34] Anchor bracket detachment method are a feasible.[12]

The drogue detachment of the four anchor points occurs when the parafoil needs to deploy. It is detached using one of the above mentioned methods and due to its high drag compared to its mass it slows down, pulling on the parafoil packing and initiating deployment of the parafoil. The parafoil detachment occurs in a slightly different manner. After catch, when the weight of the VuAB is taken up by the helicopter entirely, the parafoil control mechanisms apply brakes in order for the parafoil to experience more drag and position itself oriented backwards, after which it is decoupled. The extra drag generated by the parafoil ensures that it moves back, clear of the VuAB structure and its connection to the helicopter. Detachment would be done after confirmation is given that the load of the VuAB is entirely taken on by the helicopter and the control mechanism on the parafoil has lowered the trailing edge.

Volume and mass sizing of these detachment systems is not done due to a lack of available sources. Therefore, it is assumed that these are incorporated in the sizing of the entire parachute system, stated in Section 4.3.5.

4.4. Catch

This section discusses the recovery phase of the mission. This is done by first discussing the coupling method in Section 4.4.1, then the catch mechanism on the helicopter in Section 4.4.1, the loads introduced by performing the catch manoeuvre in Section 4.4.2 and finally the helicopter stability in Section 4.4.3. This section will cover function F 3.4.2 and F 3.4.3 from Figure 2.8.

4.4.1. Coupling

In deciding which coupling method has to be used, a literature study is done on methods for retrieving craft using a helicopter. During this study the following is found: the large aerodynamic drag and the flapping motions of collapsed of partially collapsed parachutes in helicopter tow make it impractical to tow parachutes of about more than 45 feet in diameter with the available helicopters [33]. As the MegaFly system has a span more than three times bigger than the mentioned 45 feet it is decided that in order for a helicopter to tow it the parafoil needs to be detached entirely[13]. In order to make this detachment possible only methods inducing no interference between the helicopter towing line and the parafoil are considered. Additionally, due to the high mass of the VuAB a large, heavy load helicopter is to be used to perform the retrieval. This might induce downwash effects on the parafoil, which might have a negative effect on the parafoil's flight dynamics. The exact aerodynamics involved in this are not investigated in this report, however, only retrieval methods allowing for a distance of two rotor

[12] Private contact, Airbus Defense and Space (client), J. Offerman
[13] Private contact, Airbus Defense and Space (client), J. Offerman

diameters[14][15][24] between the helicopter and the parafoil system to exist are considered in order to mitigate these potential effects.

Coupling methods

Through the insights gained in the literature study three potentially viable methods are generated. Recovery methods requiring pole assemblies are discarded due to their relatively high mass (considering the two rotor diameter recovery distance) for recovering a craft as heavy as the VuAB, reducing the effective altitude at which the helicopter is able to perform the recovery. This effective altitude for recovery is discussed in more detail in Section 7.1.3.

- Method 1: a line is attached to the VuAB in front of the parafoil, after which it is attached to its leading edge and trails over and after the parafoil. This line is then caught using a hook which is attached to a line below the helicopter, after which the loads are transferred from the parafoil to the helicopter. This method is shown in Figure 4.29a, depicting the main catch load line in red.
- Method 2: an attachment directly on the VuAB itself. This can be done using either a line on attached to the rear of the VuAB, which the helicopter catches, or a helicopter assembly attaching directly to either the front or back of the VuAB. The former is shown in Figure 4.29b, depicting the main catch load line in red.
- Method 3: Figure 4.29c displays a method in which a tandem parachute combination is used, where the smaller parafoil is used as the location where the hook can attach. The smaller parafoil has its own line able to carry the lift of the entire parafoil. This method is shown in Figure 4.29a, depicting the main catch load line in red.

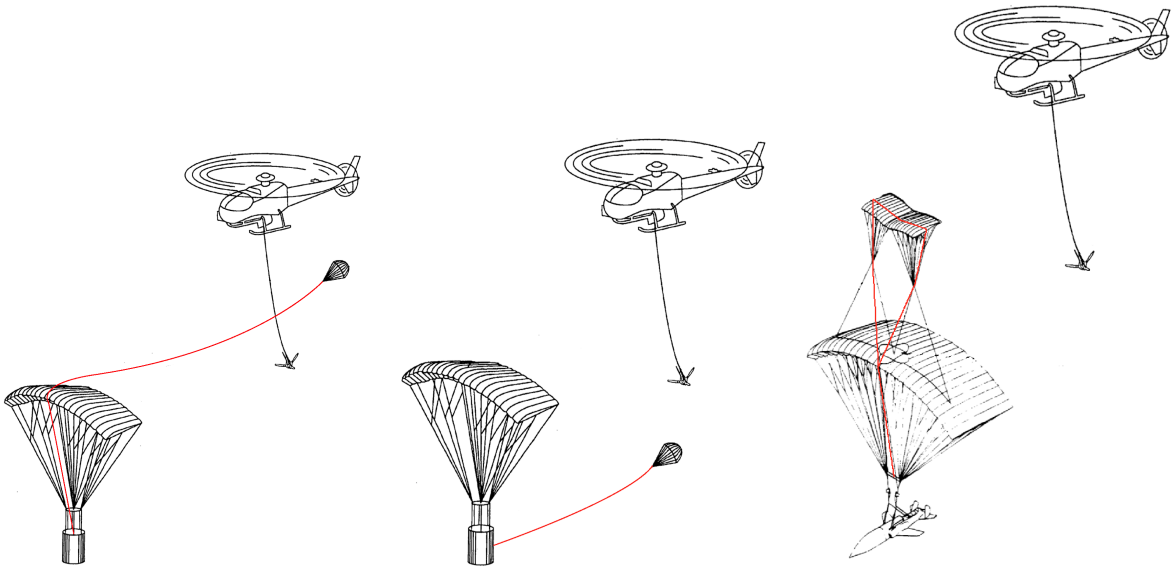

(a) Method 1: retrieval method using a trailing line behind the parafoil

(b) Method 2: retrieval method using a VuAB attachment

(c) Method 3: retrieval method using a tandem parafoil combination

Figure 4.29: Methods for coupling the VuAB to the helicopter[16]

Method 2

Method 2 is discarded for the following two reasons. First, connecting the helicopter to a line attached to the back of the VuAB is possible, however, this would mean that the parafoil detachment is hardly possible as it is positioned in front the line connecting the helicopter and the VuAB. Thus, detaching the parafoil would interfere with the catch line of between the helicopter and the VuAB. Second, attaching the helicopter to the front of the VuAB is not preferred as for this an attachment has to be present on the side of the VuAB. This has to either be present during launch, which involves negative aerodynamic effects, or it can appear after re-entry, which is unnecessarily complex.

[14] https://www.faa.gov/documentLibrary/media/Advisory_Circular/AC_90-23G.pdf, [12-01-2018]
[15] http://wikirfm.cyclicandcollective.net/ground-lessons/downwash/, [12-01-2018]

Method 1

This leaves method 1 and 3. First, method 1 is investigated. In order to position the line in a stable longitudinal location it would need a small drogue chute attached to it. In order to determine whether a parachute is necessary and possible to ensure a stable longitudinal position behind the parafoil an estimation is made on the mass and length of the line and the forces it might induce on the parafoil. This estimation is made assuming a longitudinal length of 63 meters for the line, neglecting the line section from the leading edge of the parafoil to the VuAB. This is derived from the fact that the chord of the parafoil is 16.3 m and a distance of two rotor diameters (one rotor diameter is 24 m, the choice for the helicopter type is discussed in Section 7.1.3) is chosen in order to minimize aerodynamic effects of the helicopter rotor that would affect the parafoil, as stated before. Taking a line that is able to carry the maximum loads that it would have to take (discussed in Section 4.4.2) a mass of 65.96 kg is found [64]. This line material is chosen as it has a high Young's modulus and thus a low strain (in the order of 0.003989). This low strain is desirable as the VuAB has to be landed using the line as well. During landing elongation and shortening of the line should be minimal as to not damage the VuAB during landing. In order to size the parachute and the loads it will exert on the parafoil it is assumed that the orientation of the parachute is along the line of the wind velocity travelling along the VuAB. Using a general drag coefficient of 1.75 for a parachute [17] the required area of the parachute is calculated. This is then iterated upon using the model for the atmospheric flight Section 3.1.4 and a diameter of 4.25 and an area of of 14.20 m^2 is found for the parachute. The atmospheric flight model outputs a decrease in glide range from 27 km without the drogue chute carrying the drogue line to 13.8 km, as well as an increase in downward velocity with the drogue chute. Both are not desirable as they decrease the time the helicopter has for retrieving the VuAB. The main reason why this retrieval method is not an option is due to the longitudinal force of 2878.53 N the drogue chute induces on the leading edge of the parafoil, where the line passes along and over the parachute. The parafoil is not able to cope with these loads. The parafoil would have the risk of being damaged due to the friction the line introduces and its aerodynamics would significantly change due to the force working on the leading edge[18].

Method 3

This leaves method 3, the tandem parafoil configuration. The secondary parafoil would be located above the leading edge of the main parafoil, connected directly to the VuAB with a line which is capable of coping with the loads during the recovery operations with the helicopter. Whereas method 1 induces longitudinal forces on the leading edge of the parafoil due to a drogue parachute to keep a line in stable longitudinal position behind the main parafoil, this method does not necessarily induce forces on the main parafoil. In order to minimize these forces, the secondary parafoil is designed to have the same lift over drag ratio as the MegaFly system. The size of it is estimated based on the lift it has to provide, which is the mass of the line it is required to carry. Using the same line characteristics as in the previous paragraph and a length of 54.4 m it is estimated that the secondary parafoil has an area of 18.71 m^2, a span of 7.71 m and a chord of 2.43 m. The length of the line is estimated as follows: 30 m for the line from the VuAB to the leading edge of the parafoil, two times 8.41 m (assuming a secondary parafoil height of 7.5 m) for the lines going from the leading edge of the main parafoil to the edges of the secondary parafoil and one line covering the secondary parafoil span of 7.71 m. In essence, the lines from the leading edge of the main parafoil loops along the secondary parafoil, in order to make a helicopter able to connect to it. Forces generated by local differences in velocity in between the secondary and main parafoil are assumed to be neglegible. Additionally, at the leading edge of the main parafoil, where the line of the secondary parafoil passes the line is held by a ring of sorts, allowing for up and down movement of the line, but reducing longitudinal movement. Thus effectively reducing the forces exerted on the leading edge of the parafoil to zero. The secondary parafoil is initially packed on top of first cell of the main parafoil. If the first cell is completely deployed the deployement sequence can start on the secondary parafoil [19].

As method 3 seems the most probable while exerting minimal loads on the parafoil this is chosen as the final recovery concept.

Helicopter attachment

Using method 3 the helicopter is positioned in front of the parafoil, with a line trailing behind it to which a simple hook of non-clamping design is attached in order to perform the attachment. Non-clamping design is preferred

[17] https://www.grc.nasa.gov/www/k-12/VirtualAero/BottleRocket/airplane/rktvrecv.html, [10-01-2018]
[18] Private contact, Airbus Defense and Space (client), J. Offerman
[19] https://www.google.com/patents/US6824102, [15-01-2018]

as this reduces the probability of error. Due to the required distance with respect to the parafoil no attachment can be made to the secondary parafoil using a pole of sorts as the mass of the system on the helicopter would be too big.

The line trailing the helicopter has to be supported by a drogue parachute, drogue basket, or combination of both to ensure a stable longitudinal position. For the purpose of this concept study it is assumed that even though a drogue parachute does not offer any control this is sufficient for now, as not enough data is found on controllable drogue basket designs. The line has a length of 49 meters, of which it is assumed that the drogue parachute has to support half its mass, whereas the helicopter carries the other half. Additionally, a basic mass estimation for the attachment component is added [64]. This leads to a drogue parachute with an area of 7.17 m^2 and a diameter of 3.02 m.

A conservative mass estimation of the catch mechanism on the helicopter is made based on reference data [45], resulting in a total mass of 738.8 kg. This includes the entire hoist system: a drum assembly, reeving system, hydraulic lines, valves, electric system components, helicopter drogue line and drogue parachute.

Recovery line length

The tandem parafoil catch method is shown in Figure 4.30. As can be seen, the line during recovery is all the stated lengths in the figure added together. The length of 30 m is the length of the line from the VuAB attachment tot the leading edge of the main parafoil. The 8.41 m is the length of the line from the leading edge of the main parafoil to the tips of the secondary parafoil. The 3.8 m is half the span of the secondary parafoil (adding the latter two together gives the length of the line between the leading edge of the main parafoil and the helicopter drogue line). Finally the helicopter line is 49 m. This results in a total line length during catch of 99.21 m, which is used to calculate the loads during catch in Section 4.4.2. After catch this line is reeled in as far as possible, which reduces the line length to 42.21 m. It can only be reeled in 49 m as at that point the attachment of the helicopter line to the secondary parafoil is in the way of reeling it in further.

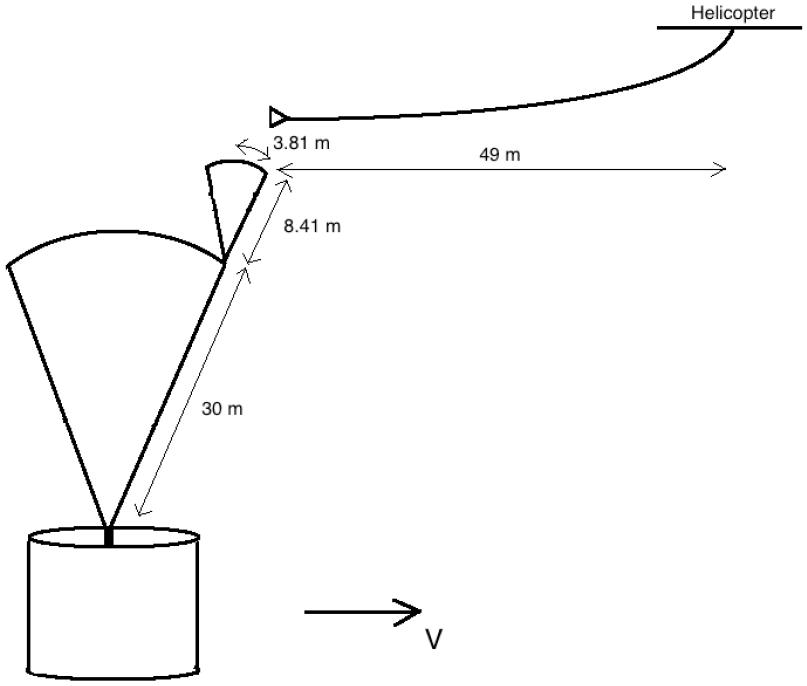

Figure 4.30: Tandem parafoil catch method line lengths

4.4.2. Catching Loads

The input variables for the model described in Section 3.2.3 are in the following three categories:

1. Assumptions:
   - Initial absolute velocity difference between helicopter and VuAB is assumed to be: $V_{h,V} = 3$ m/s;
   - Gravitational constant at height of catch: $g_{0,catch} = 9.81$ m/s^2.
2. Design parameters:

- Maximum swinging velocity of the VuAB in longitudinal and lateral flight direction of the helicopter: V_{m,S_lon} = 11.5 m/s, $V_{m,S_{lat}}$ = 1.7 m/s;
- The minimum length of the cable between the helicopter and the VuAB: l_{min} = 89.2 m;
- The maximum tension force due to the drag force on the VuAB during catch: $F_{T,D_max,V}$ = 123 m
- Mass of the VuAB at the moment of catching: $m_{V_{catch}}$ = 7173 kg;
- Mass of the attenuation system including elongation cable: m_{att} = 738 kg.

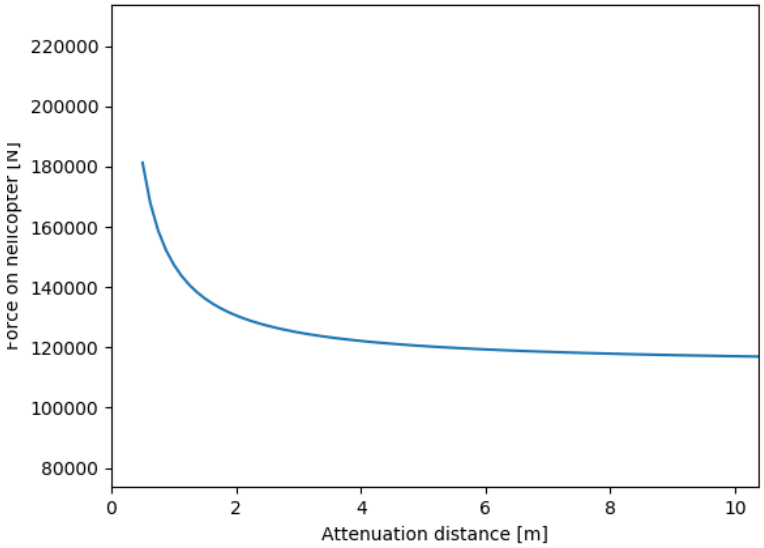

Figure 4.31: The force on the helicopter as a function of the attenuation distance.

3. The iteration parameters are:
   - VuAB catching height h_c in m;
   - Maximum allowable helicopter payload weight at the catching height: $m_{max,h,p}$ in kg;
   - Attenuation distance d_a in m.

In the model output from section 3.2.3 visualised in Figure 4.31 it can be seen that the added return of extra attenuation length diminishes significantly after 6 m Combined with the helicopter choices discussed in Section 7.1.3, the attenuation distance is set at 8 m at an absolute velocity difference between the VuAB and helicopter of 3 m/s at the moment of catch.

4.4.3. Helicopter Stability

In order to use the model outlined in Section 3.2.4 boundary and input values need to be determined, these values are recapped in Table 4.7. Sea-level values are used for g_0 and ρ. Geometry of the VuAB comes from the client. The total mass of the VuAB with the recovery system is shown in Table 4.13. The VuAB velocity at catch is an output from the atmospheric flight computed using the model in Section 3.1. The helicopter velocity at catch uses the delta-V from the attenuation device design in Section 4.4.2. As the helicopter will match its rate of descent with the VuAB during catch, only the longitudinal velocity is used.

The drag coefficient is estimated through the Reynolds number in Equation (4.29). From Figure 4.32 a C_D of 0.75 was taken. The frontal area of the VuAB during the catch is shown in Equation (4.30)

$$Re = \frac{\rho_0 \cdot \pi \cdot D_{VuAB} \cdot v_{VUAB}}{2 \cdot \mu} = 1.15 \cdot 10^7 \tag{4.29}$$

$$S_{VUAB} = h_{VUAB} \cdot D_{VUAB} = 27.7\text{m}^2 \tag{4.30}$$

The total cable length from the VuAB to the helicopter, l, is calculated using the diagram in Figure 4.30, the following parameters: d from Table 4.2, the distance between parafoils and catch parafoil span from Section 4.4.1 and the length of the line on the helicopter side from Section 4.4.1, l_{cable}. l is computed with Equation (4.31).

Table 4.7: Input variables for the helicopter stability model

Parameter	Symbol	Value
Gravitational acceleration at sea level	g_0	9.81 $\frac{m}{s^2}$
Air density at sea level	ρ_0	1.225 $\frac{kg}{m^3}$
VuAB height	h_{VUAB}	5.134 m
VuAB diameter	D_{VuAB}	5.4 m
VuAB Drag Coefficient	C_D	0.75
VuAB mass	m_{VUAB}	7172 kg
Cable length	l	99.2 m
VuAB velocity	v_{VUAB}	18 $\frac{m}{s}$
Helicopter velocity	v_{Heli}	21 $\frac{m}{s}$

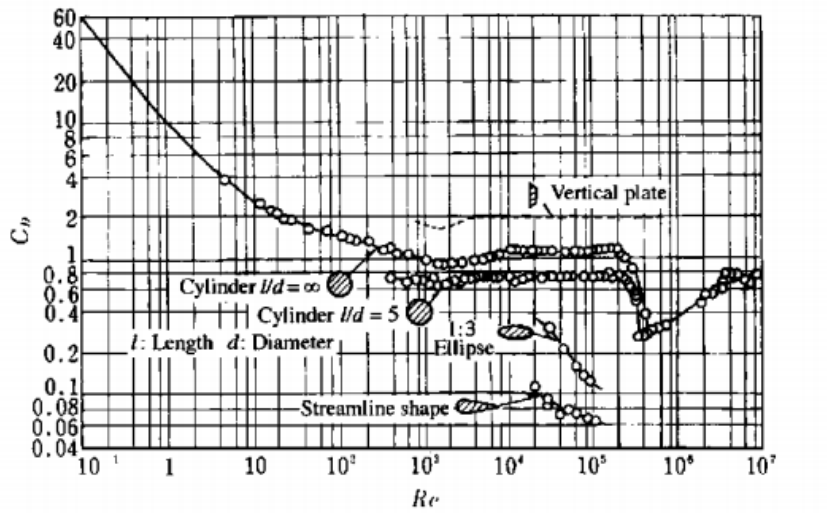

Figure 4.32: Variation of cylinder drag coefficient with Reynolds number

$$l = d_{parafoil} + \sqrt{h_{catch}^2 + \left(\frac{b_{catch}}{2}\right)^2} + \frac{b_{catch}}{2} + \frac{b}{2} + l_{cable} = 99.2\text{m} \tag{4.31}$$

Using the desired performance for cargo helicopters in lateral position from [27] of 3 ft, initial lateral pendulum conditions are derived. Similarly the initial angular velocity laterally is acquired by decomposing the velocity vector using a heading uncertainty angle [27].

The initial angular conditions for the longitudinal pendulum are determined at the moment the cable is fully extended and begins to exert a force on the VuAB. At this point the helicopter is flying 2 rotor diameters in front of the VuAB or 48 m. The angle can be worked out using the total cable length l, yielding 29°. The initial angular velocity is determined from the pre-catch delta-V (3 m/s) and the length l. At the point the swinging begins, the attenuation device has already made up for the difference, however it is deemed to be a more conservative analysis by accounting for this velocity difference. The initial pendulum conditions are shown in Table 4.8.

The distance from the helicopter attachment point to the C.o.G. of the helicopter, d, is estimated to be

Table 4.8: Initial Pendulum Conditions for the model in Section 4.2

	θ_0 (rad)	$\dot{\theta}_0$ (rad/s)	$\ddot{\theta}_0$ (rad/s^2)
Lateral	0.009	0.018	0
Longitudinal	- 0.49	- 0.030	0

1.94 m from technical drawings of the CH-53K. Finally the helicopter inertias about the body X and Y axes is determined. Assuming these values are the same as those from a mathematical model of a CH-53, I_{xx} and I_{yy} come out to 56,000 and 268,000 kg/m^2 [63]. The mass of the helicopter, m_{heli}, is taken as 38,400 kg [63].

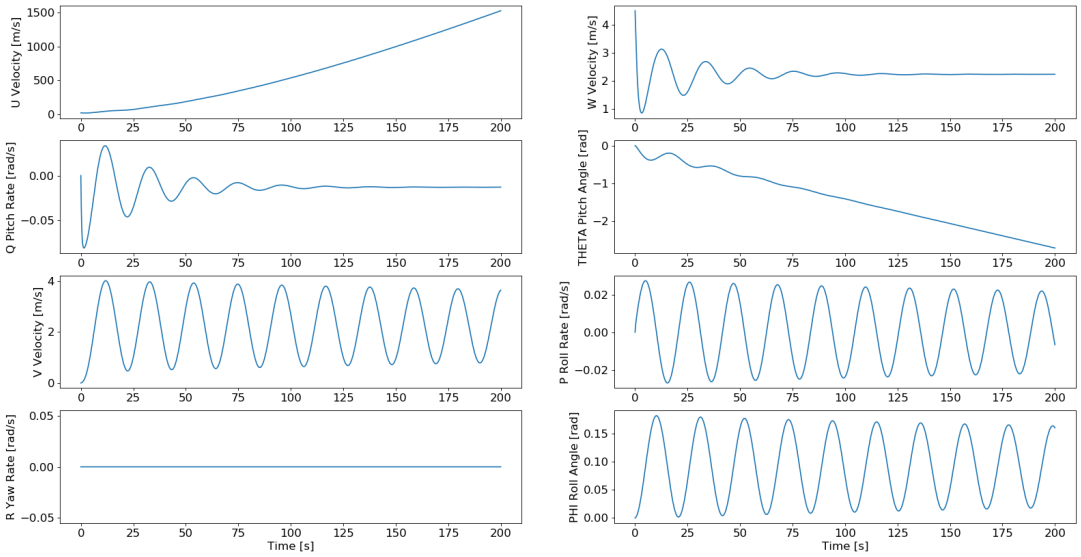

Figure 4.33: Helicopter states with no pilot inputs

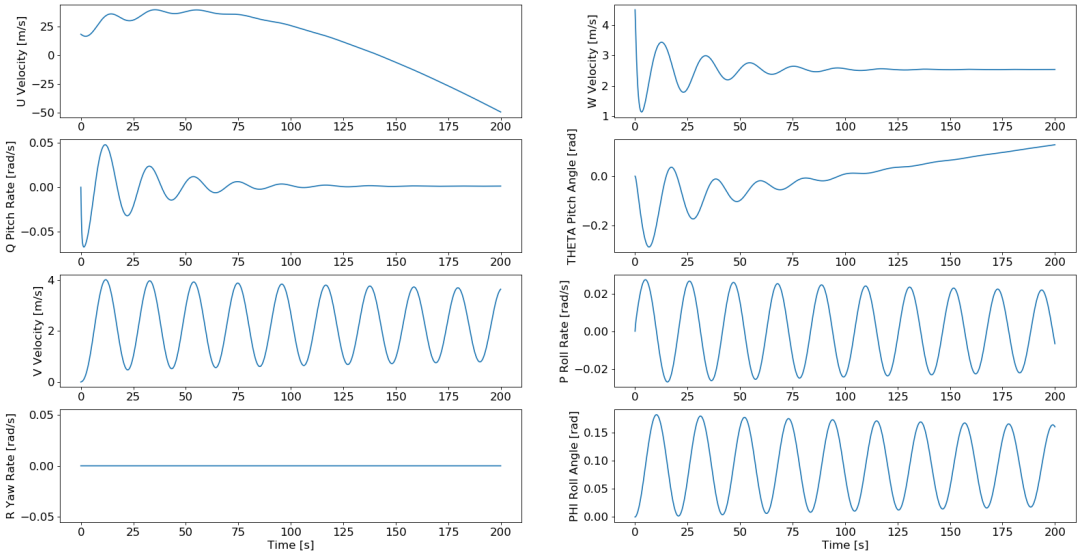

Figure 4.34: Helicopter states with constant δ_b input of -0.0608728

The time development of the helicopter states without control surface inputs is shown in Figure 4.33. Upon inspection u and θ appear to be unstable. ϕ, p and v seem to be neutrally stable at acceptable amplitude values, this behaviour is due to the lateral swinging of the VuAB as their peaks align in time with one another and the VuAB swinging. W and q demonstrate stable behaviour, with a non zero steady state that can be corrected to

zero by pilot inputs.

Pitch correction

The behaviour in u follows from the behaviour in θ which in turn is a result of q converging to a non zero value. To correct this the input matrix is extended to include the pilot inputs. The appropriate changes are made to the B matrix to accommodate this. With simple trial and error δ_B is set to a constant value of -0.0608728 rad. The helicopters response is plotted in Figure 4.34.

With the pitch rate converging much closer to 0 (order 10^{-5} rad/s) the largest θ angle is reduced by an order of magnitude. With some tweaking the unstable behaviour displayed near the end of the plot can be mitigated, by changing the input around 100 seconds. The u velocity also displays diverging behaviour around the same time. If the proposed tweak to the δ_B input is followed through on, the u velocity will also converge.

Roll behaviour correction

The asymmetric response of the helicopter is very slightly damped with very low amplitude. In a further investigation into helicopter stability, a PID controller could be implemented to make the roll rate, roll angle and Y velocity converge to 0 in a more aggressive manner. As the stability coefficients in the A matrix used in this model are for a scout/attack helicopter. It is conceivable that these stability coefficients lead to more agile and unstable response to inputs, as this is desirable behaviour for vehicles of that class.

4.5. Electrical Design

This section contains the design of the electrical system, including the communication and data handling, sensors and the power supply.

4.5.1. Data and Communicational Flow Diagrams

Before an estimate can be made for the sizing of the Communication and Data Handling system, one must know what kind of communication and data flows are present in the system. By knowing this, the required components can be determined and an appropriate sizing estimate can be made. Also, a link budget can be presented, if a decent data flow diagram and a communication flow diagram are present. The data flow diagram shows all data flows within the system, whereas the communication flow diagram shows the interaction with the system and its environment. The data flow diagram can be seen in Section 4.5.2.

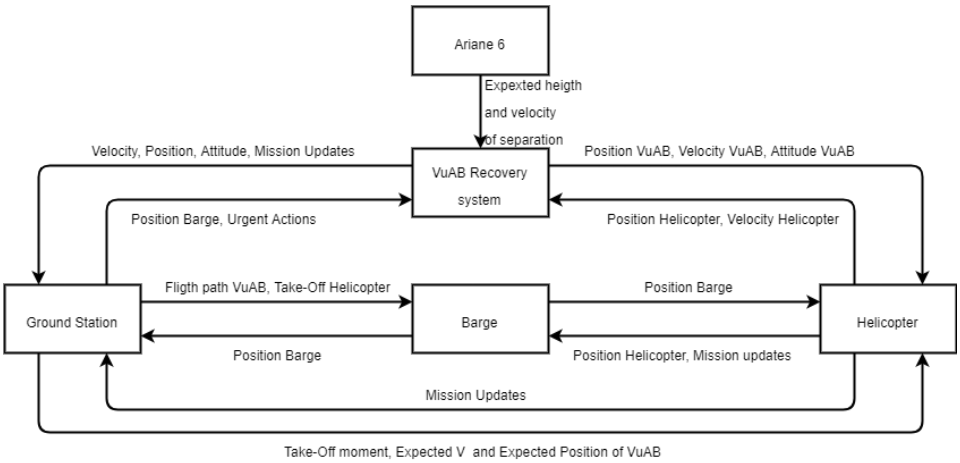

Figure 4.35: Communication Flow Diagram

The communication flow diagram is shown in Figure 4.35. As mentioned before, this diagram shows the interaction of the system with its environment. All the communication links are shown in this diagram. The first and most important link is that of the system with its ground station. The system sends all its data to the ground station. This includes the velocity of the system, the position and attitude of the system, but also all the mission updates. These are all actions performed by the system. The ground station, sends the position of the ship to the system. This allows the system to change its flight path when needed to reach the landing area. Also, the ground

station is always able to interfere with the system and to take over control when the system itself malfunctions. As mentioned before, the position of the ship is send to the system by the ground station. So, the ground station is also connected to the ship. The ship sends its position to the ground station and the ground stations sends the flight path of the VuAB to the ship, by doing so the ship can change its position to decrease the actions needed for the VuAB to reach the landing area. Also, the ground station tells the ship when the helicopter on the ship needs to take-off. This helicopter is connected with the ground station, as well as the ship and the VuAB. The communication with the helicopter becomes active when the VuAB approaches the landing area. The ground station tells the helicopter when to take-off and what the expected position, velocity and flight path of the VuAB are. The helicopter keeps the ground station updated on the mission. When taking of, the helicopter also comes in contact with the ship and the VuAB. To the ship the helicopter sends its position and the mission updates and from the ship it receives the position of the ship itself. So, when the helicopter catches the VuAB, it knows where to return. The helicopter also has a direct link with the VuAB, this assures a minimal delay, because each second is essential for the catch. The VuAB sends its position, velocity and attitude to the helicopter. The helicopter sends its position and velocity to the VuAB. They both adjust themselves to achieve the most optimal catch position. This of course is the most critical part of the mission. Another link is the link of the VuAB and the Ariane 6. The Ariane 6 sends the VuAB the expected height and velocity op separation. This is a one-way link, because the VuAB is inactive untill separation. This link ends when the VuAB is separated from the VuAB.

4.5.2. Communication and Data Handling Sizing

The most important part of the Communications and Data Handling system is the onboard computer. The heart of this computer is the CPU. So, it is essential to have a CPU which can handle all data, commands and communication throughout the mission. To determine the appropriate CPU, first a look is given to the different components and the memory and computing power they need. In the table below, Table 4.9, the memories needed and the computing power of the different components are listed [50]. This table includes the RAM and ROM of the different component as well as their throughput in KIPS. These two are a measure to choose the right CPU. These values need to be multiplied by 4 [50]. This is due to the fact that the first estimations for the conceptual design double once the final design phase is entered. Also, by doing this one will account for redundancy. For the different actuators of our system, like the aeroshell and parafoil deployment, no information was available for the needed computing power. However, these are simple commands and will not require a lot of computing power. So, it is assumed that the factor of 4 also accounts for these components, which is a fair assumption. Also, the GPS and accelerometers used are covered by this margin. Additionally, control of the steering of the parafoil is done by the CPU. A value is used for autonomy, which partly includes the steering of the parafoil, the remainder is assumed to be accounted for in the factor of 4.

Now that the needed computing power is known, a suited CPU can be chosen. This CPU needs to handle a RAM of 0.27 MB and a throughput of 820.8 KIPS. For the recovery system the RAD750 CPU is chosen from BAE systems [66] with a RAM of 4 MB and handling of 2.1 MIPS it fits the needs of the mission. The CPU cannot act on its own and needs a single-board computer and memories as well as other components. These are all chosen from the same brand to ensure perfect integration [67]. A drawing of this architecture can be seen in Section 4.5.2. This is the data flow diagram, provided by the manufacturer. For the memory size, the EEPROM of 4 MB is chosen. According to Table 4.9 this is quite enough. The power this system will use is 14 W [67].
Another part that must be sized is the antenna. The antenna needs to perform during all mission phases, so it needs a high antenna gain. But because the VuAB can not interfere with the current design of the Ariane 6, the option of an out-board antenna was discarded. Instead of this retro directive antenna arrays are used which can be placed on the outside of the VuAB without interfering with the existing system. A drawing of this can be seen in Section 4.5.2. For optimal gain, these elements are place under an 90^o angle. This antenna will have a gain of 15-20 dB [56].

4.5.3. Ground Stations

After separation, the VuAB will be in contact with the ground using the antenna's described in Section 4.5.2. The ground stations used for this communication are chosen to be a selection of the ground stations used by the Ariane 6. As can be seen in Section 4.5.3[20], the ground stations of the Ariane 6 do not cover the full ground track. Between the range of the Natal and Ascension ground stations and the Ascension and Libreville ground stations there is a short period in which no contact is possible. The first stage and second stage separation will take place in the range of the Galliot ground station [10], after which the same ground track is followed and the

[20] `http://spaceflight101.com/ariane-5-va226/ariane-5-va226-launch-profile/`, [18-01-2018]

Table 4.9: Memory and throughput estimates [50]

Function	Memory (Kwords)		Throughput
	ROM	RAM	KIPS
Command	1	4	7
Telemetry	1	2.5	3
Rate Gyro	0.8	0.5	9
Kinematic Integr.	2	0.2	15
Error	1	0.1	12
Precession	3.3	1.5	30
Thruster	0.6	0.4	1.2
Autonomy	15	10	20
Monitors	4	1	15
Fault correction	2	10	5
Power	1.2	0.5	5
Thermal Control	0.8	1.5	3
Kalman Filter	8	1	80
Total	40.7	33.2	205.2
Total Bits	$666.8 \cdot 10^3$	$543.9 \cdot 10^3$	
Total Bytes	$83.4 \cdot 10^3$	$68.0 \cdot 10^3$	
Total MB	0.083	0.068	
Total · 4	0.33	0.27	820.8

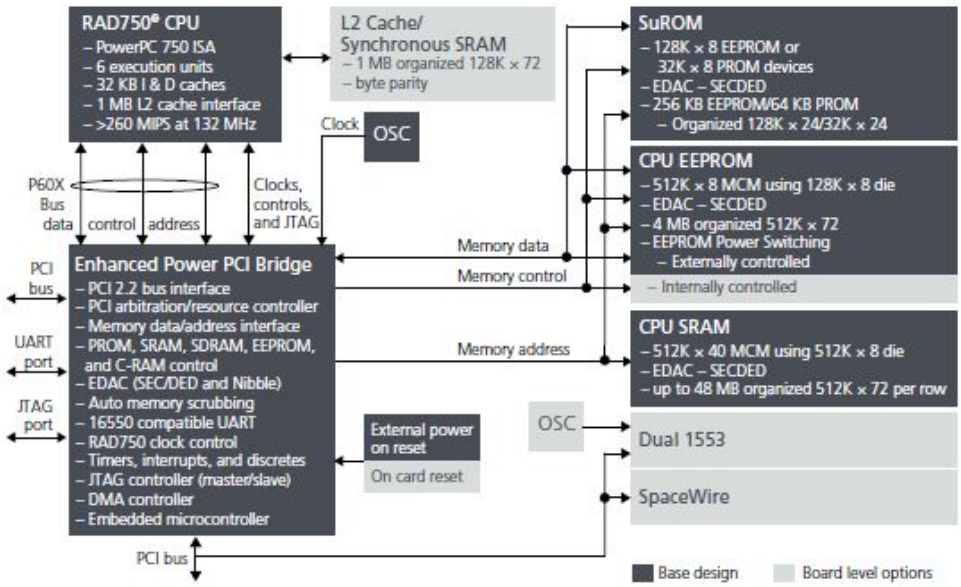

Figure 4.36: RAD750 6U Compact PCI, single-board computer, flexible architecture [67]

function of ground station will be taken over by the Natal ground station. Afterwards, the VuAB is expected to land in the range of the Ascension ground station. As the altitude of the VuAB will decrease over the flight trajectory, contact with the ground station will at some point be lost. As no information on the coverage of these ground stations is available at the moment, it is assumed that no contact with the ground stations will be possible during the atmospheric flight as the altitude will be to low. Therefore, it is chosen to integrate a (small-scale) antenna on the boat, which will serve as the ground station during atmospheric flight and catch.

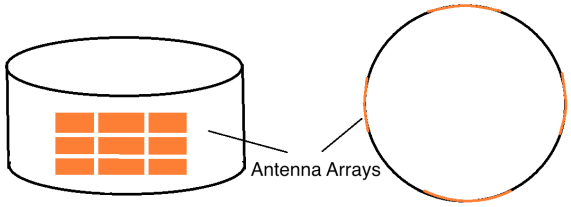

Figure 4.37: Sketch of the antenna arrays on the VuAB, not scaled

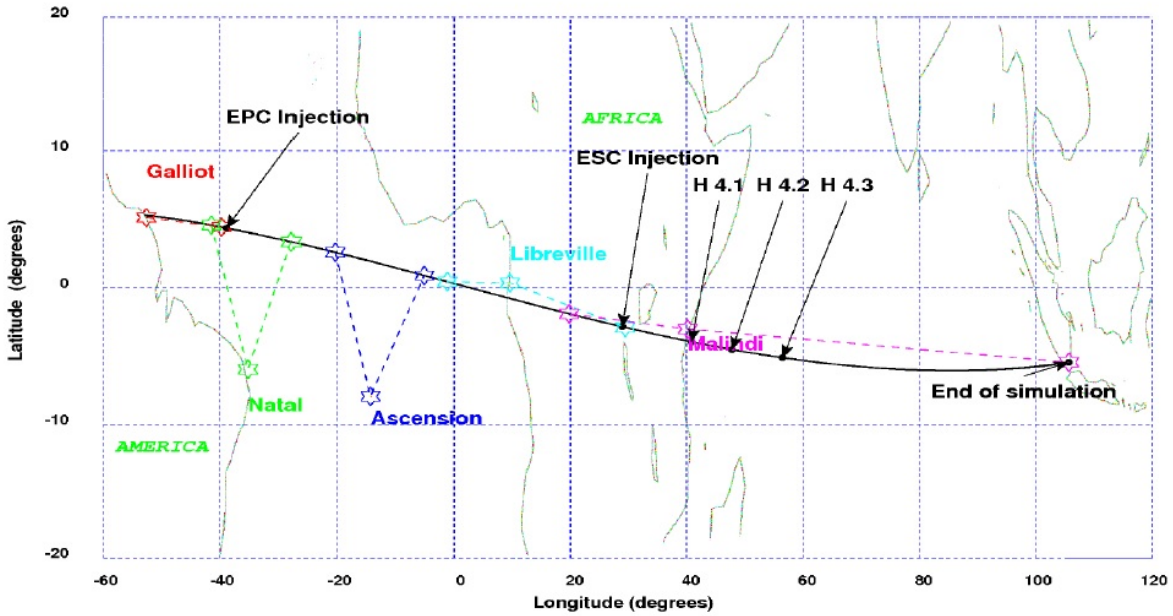

Figure 4.38: Figure showing the ground track of the Ariane 6 with the ground stations and their range of contact over the ground track

4.5.4. Sensors

The sensors of the recovery system are chosen in order to provide for accurate position and attitude determination throughout the entire mission. The attitude should be accurately determined at all times, while the altitude and position with respect to the ground should be available at certain moments in flight, such as during the start and ending of the re-entry phase, during deployment, atmospheric flight and catch.

As an integration error will be built up throughout the mission when using only gyroscopes and accelerometers and as a high accuracy is required for the catch manoeuvre, a GPS sensor is added which will be able to correct and improve the accuracy of the system before and after the blackout. Interferometric fiber-optic gyro's are chosen due to the high reliability, cost effectiveness and off-the-shelf availability. The sensors used for sizing can be found in Table 4.10.

Table 4.10: Suitable sensors for the recovery system, used for sizing of the system

Component	Product	Accuracy	Power	Weight [kg]	Size HxWxL [mm]
Gyroscope	µFORS-3U, NG	≤ 3.0deg / hr	2.3 W	0.15	21 x 65 x 88
Accelerometer	B-290 TRIAD, NG	0.2 %	0.8 W	0.08	62.8 x 50.8 x 12.6
GPS	SpaceNav, BAE Systems	1 PPS	6 W	1.6	206 x 90 x 110

4.5.5. Power System

Throughout the mission, several components need power. Therefore, a separate power supply is sized for the VuAB in order to provide this power. The main components using power and their characteristics are shown in Table 4.11.

Table 4.11: Characteristics of the main components using power throughout the recovery mission

Component	Mission Phase	Power	Time [s]	Power Consumption	Voltage	Peak Power
Transmitter	Full mission	8 W	1754	3.9 Wh	24 V	8 W
Receiver	Full mission	8 W	1754	3.9 Wh	24 V	8 W
Parafoil (AGU)	Atmospheric Flight	26 W	1020	7.08 Wh	24 V	75 W
Gyroscopes (3x)	Full mission	6.9 W	1754	5.2 Wh	5 V	6.9 W
Accelerometer	Full mission	0.8 W	1754	0.6 Wh	5 V	0.8 W
GPS	Full mission	10 W	1754	4.87 Wh	24 V	10 W
CPU	Full mission	14 W	1754	13.3 Wh	5 V	14 W
Total	-	**106.9 W**	-	**38.8 Wh**	-	**283.7 W**

The power system is optimized for the short mission with a relatively high peak power with respect to the average power. For the sake of refurbishability a secondary (rechargeable) battery is chosen, using Lithium-Ion as the main source of power. These batteries have a specific energy density of 110 Whr/kg and are common used batteries for space applications [50]. As the largest share of the components require a voltage of 24 V, the battery have an output of 24 V. The battery cells are placed in parallel in order to be able to cope with the large difference in peak and average power, and therefore the large difference in Ampère. Components requiring a lower voltage, such as the gyroscopes, use DC-DC converters to change the voltage. For sizing DC-DC converters of VPT (SVSA2800S [21]) are chosen, with an efficiency of 65 % and a mass of 0.015 kg. Typically, the cabling accounts for 20 % of the total mass of the power system [50]. Taking these figures and the numbers stated in Table 4.11, a total power consumption of 43.6 Wh is found. With a depth of discharge of 0.5 [50], the total mass for the power system, including batteries, cabling and the DC-DC converters is 0.98 kg.

The power system is shown in the electrical block diagram, showing all components using power, with an indication of the voltage through the cabling. The electrical block diagram can be found in Section 4.5.5.

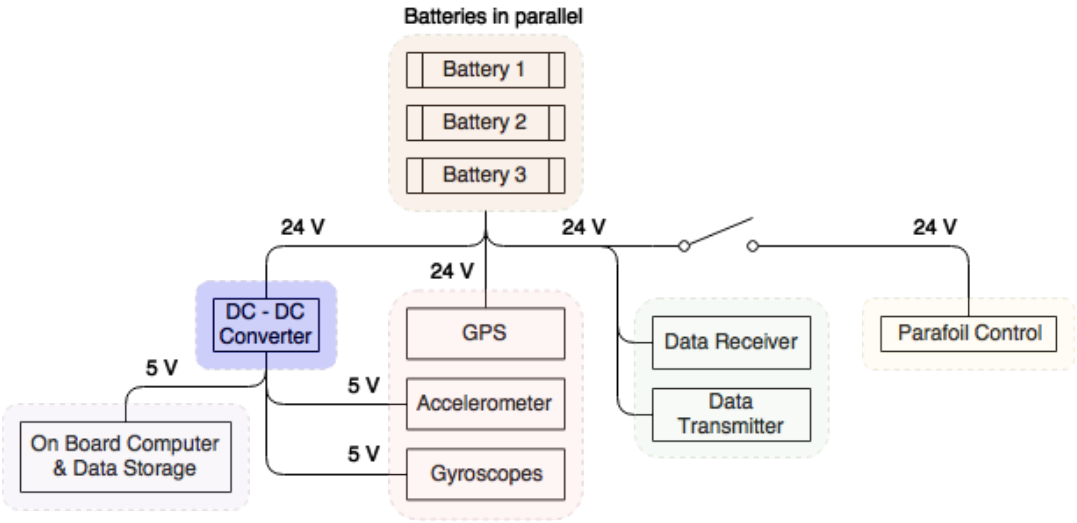

Figure 4.39: The Electrical Block Diagram shows all components using power and their mutual interactions

4.6. Configuration and Lay-Out

In this section the process of synthesizing the designs of components of the system is presented. In Section 4.6.1 the iteration steps are explained, in Section 4.6.2 the masses of all components are displayed and integrated into system masses during every stage of the mission and in Section 4.6.3 the system is integrated with the VuAB.

[21] http://www.vptpower.com/wp-content/uploads/downloads/2016/10/DS-SVSA2800S-7.0.pdf, [10-01-2018]

4.6.1. Integration

Once all the individual design elements are sized, an iterative process begins that will ensure the required reliability and functionality of the system once all the elements are integrated with each other. Figure 4.40 illustrates this process schematically. As a starting point, all the design parameters for the different design elements are taken to be the values as set by the requirements. This iteration process is run until all the updated values converge to within 2% difference.

Some notes on the aforementioned figure. It is important to keep in mind that the Position Error Probability (PEP) is a function of the altitude. The desired end condition at the end of the parafoil flight is a point at an altitude of 1.4 km. This point is within the bounds of the re-entry PEP. If the mission proceeds at its nominal conditions, the parafoil simply uses its EM-controller to spiral down. This choice is made in light of reducing the operational complexity of the mission. The helicopter range is computed by assuming an average velocity equal to the cruise velocity and just travelling at that velocity for the flight time of the parafoil from end of deployment altitude to 4 km. To mitigate mission risks, the helicopter is positioned at 4 km altitude, ready to start matching velocity vectors with the parachute system. If the helicopter is incapable of travelling such a distance in the given time, another choice needs to be made. The same reasoning goes for the catch starting altitude in light of the amount of time that can be used to perform the catch manoeuvre.

4.6.2. Technical Resource Budget

Having iterated the design to achieve internal consistency, the component designs are compiled to form the system characteristics. The total component mass is shown in Table 4.12, the variation of component mass during the mission phase including which parts are jettisoned to reach this new mass is shown in Table 4.13. The power budget is displayed in Table 4.11.

Some components are included in Table 4.12 without any other information to display. If this is the case, the mass and centre of gravity of this component has been included in the mass and volume of the previously listed component. For example, the mass of the Separation Mechanism Skirt Ring includes the mass of the Pyro Charges and that of the Electric Control.

4.6.3. Configuration

This section concerns the packaging of the recovery system inside the VuAB. Packaging the entire system before launch poses some difficulties. The aeroshell, parafoil and drogue chutes all have to be packaged in a relatively small volume where they can also be deployed successfully. The overall layout is shown in Figure 4.41, Figure 4.42 and Figure 4.43.

The packaging has to fulfil the following requirements:

- **FUNC-PERF-INT-D:** the recovery system shall not displace the centre of gravity laterally more than 50 mm in any direction during launch;
- **FUNC-PERF-INT-E:** no component of the recovery system shall be placed beneath the structural cross. The heat effects during launch from the Vulcain engine are too high;
- **FUNC-PERF-INT-F:** no modification to the VuAB will be required to accommodate the packaging of the recovery system;
- **FUNC-PERF-INT-G:** no component of the recovery system shall be placed above the lower part of the first stage LH2 fuel tank;
- **FUNC-PERF-INT-H:** parts placed on the outside of the skirt shall take into account the boosters in a 4 booster configuration;
- **FUNC-PERF-INT-I:** the packaging shall take the fuel lines into account while they are still attached to the VuAB.

The packaging during the pre-separation is the most restrictive situation. At the lowest point of the first stage fuel tank (in the centre), the longitudinal distance to the cross is about 70 cm. At most this distance is 240 cm (at the skirt). The component that requires a large volume and this extra height at the edges is the aeroshell. In Section 4.2.6, a unique aeroshell packing and deployment technique is devised that can be packaged off of its deployement axis and fits these volume constraints. This does create difficulty for fulfilling the centre of gravity requirement as the aeroshell. The centre of gravity in the Y direction defined in Table 4.12, of the aeroshell is located 0.94 m in Y.

The packed parafoil system (the entire system, including drogue parachute, secondary parafoil, control unit and a deployment device) is quite large at 1.03 m^3. However, there is relative freedom in the dimensions of the package as it can be packed in any way that still allows the right order of deployment. It must be attached to the structural cross to reach its vibration requirements. The choice is made to place the package as far to the opposite

Table 4.12: Breakdown of components masses in the system. X and Y are defined as perpendicular and parallel to the orientation of the aeroshell attachment

Assembly	**Component**	**Quantity**	**C.o.G. in Y (mm)**	**C.o.G. in X (mm)**	**Total mass [kg]**
Thrusters	Thrusters	16	0	0	32.0
	MON Tank	4	0	0	2.0
	Pumps	-	-	-	-
	Fuel Lines	-	-	-	-
	Valves	-	-	-	-
	MMH Tank	4	0	0	2.0
	Pumps	-	-	-	-
	Fuel Lines	-	-	-	-
	Valves	-	-	-	-
	Fuel	-	0	0	20.0
Separation Mechanism	L-rings	2	0	0	108.0
	Skirt Ring	1	0	0	20.0
	Pyro charges	-	-	-	-
	Electronic Control	-	-	-	-
	Fuel Line Separation	1	-1.35	0	25.6
Aeroshell	Aeroshell	1	0.938	0	1409.0
	Pump	-	-	-	-
	Attachment	1	1.35	0	383.4
	Sharp Edge Cover	1	0	0	23.9
Parafoil and Chutes	Drogue Chute	1	-2.11	-0.648	56.4
	Mortar	1	-2.11	-0.648	31.2
	Parafoil	1	-2.11	-0.648	522.5
	Package attachment	1	-2.11	-0.648	12.1
	AGU	1	-2.11	-0.648	39.2
	Chute Attachment	4	-2.11	-0.648	0.1
	Secondary Parafoil	1	-2.11	-0.648	22.4
	Retrieval Cable	1	-2.11	-0.648	68.3
Electronics	CPU	1	-	-	1
	Battery	1	-	-	1.1
	Wiring	-	-	-	-
	Gyroscope	3	-	-	0.5
	Accelerometer	1	-	-	0.08
	GPS	1	-	-	4.4
	DC-DC converter	3	-	-	0.05
	Antenna	4	0	0	4
Total			**44**	**37**	**2789**

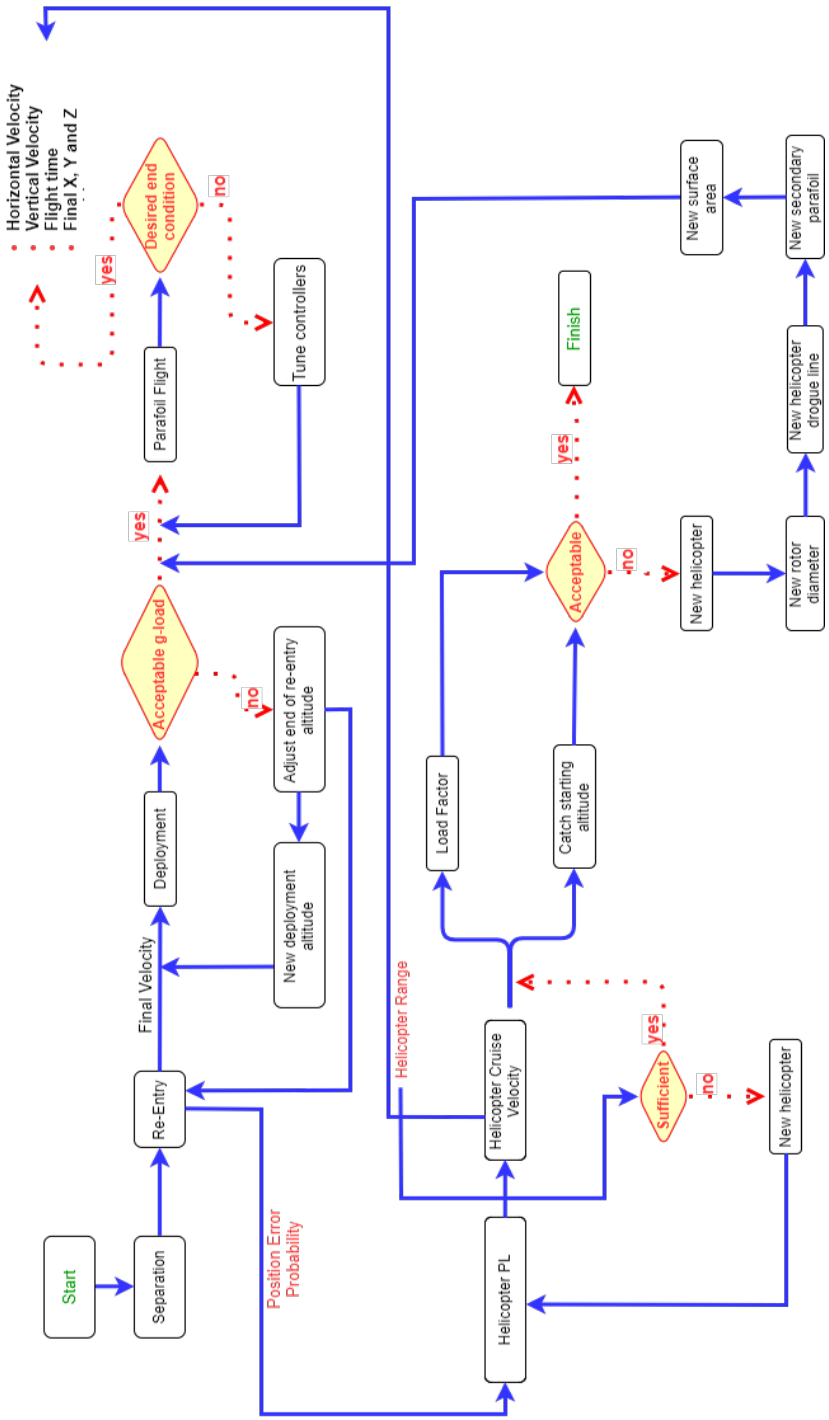

Figure 4.40: Iteration strategy flow diagram used in the design integration

side of the aeroshell as to counter the centre of gravity shift due to the aeroshell centre of gravity in Y. The centre of gravity of the parafoil system package is -2.11 in Y and -0.648 in X.

Many components do not cause a shift in centre of gravity because of a symmetric placement in the VuAB. The following components cannot be placed in such a way as to correct the centre of gravity shift from the aeroshell:

- Thruster assembly;
- Separation mechanism assembly (except for fuel line separation);
- Sharp edge cover;

Table 4.13: Variation of system mass during a mission, including the components jettisoned

Mission Stage	**Jettisoned Parts**	**Recovery System Mass [kg]**	**VuAB Total Mass**
Launch	-	2789	9664
Separation	1xL-ring + Skirt Ring + Fuel Line Separation	2690	9564
Space Flight	Thruster Fuel	2670	9544
Re-Entry	-	2670	9544
Drogue Deployment	Inflatable Heat Shield + Shield Attachment	877	7752
Parafoil Deployment	Drogue Chute	820	7695
Catch	Parafoil	298	7173

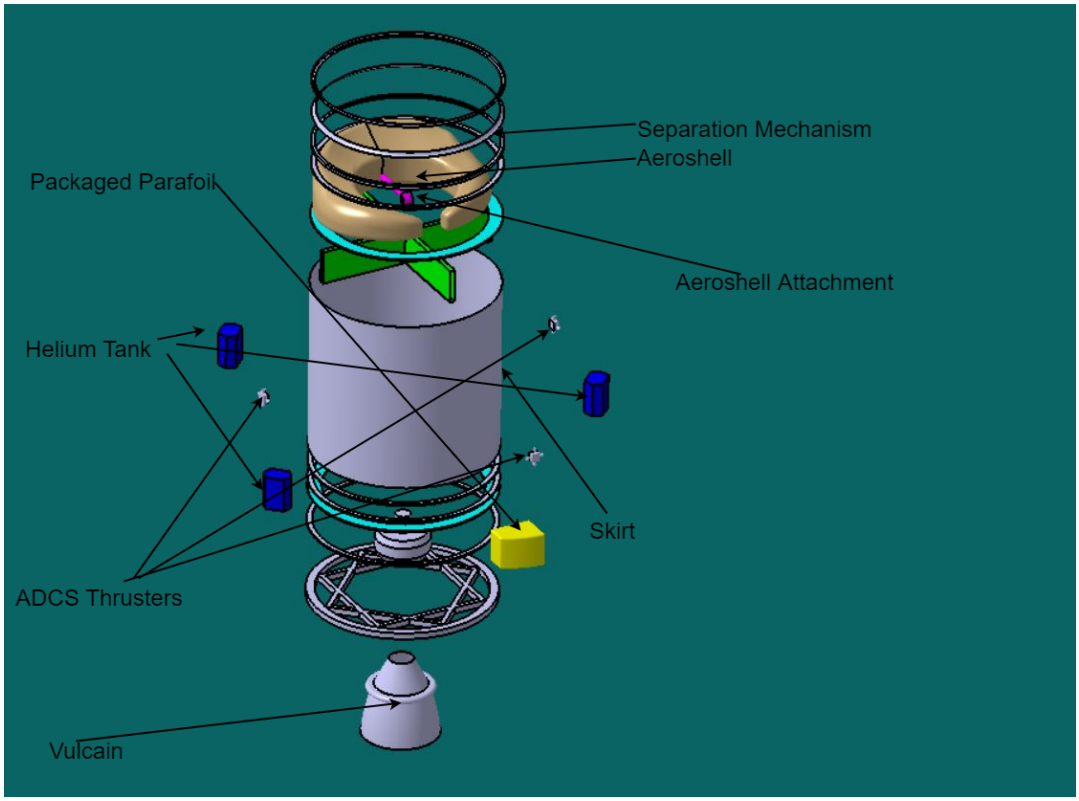

Figure 4.41: An exploded view of the design during pre-separation indicating important components

– Antennas.

The remaining components that can shift the systems overall centre of gravity amount to 1% of the recovery system mass. Therefore, they are neglected in the centre of gravity calculation. When combining the results, the magnitude of the centre of gravity shift from the longitudinal axis is 57 mm off. It is 37 mm off in Y and 44 mm off in X. The off centre placement of the parafoil in X is more critical than that of the heat shield in Y. Seeing as there is quite some freedom in the positioning and dimensions of the packed parafoil, this can be mitigated quite well.

4.6.4. Hardware and Software Block Diagrams

The hardware and software diagrams serve to illustrate the components of the product and their mutual relationships. While the Hardware Diagram describes all main hardware present, the software diagram describes the working of the on-board computer. The Hardware Diagram can be seen in Figure 4.44 and the Software Diagram

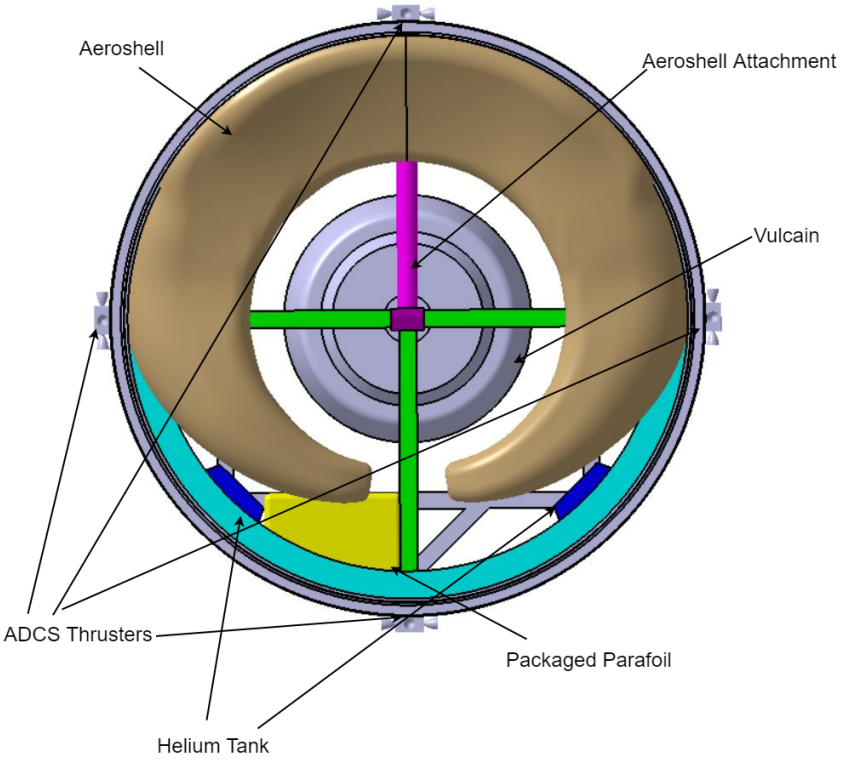

Figure 4.42: A top view of the design during pre-separation indicating important components

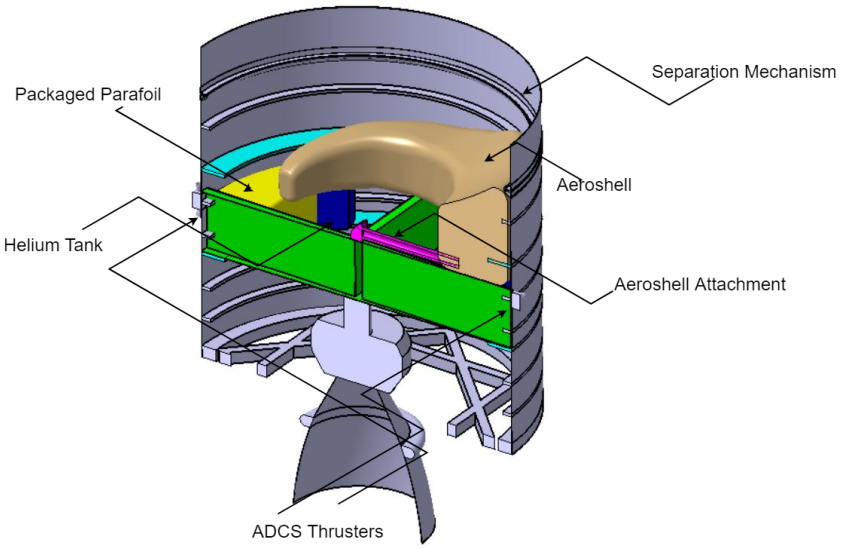

Figure 4.43: A section view of the design during pre separation indicating important components

in Figure 4.45.
In the Hardware Diagram the different blocks represent the different components of the system. The thick arrows represent the command flow, whereas the thin arrows represent the data flows. Next to the arrows, one can see the data or commands going through that arrow. The purple box represents the CPU and the battery is shown in green. The different inputs are represented by the orange boxes and the yellow boxes stand for the telemetry components. The blue boxes show the command centres and the actuators are shown in blue.
The Software Diagram sketches the action within the on-board computer. In the on-board computer, the data

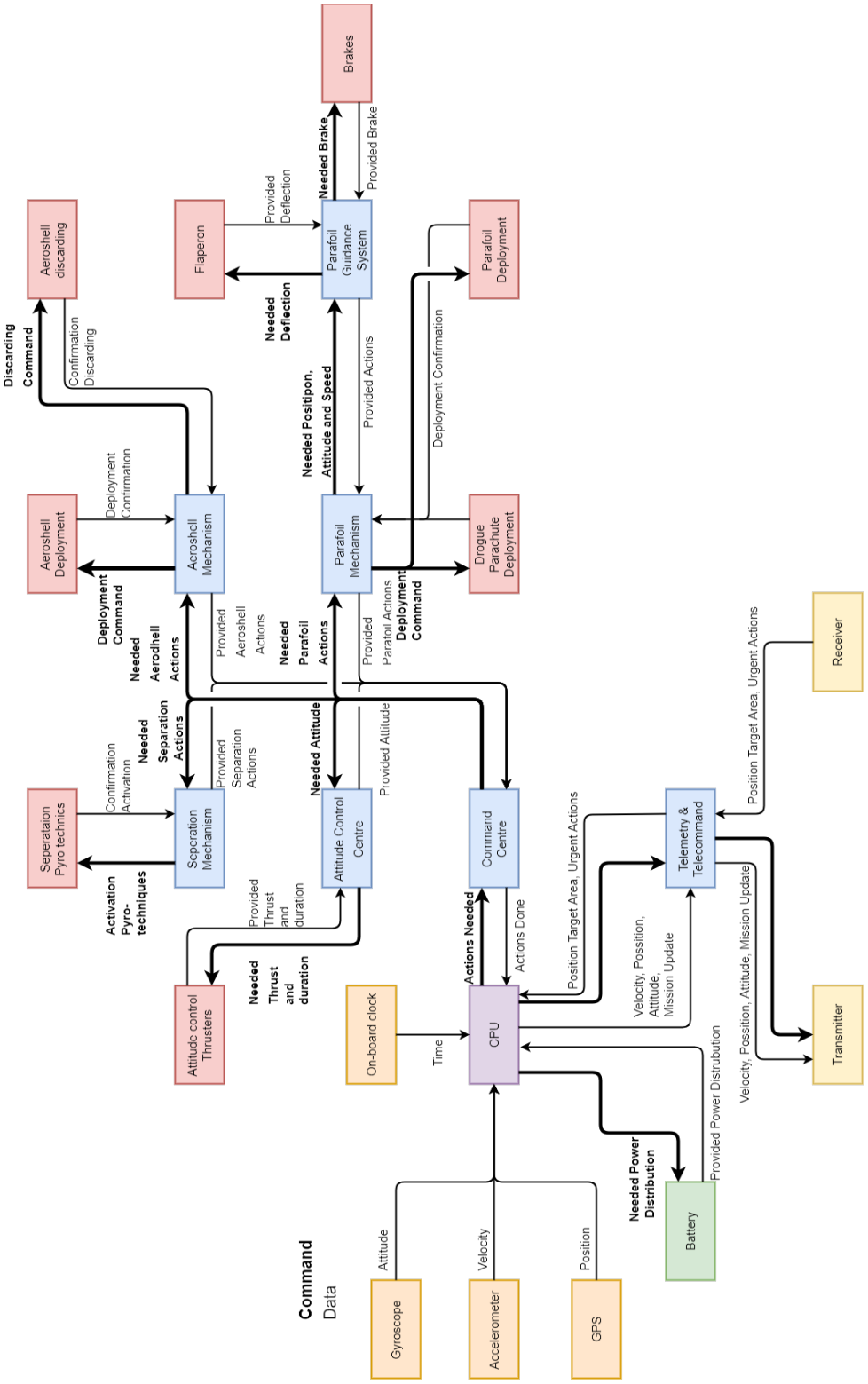

Figure 4.44: The Hardware Diagram of the VuAB recovery system. The thick arrows indicate the command, while the thin arrows indicate the data flow

from the sensors is compared with the mission data. If these values do not correspond, then the CGU send a signal to the different command centres to change the values needed. When they correspond this signal stops. Everything that is done is stored in the memory. The specific pieces of hardware used can be seen in the Hardware

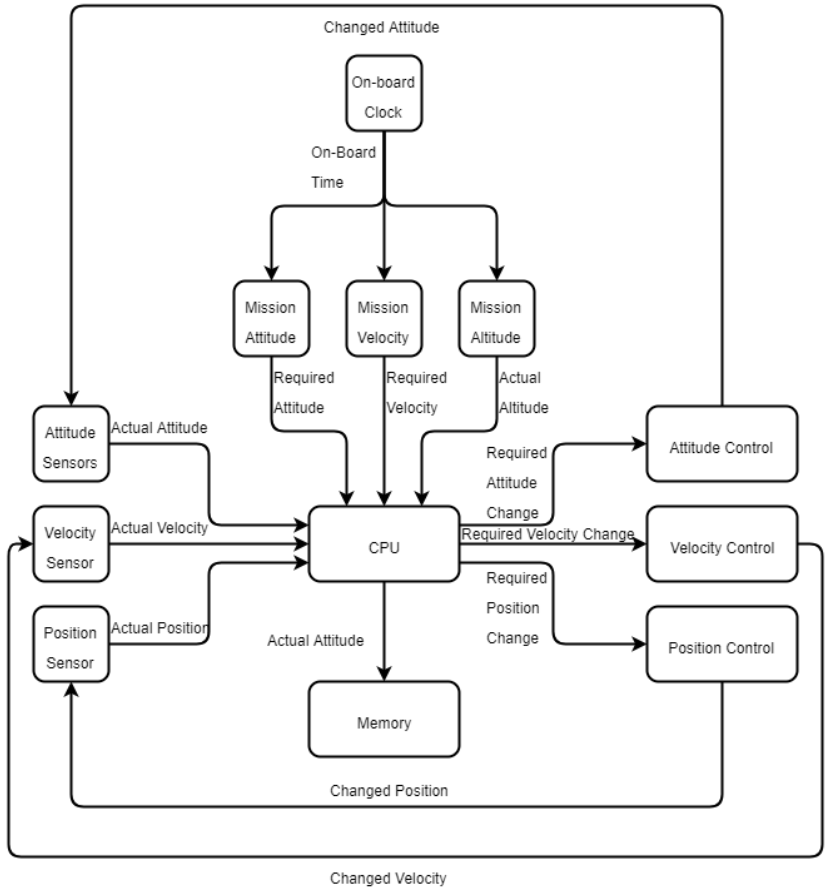

Figure 4.45: The Software Diagram of the VuAB recovery system. It indicates the working of the on-board computer

Diagram.

5

System Design Analysis

Now that all the different system elements have been designed and integrated together, an analysis on the general system design can be performed, to evaluate several key performance indicators. Section 5.1, will cover a system sensitivity analysis, section 5.2 will cover the design sustainability, section 5.3 will cover the RAMS aspects of the design, section 5.4 will cover the risk analysis of the design and finally section 5.5 will conclude the system design analysis by presenting the requirements compliance matrix and provide an overview of which requirements have and have not been met.

5.1. Sensitivity Analysis

Sensitivity analysis have been performed throughout Chapter 4, for the different system elements used throughout the different mission phases. These analysis provide insight into the design boundaries of those elements. Likewise, its important to perform a similar analysis on the complete system, to get insight into the systems robustness and to its tolerances towards different mission conditions.

Since all the subsystems and the different design elements were already designed taking into account tolerances for different mission phase conditions, the only factor that can influence the mission condition and boundaries of the system as a whole is the start of the mission, the separation of the first stage of the Ariane 6 launcher.

An analysis was performed on what is the maximum allowable percentage difference from the nominal conditions the system can tolerate in the horizontal velocity and altitude at separation. The starting point of this analysis is to compute what the maximum allowable radius from the nominal re-entry point. Its important to realize their are two distinct factors involved when setting this allowable radius. The parafoil and the helicopter. More specifically the parafoil dictates the flight time from 8km to 1.2km which in turn leads to the total ground track the helicopter can cover during that time.

Simulations performed using the atmospheric flight model, show that from right after deployment to 1.2 km altitude the flight time equals, 1022 seconds, or approximately 17 minutes. During this time, assuming the helicopter travels at its cruise speed of 315 km/h, the helicopter is able to cover a distance of 89km. A safety factor of 0.9 is applied to take into account the time the helicopter takes to take-off and climb to its cruising altitude. This gives a final range of 80km. This range is illustrated in Figure 5.1 as the most outer circle.

Any re-entry location that will lead to an elipse that has its center point anywhere on the perimeter of this circle, as depicted by the grey elipse to the left of Figure 5.1, for half of the ellipse (as shown by the red dots) recovery wont be able to be performed, since it outruns the ground the helicopter can cover.

Finally, its important to take into account the fact that the parafoil can glide. The same simulations as before resulted in a total ground track covered of 18km by the parafoil. Taking a safety factor of 0.8 to account for wind disturbances and the time it takes to manoeuvre, this results in a total ground track of 14.4km. This means that the maximum allowable radius can be further extended by 14.4km, since the parafoil can always turn back and glide that distance towards the range limit of the helicopter. This is depicted as section 3 in Figure 5.1

It is noted that during the re-entry phase a blackout period will occur caused by plasma generation on the surface of the heat shield. Due to the high level of electronic density no communication with the ground will be possible [40] and any navigation signals will also be interfered with [75]. Therefore, it is chosen to use a set of gyrometers and a accelerometer to determine the attitude of the VuAB throughout the mission. These

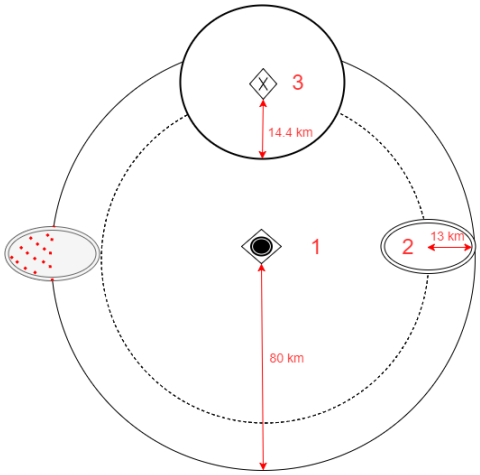

Figure 5.1: Schematic of the limits and boundaries that set the maximum allowable recovery radius.

sensors don't need any communication and will therefore be able to keep providing accurate data to the system. Three gyroscopes will determine the angular accelerations, while the accelerometer will determine the linear accelerations in three directions. By using the data of the Ariane 6 as an input before separation, the system is now able to determine the attitude, altitude and position with respect to the ground by integrating the accelerations obtained by the sensors.Bringing all these three aspects together results in a relationship for the maximum allowable accuracy of:

$$r_{allowable_{max}} = 80 - 13 + 14.4 = 81.4km. \tag{5.1}$$

Given this range, a simulation was performed that outputed for different deviations from the nominal horizontal separation velocity and separation altitude, the corresponding deviation from the nominal position of the system after re-entry. The results are illustrated in Figures 5.2, 5.3 and 5.4, 5.5 and presented in Tables 5.1 and 5.2 respectively. The results presented in these tables indicate what are the limits.

For each of the two type of deviations, two plots are provided. For one boat, one helicopter configuration and for two boats and two helicopter configurations. The later uses twice the maximum allowable radius. Note, that in the plots for the one boat, one helicopter configuration, the red lines represent a value of 81.4 km, maximum allowable radius for recovery, while for the two boats, two helicopters configuration, a value of 162.8 km is used.

Table 5.1: Results of sensitivity analysis on the maximum allowable deviations of the horizontal velocity at separation.

Configuration	Lower Bound	Upper Bound	Units
1 boat, 1 helicopter	-42.9	40.3	$ms^{-}1$
2 boats, 2 helicopters	-88.7	78.2	$ms^{-}1$

Table 5.2: Results of sensitivity analysis on the maximum allowable deviations of the horizontal velocity at separation.

Configuration	Lower Bound	Upper Bound	Units
1 boat, 1 helicopter	-8100	8268	m
2 boats, 2 helicopters	-16017	16693	m

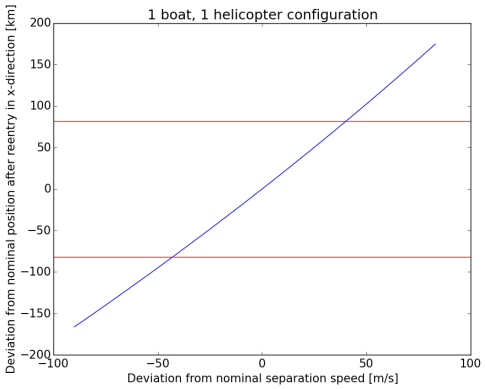

Figure 5.2: 1 boat, 1 helicopter configuration; maximum allowable deviation from nominal horizontal separation velocity.

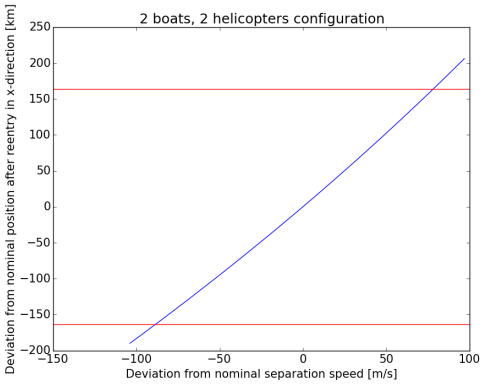

Figure 5.3: 2 boats, 2 helicopters configuration; maximum allowable deviation from nominal horizontal separation velocity.

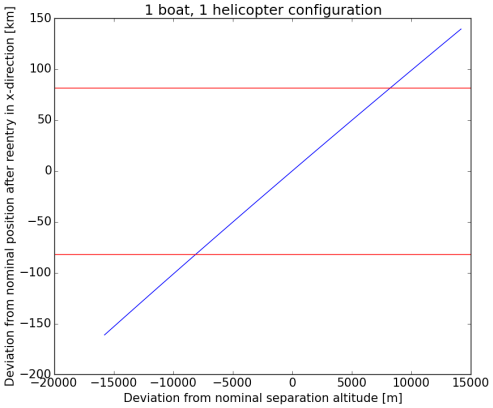

Figure 5.4: 1 boat, 1 helicopter configuration; maximum allowable deviation from nominal separation altitude.

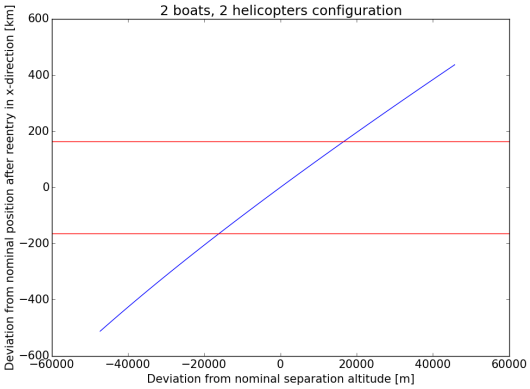

Figure 5.5: 2 boats, 2 helicopters configuration; maximum allowable deviation from nominal separation altitude.

The results presented above indicate what are the limits of the design, and within which boundaries the system is able to cope with deviations and still lie within the required level of reliability.

Its important to note that this sensitivity analysis only takes into account the two variables discussed above. However, there are other variables, that for the purpose of this analysis were kept constant, that if changed can have an enormous impact on the mission boundaries. Inclination angle, horizontal distance covered during the ascent of the Ariane 6 and vertical velocity are examples of factors that can affect the point of re-entry and hence the certainty of recovery.

5.2. Sustainability Analysis

This section describes how sustainability is approached in this project, explains the procedures used to ensure incorporation of sustainability trough-out the complete project. Then the outcome of that design process is presented in terms of sustainability contribution by the design. In the baseline report the Technical sustainability Assessment Tool (TSAT) is developed, based on the Tripple Bottom Line framework.

It incorporates a broad range of subjects of consideration for a sustainability assessment that is specifically designed to use in projects. The TSAT is built up out of the 3 main subjects: People, Planet and Profit, which in turn are evaluated for the 3 levels: Project Pre-Phase, Project Execution and Operation of the asset. These subjects are modified into a set of concise questions, to maximize their relevance to this project.

The TSAT is used to incorporate sustainability throughout the design. And the TSAT is used to create insight in the sustainability of different design choices. The procedure starts when a project member has to make a design choice that is not enforced by the requirements, then different options are inputs in the TSAT. The questions in the TSAT are weighted based on importance for the design choice. Next the design options are graded on

the different sustainability questions. For example, criteria 2.2.5 and 3.2.5, with <level>.<subject>.<question number in subject> are represented by the question: "Direct amount of non-locally produced, non-green energy in kWh used?". This question is then weighted per question, and then graded per design option. The highest score is considered the most sustainable design option at that moment of consideration. The sustainability score of the TSAT is then taken into account for the design choice.

To increase the effectiveness of this procedure, the technical sustainability assessment output of the midterm review; the TSAT scores for the mid-air retrieval is evaluated, and the critical points in the sustainability of this mission are highlighted and shared with the group to increase the awareness of sustainability improvement possibilities.

With this increased awareness the grading of the TSAT subjects is done by the project members themselves in stead of the Sustainability Manager. The reason for this shift is the specific, in depth knowledge and consequences on the subjects that are evaluated that can be represented more accurate and time-wise efficient if it can be done by the project member that works on it.

An additional benefit of this approach, is the experience project members get, getting used to doing a sustainability analysis for their design choices. This increases the likelihood of usage after the project has finished since it increases the accessibility to the sustainability assessment procedure. The Sustainability Manager remains responsible for the sustainability within the project and checks the sustainability procedures and TSAT evaluations. The procedure led directly to the following major decisions with respect to the absolute sustainability of the project:

1. The aeroshell, parafoil and parafoil will all be retrieved after it has fallen in the ocean.
2. The parafoil and parashute will be inspected after retrieval to determine if they can be reused in the future.
3. The 5^{th} launch per engine will fly without recovery system since the engine is not reusable any more.

To evaluate how this project contributes to sustainability, it is compared to the current mission procedure of the Ariane 5. The Vulcain 2.0 engine is discarded after every launch, whereas with the VuAB retrieval, the Vulcain 2.1 engine can be refurbished and re-used up to 5 times.

The production and refurbishment are complex processes and the level of detail of the design in this stage renders a complete and accurate LCA beyond the scope of the project. To get an effective estimate on the contribution of this project to the sustainability, the overlap between environmental and cost improvement is assumed to represent the sustainability improvement.

An example that illustrates this relation is for example the milling of a part from raw solid materials. This generally requires a lot more mass input material which is converted to waste and can be quite labour intensive. If the same part can be re-used after cleaning inspection it has a significant impact on the overall sustainability.
In the difference in total costs between retrieval and no retrieval (current situation) for the VuAB and Vulcain combination is estimated at 2.8 M Euro for the worst case. That implies a rough overall sustainability improvement of at least 4 % for the VuAB retrieval and reuse, compared to the current situation without VuAB retrieval.

5.3. RAMS

This section describes the consideration and comparison of reliability, availability, maintainability and safety (RAMS) for the final design described in Section 4.6. These aspects are closely related and together determine the performance quality of the product. At this point in the design process it is difficult to come up with qualitative figures for the RAMS, as the design is still conceptual and there are many uncertainties and unknowns. Therefore the main focus is on the major component that have been researched the most. First reliability will be discussed in Section 5.3.1, then availability in Section 5.3.2. Followed by maintainability in Section 5.3.3 and the section is concluded by safety in Section 5.3.4.

5.3.1. Reliability

Reliability is stated by the Institute of Electrical and electronics engineers as follows: The ability of a system or component to function under stated conditions for a specified period of time. From this one can say that reliability is the rate of success, which is specified by the following: Reliability = 1 – Probability of failure. So, to increase reliability, the rate of failure should be minimised. To minimise this rate of failure, the critical points during the mission are analysed and a mitigation plan is come up with. This can be redundancy in the systems, by means of a fail-safe design. Another option is to design the system safe-life, which means that larger safety-factors are applied, to ensure that the system does not fail during the its life-time. The critical points are the points where a failure could harm the whole mission. The critical points of the mission per subsystem are specified below, together with their reliability.

Space Flight

For the space flight part there are two systems which can be deemed critical. One is the separation mechanism between the VuAB and the 1^{st} stage of the Ariane 6. The other critical system are the attitude control thrusters.
First a look is taken into the separation mechanism. The separation mechanism is the first critical point during the mission. If the system fails to separate from the 1^{st} stage, the whole mission will fail. On the VuAB, the same separation mechanism is used as the one on the Ariane 6. This is an off-the-shelf product, delivered by the company RUAG. According to the statistics provided by this company, the separation mechanism has a success rate of 100 % over 600 flights [53]. So it is assumed that nothing will go wrong here.

The thrusters used in the system for attitude control are also thruster from the shelf. With more then 2000 of these thrusters flown into space, they have proven to be very reliable. Also, it has to be mentioned that the thrusters are placed fail-safe. There are plenty of thrusters to manoeuvre if one or more thrusters fail.

Aeroshell

Due to the tight space within the VuAB, a custom deployment mechanism is designed to ensure a proper deployment of the aeroshell. This is also a very critical point of the mission. If, by any chance the aeroshell would not deploy, the VuAB would burn in the atmosphere. A fail-safe design could not be applied for this mechanism due to the afore mentioned lack in space. So, this system is designed to be safe-life to reduce the probability of failure. The life-span of this mechanism is one flight only, because it will be discarded after re-entry. So, a safe-life design will not impose very high demands and the added weight will be relatively low. The aeroshell is inflated by releasing a valve, so extra valves are included in case that one valve fails to open. By doing so, this part of the mechanism will be fail-safe. After re-entry, the aeroshell needs to be discarded. Otherwise there would be no space for the parafoil to deploy. To discard the aeroshell, a pin is released. Cutting through steel beams, or using pyrotechnics, is not feasible within the VuAB. So, this system cannot be designed to be fail-safe, nor to be safe-life. A stronger connection will only increase the probability of failure.

Parafoil System

When entering the atmospheric flight after re-entry, the system deploys the parafoil to ensure a safe descent. This parafoil is deployed by means of a drogue chute, which in turn is deployed from a pressurized tube. Without the parafoil, the system would crash in to the ocean if the parashute would not deploy, destroying the VuAB together with it. The drogue chute and parafoil itself need to be safe-life designed, again due to the lack of space. An extra drogue chute or parafoil would be perfect for redundancy, but it does not fit in to the VuAB. A safe-life design will not require much change, because the drogue chute and parafoil will be discarded after each flight in the current design. The parashute and parafoil can be designed safe life by adding extra cables between the both the parashute and AGU and between the parafoil and the AGU. The AGU has an essential function in directing the VuAB to the landing area. Because this is an off-the-shelf product, no problems are expected. But if the AGU would fail, it has the option to be remote controlled by the ground-station. This extra redundancy minimizes the probability of AGU failure. After the system is caught by the helicopter, the parafoil is detached from the VuAB to prevent unexpected loads on the helicopter. This is done by cutting the main cables of the parafoil. A fail-safe system is considered with extra pins to cut through the cable if the first pin fails.

Catch

To land the VuAB safely it must be caught in mid-air. Otherwise the VuAB will splash into the ocean, or crash on the barge, which will both destroy the Vulcain engine. The catch is the phase of the mission which includes the most risk. To lower the probability of failure, the helicopter should aim to catch the VuAB as high as possible. By doing so it will have more chances of catching it, if it would miss the VuAB the first time. Another important factor is the cable connecting the helicopter with the VuAB. This cable should be able to withstand all the loads and should not snap. To ensure this, the cable is designed to be safe-life.

Electrical Systems

The on-board computer is essential for proper system operation. It handles all commands and all communications. To ensure that the system will not fail due to a failure of the on-board computer, an extra computer is added for redundancy. The antenna used is divided into different arrays and if one of the arrays would fail, the other ones will keep up the link with the environment. The system has a broad spectrum of sensors. This automatically builds in a fail-safe system. So, if one of the sensors would fail, the other sensors could be used to continue the mission. To account for power failing, an extra battery can be included. This will not significantly influence the

design, because the batteries are relatively small with a low mass.

So, to conclude, one can say that the system has a reliable design. Because of the limited space in the VuAB, most systems are designed to not fail during the mission. Where in other systems this would mean an enormous increase in mass, for the VuAB Recovery System (VRS) it does not add much of an extra weight. This is since most of its components are discarded after each flight. So, the system can be made more reliable, without adding much of a mass.

5.3.2. Availability

The availability, is defined as the probability that the system is available to perform when it is required to perform. So, for this project it means that the VRS is ready for use for each launch of the Ariane 6. According to the client, Airbus Defence and Space Netherlands, the Ariane 6 is going to be launched 12 times a year. So that means that the system has approximately one month to become ready. The availability of the VRS depends on the following 3 main processes:

- Manufacturing of the discarded components;
- Maintenance of the retrieved components;
- Refurbishment of the VuAB.

These three processes must be performed before each launch. If this is possible in one month, then there is no problem for the availability of the system. Starting the manufacturing of the parts discarded during the mission, one can say that most of the systems are off-the-self products and, once fully developed, they will be produced in batches. Due to this, new parts will always be available. The maintenance of the components which are going to be reused is discussed in the following section. But one can already say that most of the big components of the VRS are going to be consumed fully. So, maintenance is largely performed on the smaller parts. This means that one month is enough time to perform all the required maintenance tasks. The last part that can affect the availability is the refurbishment of the VuAB. According to Section 7.2 this will last for approximately 6 months, together with the transportation adn the assembly. So, to ensure that each launch can be performed, it is planned to use a total of 4 Vulcain engines, together with 7 VuAB's, including one for redundancy. By doing so the VRS will be available to be launched into space with the Ariane 6 each month.

5.3.3. Maintainability

For the maintainability, only the recovery system is considered. The maintainability or refurbishability of the other components of the VuAB are touched upon in Section 7.2. Before starting an analysis on the maintainability of the VRS, first it is determined which parts are fully consumed and which will be maintained. All the main components of the VRS are considered below according to the mission profile and determined if they will be maintained or discarded. The components which are fully consumable do not have to be taken into account for maintainability.

Space Flight

The Separation mechanism to separate the VuAB from the 1^{st} stage is fully consumable, because it uses pyro-techniques to destroy the structure around it. The attitude thrusters used are bi-propellant thrusters. Theses thrusters are reusable in theory, because they also are re-ignited in space for attitude control. The tanks, pumps, fuel lines and valves are all going to be reused and must be considered for maintainability. The fairings of the thrusters, which are attached to the thruster clusters are separated in space, so they are fully consumed. The cluster itself, which attaches the thrusters to the VuAB are also reused and need to be considered.

Aeroshell

The aeroshell is discarded after re-entry, together with its deployment mechanism and pumps. After this they are planned to splash into the sea. This makes the attachment mechanism unusable, because it is made of aluminium. Also, the pump which inflates the aeroshell are fully consumed. The aeroshell is also not expected to survive the ocean water and will be replaced. To protect the aeroshell from the sharp edge of the separation line, a mechanism is used to cover this sharp edge. This mechanism is planned to be reused.

Parafoil System

The parafoil system consist of different chutes. The first one to deploy is the drogue chute, which is followed by the main parafoil together with the 2nd parafoil on top of it. From these three chutes, only the second parafoil stays attached to the VuAB. Both the drogue chute, as well as the main parafoil are discarded into the sea. The

contact with the ocean water make these chutes impossible to reuse. The attachment of the parafoil stays within the VuAB and is considered for maintainability. This also holds also for the AGU and the mortar, which deploys the first drogue chute. The catch cable is also reused and considered for maintainability.

Electronics

The electronics include the CPU and the battery as well as the sensors and the antenna. They are all planned to be reused, so all of these needs to be taken into account when analysing the maintainability of the whole recovery system.

Now it is known which of the components are going to be reused and so need to be maintained. With this information a maintenance diagram can be made. This diagram can be seen in Figure 5.6. The maintenance diagram visualises a difference between corrective maintenance and preventive maintenance. Corrective maintenance is performed for components which need repair. Preventive maintenance is performed to ensure that that the component will survive the following mission. Preventive maintenance can be divided into periodic maintenance and condition-based maintenance. The first one is performed after each mission, the other is only performed of the component needs maintenance. These components are judged after each mission to see if they need maintenance.

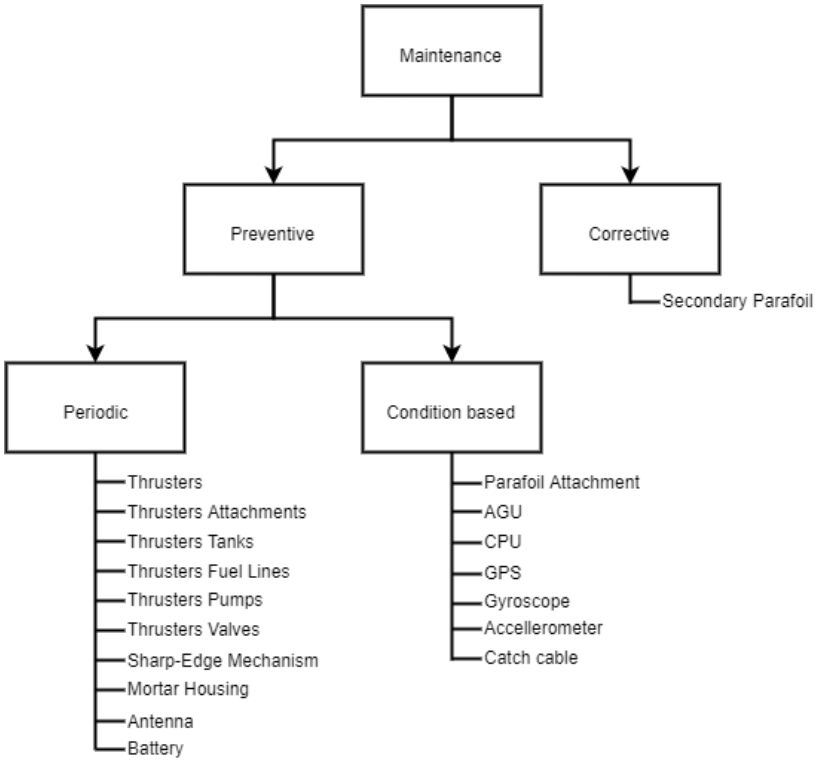

Figure 5.6: Maintenance diagram of the recovery system

Periodic Maintenance

Periodic maintenance for this mission means that these components are going to be maintained after each mission. This includes different types of maintenance. The thrusters' attachments, fuel lines, pumps and valves will be inspected and tested to see if there are no leakages. The thrusters themselves, together with the fuel tanks are substituted to routine maintenance. This includes inspection but also cleaning and, for the tanks, refilling. The sharp-edge mechanism is also substituted to routine maintenance, which includes also lubrication of the mechanism and cleaning. The mortar housing needs to be re-pressurized, so it will also undergo a routine maintenance. The antenna, which is on the outside of the VuAB, will have to be cleaned after each launch. And at last, the battery for power supply needs to be recharged after each mission.

Condition-based Maintenance

Condition based maintenance only occurs when the components listed are in need of maintenance. To know if this is the case, the electric devices are constantly monitored. Because they are always in contact with the ground station, this can be easily judged upon. The parafoil attachment is inside the VuAB and is not exposed to the harsh conditions on for example re-entry. It also does not need to be refilled like the mortar housing. So, this part is only inspected for cracks, like the catch cable.

Corrective Maintenance

The only component that will need a repair after the mission is the secondary parafoil. Because this parafoil is caught with a hook, it will be damaged in such a way, that the reuse of it without a repair is dangerous. So, after each mission this parafoil will be repaired and reused.

Another part that needs maintenance are the ground supports, like the helicopter and barge. These only need to be inspected after a certain amount of missions. The catch mechanism of the helicopter needs to be service maintained after each flight.

5.3.4. Safety

Safety is the grade in which the system can be operated, without causing any harm to its surrounding, including people. Also, it includes the damage to the environment in case of a failure. In this section first, it is determined how safe the system is when operating in normal conditions. After that, one can see what the plans are for safety if the system fails.

When operating under normal conditions, the system is designed to be safe. An example of this is that after the catch, the parafoil is discarded so that the pilot of the helicopter can easily carry the VuAB without any impulsive loads. Also, the discarding mechanism is designed in such a manner that the parafoil will not enhance any harm to the helicopter pilot when discarded. Another example of safety is that the path in which the whole mission occurs is closed to other aircraft or boats other then the helicopter and barge needed for the mission.

This also is important in case of failure. Would the VuAB fail in air, causing it to fall down, its surrounding would be clear from any aircraft or boats. By doing this a collision with another vehicle is prevented. So, any during the whole mission, the whole mission path and ground track is cleared from other vehicles. Another situation where failure can occur is during launch. Here the VRS is in-active. But the system is designed such that no harmful gasses will flow into the air in case of a fire. Also, the system does not imply an extra danger for the existing Ariane 6 design.

The system is monitored at every stage of the mission. This allows the observers to detect an error immediately and it gives them the chance to mitigate the problem. If that is not possible, an appropriate contingency plan can be executed. With these measures, the VRS will not imply any danger on its surroundings and will be deemed safe.

5.4. Risk Analysis

This chapter contains the assessment and mitigation of technical risk at system and subsystem level. Risks concerning project procedures, planning and scheduling have been discussed in the Project Plan [72] and are not included in this analysis. Risk is part of any design project and so, managing these risks is an important part of such a project. Risk can never be avoided completely, but when managed well risk can be reduced. Risk management shall be a continuous process throughout the project to ensure the final result meets all requirements.

Risk is defined as a product of the probability of a risk event happening and the impact the event will have on the system or mission [20]. This way identified risks will be assessed, showing which events pose the highest risks. For these risks a mitigation strategy is developed in order to reduce the probability, the impact or both. The goal of mitigation is making sure all risks are small enough to justify continuance of the project in the current manner.

The risk identification and risk assessment steps are described in Section 5.4.1. In Section 5.4.2 a description of the risk analysis and risk mitigation is found.

5.4.1. Identification and Assessment

In this section possible risk events are identified and assessed by quantifying the probability and impact of all risks. Both probability and impact are scaled to a number between 1 and 5. A probability of 1 is for highly unlikely events and a probability of 5 is for nearly certain events. More information on the probability scale can be found in Table 5.3. An impact score of 1 means the impact on the mission is negligible and an impact score

of 5 means the impact is catastrophic for the mission. More information on the impact scale can be found in Table 5.4.

Table 5.3: Probability scaling

Probability	P-value	Scalar
Very likely	0.5-1.0	5
Likely	0.2-0.5	4
Possible	0.05-0.2	3
Unlikely	0.02-0.05	2
Highly unlikely	0-0.02	1

Table 5.4: Impact scaling

Impact	Result	Scalar
Catastrophic	Mission failure	5
Critical	Questionable mission success	4
Substantial	Some reduction in technical performance	3
Marginal	Minimal reduction in technical performance	2
Negligible	No reduction in technical performance	1

In Table 5.5 the identified events with their probability and impact scores can be found. Although the design has been developed quite extensively since the start of the project it can still be difficult to get accurate probability values for the risk events. In these cases the score is set higher rather than lower to make sure risks are not easily underestimated. Also a justification for the assigned scores for every risk event is listed.

- **SPACE-01** The chance of separation failure is extremely small. The company producing the separation mechanism claims a 100 % success rate [53]. Complexity however, is increased by the need to cut the fuel lines connecting the fuel tanks to the Vulcain engine. The impact of separation failure would be catastrophic, as it is not possible to recover the complete first stage with this recovery system. The separation will introduce loads on the VuAB causing rotations. These will be counteracted with the ADCS system.
- **SPACE-02** The ADCS system stabilises the system after separation and provides the proper attitude for re-entry. Failure could be catastrophic if the wrong attitude causes the aeroshell to deploy in the wrong direction. The probability is unlikely, as the reliability of bi-propellant thruster systems is generally high.
- **AEROS-01** Failure to deploy the inflatable aeroshell would be catastrophic as the VuAB is not protected from the heat generated upon re-entry. It would cause complete mission failure. For the deployment a mechanical arm is deployed to centre the shell before it is inflated. The system is not very complex, but does rely on a single actuator. The probability of failure is expected to be very low.
- **AEROS-02** Proper discarding of the aeroshell is required to ensure the success of the following mission phases. Failure may cause blockage of the drogue parachutes and parafoils or may introduce the system to unexpected loads. The rotation caused by deflating the aeroshell might not be stable and the VuAB could start tumbling. Releasing the aeroshell while tumbling might cause extensive damage. The release system itself is very simple, making the probability of failure small.
- **DROGUE-01** There are several ways for the drogue parachute to fail to deploy. It could not deploy at all, get stuck upon deployment or rupture due to the aerodynamic forces coming with deployment for example. All would be critical or catastrophic as the parafoil is not able to deploy without the drogue parachute. The probability of deployment failing is not expected to be high, as parachute systems have been used and tested for a long time and the deployment is generally reliable.
- **DROGUE-02** After parafoil deployment the drogue parachute has to be discarded. The chute staying attached would introduce loads on the parafoil that would cause it to fail, which would cause complete mission failure. The system used to separate the drogue parachute from the rest of the system is very simple and has been widely used. The probability of failure is expected to be very low.
- **PARA-01** For the parafoil deployment a mortar is used. This is a widely used way for deploying large parafoils and parachutes. It is a proven concept that is considered reliable at the altitude at which it is used. Failure of the parafoil would be catastrophic as it is the main way of deceleration and without it the attachment point for the mid-air retrieval does not deploy.
- **PARA-02** The parafoil is controlled to make sure it arrives within reach of the helicopter and can fly steady and straight for mid-air retrieval. The system is expected to re-enter well in reach of the helicopter. Even when gliding in the wrong direction it stays within range. Failure of the control system might cause problems at the retrieval if it causes the system to not fly straight. The control system that is used is simple and works with only 2 actuators, one for the aileron on each side of the parafoil. Generally the reliability for these actuators is high, but they do pose single points of failure.
- **PARA-03** When the VuAB is attached to the helicopter the parafoil has to be discarded to make steady flight with the coupled system possible. The drag induced by the parafoil would make this impossible,

Table 5.5: Risk assessment for the VuAB recovery system

Nr.	Risk event	Probability	Impact
SPACE-01	Propellant tank separation failure	2	5
SPACE-02	ADCS failure	2	5
AEROS-01	Aeroshell deployment failure	1	5
AEROS-02	Aeroshell discarding failure	2	5
DROGUE-01	Drogue parachute deployment failure	2	5
DROGUE-02	Drogue parachute discarding failure	1	5
PARA-01	Parafoil deployment failure	1	5
PARA-02	Parafoil control failure	2	3
PARA-03	Parafoil discarding failure	1	4
CATCH-01	Failure to link VuAB and helicopter	2	5
CATCH-02	Helicopter capacity overload	2	4
CATCH-03	Helicopter stability failure	1	4
OPER-01	Missing helicopter catch range	5	5
OPER-02	Boat failure	1	4
OPER-03	Helicopter failure	1	5
OPER-04	VuAB drop-off failure	2	4
OPER-05	Transport failure	4	2
OPER-06	Refurbishment/maintenance delays	5	4
CDH-01	Communication link failure	1	4
CDH-02	Sensor failure	4	5
CDH-03	Data handling failure	2	4
ELEC-01	Electrical power system failure	3	5
STRUC-01	Structural failure during launch	2	5
STRUC-02	Unexpected loads during launch	4	3
STRUC-03	Structural failure during re-entry	1	5
STRUC-04	Unexpected loads during re-entry	4	1
STRUC-05	Drogue parachute attachment failure	1	5
STRUC-06	Parafoil attachment failure	1	5
STRUC-07	Catch attachment failure	2	5
PROJ-01	Development goes over financial budget	4	2
PROJ-02	Development goes over time budget	3	4
PROJ-03	Operating costs of system go over budget	2	4
PROJ-04	Reliability requirement is not met	3	3

possibly causing the helicopter to fail. The system used for detachment is similar to that for the drogue parachute. A simple system that has been tested and used so probability of failure is expected to be small.

– **CATCH-01** In order for the helicopter to lift the VuAB, the two need to be structurally linked. Although this is a complex, high-precision manoeuvre, there is quite some time in the flight plan for the helicopter to line up with the VuAB, then attach the linking components and finally lift the VuAB when the air density is high enough for the helicopter to be able to lift the mass of the VuAB. The probability of failing to link is expected to be low due to the extensive time span for the manoeuvre. The impact would be catastrophic, as failure to link would result in a splashdown for the VuAB.
– **CATCH-02** If the mid-air retrieval is performed in non-ideal conditions the load factor might be higher than predicted. Also, capacity overload could be the consequence of attempting a catch at an altitude that is too high. In this case the helicopter starts dropping until it is able to produce enough lift at a lower altitude. A capacity overload for a short period of time will not have large impact on the mission, but if the overload can not be compensated the impact could be catastrophic.
– **CATCH-03** As said the parafoil would cause stability issues when not properly disposed, but these issues could also arise without the parafoil. Weather conditions, catch manoeuvre offsets or other factors impacting the flight dynamics could cause the VuAB to have significant swing beneath the helicopter. This could have a critical impact. The stability of the combined system is simulated and the chance of it being unstable is deemed very small. All destabilising effects can relatively easy be compensated by control

inputs from the helicopter pilot.

- **OPER-01** Missing the helicopter catch range would have a critical impact. As stated before, the VuAB splashes down in the water if the helicopter does not pick it up and this would ruin the recovered elements. The chance of missing the range is expected to be high, as the sensitivity analysis (Section 5.1) showed that small deviations in the separation velocity cause the VuAB to end up outside of the helicopter flight range.
- **OPER-02** For the retrieval operation a boat is needed from which the helicopter operates. Failure of this boat could have a big impact on the mission as it might not be able to get the helicopter within flight range of the VuAB. This would result in catastrophic failure. The probability for this happening is expected to be very small. The boat can be extensively tested and inspected before take-off.
- **OPER-03** Failure of the helicopter, not necessarily during the catch, but in general would result in the same catastrophic failure as boat failure. The VuAB has no way of properly landing without the helicopter. The chance of this happening is considered negligible. The helicopter can be fully tested and inspected before departing with the boat, so the chance of it not functioning properly is extremely small.
- **OPER-04** After the VuAB has been picked up by the helicopter it has to be put down on the boat for transport. It is expected that this can be done in a very controlled manner with low velocities. Still the VuAB might be vulnerable in certain places and damage to critical systems could be done when not touching down properly.
- **OPER-05** The chance of causing significant damage during transport is expected to be very small. However the chance of delays during transport are expected to be higher. They could impact the mission negatively when the delays are too extensive, but in general the impact is expected to be low.
- **OPER-06** Delays during refurbishment and/or maintenance could occur due to different reasons. The turnaround time is limited by the next scheduled launch for the Vulcain engine to be refurbished. If this time limit is not met this could have critical cost impacts on the project. The maintenance of the recovery system itself is expected to have a small chance of causing delays. The refurbishment of the VuAB however is a complex operation with many disassembly and assembly steps which are time consuming and have a high probability of causing delays.
- **CDH-01** Communication with the ground station is very important during the atmospheric decent phase. The helicopter needs to continuously be updated on the position of the VuAB to be able to properly position itself for the retrieval manoeuvre. Loss of this communication would be mission critical. The probability of losing contact is considered very small, as the VuAB is outfitted with 4 antennas of which 2 are always in line of sight of the ground station.
- **CDH-02** The system contains sensors providing critical information to the different control systems. Failure of these sensors could have varying impacts on the mission with critical failure as a worst case. The chance of failure is relatively high as there are a number of different sensors of which only one of each is fitted in the system. This produces a number of single points of failure.
- **CDH-03** Data handling failure has an impact similar to sensor failure. Wrong interpretation of sensor data could lead to wrong control inputs which could impact the mission critically. The CPU used for data handling is a tested and used model designed for space flight. However, there is only one on board, so it is a single point of failure.
- **ELEC-01** Failure of the electrical power system would be catastrophic at any point in the mission. In every mission phase the system relies highly on the electrical power system. For a single battery the chance and impact of failure are relatively high.
- **STRUC-01** The launch is a critical load case, especially for vibrational loads. Structural failure during this phase has a catastrophic effect on the remaining part of the mission. The probability of this failure mode is expected to be small as the critical structural components are designed for this load case with appropriate load factors.
- **STRUC-02** There are estimations for the loads encountered in launch, but the load case is very complex and thus difficult to model. This gives a possibility of encountering unexpected loads during the launch. The impact could be substantial.
- **STRUC-03** The load case for re-entry is expected to be less critical than the load case in launch, so the chance of failure is lower. For some components the loads are higher than during launch, so failure is still possible. The most critical parts are the aeroshell and it's attachment. Failure of these components would have catastrophic impact on the mission.
- **STRUC-04** For the same reasons as for launch loads the encountering of unexpected loads during re-entry is likely. However, the impact is scaled lower because the loads are expected to generally be lower during

re-entry than those encountered during launch.
- **STRUC-05** The probability of attachment failure for the drogue parachute is highest at the moment of its deployment as that is the moment with highest loading. The probability of structural failure of the attachment is expected to be low as the attachments are designed for the worst case scenario with an added safety factor. The impact would be catastrophic as the parafoil cannot deploy without the drogue parachute.
- **STRUC-06** Also for the parafoil attachment the loading is most critical during deployment. The probability of failure is the same as for the drogue parachute attachment. Failure of the attachment would be catastrophic.
- **STRUC-07** During the catch manoeuvre the loads are transferred from the parafoil attachment to the catch attachment, because the parafoil is discarded. The load on this attachment is highest right after the moment of attachment. Failure would be catastrophic, as the parafoil is discarded at that point, so the VuAB has have no way of generating lift when it is dropped from the helicopter. For the probability the same goes as for the parachute and parafoil attachments, except that this load case is more critical. This slightly enlarges the failure probability.
- **PROJ-01** Even after the more detailed design phase it has proven difficult to come up with reliable development cost figures. The estimations that are made in Chapter 8 are conservative, but still the probability of going over this budget is expected to be high. The impact of overshooting the development budget is not very high. With the current expected profit margins a higher cost for development would not directly endanger the project.
- **PROJ-02** The schedule for further development of the system to have it ready for flight by 2022 does not have much room for delays. The schedule as presented in Section 9.4 seems feasible, but if any large problems arise during any of the phases this might cause the development to overshoot the 2022 deadline. The impact of these delays could be high. At some point it might not at all be feasible to continue the project as the costs might exceed the profits.
- **PROJ-03** The operating costs are estimated to a more certain level than the development costs, so the chance of going over budget is smaller. The impact would be much larger, as the operating costs add up over the number of launches and directly decrease the profit per launch.
- **PROJ-04** At this phase in the development of the system it is still very difficult to estimate the reliability. That makes it probable that the requirement will not be met. The impact of not meeting the requirement would be largely financial, as failure of the system costs a lot of money. Failure during the helicopter phase could result in loss of human life which is by any standard unacceptable.

In Figure 5.7 the risk events are mapped, before mitigation is applied. The events closest to the top right corner pose the greatest risks as they have both high probability and impact. These risks need mitigation to ensure they do not pose a threat on the future of the project.

5.4.2. Analysis and Mitigation

In this section the risk events mentioned in Section 5.4.1 are further investigated. More specifically, ways to mitigate the high risk events are explored. For the risks, ways to decrease the probability, impact or both are considered. In some cases the mitigation involves actions or processes that are to be used in later phases of the development. It should be closely checked that the mitigation is actually carried out in order to reduce the risk. Below the mitigation strategy for the different risk events is listed.

- **SPACE-02** The probability of ADCS failure is reduced by using four sets of 4 thrusters. This way there is no single point of failure in the ADCS system. Most rotations have direct redundancy, other rotations can be achieved by doing two rotations in series with other thrusters. New probability: 1.
- **DROGUE-01** The impact of drogue parachute deployment failure is decreased by splitting the drogue parachute into two. Together they provide the same properties as a single parachute, but if one fails, the other would still work. It would then take longer to decelerate to the required velocity, but it eventually will. The failure would now only be catastrophic if both parachutes fail. New impact: 3.
- **OPER-01** The probability of missing the landing zone can be reduced by enlarging the landing zone. This can be done by using 2 boats with 2 helicopters. The sensitivity analysis in Section 5.1 shows that this would increase the compatible separation velocities. New probability: 3.
- **OPER-03** To reduce the impact of helicopter failure two helicopters can be taken on the boat. One for redundancy. New impact: 3.
- **OPER-04** To reduce the touch down impact the boat could be fitted with a simple net or airbag construction. The impact will generally be small, so no large or expensive equipment is needed. This would reduce the impact for this risk event. New impact: 2.

Catastrophic	AEROS-01 DROGUE-02 PARA-01 OPER-03 STRUC-01 STRUC-03 STRUC-05 STRUC-06	SPACE-01 SPACE-02 AEROS-02 DROGUE-01 CATCH-01 STRUC-07	ELEC-01	CDH-02	OPER-01
Critical	PARA-03 CATCH-03 OPER-02 CDH-01	CATCH-02 OPER-04 CDH-03 PROJ-03	PROJ-02		OPER-06
Substantial		PARA-02	PROJ-04	STRUC-02	
Marginal				OPER-05 PROJ-01	
Negligible				STRUC-04	
	Highly unlikely	Unlikely	Possible	Likely	Very likely

Figure 5.7: Risk map of the VuAB recovery system before mitigation

- **OPER-05** The probability of transport delays can be reduced by closely keeping track of the transport channels and keeping delays in mind when scheduling transports. However, this does induce costs. New probability: 2.
- **OPER-06** The probability of delays can be reduced by extending the available time for refurbishment. To do this extra VuABs and Vulcain engines would have to be available. Refurbishment is expected to take three months, but by using 4 VuABs, an extra month is available to cover any delays. New probability: 2.
- **CDH-02** To lower the impact of sensor failure redundancy can applied. Taking a full second set of sensors is feasible as the weight and costs of these sensors is low compared to the level of risk it mitigates. New impact: 2.
- **ELEC-01** In order to lower the impact of electrical failure the battery would be split into two batteries that both have enough energy to power the whole mission. This removes the single point of failure. New impact: 2.
- **STRUC-02** The impact of unexpected loads can be reduced by using appropriate safety factors. There might then still be unexpected loads that are encountered during launch, but they would not cause the system to fail. However, the safety factor should not be too high, as this would mean that unnecessary mass is added to the system. New impact: 2.
- **STRUC-05**, **STRUC-06 STRUC-07** The attachments all consist of several attachment points. These points will be designed so that every one of the attachment points can carry the total load that is encountered. This reduces the impact of attachment failure. New impact: 3.
- **PROJ-01** To reduce the probability of going over the development budget more research would have to be done. When more accurate figures are obtained, proper contingencies can be applied and the chance of going over budget is reduced. New probability: 2.
- **PROJ-02** By keeping a tight handle on the project planning and keeping a close look at planning and project related risk both the impact and probability of running out of time can be reduced. Problems that are found in early phases can generally be solved with relatively low impact. New probability: 3. New impact: 3.
- **PROJ-03** The probability for this risk can also be lowered by doing further financial research. Also, applying proper contingencies in earlier phases of the further development is important to make sure the

budget is not exceeded. New probability: 1.

– **PROJ-04** The reliability of the system can be more accurately estimated later in the design process. Reacting adequately to any findings that might endanger the compliance with the reliability requirement would lower the probability of this happening. New probability: 2.

Catastrophic	SPACE-02 AEROS-01 DROGUE-02 PARA-01 STRUC-01 STRUC-03	SPACE-01 AEROS-02 CATCH-01	OPER-01		
Critical	PARA-03 CATCH-03 OPER-02 CDH-01 PROJ-03	CATCH-02 OPER-06 CDH-03			
Substantial	OPER-03 STRUC-05 STRUC-06	DROGUE-01 PARA-02 STRUC-07			
Marginal		OPER-04 OPER-05 PROJ-01 PROJ-02	ELEC-01 PROJ-04	CDH-02 STRUC-02	
Negligible				STRUC-04	
	Highly unlikely	Unlikely	Possible	Likely	Very likely

Figure 5.8: Risk map of the VuAB recovery system after mitigation

Not all risk events can be mitigated, but the highest risk factors can be. Figure 5.8 shows a mapping of the risks with their new scores after mitigation. When comparing this map to the map without mitigation (Figure 5.7) it can be seen that in general the risks moved from the upper right to the lower left corner. This means overall risk is reduced. It can also be seen that there are almost no risks close to the upper right corner. Only the missing of the landing zone due to an offset in separation speed remains a significant concern even after risk mitigation. In the future of the project this should be kept in mind. The risk could be lowered by extending the landing zone even further, but at this point that does not seem financially feasible. For reducing the risk in the future research should be done in reducing the variance in separation speed so that the landing zone can stay small.

5.5. Requirements Compliance Matrix & Feasibility Analyis

The progress in completing the deliverables and requirements defined in the Baseline Report are presented in Table 5.6 and Table 5.7. The requirements evaluated to be stakeholder requirements have been presented with an asterisk next to the requirement identifier. The compliance of the design can achieve four different ratings:

– **Full Design Compliance:** Design complies with requirement. No indication of complications in further phases. Represented by ✓
– **Marginal Design Compliance:** Design complies with requirement. Reason to believe complications may arise down the line. Represented by ~
– **Non Compliance:** Design does not currently comply with requirement. Represented by ×
– **Not Investigated:** Design does not comply with requirement because it could not be investigated yet. Represented by –

Every deliverable or constraint that has not been assessed to have Full Design comlpiance (✓) is justified below.

– **Not Investigated Requirements**: These requirements were considered to be outside the scope of the DSE project and require confidential information from the client not available at this stage. These requirements were still included as they remain relevant if the design were to advance to further stages.

Table 5.6: Stakeholder Deliverable & System Requirement Compliance

Identifier	Requirement	Compliance	Found in:
STKH-DEL-01	The safety and reliability of the full recovery system shall be included in the design trade-off process	✓	Midterm Report
STKH-DEL-02	The system sustainability index shall be included in the design trade-off process	✓	Midterm Report
STKH-DEL-03	The reusability of the recovery system shall be included in the design trade-off process	✓	Midterm Report
STKH-DEL-04	The payload penalty from extra mass induced by the recovery system shall be included in the overall cost modelling and Return of Investment analysis	✓	Section 8.3
STKH-DEL-05	The refurbishment operation costs of the key components shall be included in the overall cost modelling and Return of Investment analysis	✓	Section 8.2.3, Section 8.3
STKH-DEL-06	The extra costs for the recovery systems shall be included in the overall cost modelling and Return of Investment analysis	✓	Section 8.2.3, Section 8.3
STKH-DEL-07	The retrieval operations of the key components shall be included in the overall cost modelling and Return of Investment analysis	✓	Section 8.2.3, Section 8.3
STKH-DEL-08	The designing, testing, integration of the full recovery system shall be included in the overall cost modelling and Return of Investment analysis	✓	Section 8.2.2, Section 8.3
STKH-DEL-09	The number of launches for which the key components are reused shall be included in the overall cost modelling and Return of Investment analysis	✓	Section 8.2.3, Section 8.3
STKH-DEL-10	A complete system breakdown shall be used in design phases	✓	Section 4.6
STKH-DEL-11	Recovery from either sea or land shall be included in the design options development.	✓	Mid Term Report
FUNC-PERF-MISS-A	The Mission Support shall be informed of all Mission Essential Data	✓	Section 4.5.3
FUNC-PERF-STRC-A	The system shall not experience critical failure due to forces in all directions during any mission phase	✓	Chapter 4
FUNC-PERF-STRC-B	The system shall not experience critical failure due to vibrations in all directions during any mission phase	✓	Section 4.2.7, Section 4.3.6
FUNC-PERF-STRC-C	The system shall not experience critical failure due to the environment during any mission phase	✓	Section 4.2.3, Section 4.1.3
FUNC-PERF-STRC-D	Deflections of the system under load shall not lead to a loss of functionality during any mission phase;	~	Section 6.1.3
FUNC-PERF-STRC-E	The payload shall be secured for the duration of the mission	✓	Chapter 4

Table 5.7: System Requirement Compliance

Identifier	Requirement	Compliance	Found in:
FUNC-PERF-GNC-A	The system shall return to a predefined landing zone with an accuracy of 50 m	✓	Section 4.3.2
FUNC-PERF-GNC-B	The system shall determine its attitude, position and velocity at predefined moments of the mission	✓	Section 4.3.2
FUNC-PERF-GNC-C	The system shall be able to determine the necessary moments for changes to its trajectory	✓	Section 4.3.2
FUNC-PERF-GNC-D	The system shall be able to enact the necessary changes to its trajectory as planned	✓	Section 4.3.2
FUNC-PERF-GNC-E	The system shall be able to control all system actuators	✓	Section 4.3.2
FUNC-PERF-GNC-F	The system shall identify critical failures and enact contingency plans for those situations	~	Section 4.3.2
FUNC-PERF-TLM-A	The telemetry system shall be designed to be integrated with existing Ariane 6 ground systems	✓	Section 4.5.3
FUNC-PERF-TLM-B	The telemetry system shall communicate essential mission data with the ground	✓	Section 4.5.3
FUNC-PERF-TLM-C	The telemetry system shall communicate the ocurrence of mission defining events to the ground	✓	Section 4.5.1
FUNC-PERF-REC-A	The recovery system shall disipate the kinetic and gravipotential energy of the VuAB	✓	Section 4.2.3, Section 4.3.2
FUNC-PERF-REC-B	The recovery system shall return the payload to Earths surface in conditions where refurbishment costs will be less than 6 M Euros	✓	Section 8.2.3
FUNC-PERF-REC-C	The recovery system shall ensure the landing velocity will not exceed 5 m/s	✓	Section 7.1.5
FUNC-PERF-REC-D*	The key components of the Vulcain Aft Bay of the 1st stage of the Ariane 6 that shall be recovered, refurbished and reused are the frame, the turbopumps, pyrotechnic devices, the engine, the nozzle	✓	Section 4.6
FUNC-PERF-OPS-A	The logistics of delivery, transport, integration with Ariane 6, retrieval and refurbishment shall not cause delays of more than 7 days each	–	
FUNC-PERF-INT-A	The operation of the recovery system shall not excessively impede normal operation of the Ariane 6 during the pre-launch, launch and separation	~	Section 4.6
FUNC-PERF-INT-B	The integration of the recovery system shall not require redesign work or modifications to the Ariane 6 costing more than 20 M Euros	–	
FUNC-PERF-INT-C	The integration of the recovery system shall not require redesign work or modifications to the Ariane 6 costing more than 26 weeks	✓	Section 7.2
FUNC-PERF-INT-D	The centre of gravity of the recovery system and VuAB may not be more than 50 mm off the longitudinal axis during launch	×	Section 4.6
FUNC-PERF-INT-E	No component of the recovery system shall be placed beneath the structural cross	✓	Section 4.6
FUNC-PERF-INT-F	No modification to the VuAB will be required to accommodate the packaging of the recovery system	✓	Section 4.6
FUNC-PERF-INT-G	No component of the recovery system shall be placed above the lower part of the first stage LH2 fuel tank	✓	Section 4.6
FUNC-PERF-INT-H	Parts placed on the outside of the skirt shall take into account the boosters in a 4 booster configuration	✓	Section 4.6

Identifier	Requirement	Compliance	Found in:
FUNC-PERF-INT-I	The packaging shall take the fuel lines into account while they are still attached to the VuAB	✓	Section 4.6
FUNC-PERF-REF-A	The final landing site shall be determined and communicated to the on-site team with an accuracy of 1 km	~	Section 5.1
FUNC-PERF-REF-B	The retrieval of the system shall take no longer than 30 days	✓	Section 7.1.1
FUNC-PERF-REF-C	The refurbishment apparatus shall be operational before the recovery system is fully operational	✓	Section 7.2
FUNC-PERF-REF-D	The refurbishment of the key components of the VuAB shall not take longer than 1 year	✓	Section 7.2.2
FUNC-PERF-REF-E	The reliability of the key components of the VuAB shall be 90% of the original reliability of the components	✓	Section 7.2
FUNC-PERF-REF-F	The reliability of the A6 launcher using refurbished VuAB key components shall be 90% of the original reliability of the A6 launcher	✓	Section 7.2
FUNC-BUD-A*	The increased total weight of the A6 launcher with the installed and operable recovery system versus an A6 launcher without recovery system shall not exceed 3000 kg	✓	Table 4.13
FUNC-SRR-A*	Success rate of the recovery system shall be at least 0.8	~	Section 5.3.1
FUNC-SRR-B	The models used on board of the recovery system shall be verified with an accuracy of 1%	–	
FUNC-SRR-C	The models used on board the recovery system shall be validated with an acurracy of 5%	–	
FUNC-SRR-D	The models used during the design of the recovery system shall be verified with an accuracy of 1%	×	Chapter 6
FUNC-SRR-E	The models used during the design of the recovery system shall be validated with an accuracy of 5%	–	Chapter 6
FUNC-SRR-F*	All the personnel involved in testing, integrating and operations involving the recovery system shall not be exposed to serious danger.	~	Section 5.3.4 Section 4.1.3, Section 4.4
FUNC-SRR-G*	The recovery system shall have safety measures for launch failures	✓	Section 5.3.4
CONS-TIME-A*	The recovery system shall be fully operational 2 years after the 1st A6 launch, where the first A6 launch is envisaged in 2020	✓	Section 9.4
CONS-COST-A*	A 15% cost reduction for an Ariane 6 launch shall be established after 5 years of Ariane 6 operations	✓	Section 8.3
CONS-COST-B	The VuAB shall be reusable at least 10 times before reaching EoL	×	-
CONS-COST-C	Refurbishment of the VuAB shall cost no more than 10% of the overall VuAB cost after 5 years of operation	✓	Section 8.3
CONS-COST-D	The recovery system shall cost no more than 30% of the overall VuAB cost after 5 years of operation	✓	Section 8.3
CONS-SUST-A	The Sustainability estimation system shall have a relative	✓	Section 5.2
CONS-SR-A*	All components present in the recovery system shall have a Technology Readiness Level of at least 5	✓	Midterm Report, Section 4.6.3
CONS-SR-B*	All sub-systems present in the recovery system shall have a Technology Readiness Level of at least 5	✓	Midterm Report, Section 4.6.3

- **FUNC-PERF-STRC-D:** The structural elements of the system were designed to remain within the elastic deformation regime. A full in depth analysis on allowable deflections and compliances was excluded. This can be done better at a further stage using a FEM analysis when the geometries and loading become more complex. For this FEM to be accurate, more (confidential) information regarding the structural properties of the VuAB must be known.
- **FUNC-PERF-GNC-F:** The design of the parafoil control system is currently not equipped to handle failure situations. The current framework can easily be adapted to flight with inactive control surfaces. The largest challenge would lie in the recognition of those situations by the system.
- **FUNC-PERF-INT-A:** The recovery system has been designed to make the integration as simple as possible. It is clear that when modifying a design, such as the A6 that is far into detailed design, the complexity of integration increases the deeper it is looked at. For this reason this requirement was marked as marginally compliant.
- **FUNC-PERF-INT-D:** With the current packaging this requirement is not reached, as the value is at 57 mm. The most critical reason for not reaching the requirement is the packaging and position of the parafoil. It was positioned so as to counteract the C.o.G. shift of the aeroshell, a part that weights almost 3 times more than the parafoil. The positioning of the parafoil contributed to a C.o.G. shift in a direction without counterweight. By tweaking the centroid of the parafoil, the requirement can be reached by balancing the two directions of C,o.G. shift to reduce the magnitude of the overall C.o.G. shift. Alternatively, modifications to the VuAB that make packaging of the recovery system easier could resolve this problem altogether. The worst solution would be to use the margin from the weight requirement as a ballast to help the C.o.G. location.
- **FUNC-PERF-REF-A:** The sensitivity of recoverability versus uncertainties in separation altitude and velocity is extremely high. As the expected uncertainty of the Ariane 6 in these parameters is uncertain, this parameter was marked as marginally compliant. If problems arise multiple boat configurations can be attempted. Otherwise some form of controllability during re-entry can lead to a sufficient correction in final landing location. An example of a control system can be to gimbal the engine to shift the C.o.G. to change flight angles sufficiently to correct the trajectory.
- **FUNC-SRR-A:** This requirement is marked as marginally compliant, for 2 reasons. Firstly, the marginal compliance of FUNC-PERF-REF-A impacts the success rate from Section 5.3.1 considerably. Secondly, there are many ways to come to this number. The originally proposed method was a product of all the component reliabilities. This method proved to be difficult to use as reliability numbers are difficult to come by for some components. It is entirely possible that this method yields an unsatisfactory success rate. If this were to happen, more redundancy or better components could be used, increasing the system mass. Otherwise, deployment of the parafoil and chutes at a lower altitude can lead to better deployment reliability. In this case gliding performance is sacrificed.
- **FUNC-SRR-D:** The quality of verification procedures and sources varied between models. To make this a Fully Compliant requirement, more time and a standardised effort is required. The models and design tools outlined in this report would be expanded upon for a detailed design phase. In that case there will be time available to improve this aspect.
- **FUNC-SRR-F:** The effects of radiation on the system was looked at briefly in this report. To achieve Full Compliance, the equipment, handling of the equipment and working attire of the retrieval, refurbishment and reassembly team needs to be investigated. Furthermore using a pilot for the helicopter catch relegates this to a Marginal Compliance requirement. Despite the analysis on the feasibility of the catch, a critical failure will lead to high impact consequences. The best way to mitigate this risk is to make the entire catch operation automated (as Falcon 9 does). This is possible but is far outside the scope of this project.
- **CONS-COST-B:** This requirement was not achieved as after the formulation of the requirements the client stated the limit of Ariane 6 engine reuses was 5. The business case was adapted to this as a result, however as the recovery system costs were lower than initially projected, the cost reduction was not affected to the point of not meeting its requirement. Effectively the requirement is now reformulated to read: "The VuAB shall be reusable at least 5 times".

6

Verification and Validation

The purpose of this chapter is to summarise the verification and validation strategies, execute the validation and suggest further verification and validation procedures. It is important to note that the verification execution of the models and the sub-system designs is conducted in Chapter 3 and Chapter 4 respectively. This is done for the ease of understanding and reading. This chapter simply provides the verification methods and procedures in each design phase.

6.1. Verification

The purpose of verification is to make sure that the models used and designs made comply with the imposed conditions and requirements, respectively. This is an internal process that is carried out at different levels of the design. The design process can be split up in several main design phases that each require adequate and unique verification. The first phase is the simulation tools and models created. The next phase includes the sub-system designs and optimization. The last phase is the sub-system integration after which the final design is the output. The applied verification strategies in each phase are so different that they will be emphasized upon in separate sections.

6.1.1. Model Verification Strategy

The verification strategy of the models is based on the suggested strategy as proposed in the mid-term Review [71]. The purpose of model verification is to prove that the simulation model accurately represents the chosen physical model. Similar to a design, a model includes many 'sub'-models which each are composed of units of code. Each level requires adequate verification. From lowest level being units codes to highest level being the fully integrated model, the applied strategy is as follow:

- **Unit test:** The purpose of unit tests is to verify that a functional unit of the model (feature), it in its standalone format, works as intended and the outputs are correct. This can be done in two ways. One is to determine an analytical solution and compare the results. Second is to retrieve a reference value from external literature and with the same parameters and input values compare the final result.
- **Integration test:** Integration tests verify that the accumulation of features work together as intended.
- **System test:** Is similar to a unit tests, but on a higher level as it verifies that the output of the model is as intended. The model is verified by evaluating if the model outputs the correct numerical value for a given input value from all the input features.
- **Acceptance test:** Finally, the acceptance test is based on the accuracy in terms of percentage difference (PD) of the final system output. The error at unit test level might cause some or even all the outputs after that to scale in PD as well (cascade effect). It is important to make sure that this accumulation of error is not incrementing itself in the output and in further dependencies.

Each model as discussed in Chapter 3 will perform model verification and apply the strategy as discussed in this section. In the sections, a required accuracy will be defined which result from the system accuracy requirements.

6.1.2. System Verification Strategy

Each subsystem as described in section Chapter 4 will need to be evaluated for compliance with the expected performance. This is also true for the fully integrated system. The verification strategy must include the following

parameters: The verification method, verification level and the applicability. Subsystem and system design will be verified by means of at least one of the following four methods. The four methods are as follows:

- Analysis
- Demonstration (review of the design)
- Inspection
- Test

At this stage in the design process, the only verification methods that are applicable to the system design is a review of the design and analysis. Components are not manufactured and therefore cannot be verified by tests nor inspection. The designs of the (sub-)systems are optimized to meet the function requirement for several design parameters such as mass, size, power budget. A design review to verify that the requirements have been complied with is done in Section 5.5. Moreover, verification by analysis is performed to a limited extend. In Chapter 4, each sub-system performs its part in this verification. Where applicable, each subsection performs a functional, operational or control analysis to verify the design. This is different for every subsystem. It must include the specified method, level and explain why the tests are applicable to the design. As a further analysis, the results can be compared to existing systems for reference. The fully integrated system is verified by means of configuration analysis, a RAMS analysis and several speciality analyses such as operations, costs, sustainability, risk and producibility.

Ideally, verification shall be performed to the lowest component level possible. However, regarding the scope of this feasibility study, many components and units are not defined into great detail. For this reason the level of verification is limited to the subsystems and the integrated system.

6.1.3. Further System Verification

The scope of this feasibility study limits the verification methods that are executed. The purpose of this section is to provide additional methods on how the design at this stage in the design process, with the respective level of detail, can be further verified using more advanced tools.

Simulation and Models

- The space trajectory can be further verified by means of analysis. The General Mission Analysis Tool (GMAT) and the TU Delft Astrodynamics Toolbox (Tudat) can be used to verify the current space trajectory model.
- The Re-entry trajectory model can also be verified with the Tudat. This does not only apply to the calculated trajectory but also the re-entry dynamics.
- The atmospheric flight trajectory model can be further verified by means of comparison to an analytical method. The current method of determining the trajectory is based on a numerical analysis. (Runge-Kutta)

System Design

- The current detail of design of the design of the aeroshell allows for verification via CFD involving the steady solution of the reacting Navier-Stokes equations.
- The type and thickness of the TPS is known, this allows for the verification that the chosen TPS will be able to endure the thermal loads and dynamic loads experienced during re-entry by testing it with an arc jet. Arc jets are much used TPS testing methods and can sample dynamic pressure, heatflux, enthalpy and shear stress for long periods of time. [19].
- The parafoil is an off-the-shelf parafoil. This means we are not limited by the fact that a full detailed design has to be made before testing can be done. However, due to the shear size of the parafoil, a wind tunnel test is not feasible. Components such as the fabric, chords, the fabric-chord attachments can be tested for tensile strength and dynamic pressure.
- The ability of the control actuators to provide the needed moment can be verified in a wind-tunnel.
- Tension tests will be conducted to verify the strength of the cable that will carry the VuAB when suspended under the helicopter.
- Full Finite Element Analysis of structural components of recovery system and VuAB for stresses and deflections.

6.1.4. Detailed Design Verification Methods

When the detailed design is completed, verification can be done on the lowest level. As seen across the space engineering industry, this will involve heavy testing and certification. Verification is often the most expensive

and time-consuming phase in the development of a space product. All components must be either certified or otherwise verified to function as required. At this stage it is not feasible to give a full overview of verification methods for all components. The focus will be on the most critical systems and functions such as the aeroshell and the VuAB catch operations. Since the parafoil is off-the-shelf and certified, there will be no emphasise on the parafoil verification. Subsystems such as the aeroshell can be prototyped for full scale testing, an example verification procedure for the aeroshell is given below. Note that overlap between verification and validation exists, this is so because certain tests can, for example, be used to verify material properties as well as validate models.

- The aeroshell can be prototyped and design parameters verified by tests. Its packing volume and weight can simply be measured. The Small Probe Reentry Investigation for TPS Engineering (SPRITE), which is a type of arc jet test in will be performed to verify the thermal load capabilities [43]. Moreover, a structural analysis test can be conducted to verify the material properties of the inflatable aeroshell as well as the overall stiffness and deformation. The following aerodynamic properties of the aeroshell can be verified in the National Full-scale Aerodynamics Complex (NFAC): deformation due to aerodynamic effects, lift, drag and moment generation at various angles of attack.[21] This will also serve as a validation to the models.
- The helicopter catch mechanism, as well as the VuAB catch mechanism can undergo a structural analysis by a test where the expected loads are exerted on the cable and break system. The effects of the catching cable on the parafoil performance must be verified, this can be done by a flight test with a simple dummy mass with the same mass as the VuAB. The performance of the secondary parafoil can be verified by means of simple wind tunnel tests.

6.2. Validation

Since the nominal operation for the recovery system involves a very expensive Ariane 6 launch, standard validation procedures, by means of operational experiments, do not often apply. However, the designs of subsystems can be validated by means of simplified tests. Many functional verification tests serve as validation to the models.

- The packaging and lay-out inside the VuAB can be validated on the ground as soon as the design of the Ariane 6, and the VuAB in particular is fixed and manufactured.
- The aeroshell deployment performance will be validated in large vacuum chambers under the verified atmospheric conditions.
- Load tests can validate the structural integrity of the toroids that are part of the aeroshell. It would be conducted by fixing the centrepiece of the aeroshell to the floor and inducing loads by a random input shaker, see Figure 6.1c [1].
- To validate the performance of the parafoil a high altitude drop test will be conducted. This will be conducted similar to that of the Guided Parafoil High Altitude Research conducted by Airborne systems [13]. This can and will at the same time serve as a validation to the atmospheric flight model, as well as the deployment. Aspects of the catch, such as the helicopter 'catching' the cable as well as parafoil discarding may be validated by means of a comparable test.
- The helicopter stability model and performance as well as landing operations are validated by flying the last mission phase with a dummy mass suspended from the helicopter.

(a) Arc Jet test (b) HIAD testing in NFAC (c) HIAD structural test article

Figure 6.1

[1] https://www.nasa.gov/centers/armstrong/Features/HIAD_decelerator_system.html, [23-01-2018

7

Operations, Refurbishment and Production

This section concerns with the operations involved in the recovery of the VuAB. First the recovery operations are analysed in Section 7.1. Then the refurbishment strategy (Section 7.2) and the production plan (Section 7.3) are discussed. This section likewise Chapter 4 will cover all of the functions within F 3.5, F 3.6 and F 3.7 from Figure 2.8 and Figure 2.9.

7.1. Operations

This section contains the operations of the VuAB recovery. First a general outline of the operations is stated in Section 7.1.1, after which an Operational Flow Diagram (OFD) is presented in Section 7.1.2. Finally the operational costs are discussed in Section 7.1.4.

7.1.1. General Outline

In order to be able to recover the VuAB using a helicopter its estimated recovery location is to be known. At an altitude of approximately 8 km, just before the parachute systems starts deployment, an estimation on the landing locations can be made. A plot showing a range of 1000 possible descent locations as red dots is shown in Section 7.1.1 (Section 3.1.3), where both axes represent the meters, in x and y direction. As can be seen, the descent locations are spread out in an ellipse of approximately 26 km by 4 km.

The parafoil control system is designed in such a way that it starts loitering from deployment onwards, from an altitude of 7.3 km to an altitude of 4 km. From an altitude of 4 km it orients itself towards the boat and keeps the same heading until it is retrieved by the helicopter. This is done as the catch method described in Section 4.4.1 needs a constant velocity vector in order for the helicopter to be able to hook onto the secondary parafoil. The altitude of 4 km is chosen to stop loitering as this is the approximate operating ceiling of the helicopter (The helicopter choice is stated in Section 7.1.3) and thus the point from which the helicopter can align its velocity vector with that of the VuAB.

From the altitude of 4 km the parafoil takes 8 minutes to descend to an altitude of 1.4 km. During this period the helicopter aligns its velocity vector to that of the VuAB. The altitude of 1.4 km is set as this is the maximum height for which the chosen helicopter can cope with the maximum loads exerted on the helicopter. In section Section 7.1.3 this is elaborated upon in further detail.

Two ships are involved in the recovery process. One ship on which the VuAB is landed which comes from the Ariane 6 launch site in Kourou and transports the VuAB to its refurbishment site in France. Another ship has the sole purpose of transporting the helicopter from the launch site to the recovery site and returning it to that same launch site. This is done to reduce the operational costs, as stated in Section 7.1.4. During recovery, both ships are at the median of the range of landing locations. Placing the ships at this location the has the highest probability of the VuAB descending in close proximity to the ships. Thus, this reduces the distance the helicopter has to fly in most cases, thereby reducing cost, the risk involved (as the performed operation is as small as possible) and decreasing the effects on the environment. By placing the ships in the middle the maximum distance the helicopter will have to fly to reach the VuAB is approximately 26 km, back and forth both included. This length is derived using twice the farthest distance from the median of the ellipse in Section 7.1.1. In case the VuAB stops loitering close to the ships and overshoots them, it can glide for about 12 km, which the helicopter can cover.

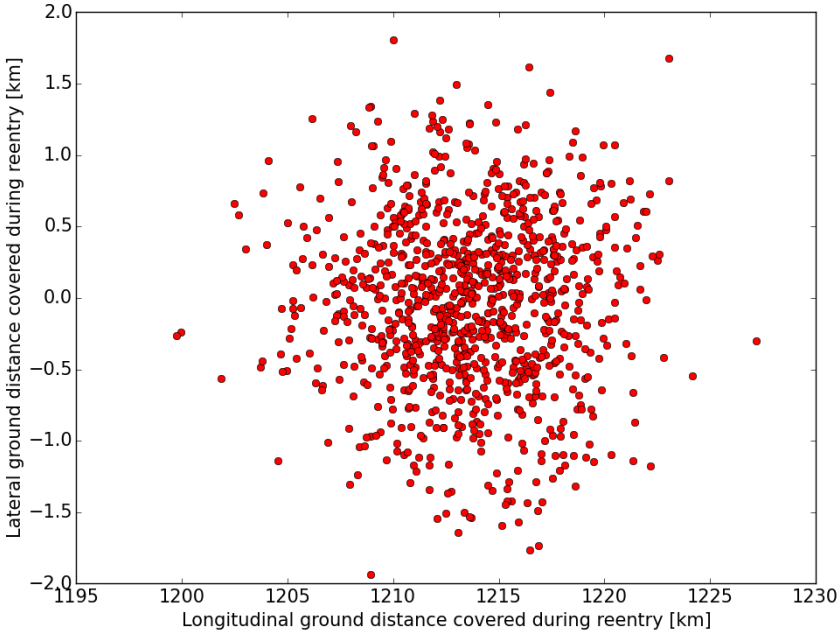

Figure 7.1: Approximate descent locations estimated at 8 km altitude

The time it takes for the VuAB attached to the parafoil to descend from 7.3 to 4 km is 9 minutes. At 7.3 km altitude of the VuAB the helicopter is already in the air and at 4 km the helicopter should be in close proximity to the VuAB. In order to arrive at the parafoil in the case that the parafoil is at the farthest possible distance, 13 km away, it would have to travel 13 km in 9 minutes. As the cruise speed of the helicopter is 315 km/h [41] the distance the helicopter can fly in 9 minutes is 45.94 km, leading to the conclusion that the distance of 13 km should not pose a problem.

7.1.2. Operational Flow Diagram

Section 7.1.2 shows the operational flow diagram of the recovery operations described above. The objects denoted by the main number '1' (blue), state the VuAB locations. These are used in order to time certain events in the recovery operations process. The latter are denoted by the main number '2' and are shown in yellow.

7.1.3. Helicopter Choice

In order to see which helicopter is suitable the maximum loading that is experienced during catch has to be known. It is shown that the loading during catch is the critical load case. For an attenuation distance of 8 m the maximum load experienced during catch is approximately 123 kN Section 4.4.2. The 8 m attenuation length is chosen as from this point onwards increase in this attenuation length does not decrease the load by a sufficient amount. Using an ISA atmospheric model the maximum load capacity per altitude is calculated. Subtracting from this the loads introduced by the attenuation system, fuel and pilot mass a calculation results in the maximum payload capacity per altitude, which is shown in Figure 7.3. Comparing this to the catch load the helicopter would need to be able to cope with results in the altitude to which a helicopter type can carry the catch load. This is shown in the right column of Table 7.1. It can be seen that only the Sikorsky CH-53E and CH-53K are capable of carrying this load. Additionally, it can be seen that the CH-53E is only capable of performing the catch manoeuvre at an altitude of 190 m, which is deemed to low as this leaves almost no margin for error. Therefore, the CH-53K is chosen as the helicopter for retrieving the VuAB, which is able to perform the catch manoeuvre at 1.4 km. From this altitude the helicopter has an estimated time of 4.5 minutes to perform the catch. The helicopter mission profile is as follows. At the parafoil deployment altitude the helicopter is in the air. In the time the VuAB descends from 8 to 4 km altitude (9 minutes) the helicopter flies to the VuAB. From the 4 to 1.4 km altitude the helicopter aligns its velocity vector with that of the VuAB, for which it has 8 minutes. From the altitude of 1.4 km the helicopter performs the catch manoeuvre, after which it returns the VuAB to the ship

Table 7.1: Helicopter types, their respective payload capacities at ground level and altitudes for the maximum load during catch (123 kN)

Helicopter Type	Load capacity [kg]	Max altitude for catch Load [m]	Time to ground level [min]
Sikorsky S-64F	11,364	Not possible	-
Columbia Model 234	11,818	Not possible	-
Sikorsky C-53E	14,500	190	0.63
Sikorsky C-53K	15,600	1,200	4.01

Table 7.2: Operations cost, averaged for both landing locations

Cost type	**Price [Euros]**
VuAB shipping charter	132,404
Helicopter shipping charter	22,537
Helicopter lease	964,000
20 % margin	215,260
Total	**1,291,565**

bound for France and lands it. Finally, it retrieves the parafoil as it is not sustainable to leave the object in the water. Finally it lands on the ship bound for Kourou and is returned to the port.

7.1.4. Operational Cost

In order to estimate the cost of operations an estimation has to be made on the way the VuAB is transported. As both landing locations, the middle of the Ocean for a GTO launch (80 % of launches)[1] and to the right of Canada (20 % of launches), are in open water a ship is needed. The size of the VuAB imposes a significant constraint on transportation due to its size and therefore it can not be transported by an aircraft. Therefore, all the transportation is done by ship. Landside transportation cost would occur either to and from the ship to the Kourou launch facility or to and from the ship to the Airbus refurbishment facility in France. As these distances are minimal and the fact that both of these facilities are already capable of transporting large objects over land it is assumed that these costs can be neglected. This leaves the costs of the ship and helicopter lease as the main drivers for the operational costs.

For both landing sites a cost estimate is made which is then averaged based on their ratio. For the shipping costs actual ship charter rates and average sailing speed are used [2]. For the Mid-Air Recovery helicopter costs are incorporated, these are computed using actual helicopter charter rates for the Erickson S-64F [3], capable of lifting loads of 12,500 kg . This does not suit the needs of the recovery, but it is assumed that this gives a good estimation of the costs.

Initially costs are estimated for a ship and helicopter leaving from Kourou, performing the recovery operations, shipping the VuAB to France and from there returning to its port in Kourou. However, it is cheaper to have two ships leaving from Kourou initially, one for the VuAB landing and shipping and one for the helicopter. After the catch is performed the helicopter is returned to Kourou immediately and the VuAB is shipped towards France, for which it is secured in such a way that it is protected from the humidity, water and salt during its transport. Additionally, during the transport the first system checks on the VuAB are done, in order to speed up the refurbishment process. Costs for the entire recovery operation are stated in Table 7.2. In the table it can be seen that there is a 20 % margin. This margin is used to account for aspects not incorporated such as the personnel onboard the boats. The total operation costs are taken into account in the business analysis in Chapter 8. Travelling from Kourou to the recovery location takes on average 5 days and travelling from the recovery location to France takes on average 8 days. Including one day for performing the recovery the total from Kourou to France including recovery comes down to 14 days, whereas returning from France to Kourou takes approximately 10 days.

7.1.5. Landing Operations

As the VuAB will be transported using a ship the helicopter will need to put it down on the ship. This section looks into multiple landing devices that might achieve this. In the following landing system analysis it should be noted that the VuAB will approach the landing site with its nozzle oriented downwards, which is also a protruding

[1] Private contact, Airbus Defence and Space (client), H. Cruijssen

[2] `http://www.vhss.de/index.php?id=28&L=1`, [27-01-2018]

[3] Private contact, E-mail, Erickson Incorporated, M. Vaji

object. Additionally, it should be noted that the helicopter system allows for the cable to be reeled in. Hence, the VuAB is reeled in so that the VuAB is located 42.21 m below the helicopter attachment, maximising control of the helicopter on the VuAB. This 42.21 m is derived from the fact that this is the length of the VuAB to the top of the secondary attachment, from which it can not be reeled in further (This can be seen in Section 4.4.1). Lastly, it should be noted that the system is carried by a helicopter, which is able to hover and thus reduce its vertical descent velocity to zero, the impact with which the VuAB will land can be at low velocity (< 1 m/s). However, for the purpose of taking into account flight instability, wind gusts during and after landing and extra loads that might arise during transport a descent velocity of 2 m/s is assumed. This is just within acceptable landing limits for aircraft, a velocity greater than this would be characterised as a hard landing [6]. Landing with this velocity and reducing the velocity to zero in half a second results in an impact force of 39.37 kN that the landing system would have to cope with.

Due to the low descent velocity and the pinpoint accuracy the helicopter can deliver it is not necessary to have the landing structure available on the VuAB itself. This is also not desired as this increases the mass of the VuAB system. The following landing systems can be implemented on the landing site on the ship and thus are investigated in this section: a pneumatic bag attenuation system, foam filled landing bags, a soft landing on a fixed structure and a landing on a soft material without accompanying structure (e.g. rubber) [33].

While the pneumatic bag and foam filled attenuation systems might be able to do the job, they are discarded due to the fact that they pose several clear disadvantages. Systems landing on these have a tendency to topple, bouncing or rolling of. Additionally, there is also the risk of bouncing. Lastly, as stated, the VuAB nozzle is a protruding object. While it might be capable of withstanding some loading, this is not desired as it is a part of the key components the project is designed to re-use. When landing on a pneumatic bag or foam filled bag attenuation system the nozzle will be the first part of the VuAB that will come into contact with the landing surface. This is also the main reason that the landing on a a soft material without accompanying structure is discarded. As the soft landing on a fixed structure does not necessarily have this disadvantage this method is investigated in more detail below.

Soft Landing on a Fixed Structure

When investigating this option it is important to see whether there is a structure on the VuAB itself capable of carrying the loads involved in landing. One of the main structures in the VuAB that might be able to do this is the load bearing structure accounting for the boosters. The boosters of the VuAB, 2 for the Ariane 62 configuration and 4 for the 64 configuration are attached to a support structure present in the VuAB (Figure 7.4a), which absorbs the main portion of the loads they exert. As can be seen in Figure 7.4b the structure is located on the bottom of the VuAB. Using this load bearing structure in order to set the VuAB down might be a good solution if the structure is capable of supporting the forces. The boosters are each capable of providing a thrust of 4,500 kN [4]. Thus, the structure should be capable of taking 18,000 kN of thrust in the case all four boosters are attached. The force that would be exerted on the structure in touchdown configuration are 96.55 kN. Adding to this the forces introduced by a hard landing and a safety factor of 1.5 this would be 199.2 kN. This is only a small percentage (0.74 %) of what the boosters exert on the structure and thus the structure is able to cope with the loads during landing and its landed configuration.

This landing structure has not yet been designed, but can be designed in such a way that contact points will only exist on the booster load structure, and none will be exerted on the nozzle or other components of the VuAB. Additionally, it can be designed in such a way that no components will have to be added to the VuAB itself. For example, this can be done by creating a hollow circular structure to which the VuAB will be set down on its booster load bearing structure and adding rubber contact points to reduce the impact and any damages that might occur with that. The hollow part is where the nozzle of the Vulcain engine is located in its landing position. This system has to be able to carry the load of 199.2 kN. Additionally, it can be done using several struts on which the VuAB booster load bearing structure touches down. While swing during landing might be a significant factor, the Vulcain engine nozzle is 2.1 m, whereas that of the VuAB and with it the booster load structure is 5.4 m. This leaves a margin of 1.65 m on either side during landing, enough to account for minor swing that might occur during landing. Certainly when taking into account that there is no time constraint on the landing apart from the amount of fuel in the helicopter slowing landing operations and thereby reducing swing is possible.

[4] http://www.avio.com/en/ariane/ariane-6/p120c-motor/, [11-12-2018]

7.2. Refurbishment

The refurbishment is an integral part of the recovery and re-use mission of the VuAB. This section will outline what parts shall be considered for refurbishment and how the refurbishment will take place.

7.2.1. Refurbished systems

The main components of each system shall be evaluated and categorised as a consumable or a refurbishable component. The systems are the VuAB, the Vulcain engine and the recovery system. These are the systems that are evidently retrieved after an Ariane 6 launch. An important note is the the VuAB can be refurbished up to five times, as established by Airbus Defence and Space. The components of the VuAB are categorised as follows:

Refurbishable

- The VuAB skirt
- The Vuclain supportcross
- The external booster support bottom ring
- The liquid oxygen external fuel pipes

Consumable

- Separation Ring
- VuAB-Vulcain Interface
- Main fuel pipe of liquid oxygen tank

The components of the Vulcain 2.1 engine are catagorized as follows:

Refurbishable

- Nozzle
- Fuel and liquid oxygen injection pumps
- Structure
- Combustion chamber
- Internal Vulcain engine piping

Consumable

- Liquid oxygen tank connection
- External pipe connections

The refurbishability of the recovery system itself will be analyzed in depth as Maintainability in Section 5.3. However, a note must be made regarding the parafoil, parachute and the aeroshell. This is so because even though these components are currently discarded, these sub-systems prove great potential for refurbishment and re-use. All the sub-systems are manufactured by the same company Airborne Systems. Therefore, these three sub-systems are taken into consideration for the refurbishment strategy.

7.2.2. Refurbishment Strategy

The strategy for refurbishment is as follows: The retrieved VuAB will be brought to the Lower Liquid Propulsion Module (LLPM) assembly site, after which it will be dismantled. Next, the sub-systems will be brought to the manufacturer of that specific sub-system. At these locations refurbishment will take place. Once refurbished, the sub-systems will be as good as new and ready for shipment to the assembly site to be made ready once again for operations. This last stage, in which the refurbished (or original) sub-systems are assembled to the VuAB and evidently to the LLPM is covered in greater detail in Section 7.3. The refurbishment process as described above is depicted in more detail in Figure 7.5.

The refurbishment of outsourced and delivered sub-systems, such as the Vulcain 2.1, the VuAB and possibly the parafoil, parachute and aeroshell will be conducted to the same standard. Much of the structural characteristics of the above mentioned sub-systems is classified information and is not provided by the companies. Therefore, exact refurbishment strategies and tests cannot be specified for each sub-system. However, a general strategy and quality assurance procedures are defined. In chronological order, the refurbishment will be conducted as follows:

1. **Disassembly of sub-system** The sub-systems will be disassembled to component level. For the VuAB this means that the (if possible) support cross and booster support ring are separated from the skirt.
2. **Structural Health Monitoring** All components will be carefully inspected for damage. This will involve the following methods: observe, measure, gauge, (non-destructive) test. The inspection must include geometrical (buckling, deflection), material (plasticity, residual stresses), environmental (UV, thermal) and age related (fatigue) factors. A few specific examples of a tests that can be conducted are vibrational analysis and ultrasound tests. [25]

3. **Analysis of Inspection** The damage size shall be determined as well as the effect on the structural integrity. This will be reported.
4. **Perform Corrective Maintenance** If needed and possible, maintenance can be performed: corrective maintenance on demand. It involves fault diagnosis, fault correction and function check-out.
5. **Re-usability decision** The standard that will be applied is that the performance of the component must be 95% of that compared to the performance at beginning of life. If this cannot be achieved through repairs, then the component will be replaced.

The last aspect of refurbishment is to indicate the refurbishment time. Once again, each step in the refurbishment process will be evaluated for duration. Refurbishment is completed when the components is ready for assembly. Assembly and testing time is covered in the Production Plan.

1. **Disassembly** 2 weeks.
2. **Transport to refurbishment site** 1 week.
3. **Disassembly of sub-system** 2 weeks.
4. **Inspection** 4 weeks.
5. **Analysis of Inspection** 1 week.
6. **Maintenance** The total repair time is the accumulation of logistic delay and active maintenance time. Active maintenance time is composed of fault localisation time, fault correction time and check-out time.[25] 2 weeks.

7.3. Production Plan

The production plan shows the components of the system, in which order they are assembled and in which order they are integrated on the existing system. The process for manufacturing and refurbishing the VuAB will differ over time. This is because of the fact that some components will have to be manufactured every time as they are consumables and not re-used, while other components will have to be refurbished. A component, however, can not be refurbished over and over again and will have to be checked for damage and performance. The production plan has been developed in such a way that it indicates whether a component can be refurbished or not. When a activity shows that a component will be refurbished, this can therefore mean that the component will be refurbished only once and will then be manufactured again, while other components may be refurbished 5 times before they are replaced.

In this production plan parts of the VuAB, which are from an existing design and not from the new design, are shown as well, as they are being refurbished. This gives an overview of which existing components can be refurbished and in which order they are assembled according to the new design.

The production plan is shown in Section 7.3. As can be seen, the production starts with manufacturing and refurbishing the main structural parts of the VuAB and assembling them, as shown in activity 1.0. Meanwhile, the added structural elements are manufactured and refurbished and integrated on the existing structure, as shown in activity 2.0. Then, the Vulcain engine has to be integrated in the structure. It should be refurbished first, however, which can happen during or before assembling the structural elements already. This is shown in activity 3.0. Some components will have to be mounted on the outer structure of the VuAB, as shown in activity 4.0, while most of the new components of the recovery system will be located on the inside of the VuAB, as shown in activity 5. Activity 4 and 5 can be done in parallel or one after the other, in which the order does not matter. Finally, the VuAB will be integrated on the Ariane 6 using the separation rings and by coupling the fuel lines.

Finally, the time it takes to assemble the VuAB is estimated. In this estimation, all components are considered to be ready or refurbished at the moment of assembling. Therefore, it concerns all assembling and integrating activities, indicated as the green activities in the production plan.

- **Activity 1.0**: Assembling the existing structural elements is estimated to take 3 weeks, including inspection and assuring to variations in geometry are dealt with;
- **Activity 2.0**: Integrating the additional structural elements is then estimated to take 1 week;
- **Activity 3.0**; Integrating the Vulcain engine in the structure is also estimated to take 1 week;
- **Activity 4.0**: Integrating the outer elements on the VuAB is estimated to take 3 days, as just a few components are involved in this process, assuming the thruster system to be assembled as far as possible;
- **Activity 5.1**: Assembling the parafoil system package is estimated to take 2 days, and integrating it on the structure another 1 day;
- **Activity 5.2**: The same holds for the C&DH and Power package, 2 days for assembling and one day for integrating;
- **Activity 5.3**: Integrating the cabling on the VuAB is estimated to take 1 week;

- **Activity 5.4**: Packing the aeroshell and integrating it on the attachment is estimated to take 1 week as well.
- **Activity 6.0**: Integrating the VuAB with the rest of the LLPM is estimated to take 2 weeks.

7.4. Turnaround Time

Multiple VuAB's need to be operational at all times. This is so because the full turnaround time, that is the time it takes between two launches for a single VuAB is longer than the expected Ariane 6 launch frequency. The turnaround time is composed of 4 stages. In order of operations: Transport from landing zone to disassembly site, refurbishment, assembly, and last the transport from assembly site to launch site, and lastly the integration with the launch vehicle The transport from the landing site in the middle of the Atlantic Ocean to Arianespace in Les Mureaux, France takes 10 days according to the equations established in Section 7.1.4. The full refurbishment process takes 12 weeks. The assembly of the VuAB and integration with LLPM takes 7 weeks, because some activities can be performed in parallel. The transport from Les Mureaux to the launch site in Kourou, French Guiana takes 9 days. The duration of LLPM integration and testing with the launcher takes up to 8 weeks.[5] This leads to a cumulative turnaround time of just under 30 weeks, which is just short of 7 months.

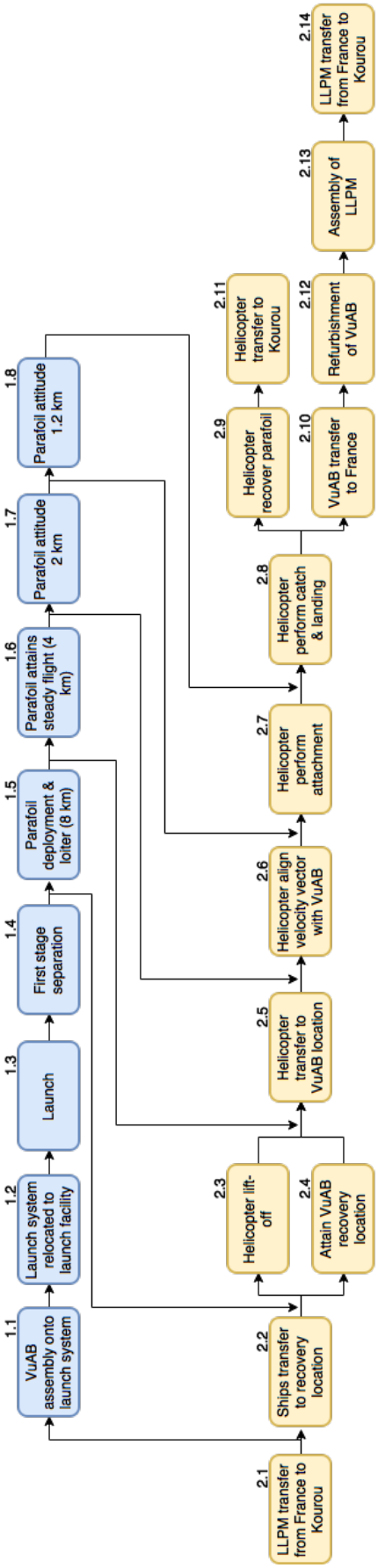

Figure 7.2: Operational flow diagram

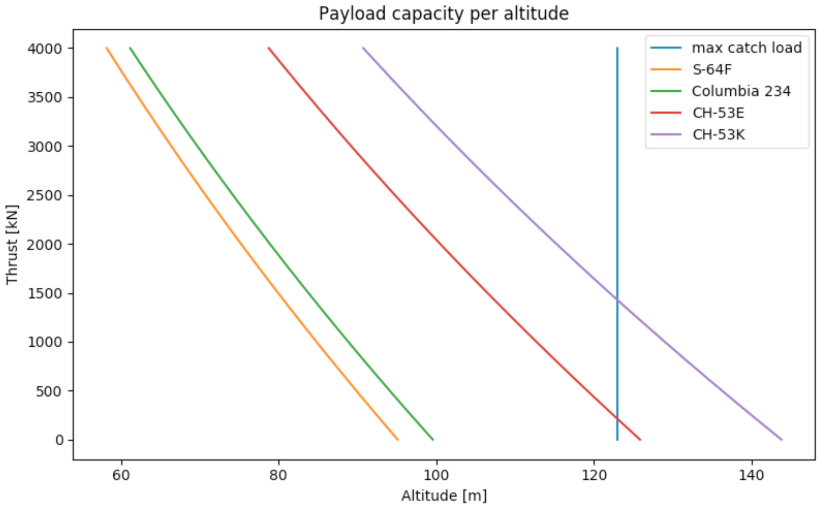

Figure 7.3: Payload capacity per helicopter versus altitude, along with the maximum catch load

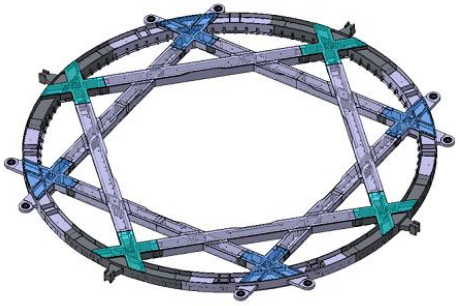

(a) Booster load bearing structure

(b) VuAB cut showing the location of the booster load bearing structure

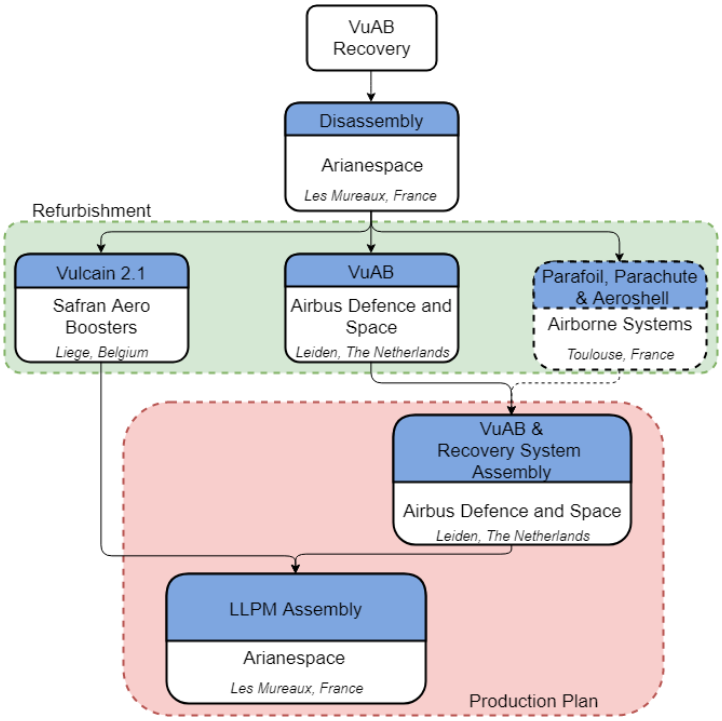

Figure 7.5: Schematic representation of the refurbishment process

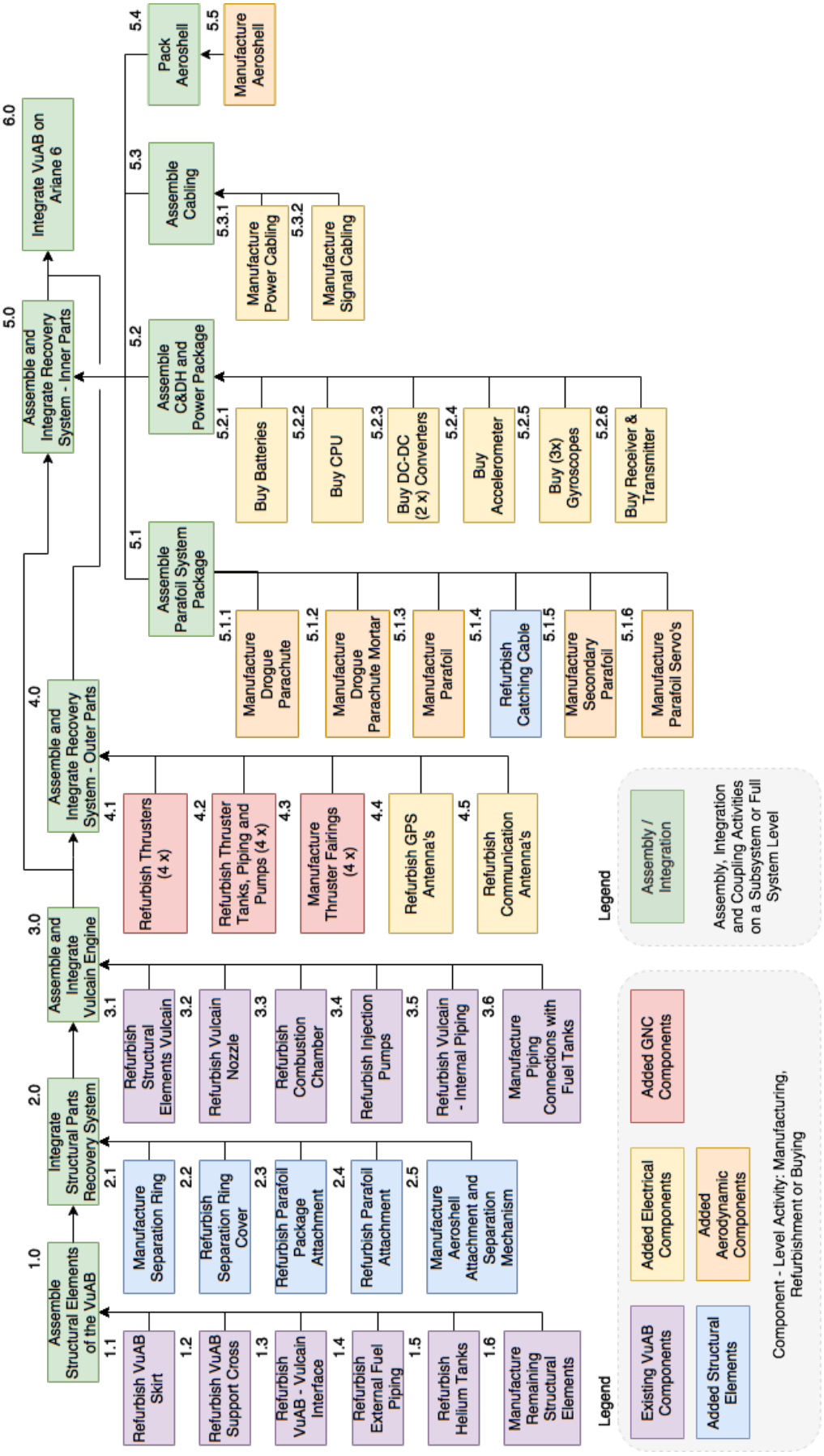

Figure 7.6: Production Plan of the VuAB, combining existing and added components.

8

Business Case Analysis

With the system designed and defined, the expected business case of the recovery system can be analysed. The analysis of the business case is divided into three different sections. Section 8.1 treats the market analysis [72], in which the market forecast, segmentation and competition are analysed. Section 8.2 treats the cost breakdown structure, which shows the breakdown of the individual cost components of the reusable Ariane 6 program, which are then taken into the Return on Investment analysis in Section 8.3. The return on investment analysis shall provide the final determination of the potential profitability of the recovery system.

8.1. Market Analysis

This section concerns an analysis of the market the VuAB recovery system is subject to [70]. This is done in order to get a view on competitors, customers, prices and possible opportunities. The first part is stated in the Global Picture (Section 2.1), after which defining and segmenting the market in Section 8.1.1 is done. Then the dynamics of the market are explained in Section 8.1.2. An analysis on the competitors and customers is made in Section 8.1.3 and Section 8.1.4, respectively. Finally, a conclusion is drawn which is presented in Section 8.1.5.

8.1.1. Market Definition and Segmentation

This section concerns the definition and a segmentation analysis of the market. In this case, a market is *a pocket of latent demand* [20]. The market that the Ariane 6 Launch Vehicle enters in and is analysed in this chapter is the market for Orbital Launchers, in particular the market for the Heavy Lift Orbital Launch Vehicles [42], as this is the category the Ariane 6 belongs to. This category concerns the launch vehicles that are capable of lifting 20 to 50 metric tons into Low Earth Orbit (LEO).

Then, market segmentation is applied. A market segment is *an identifiable group of customers with requirements in common that are, or may become, significant in determining a separate product strategy* [20]. The first segmentation that is applied is the segmentation based on the type of satellite. This concerns the following types: commercial communications, civil/military communications, Earth observation sciences, R&D, navigation, military surveillance, scientific and meteorology. The second segmentation is on the type of customer: institutional versus commercial. This segmentation is important since for both the Ariane 6 Launch Vehicle and for space launch vehicles in general, the amount of institutional customers is substantially higher as opposed to other markets. The third segmentation made is a geographical one. The importance of this segmentation becomes clear from the fact that from a historical standpoint there is quite a set of (potential) customers that chose to go for a certain launch vehicle operator for other reasons than lowest pricing. Amongst these reasons might be logistics and institutional ties.

An additional market might be addressed. The non-satellite industry related to the satellite industry. This made up about 38% or 127 Billion USD of the global space market in 2015 [60]. It has been decided not to pursue this market as this project focuses solely on the implementation of a reusable Vulcain Aft Bay.

8.1.2. Market Sizing

This section concerns the current state of the market and its segments and where it's headed, as identified in Section 8.1.1. This is done by first analysing the general market status and growth, after which the same is done

for the segments mentioned in Section 8.1.1. Due to the lack of sufficient necessary data for analysing all the segments at this point, the required data that is missing is derived from available, more general resources [20].

General

Overall, the global satellite industry has shown tremendous growth over the years. From 2005 to 2015 the industry has doubled in size [60]. The average number of satellites launched per year in the time period of 2011-2015 increased by 36% compared to the previous 5 years [60]. It should be noted that small (<500 kg [37]) satellites posed the largest contribution to this growth, which do not fall under the category of relevant customers for the Ariane 6 Launch Vehicle. It is expected that the trend of the decrease in satellite size and frequency of launch of the small satellites keeps increasing and that the market for large satellites (>1000 kg [37]) will also experience growth [60], however, at a potentially slower rate. This is mainly due to the large influence of communication satellites, which are in most cases large satellites, even though the average mass is shrinking (Figure 8.2) due to increasing technology levels.

Of the entire global satellite market revenue only a small percentage, about 2.5% [60] is attributed to the global launch industry. This sector has seen a growth period after which it currently is constant, with an average launch market revenue of 5.6 billion USD (Figure 8.1). No forecast data is present, therefore it is assumed that the market revenue shall remain constant for the foreseeable future relevant for this report as there is no indication otherwise.

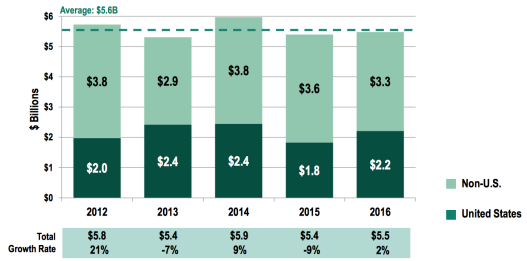

Figure 8.1: Commercial launch market trend [60]

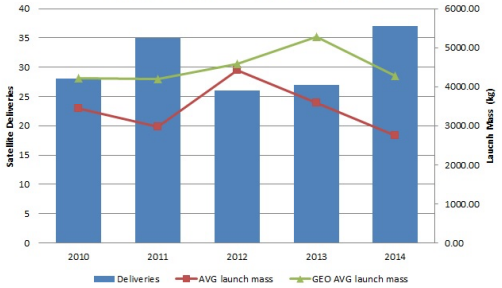

Figure 8.2: Communication satellite sizes over the years [30]

Segment - Satellite Type

As can be seen in Figure 8.3 the communication satellites (commercial & civil) account for 42% of all manufactured satellites in 2015. Additionally, the military surveillance satellites account for about 36%. Military surveillance and especially communications satellite are predominantly large satellites (see Figure 8.2) and thus form a large portion of the potential customers for a launch using the Ariane 6 Launch Vehicle.

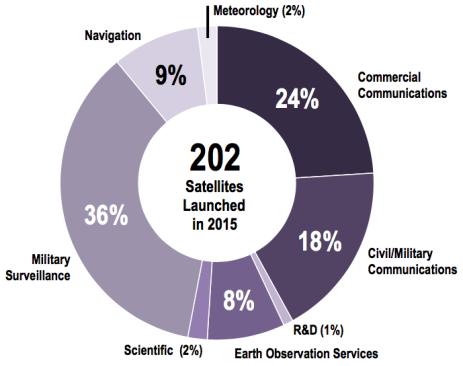

Figure 8.3: Value of manufactured satellites per type

Segment - Customer Type

It is found that of the two main customers, types institutional and commercial, currently the institutional customers make up the biggest sum of projects. This is shown in Figure 8.4. As can be seen in the figure the institutional customer presence in the space launch market has increased by about 36% in the last 10 years. This

increase is partly attributed to the fact that the US government does not have full space launch capability at this point and is forced to find that capability elsewhere. Additionally, the European Union has two large projects running, Copernicus and Galileo, leading to a significant amount of launches into space. This can be seen in Figure 8.5, by looking at the data for sales to European public entities, which has seen a growth of 66% in the last 10 years. For the foreseeable future the US government will not have full space capability and the Copernicus project will still be under way with space launches being performed. The Galileo project has its last launch projected before 2020. Concluding, it is assumed that the institutional percentage of the customers shall not exceed its current value of 68%, and might become a bit lower. Therefore, it is assumed that this value shall be around 65% for the foreseeable future.

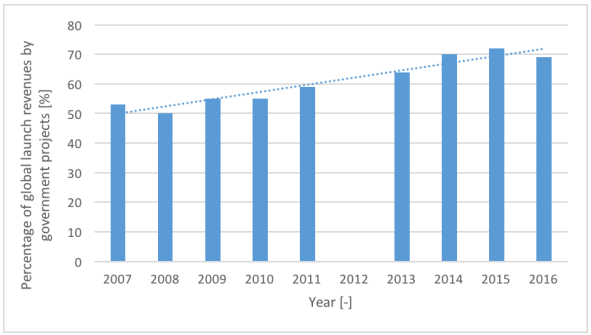

Figure 8.4: Percentage of global satellite launches ordered by institutional customers

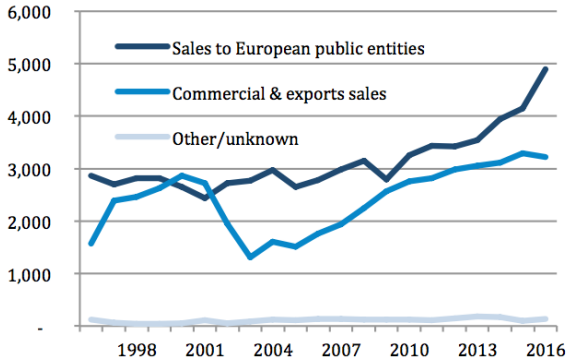

Figure 8.5: European satellite launch revenue as ordered by institutional customers [23]

Segment - Geographical

As can be seen in Figure 8.6, computed through historical data [60], the commercial space market is predominantly occupied by launches performed by the US government or companies from the United States. A bit more than 20% of the commercial launch market is in European hands. Between 10 and 20% is occupied by other regions. As for revenue, Europe's market share is higher, about 40% for the last 3 years. This can be seen in Figure 8.7. As no sufficient data for institutional orders is found, it is assumed that a similar distribution is applicable to the institutional orders in the space launch market. Additionally, it is assumed that the European launch market occupation of 20% and launch market revenue occupation of 40% shall not deviate significantly for the foreseeable future, due to the fact that there is fierce competition but Europe's sales are strongly supported by orders from the European Union.

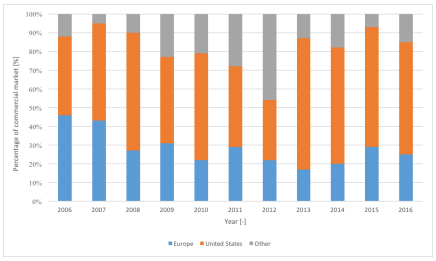

Figure 8.6: Percentage of commercial launches per region

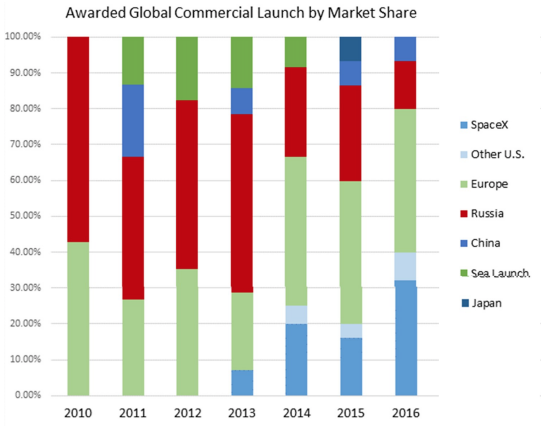

Figure 8.7: Percentage of commercial launch revenue per region (SpaceX is viewed as America)

8.1.3. Competition

The direct competitors and their prices are stated in Table 8.1. There's two methods to compare these. One method is by comparing cost per launch. While the launch price is important this automatically assumes the

maximum load capacity. In order to account for situations in which maximum loading is not the case the second method is also applied: the comparison using launch prices per kilogram. The Ariane 5 and 6 (both the 62 and 64 version) are also presented in the table to get an overview of where the Ariane 5 and 6 are and will be positioned. It is assumed that the list of competitors consists only of companies that can provide Heavy Lift Launch Vehicles as the proposed Ariane 6 Launch Vehicle is a system of this class and it is going to compete with other systems in this class. As the Ariane 6 has dual launch capabilities, meaning that it is able to launch two satellites with one launch, it can be argued that smaller satellites, offering only single launch capabilities, should also be in the list of competitors. However, it has been decided not to incorporate these in the analysis of the competitors, as an increase in scale of a launch device in general decreases cost, leading to the subsequent conclusion that these other competitors are in most cases more expensive and not a threat to the Ariane 6 Launch Vehicle. They might be competitors if their reliability is significantly higher, however, at this point the Ariane 5 has had more than 80 successful launches in a row, leading to a very high reliability rate compared to the others and it being one of the most reliable launchers currently operable [12]. In order to be a decent competitor Arianespace requires the Ariane 6's reliability to be in line with that of the Ariane 5 [11]. Therefore, the reliability rate of lower lift launch vehicles should not pose a competitive advantage for them, leading to them being excluded in this analysis.

As can be seen in Table 8.1 the Ariane 5 is currently positioned as the second most expensive launch system, looking at currently operational launch vehicles as well as not yet operational launch vehicles. The main reasons for still having customers are the aforementioned fact that it is one of the most reliable launchers at the moment and that the European institutions support the launcher. The Russian launchers are not as widely used, the exact reasons are unknown at this point but it is expected that these are mainly political, which is expected to remain this way for the foreseeable future. As can also be seen there are some competitors either operational but unproven or still in development. Of these the Chinese and Russian options as well as Blue Origin's New Glenn and ULA's Vulcan cannot be adequately analysed at this point as there is not sufficient data on this. This leaves SpaceX as the main competitor. As can be seen in the table at this point the more powerful of the two expendable Ariane 6 Launch Vehicle (64) positions itself below the pricing for the SpaceX's Falcon Heavy, whereas the less powerful version (62) positions itself above that. Making the rocket reusable might solidify the Ariane 64's position and make the Ariane 62 more competitive on this front.

Table 8.1: Competitor heavy lift launch vehicles

Status	**Company (region)**	**Rocket**	**Launch Price [USD]**	**Payload to GTO [kg]**	**Price per kg [USD/kg]**
Operational	ULA (USA)	Delta IV Heavy	400 million [8]	14,220	28,129
	Khrunichev (Russia)	Proton-M	65 million [57]	6,150	10,569
	Arianespace (Europe)	Ariane 5	165-220 million [4]	10,500	20,952
Operational, not proven	Khrunichev (Russia)	Angara A5	Unknown [32]	7,500	Unknown
	SpaceX (USA)	Falcon 9 full thrust	62 million [61]	5,500	11,272
	Calt (China)	Long March 5	Unknown [46]	14,000	Unknown
In development	Arianespace (Europe)	Ariane 64/62	90/ 75 million [5]	12,100/ 5,700	7,438/ 13,158
	SpaceX (USA)	Falcon Heavy	90 million [61]	8,000 (up to 26,700)	11,250
	Blue Origin (USA)	New Glenn	Unknown	Unknown	Unknown
	ULA (USA)	Vulcan	Unknown	Unknown	Unknown

8.1.4. Customers

This section concerns an analysis of the (potential) customers and their characteristics. As already shown in Figure 8.4 and Figure 8.5 the customer base is predominantly institutional. Currently about 68% globally [60] and about 60% in Europe [23]. Institutions focus mainly on two things; technology proof of concept and sustaining and/or increasing civil/military communications, surveillance and navigations. As for the commercial customers, as shown in Figure 8.3, in the commercial market the satellites with their primary function being communication make up the biggest portion. The customers ordering these launches are predominantly large telecommunication firms.

Both of these customer types require flexibility, affordability and reliability. Flexibility is required as the market for space launches is dependent on several variables, including satellite mass and size, launch window and orbit. Affordability is required as launching a satellite into space is expensive (see Table 8.1). A small cost reduction in percentages could potentially make launching a satellite into space millions cheaper. This is especially an important factor for the commercial customers as their main focus is creating value. Reliability is also a requirement due to the launch of a satellite being expensive, as stated before. Therefore, failure leads to significant cost increases on the customer and launch provider's end, as well as significant time delays for the customer. As such, this is an important factor to both commercial and institutional customers.

8.1.5. Market Perspective Conclusion

Looking at the growth of the market and the fact that there are already 12 launches planned for 2018 and 9 for 2019, the assumption is made that 9-12 launches yearly for the Ariane 6 is achievable. This is also in line with the client's target of 12 launches a year [7].

Because of the fact that the commercial market is very globally oriented and focused on reducing cost the geographical location of the customer shall not really pose a hurdle in acquiring customers. For the institutional customers this will pose a problem. In fact, it is expected that the only institutional launch orders will be done by European customers. With these it should be noted that they are economically motivated to support a European launcher such as the Ariane 6 as this supports their own economy as well. Furthermore, the commercial and civil/military communications and navigations satellite types made and will make up the biggest portion of the Ariane launches, as these make up the biggest portion of satellite launches in general and are predominantly large satellites needing a launch vehicle of the Heavy Lift category. The market focus should be oriented towards but not solely on these customers.

This leads to the conclusion that the market for the Ariane 6 can be defined as the following: *the market for Heavy Lift Launch Vehicles, focused predominantly on the European institutions and global commercial (telecommunication) firms, launching large satellites*.

As can be seen in Table 8.1, the SpaceX Falcon 9 launch vehicle offers the lowest cost launch option. Ariane 62 poses a direct competitor to this, certainly looking at the fact that its maximum launch payloads to GTO orbit are nearly identical. Therefore, reducing cost for the Ariane 62 is needed to make it more competitive. Furthermore, the Ariane 64 launch price is identical to that of the proposed Falcon Heavy launch vehicle. It should be noted that the Falcon Heavy maximum payload to GTO is currently set at 8,000 kg, whereas it shall have the ability to scale this up to 26,700 kg, possibly reducing launch cost. So even though the Ariane 64 is currently quite competitive it is advised to reduce costs in order to stay competitive or gain a competitive advantage. Looking at the launch cost per kg the Ariane 64 certainly is a good competitor. The Ariane 62 however, could use a cost reduction in order to increase its competitiveness.

8.2. Cost Breakdown Structure

The first step in analysing the profitability of the recovery system is a breakdown of all the individual cost components in the reusable Ariane 6 program. This section contains the so called cost breakdown structure. First an overview of the costs is graphically given (Section 8.2.1), after which the development cost and the production and operational costs are discussed in Section 8.2.2 and Section 8.2.3, respectively.

8.2.1. Graphical representation

The cost breakdown structure consists of three main elements, the development costs, vehicle costs and operational costs, which are represented in the top level of the cost breakdown structure, as seen in Figure 8.8.

The individual elements of the vehicle costs are broken down in Figure 8.9. The elements are broken down into reusable Ariane 6 components, the expendable Ariane 6 components, the recovery system and the final assembly costs associated with integrating all individual elements. Apart from the reusable Ariane 6 components,

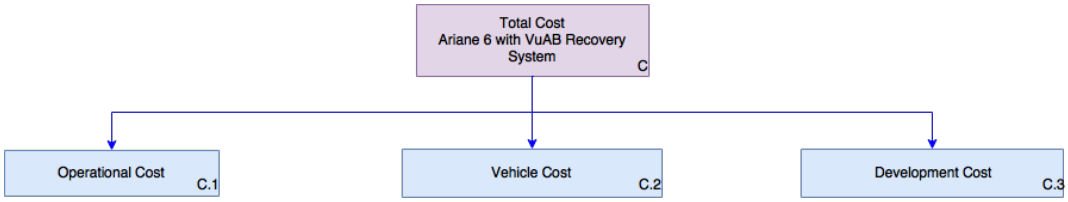

Figure 8.8: Cost Breakdown Structure - top level

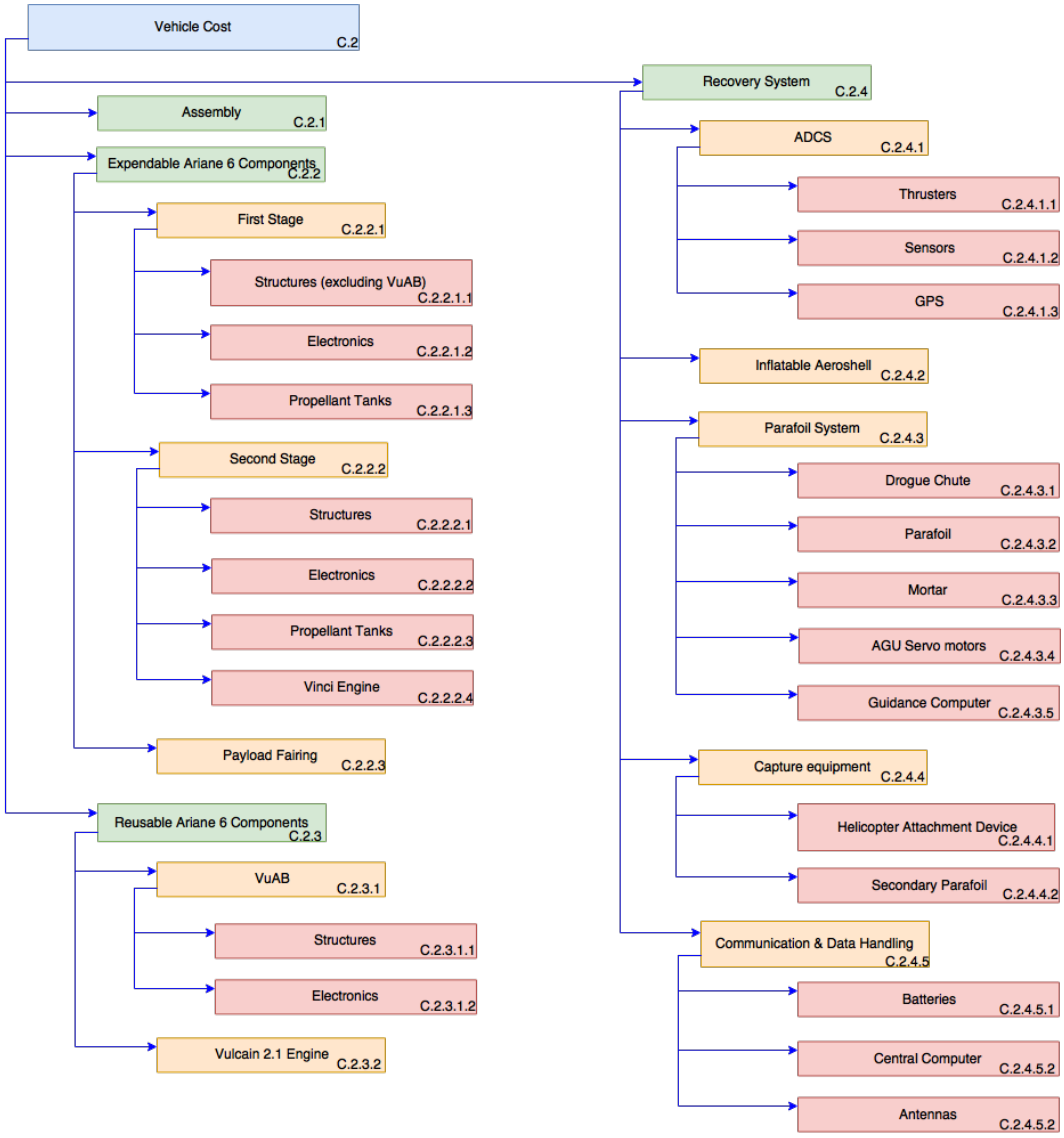

Figure 8.9: Cost Breakdown Structure of vehicle cost

the VuAB and the Vulcain 2.1, the vehicle costs are incurred upon every single launch, since of all of these components will be produced for every individual launch. The costs of the reusable components are incurred every time the engine is written off. The individual elements of the recovery cost are shown in Figure 8.11. These are mainly the launch operations, recovery and refurbishment operations. The development cost contains all the different elements that need to be developed: the aeroshell, parafoil system, additional structures, the power, GNC and ADCS systems, as well as integration, the program level and ground support equipment.

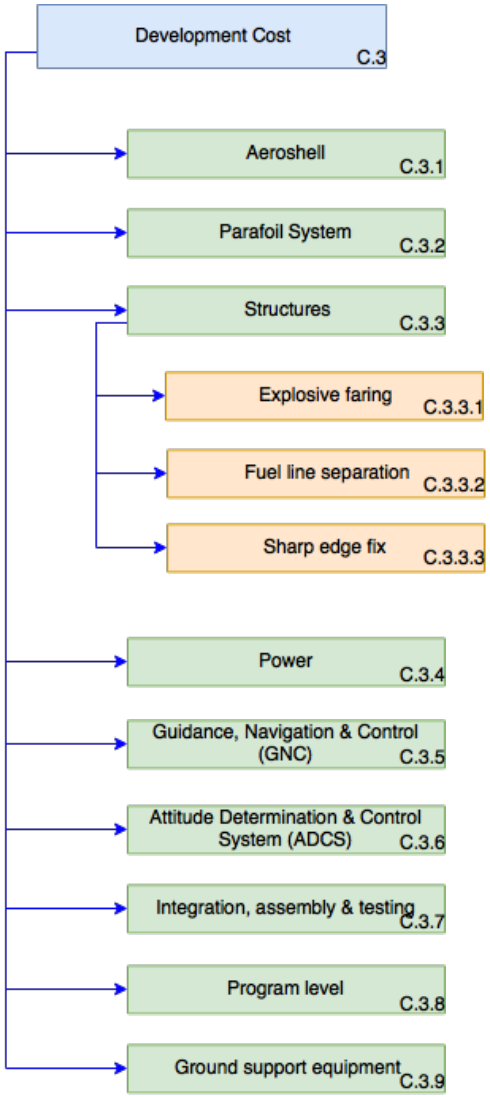

Figure 8.10: Cost Breakdown Structure of development cost

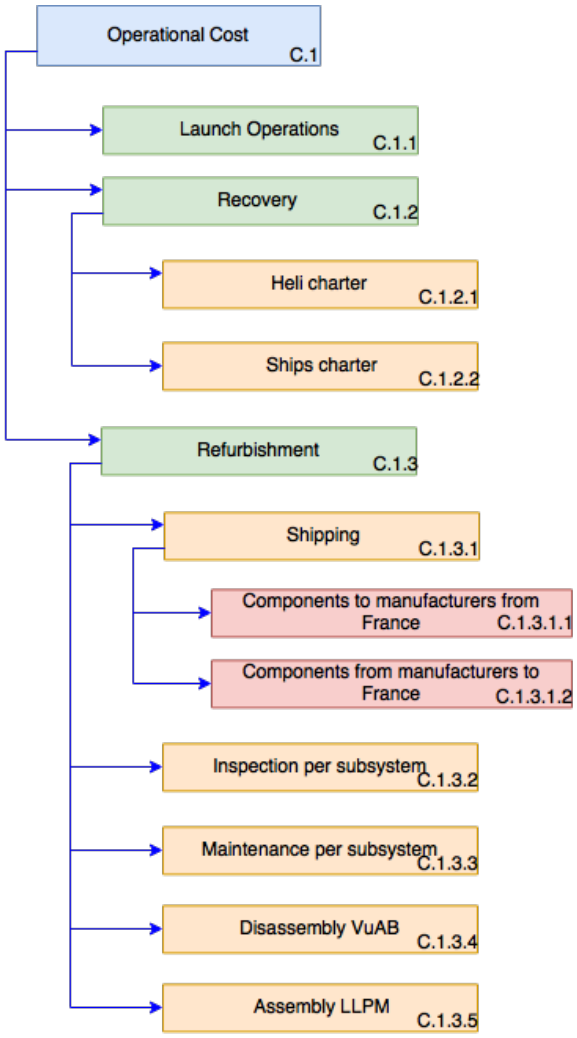

Figure 8.11: Cost Breakdown Structure of operations cost

8.2.2. Development Cost

The development costs are analysed using a parametric cost estimation method for research, development, test and evaluation costs based on statistical spacecraft data [50] [71]. Even though the recovery system itself is not an actual spacecraft it is assumed that the systems include most of the same subsystems and therefore this method can be applied.

The method applies equations derived from statistical data in which the cost per subsystem is estimated based on the mass of that subsystem. The mass input in the equations is good for a certain range, of which it can be said that a good estimate can be 25 % above and below this data range. Although a small number of inputs is not in the given range, it is assumed that the estimate is still applicable to the business research. The estimation results in USD for the year 2000, which are converted to euros for the year 2017[1][2].

For the heat shield and parafoil the development costs are difficult to estimate due to the fact that not enough (reliable) data is at hands on such specific systems. However, an estimate on heat shield development costs was found to be about 17 million USD up to and including testing[3]. As this is for a somewhat smaller sized heat shield it is assumed that a value of 20 million USD is a good estimation for the heat shield development. It is higher because of this projects bigger sized heat shield but not much higher due to the fact that its a technology that has seen quite a lot of development already. Unfortunately, Airborne Systems did not provide any data on the cost of the system. Therefore, an estimation on its development cost is made using the heat shield development cost as a reference. In this it is taken into account that the parafoil system is an off the shelf system which only has to be implemented in the VuAB system. Its development costs are estimated at 3 million USD.

Incorporating this in the development cost model comes to a total value of the development costs of approximately 83 million Euros. These are incorporated in Section 8.3.

8.2.3. Launch Cost

The launch costs are the variable costs associated with the launch of the reusable Ariane 6 launcher, which consist of the production costs and the vehicle costs. The vehicle costs consist primarily of the launcher and system production cost, while the operational costs can be subdivided into direct operational costs, indirect operational cost and refurbishment costs. The model results are evaluated for various model parameters to assure that the use of the VuAB recovery system is also economically viable under changing parameters, such as economic downturn, higher-than-expected refurbishment cost or low reliability. The client has provided data on the current expected launch costs for an expendable Ariane 6, which can be found in Table 8.2[4]. These values provide the basis for the costing models for the launch costs of the reusable Ariane 6.

The production and operational costs associated with the reusable system are derived using a parametric top down approach. This approach is chosen in favour of a more elaborate bottom-up approach due to a lack of sufficiently accurate cost data on component level. Therefore, parametric estimation is deemed the only suitable method of defining the approximate system and operational costs. The parametric approach employs the transcost model for reusable launch vehicles, supplemented by a model for responsive reusable launch vehicles [35][36]. The primary inputs are the vehicle mass, amount of vehicles produced, and a few parameters related to configuration type. The outputs are the production cost of the reusable first VuAB and a reusable version of the Vulcain 2.1. A learning factor is incorporated, which models the reduction in production cost over the length of the production run. The equations from the model can be found in Equations 8.1, 8.2, 8.3, 8.4 and 8.7. Let F_{se} and F_{sr} be the production cost of an expendable and reusable first stage and F_{ee} and F_{er} be the production costs of an expendable and reusable engine. f_4 is the learning factor associated with increasing production numbers. Since the reusable VuAB shall be part of an existing system with available cost estimates, the cost estimations are based on the existing estimates from the client and the relative mass increase and the increase in complexity for reusable launcher stages and engines. Therefore a 25% margin is taken on top of the usual engine price, as can be derived from equations 8.1, 8.2, 8.3 and 8.4 . The Cost Estimation Relationship (CER) for the new first stage cost can be seen in Equation (8.5) and the CER for the reusable engine can be found in Equation (8.6) [35] [36]. Additionally, the model indicates that the operation of a reusable system leads to a 25% pre-launch and mission control operational cost increase, due to increased system complexity.

[1] https://www.statista.com/statistics/412794/euro-to-u-s-dollar-annual-average-exchange-rate/, [20-12-2017]

[2] http://www.in2013dollars.com/2000-euro-in-2017?amount=1, [20-12-2017]

[3] https://www.space.com/16695-nasa-launches-hypersonic-inflatable-heat-shield.html, [20-12-2017]

[4] Private contact, Airbus Defense and Space (client), H. Cruijssen

$$F_{se} = 5.0 \cdot M_{expendable}^{0.46} \cdot f_4 \tag{8.1}$$

$$F_{sr} = 10.0 \cdot M_{reusable}^{0.46} \cdot f_4 \tag{8.2}$$

$$F_{ee} = 4.0 \cdot M_{ee}^{0.46} \cdot f_4 \tag{8.3}$$

$$F_{er} = 5.0 \cdot M_{re}^{0.46} \cdot f_4 \tag{8.4}$$

$$F_{sr} = 2 \cdot \frac{M_{reusable}}{M_{expendable}}^{0.46} \cdot f_4 \cdot C_{stage1} \tag{8.5}$$

$$F_{er} = 1.25 \cdot C_{Vulcain} \tag{8.6}$$

$$f_4 = 0.85^{\frac{log(n_p)}{log(2)}} \tag{8.7}$$

Table 8.2: Expendable Ariane 62 launch costs (provided by Airbus)

Cost Element	Cost (M euro [2017])	Cost Element	Cost (M euro [2017])
Vulcain 2.1	25.0	First Stage Structural Elements	6.0
Vinci	10.0	Second Stage Structural Elements	5.0
VEB (electronics)	5.0	Launch Preparations	8.0
Booster (single)	3.0	Refurbishment Vulcain and VuAB	5.3
Fairing	2.0	Pre-launch Operations	8.0

The application of the model led to the cost figures for engine production, recovery system production, refurbishment and operations, which can be seen in Table 8.3. In Table 8.3, both the first unit costs, as well as the costs for the sixtieth unit, which is currently estimated to be the final launch in the fifth year. This gives an indication of the system's costs after five years of operations, which is important for determining whether the requirement on cost reduction can be achieved. The costs decrease significantly over time, due to the applied learning factor on the production costs of the recovery system and the refurbishment of the engine and VuAB.

Table 8.3 shows high first unit costs for both recovery system production and refurbishment, which, as can be seen in the following section, can prove to be prohibitive for the return on investment. After a few years of operations, however, these costs decrease significantly, due to the steep learning curve associated with implementation of new technology. As with most existing systems on the Ariane 6, the learning curve is not applied to the engine production cost, since it is assumed that the learning curve is a lot shallower due to the client's accumulated experience with the equipment. The refurbishment cost in Table 8.3 includes both the refurbishment of the VuAB and engine, as well as the production cost of a new recovery system, which is largely not reusable at the moment.

Table 8.3: Production costs

Cost Element	First Production Unit Cost (M euro [2017])	Cost of sixtieth unit production (M euro [2017])
Vulcain 2.1R	31.25	31.25
VuAB	3.7	3.7
Recovery System	4.8	2.8
Refurbishment	10.1	7.8

8.3. Return on Investment

With the individual cost components known, an analysis of the potential launch cost reduction and profit potential compared to the expendable Ariane 62 is performed. Based on those figures, an approximation of the possible return on investment over time can be created, taking into account the number of launches per year, the maximum amount of reuses of the reusable VuAB and engine and the development cost. These analyses are conducted through the use of a python model that uses the pre-established production cost, operational cost, number of reuses and the number of launches per year.

Lifetime Cost Estimation

First of all, the launch costs for the n-th launch of the Ariane 6 including the system are plotted in Figure 8.12. What can be seen are the costs for the n^{th} launch , for a number of reuses ranging between 1 and 4. This figure for the amount of reuses was chosen, due to the fact that the client indicated that the engine will no longer be refurbishable after 5 launches. [5] The two main influences on the cost per launch that can be analysed in this plot are the learning factor and the number of possible reuses for each VuAB and Vulcain engine. The plot shows the decline of the costs associated with the learning curve, and the lower costs associated with a larger amount of reuses.

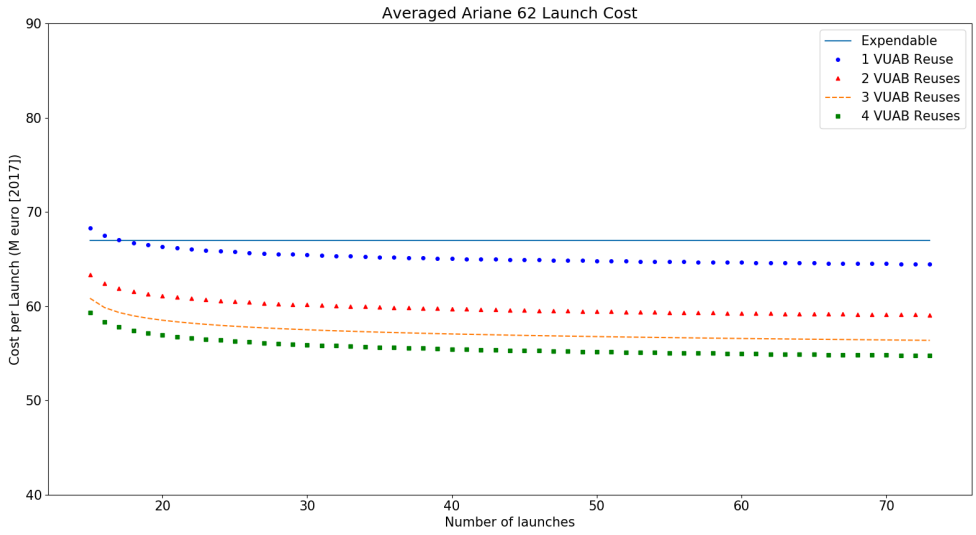

Figure 8.12: Launch costs after n-th launch for varying number of reuses

Given the development costs, and the cost estimating relationships for the launch costs, an estimation of the lifetime costs from the introduction of the recovery onwards can be performed. Apart from the individual component and operations cost, other factors such as reusability, reliability and demand for launchers strongly influences this lifetime cost estimation. Therefore, four different possible cases were drafted, after which the development of the cost per launch over time is computed and the total lifetime costs are determined. This will then serve as an input in the analysis of the profitability of the system. The four different cases are as follows:

1. Worst case, 7 Ariane 6 launches per year, maximum of 1 reuse of each VuAB
2. 10 Ariane 6 launches per year, maximum of 2 reuses of each VuAB
3. 10 Ariane 6 launches per year, maximum of 3 reuses of each VuAB
4. Best case, 12 Ariane 6 launches per year, maximum of 4 reuses of each VuAB

In these four cases, an absolute worst and best case is selected, which serve as limits of the cost analysis, and provide the minimum and maximum achievable cost reduction by implementation of the recovery system. The worst case takes the minimum expected launches per year, with only one reuse per VuAB and Vulcain engine. This limited reuse can be due to different factors such as difficulties in refurbishment, consistent adverse weather conditions at the recovery point or low reliability. The best case assumes the figure of 12 launches per year that

[5] Private contact, Airbus Defense and Space (client), H. Cruijssen

the client aims to achieve[6], in addition to assuming a perfect reliability and reusability. The two other cases assume a number of launches and reuses per system that is roughly in between the best and worst case scenario, to provide an indication of the costs given more conservative parameters. The development costs are assumed to be amortised during the first five years of operations, which explains the drop in launch cost at the start of the sixth year of operation. There are multiple advantages to this type of debt amortization, first of all, it limits the accrued interest payments over time, and second of all, the profitability after five years of operation is increased. This is however only possible if this strategy does not cause the program to incur significant losses in the first year of operation. This will be discussed in the next section.

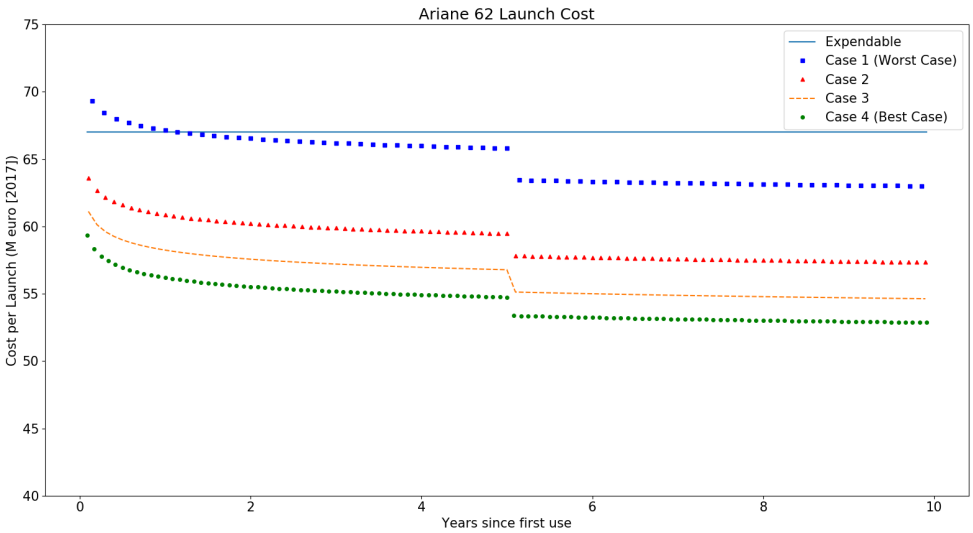

Figure 8.13: Cost per launch after a number of years of operation for four different cases. As can be seen, development costs are paid off in the first five years of operations.

Figure 8.13 shows the development of the cost per launch during the first ten years of operations. Apart from the worst case scenario, all cases realise a cost reduction from the first launch onward. This launch cost reduction initially does not meet the set requirements, due to the high first unit production costs. Table 8.4 shows the launch costs one year after the start of operations of the recovery system. In this case, the best case scenario and the scenario with a maximum of three reuses and ten launches per year already show large cost reductions, despite the amortisation of the development cost and the early stage in operations. The scenarios with 1 and 2 reuses show a small cost reduction of 0.1 million Euros and a 7.1 million Euros per Ariane 62 launch. For economic success of the system, a minimum of three reuses is therefore deemed necessary. The year one cost reduction can therefore be concluded to be within the broad range of 0. and 17.9%.

Table 8.5 shows the same parameters as Table 8.4 after 5 years of operations, when the system is supposed to realise a 15% cost reduction on a per launch basis. From the table, it becomes clear that in the third and fourth scenario, the system is capable of meeting the predefined requirement, and even exceeds it with up to 4.95 million euros. The first two scenarios show a less positive cost reduction figure, since in both cases the requirement will not be met. Therefore, it is key that the engine and VuAB can be reused at least 4 times. Additionally, it becomes evident that the development of this recovery system is especially favourable when launch demand is high, because the production costs decrease strongly as soon as production numbers increase. It can be concluded that upon the fifth year, a cost reduction between 4.1 and 15.0 million euros is possible, which corresponds to a reduction in percentages of 6.1 to 22.3% cost reduction, depending on the launches per year and the amount of reuses.

Given all the production costs, operational costs, launches per year, number of VuAB and engine reuses and the development cost, the lifetime program costs since the first deployment of the recovery system can be determined. The lifetime costs are the accumulated production, operation, refurbishment and development cost accumulated over time, and provides an insight in the total accumulated cost savings that the development of a

[6]Private contact, Airbus Defense and Space (client), H. Cruijssen

Table 8.4: Launch cost after 1 year of recovery system operations multiple predefined scenarios

Scenario	1 (Worst Case)	2	3	4 (Best Case)	Expendable
Launches per year	7	10	10	12	12
Reuses per engine	1	2	3	4	0
Constant Production Cost	26.3	26.3	26.3	26.3	30.3
Operational Cost	12	12	12	12	8
Recovery System Production	3.9	3.7	3.7	3.6	0
Vulcain 2.1	15.6	10.4	7.8	6.25	25
Refurbishment	3.6	3.4	3.4	3.3	0
VuAB	1.9	1.2	0.9	0.7	3.7
Recovery	1.3	1.3	1.3	1.3	0
Development Cost Payment	2.3	1.6	1.6	1.4	0
Total Cost	66.9	59.9	57	54.9	67
Cost Reduction	0.1	7.1	10.0	12.1	0

Table 8.5: Launch Cost after 5 years of recovery system operations for multiple predefined scenarios

Scenario	1 (Worst Case)	2	3	4 (Best Case)	Expendable
Launches per year	7	10	10	12	12
Reuses per engine	1	2	3	4	0
Constant Production Cost	26.3	26.3	26.3	26.3	30.3
Operational Cost	12	12	12	12	8
Recovery System Production	3.0	2.9	2.9	2.8	0
Vulcain 2.1	15.6	10.4	7.8	6.25	25
Refurbishment	2.8	2.6	2.6	2.6	0
VuAB	1.9	1.2	0.9	0.7	3.7
Recovery	1.3	1.3	1.3	1.3	0
Total Cost	62.9	56.9	53.8	52	67
Cost Saving	4.1	10.1	13.2	15.0	0.

recovery system can achieve. The python costing model is expanded to accumulate the total launch costs over a period of 10 years.

Figure 8.14 shows the lifetime program costs from the costing model for an expendable and a (partly) reusable Ariane 62. This shows the difference in total accumulated cost between the original expendable launcher and the Ariane 62 with the VuAB recovery system. A few assumptions are made in this analysis. First of all, it is assumed that 12 launches per year will be realised, as assumed by the client. Secondly, during the first three years of operation, the system can only be reused twice, due to lower reliability in the early phases and issues during initial integration. After three years of operation, four reuses per engine are assumed. Thirdly, the development costs will be amortized in the first five years of operation, which is one of the reasons that the plot for the reusable system in Figure 8.14 is steeper in the first five years. And finally, the model also takes into account that an inventory of 7 VuABs and Vulcain engines is needed, considering the amount of launches per year and the duration of refurbishment. This means that initially, 7 units will have to be produced, which also partly explains the high initial cost. Additionally, these will all have to be replaced at the end of their cycles, which is the reason that the lifetime cost curve has a few steeper segments, which is when new Vulcain engines and VuABs will need to be produced.

From the model, it is derived that after 10 years of operation, the total accumulated costs of the expendable and reusable systems will be 8.0 billion euros and 6.5 billion euros, respectively. That means that over a 10 year period, the system is capable of a total cost reduction of 1.5 billion euros. This is roughly the maximum achievable cost reduction, since the maximum amount of reuses is assumed after three years of operation.

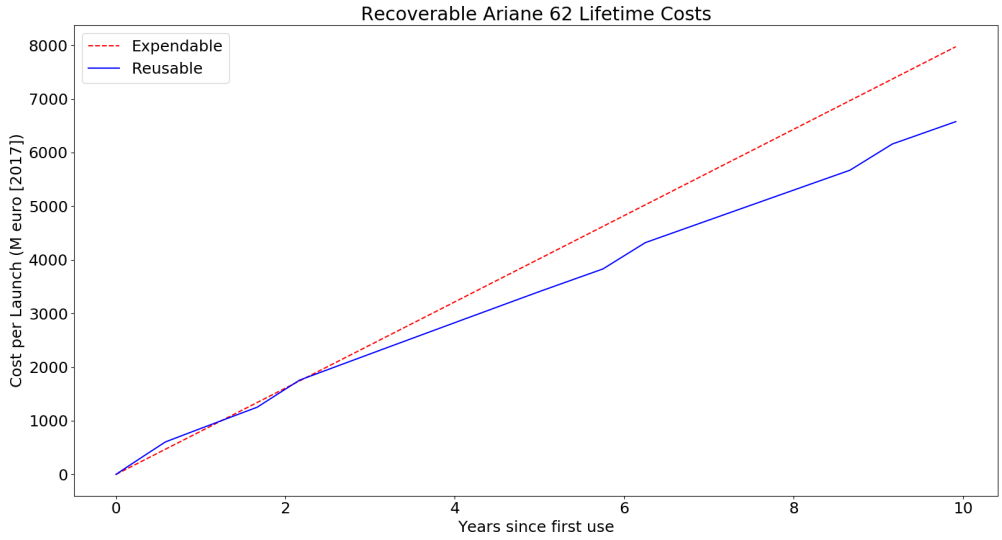

Figure 8.14: Ariane 6 lifetime costs after introduction of the VuAB recovery system.

The final part of the business case is the analysis of the profit potential. Using the lifetime cost data and the known price per launch, profit figures can be estimated. However, since the Ariane 6 incurs a 720 kg payload penalty due to the implementation of the recovery system, a new price figure had to be determined. The client at Airbus indicated that the price reduction due to a payload penalty can be assumed to be 10 000 euro /kg [7], which in this case implies a 7.2 million euro reduction in price.

With this data known, a profitability projection for the Ariane 6 can be drafted using the lifetime cost data, which can be seen in figure Figure 8.15. This projection takes into account the fact that the last launch of the recoverable system's service life, usually the fifth, the launch will be expendable without recovery system, which negates the need for recovery cost and allows for a higher payload and thus a higher price. The model prospects a total profit of 360 million after 8.5 years of operation. The profit after 10 years is slightly lower, because a replacement cycle takes place during the tenth year, which significantly impacts the profitability. It is therefore recommended that the engine replacements are spread out over time, to prevent short periods of losses.

[7]Private contact, Airbus Defense and Space (client), H. Cruijssen

Figure 8.15: Ariane 6 profits after introduction of the VuAB recovery system.

9

Future Recommendations and Development Logic

This chapter will show all preparations taken for the next steps in the design and development of the VuAB Recovery System. First, the recommendations for future design efforts as well as research prospects are given in Section 9.1, after which the general recommendations are given in Section 9.2. Section 9.3 will show all activities to be executed to produce and use the product. Finally, the Gantt chart in Section 9.4 shows the planning from now up until the first launch of the system.

9.1. Future Recommendations

This section aims to provide recommendations to the client regarding design choices and steps to be taken to improve the design and possible research topics that have prospects to improve the current design.

9.1.1. Aerodynamics

The reconsiderations include suggestions on further design and in depth analysis of the design, as well as recommendations for research that would be highly beneficial to the design.

Design Recommendations

- Investigate the aeroshell shockwave impingements with the aft section of the VuAB, including the nozzle.
- Investigate if the aeroshell can be constructed of multiple sections. The central section can be deflated and discarded to make way for the parafoil, the remaining section can be re-used in the future. Also, changing the inflation pressure of sections can allow for manipulation of the generated lift, which in turn can be used for attitude control and trajectory steering.
- Optimize the aeroshell design so that the critical section(surface of maximum heatflux) is ablator TPS and the rest is insulator TPS. This can save weight, and the insulating TPS material can be refurbished to save costs. This can be done with CFD analysis.
- Design a aeroshell attachment with a gimbal system that will cause a CG offset that will allow the control and steering of the VUAB during re-entry. This has high enough TRL levels as the technology has been demonstrated on board the IRVE-4 [21]
- Investigate the change of inertia due to deployment of the aeroshell, this will induce a rate of rotation. This must be know and can even be used for stabilizing effects.
- Investigate the change from the drogue parachute attached to the helicopter line to a drogue basket in order to gain more control over the hook attachment system.
- Investigate to what extent it is possible to reel in the VuAB (as it's towed by the helicopter) further than the secondary parafoil currently restricts this, in order to make landing operations have less probability of error.
- Investigate whether splitting the drogue parachute used to decelerate the VuAB before deploying the parafoil into two or more drogue parachutes with the same total surface area is efficient. This could increase the reliability of the system as only one large drogue parachute is used at the moment.

- Investigate the effect of the downwash of the helicopter on the parafoil. This might lead to a more efficient method for catching the parafoil.
- Investigate whether using the gimbal capabilities of the Vulcain engine is possible during reentry and whether or not this can be utilized for attitude control(center of gravity shift).

Research recommendations

- Research the insulator TPS with the aim of making the insulator operational under a higher heatflux. This has great potential and will pose multiple major advantages. The aeroshell mass will significantly reduce as shown in Section 4.2 and the aeroshell can be refurbished and reused. This will increase sustainability and reduce operational costs. The decrease in mass can lead to a snowball effect as it could allow the use of a smaller parafoil.
- The same is true for the parafoil and parachute. If material research is conducted with the aim of refurbishing the parafoil and parachute after sea water contact, it will reduce operational costs and improve sustainability.

9.1.2. Structures

- Investigate the mortar applicability to launching the drogue chute. Additionally, investigate its mass and especially volume sizing further, as the latter might turn out to be impossible to implement.
- Investigate which parachute detachment mechanism suits the mission needs the best.
- Investigate the effects of temperature fluctuations on the recovery systems, especially as these are fully exposed once the first stage and VuAB disconnect.
- Investigate the aero-structural dynamic instability of the aeroshell so the deflection during reentry can be modelled more accurately. [49]. These values have an influence on the accuracy of the re-entry. Using this analysis a more accurate prediction of the position error probability can be made.
- The loads exerted by the deployment of the parafoil and parachute on the VuAB have been determined. To optimise the design and sizing of these components the loads per cable should be determined in order to optimize cable and parafoil cell sizing.
- The durability of the components should be analysed after each recovery, and with that a prediction of refurbishment should be made. Considering the fact that high loads have to be dealt with, as well as large differences in temperature, crack propagation and durability should be analysed.
- All structural components have been designed using Aluminium 7075-T6 as this is the main source of material for the Ariane 6. Is should be investigated, however, if some elements could be made more efficiently from different materials.
- A dedicated attenuator design integrating a winch with a (modified) carbon (aircraft) brake could prove a significant weight saving with respect to the current mass estimation of the attenuator.

9.1.3. Guidance, Navigation and Control

- Apply a root-locus analysis to provide a more accurate controller tuning.
- The model developed could be improved, by taking into account some of the aspects an assumption was made, such as the drag of the payload.
-

9.1.4. Electrical System

- The antenna chosen in the design is not operational yet. It is also not know if this antenna can function both as a receiver and a transmitter, which is assumed in this design. This should be investigated.
- The link budget of the system is not yet computed. This is since the Ariane 6 is under development and not much of information is at hand about its telemetry systems. Future engineers should aim to close this link budget.

9.1.5. Operations

- Further refurbishment analysis can be done regarding modelling component failure. This will allow for predictive maintenance and can help reduce refurbishment costs and time.
- Investigate whether acquiring ships and / or helicopters might reduce the cost during operations.
- Investigate the effect of swing on landing operations in order to reduce the probability of error and damage on the VuAB in this process.

9.1.6. Sustainability

– A more exact and absolute estimate on the sustainability of the retrieval and re-use of the Vulcain 2.1 Engine can be established with a full LCA based on detailed recovery system properties such as the production processes and logistics of the refurbishment procedures.

9.2. General Recommendations

Next to the recommendations given by the different subsystems, several recommendations can be given regarding the design of the VuAB and Ariane 6 as a whole. These recommendations would enable the design of the recovery system to be improved, and no assessment on the change in overall performance of the Ariane 6 has been performed.

First of all, one of the most critical design parameters is the available volume in the VuAB, and the fact that this volume is split into several smaller parts. This results in an inconvenient way of packing the components and makes it hard to comply with the requirements on the centre of gravity. For example, some volume is available between the legs of the cross, some volume between the conical shape of the tank and the skirt, and the volume under the tank is split by fuel lines. Therefore, it is recommended to investigate whether it is possible to change the several existing structural parts of the VuAB. The structural cross supporting the Vulcain engine has now been designed in such a way that it splits the available volume of the VuAB in an inefficient way, reducing the space available for larger components. It should be investigated whether the cross can be redesigned in such a way that it takes this aspect into account, while still meeting the requirements from the Ariane 6. Furthermore, it was chosen not to locate any components under this structural cross due to thermal constraints. It should be investigated whether a thermal protection system, enabling components to be located under the cross, would be an efficient way to increase the available volume. Another way of increasing the 'efficiency' of the volume available would be to change the shape of the LH_2 tank. By flattening out the bottom part more space would become available in the middle, while reducing the volume available at the skirt, which would be more efficient for the larger subsystems such as the aeroshell. Finally, the VuAB skirt could be elongated to increase the volume of large area already available between the tank and the cross. This would increase the height of the full Ariane 6 and a thorough investigation should be done to see whether this is acceptable and an efficient way of increasing the volume available.

Secondly, the nozzle is a point of concern as it is critical for refurbishment and has not been designed for landing the VuAB on the boat. Therefore, it should be investigated whether it can be made stronger in able to cope with landing loads on the boat.

Another major improvement could be a re-ignitable rocket engine. Right now, the full concept trade-off was dependent on the fact that no re-ignition of the Vulcain engine in space is possible. This resulted in the fact that the flight trajectory of the VuAB ends in the middle of the ocean, limiting the possibilities for landing drastically. Furthermore, landing closer to land would decrease the operational costs. When a burst in space is possible and the flight trajectory would reach land, several landing options could be considered. The most critical mission phase for this design is the catch as it is sensitive to changes in the initial parameters, involvement of human beings in the catching process, the critical loading case and the small catching envelope. By reaching land different options for landing could be considered and the high accuracy of the parafoil would not be necessary, as mentioned in the midterm report. Furthermore, when reaching land it should be considered to recover the whole LLPM, as this would be possible with different landing concepts, in comparison with the landing on the ocean. Therefore, considering all reasoning as stated above, it is advised to investigate using a re-ignitable rocket engine, whether that would be the Vulcain or a different engine.

9.3. Project Design and Development Logic

The project design and development logic is used to show a logical order of activities to be executed to finalise the design and prepare for producing and using the product. It is shown by means of a diagram. The top level of this diagram showing the main activities can be found in Section 9.3. As can be seen, first the design as proposed in this report will have to be finalised, after which preparations will be taken for production, testing and operations. When the first components and subsystems are fully designed and produced they are tested, which is the 4th main activity. As soon as these tests are performed and a prototype of the VuAB is available, full scale system tests can be performed. Finally, the system can be produced for application on the Ariane 6 and the mission can be performed, after which refurbishment will take place and the mission can be performed again.

Section 9.3 shows the activities mentioned above in more detail. It shows the iterative process of optimizing

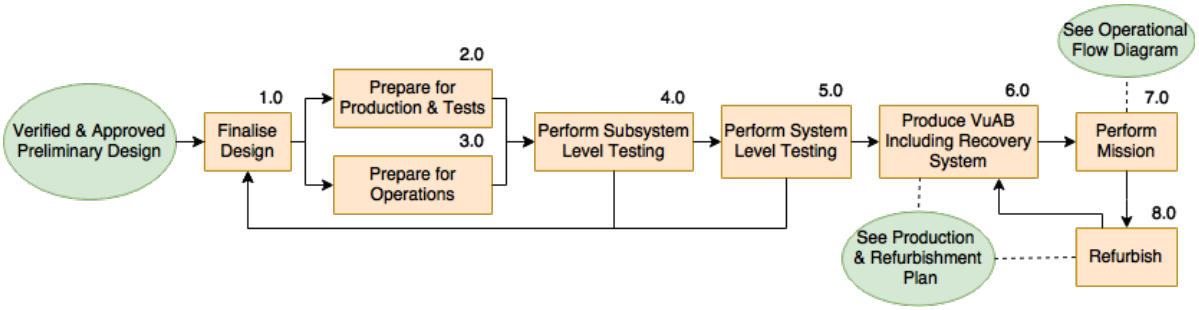

Figure 9.1: Top Level of the Project Design and Development Logic diagram, showing all main activities to be performed to produce and use the product

the design of the system, after which the design will have to be approved by for example ESA and Arianespace. The design phase is finished by providing detailed technical drawings to the production facilities. These facilities are prepared in activity 2.1, and the same will be asked from all subcontractors. Furthermore, the first materials and components will have to be ordered to start producing the samples for testing on time. Then, the preparations for testing are done, which includes developing detailed testing procedures. At the same time the operations will be prepared, by first selecting a helicopter and ensuring that the catch mechanism will be able to be integrated on the helicopter. Then, some time is taken to prepare and train the helicopter pilots for their jobs and the boat will be prepared for its job.

The testing activities provide some examples of components to be tested. In the chapter on verification and validation (Chapter 6) several testing procedures have been proposed and it is assumed that additional, detailed, testing procedures will be developed later on in the process, shown as activity 2.5.

The detailed plan for activity 6.0 can be found in the production plan Section 7.3, activity 7.0 in the operational flow diagram Section 7.1.2 and activity 8.0 in the refurbishment plan Section 7.2.

9.4. Project Gantt Chart

All activities mentioned in Section 9.3 and the logical order as shown in the diagrams are used to construct a Gantt chart showing the steps to be taken with an assigned period of time. The logic as explained in the text of the previous section is used and the Gantt chart can be found in Section 9.4. As can be seen in the Gantt Chart, a lot of tasks can be performed simultaneously, while others have to be performed in series.

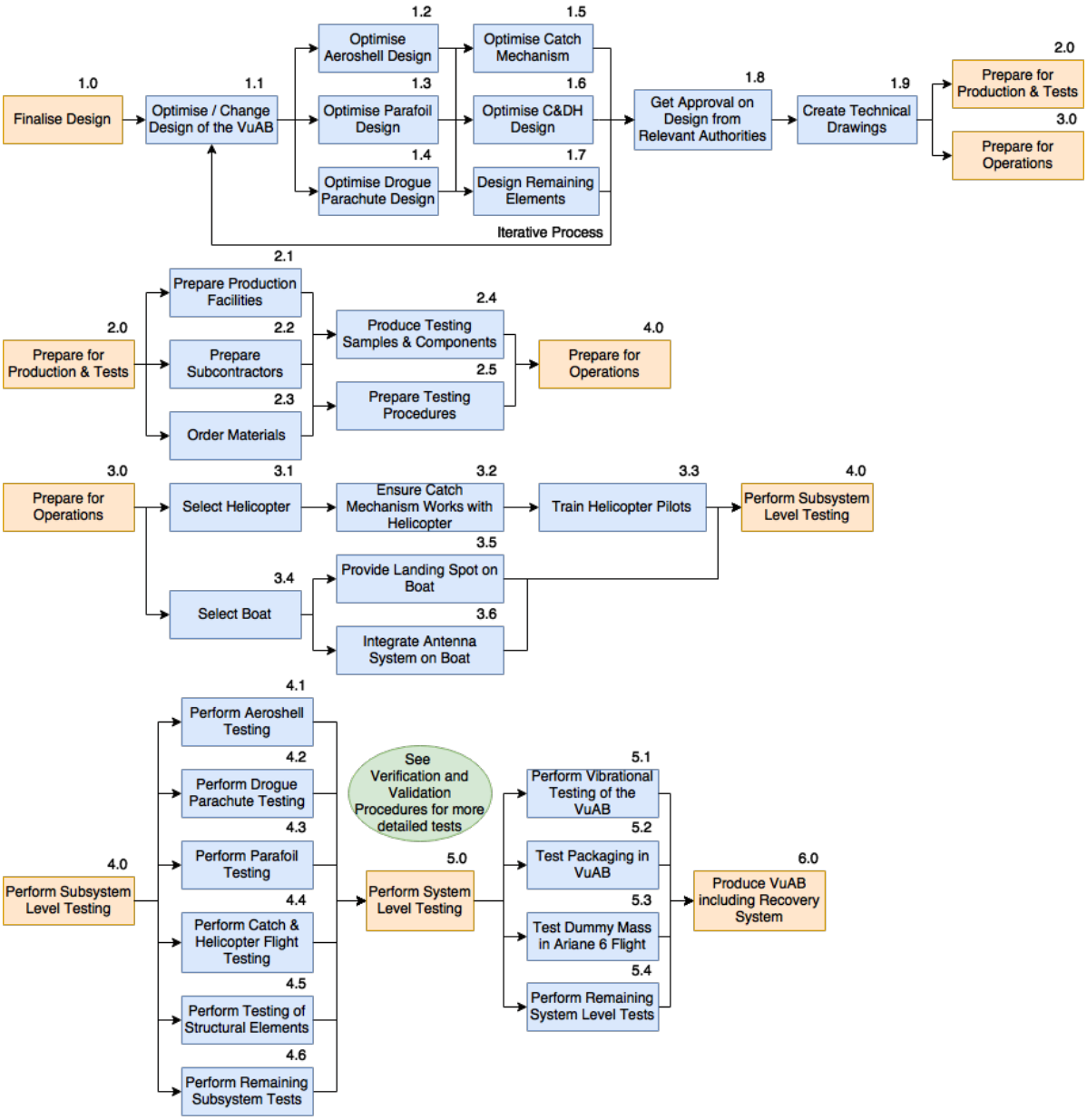

Figure 9.2: Detailed view on the Project Design and Development Logic diagram, showing all main activities to be performed to produce and use the product in more detail

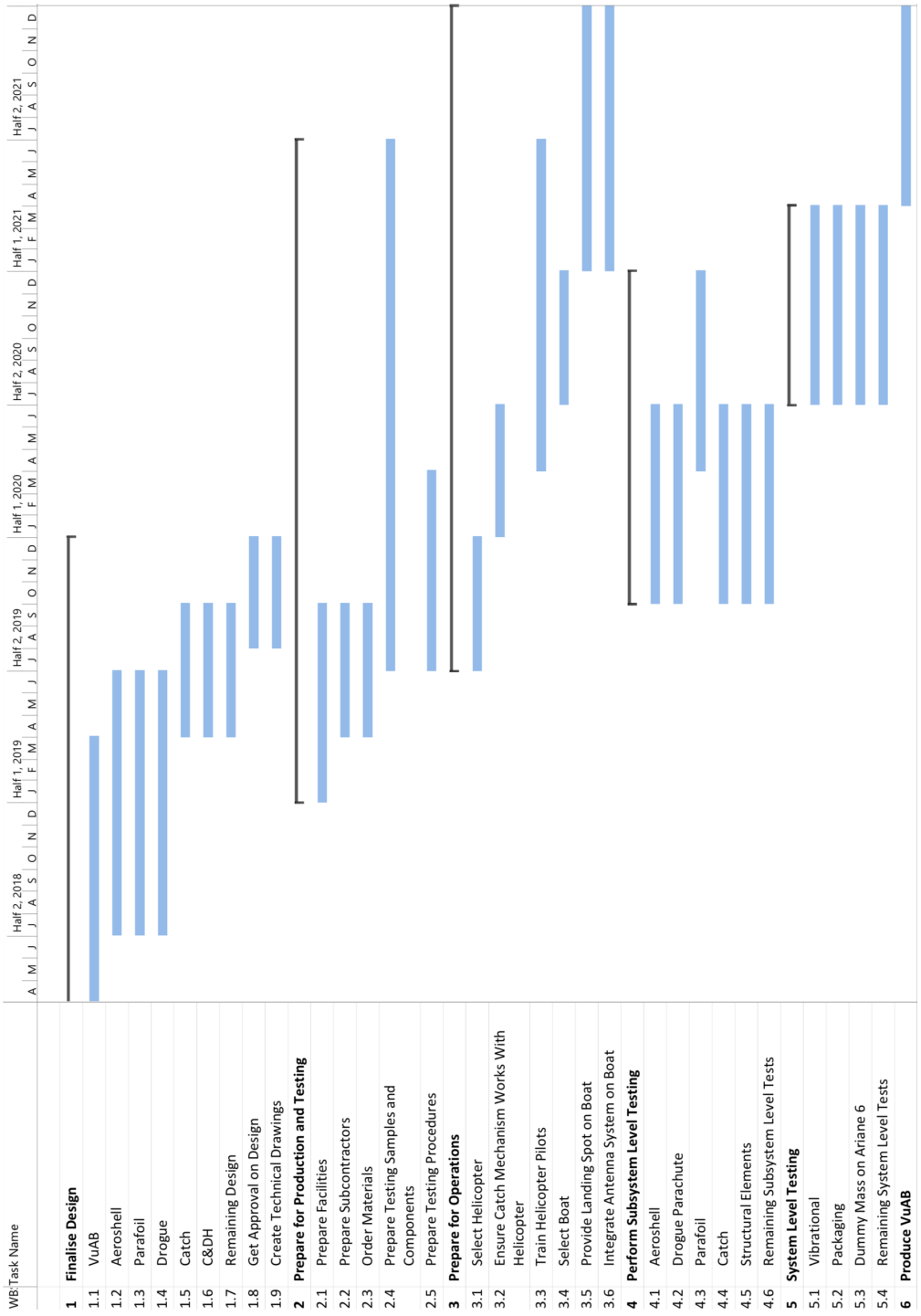

Figure 9.3: Project Gantt Chart, showing the activities to be performed up until the first launch of the recovery system

10 Conclusion

In the current competitive space launcher market innovations are important to stay on top. Currently there is a clear push for reusability of launcher parts. Not only does this reduce the launch costs, also sustainability of space flight is improved. The purpose of this project is to study the feasibility of making the Vulcain Aft Bay, which is a part of the Ariane 6 launcher currently in development by Arianespace, recoverable and reusable by adding a recovery system to the current design. In this Final Report the continued conceptual design of the Mid-Air Recovery concept that won the trade-off in the Midterm Report is presented.

The final design separates the VuAB from the first stage's fuel tanks after first stage separation at an altitude of about 160 km. It stabilises in space using small thrusters and deploys the inflatable aeroshell for re-entry at 100 km altitude. The aeroshell provides protection from the heat generated by the drag in re-entry and also stabilises the system passively due to its shape. When the velocity is low enough at 8.1 km altitude, drogue parachutes will be deployed to further decelerate and eventually pull out the controllable parafoil at 7.4 km. With this parafoil the VuAB will glide to the pre-set landing zone. At an altitude of 4 km the helicopter will start aligning with the VuAB. At 2 km altitude the helicopter and the VuAB will link and at 1.2 km the helicopter will take over the lift force from the parafoil, finalising the MAR manoeuvre.

The VuAB is then landed on a boat which will transport it to the place of assembly where it will be disassembled and distributed for refurbishment. When that is done the parts will be reused in a new Ariane 6 launcher. The refurbishment will take up to seven months for some parts, while it will take way shorter for others.

At launch the recovery system will weigh 2789 kg which is well within the 3000 kg requirement. Implementing the system will reduce the cost per launch of an Ariane 6 by up to 22 %. This reduction will put the Ariane 6 at a good position in the heavy space launch market, especially at the reliability that Arianespace currently provides with it's Ariane 5 launch record.

Although this recovery system is a feasible option that complies with almost all of the set requirements there are some recommendations for the Ariane 6 design which would greatly improve the possibility for integration of a recovery system to the design and would open up many, possibly more efficient, options that now had to be discarded during the design process. Most importantly the space within the VuAB is very limited. At this point it is of course not designed to fit a recovery system so a change there could open up a lot of options. Also a possibility to reignite the main first stage engine would provide many other options, like landing on land.

The design proposed and analysed in this report, combined with the recommendations for future design, provide a good solution for reducing the launch costs of the Ariane 6 in the future. Therefore, it is advised to move on with the design and development process.

Bibliography

[1] Dupont kevlar xp commerical product specification. DuPont Technical Data sheet, 2008.

[2] J.Rowan; J.Moran; D.S. Adams. Development and qualification of the mars science laboratory mortar deployment system.

[3] National Aeronautics and Space Administration. Orion's parachute system.

[4] European Space Agency. Ariane 5, .

[5] European Space Agency. Ariane 6, .

[6] G. Aigoin. Characterising hard landings. 2012.

[7] Airbus. Ariane 6: Europe's new way to space.

[8] United Launch Alliance. Delta iv launch services user's guide, 2013.

[9] J.D. Anderson. *Fundamentals of Aerodynamics*. McGraw Hill Education, 2017.

[10] *Ariane 6 User's Manual*. Arianespace, issue 0 revision 0 edition, May 2016.

[11] Arianespace. Ariane 6, 2017.

[12] Arianespace. Arianespace's ariane 5 launches two multi-mission satellites for fixed and mobile services, 2017.

[13] S. Dunker; J. Huisken; D. Montague; J. Barber. Guided parafoil high altitude research (gphar) flight at 57,122 ft.

[14] T. Barrows. Apparent mass of parafoils with spanwise camber. 2002.

[15] S. Dunker; J. Berland. Modularity concepts for a 30,000 lb capacity ram-air parachute. 2008.

[16] P.B.S. Lissaman; G.J. Brown. Apparent mass effects on parafoil dynamics. 1993.

[17] W.C. Young; R.G. Budynas. *Roark's Formulas for Stress and Strain*. McGraw-Hill, 2002.

[18] J.A. Del Corso; F.M. Cheatwood; W.E. Bruce III; S.J. Hughes; A.M. Calomino. Advanced high-temperature flexible tps for inflatable aerodynamic decelerators. Technical report, NASA Langley Research Center, 2011.

[19] S.J. Hughes; J.S. Ware; J.A. Del Corso. Deployable aeroshell flexible thermal protection system testing. Technical report, NASA Langley Research Center, 2016.

[20] Ir. R.J. Hamann; Prof. dr. ir. M.J.L. van Tooren. Systems engineering & technical management techniques - lecture notes, September 2006.

[21] D.K. Litton; D.M. Bose; F.M. Cheatwood et al. Inflatable re-entry vehicle experiment(irve)-4 overview. Technical report, NASA Langley Research Center, 2010.

[22] H. Wright; A. Cutright; J. Corliss; W. Bruce et al. Heart flight test overview. Technical report, NASA Langley Research Center, 2012.

[23] P. Lionnet; ASD Eurospace. The state of the european space industry in 2016 - facts and figures press release - june 2017, 2017.

[24] S.W. Ferguson. Rotorwash analysis handbook. 1994.

[25] R. Groves G.J.W. Van Bussel. Asset management: Maintenance concepts and maintenance strategies, structural health monitoring.

[26] William K. Wailes; Nancy E. Harrington. The guided parafoil airborne delivery system program.

[27] Ronald A. Hess. Analytical assessment of performance handling qualities and added dynamics in rotorcraft flight control, 2009.

[28] Dr. Sighard Hoerner. *Fluid Dynamic Drag*. 1965.

[29] Daniel J. Inman. *Engineering Vibration*. Pearson.

[30] Forecast International. Average commercial communications satellite launch mass declines again, 2015.

[31] Dr. C. Kassapoglou. Lecture slides structural analysis. 2015-2016.

[32] Khrunichev. The angara carrier rocket family, 2014.

[33] E.G. Ewing; H.W. Bixby; T.W. Knacke. Recovery systems design guide. 1978.

[34] T.W. Knacke. Parachute recovery systems design manual. 1991.

[35] D.E. Koelle. The transcost-model for launch vehicle cost estimation and its application to future systems analysis. *Acta Astronautica*, 11, 1984.

[36] D.E. Koelle. Space launch systems cost estimation as design tool. *Acta Astronautica*, 34, 1994.

[37] H.J. Kramer. *Observation of the Earth and Its Environment: Survey of Missions and Sensors*. Springer Science & Business Media, 2002.

[38] J. E. Johnson; R. P. Starkey; M. J. Lewis. Aerodynamic stability of reentry heat shield shapes for a crew exploration vehicle.

[39] A. Wiese M. Kaltschmitt, W. Streicher. *Renewable energy: technology, economics and environment*. Springer, 2007.

[40] Reynier; L. Marraffa. Aerothermodynamics investigations for earth orbital entry vehicles. 2005.

[41] Lockheed Martin. Ch-53k sikorsky king stallion helicopter, 2016.

[42] P.K. McConnaughey. Nasa launch propulsion systems roadmap, November 2010.

[43] J.O. Arnold; E. Venkatapathy; R.A.S. Beck; M.K. McGuire. Flexible ablators: Applications and arcjet testing. NASA Ames Research Center. Presentation slides, 2011.

[44] M. Naeije; W. Simons; E. Mooij. Ae4870a rocket motion - ballistic flight over the earth 1 lecture slides, 2017.

[45] R.V. Patterson; F.J. Fisch; H.O. Heyck; R.L. Jarvis; B.W. Mouring. 40,000 pound-capacity heavy-lift helicopter external cargo handling system design study. 1968.

[46] M. Xiang; Marketing Department; China Academy of Launch vehicle Technology; Beijing. The new generation launch vehicles in china, 2016.

[47] L. Marraffa; D. Kassing; P.Baglioni. Inflatable re-entry technologies: Flight demonstration and future prospects. ESA ESTEC, 2000.

[48] W.B. Pepper. Development of a parachute recovery system for a re-entry nose cone (nrv). 1977.

[49] C.J. Player. Development of inflatable entry systems technologies. Presentation slides NASA Langley Research Center, 2005.

[50] J.R. Wertz; D.F. Everett; J.J. Puschell. Space mission engineering: The new smad, 2011.

[51] N. Demidovich; D. Rasky. Technology needs for space access. Presentation slides NASA and FAA, 2011.

[52] A. V. Da Rosa. *Fundamentals of Renewable Energy Processes, 3rd ed.* Academic Press, 2012.

[53] RUAG. Payload adapters and separation systems, 2012.

[54] J.A. Samareh. Estimating mass of inflatable aerodynamic decelerators using dimensionless parameters. Technical report, NASA Langley Research Center, 2015.

[55] R. Winski; D. Bose; D. R. Komar; J. Samareh. Mission applications of a hiad for the mars southern highlands.

[56] J. Puttonen; J. Zhang; O. Puchko; J. Kurjenniemi; P. Salaris; A. Masci; R. Romanato; D. Di Lanzo; S. Falzini; N. Buchanan; H. Kim; H. Paaso; J. Seppänen; P. Järvensivu; G. Matini; A. Pagnani; I. A. Sanches. Robust telemetry system for future launchers.

[57] International Launch Services. Proton launch system mission planner's guide, 2009.

[58] M. Ward; M. Costello; N. Slegers. On the benefits of in-flight system identification for autonomous airdrop systems. 2010.

[59] S. Reza; R. Hund; F. Kustas; W. Willcockson; J. Songer. Aerocapture inflatable decelerator (aid) for planetary entry.

[60] Bryce Space and Technology. State of the satellite industry report, 2016.

[61] SpaceX. Capabilities & services.

[62] J.M. Stein; C.M.Madsen; A.L. Strahan. An overview of the guided parafoil system derived from x-38 experience.

[63] W. R. Sturgeon. A mathematical model of the ch-53 helicopter.

[64] SWR. 6x36 galvanised ws i.w.r.c.

[65] Airborne Systems. 30k megafly joint precision aerial delivery system. 2009.

[66] BAE Systems. Rad750, 2016.

[67] BAE Systems. Rad750 6u compactpci, 2016.

[68] Technavio. Global reusable launch vehicles market 2017-2021, June 2017.

[69] B. E. Tweddle. Simulation and control of guided ram air parafoils.

[70] A. Toeter; C. Dek; J. Slimmens; J.L. Overkamp; J. van Zijl; P. Areso Rossi; R. Machado; S. Hereijgers; T. Hoppenbrouwer; V. Kilic. Vuab recovery baseline review. Technical report, Delft University of Technology.

[71] A. Toeter; C. Dek; J. Slimmens; J.L. Overkamp; J. van Zijl; P. Areso Rossi; R. Machado; S. Hereijgers; T. Hoppenbrouwer; V. Kilic. Vuab recovery midterm report. Technical report, Delft University of Technology, 2017.

[72] A. Toeter; C. Dek; J. Slimmens; J.L. Overkamp; J. van Zijl; P. Areso Rossi; R. Machado; S. Hereijgers; T. Hoppenbrouwer; V. Kilic. Vuab recovery project plan. Technical report, Delft University of Technology, 2017.

[73] C. Toglia; M. Vendittelli. Modelling and motion analysis of autonomous paragliders.

[74] D. Wilde; S. Walther;. Inflatable reentry and decent technologies (irdt) - further developments. Astrium GmbH, ESA ESTEC, 2001.

[75] L. Zhao; B.W.Bai; W.M.Bao;X.P.Li. Effects of reentry plasma sheath on gps patch antenna polarization property. 2013.

[76] Alicia Cianciolo; J Davis; David Komar; Michelle Munk; Jamshid Samareh;Julie Williams-Byrd; Thomas Zang. Entry, descent and landing systems analysis study: Phase 1 report, 2010.

[77] A.M.D. Cianciolo; J.L. Davis; D.R. Komar; M.M. Munk; J.A. Samareh; J.A. Williams-Byrd; T.A. Zang. Entry, descent and landing systems analysis study: Phase 1 report. Technical report, NASA Langley Research Center, 2010.

A

Atmosphere Model

Atmospheric properties are an integral part of all the trajectory models presented in Chapter 3. Therefore, an atmosphere model was developed and used throughout all the models, such that the atmospheric properties used were consistent.

For a given altitude, denoted by h, where h $0 \leqslant h \leqslant 84852m$ the model outputs the pressure, P, temperature, T and density, ρ.

Table A.1 presents the standard mean sea level conditions used by the ISA Standard Atmosphere Model.

Table A.1: International Standard Atmosphere; Mean Sea Level Conditions

Parameter	Value	Unit
T_0	288.15	K
P_0	101325	Pa
ρ_0	1.225	kgm^3
g_0	9.81	ms^2
R	287.00	$Jkg^{-1}K^{-1}$

Where g_0 is the gravitational constant and R is the specific gas constant for dry air at standard conditions.

The ISA standard atmosphere divides the atmosphere into 7 main layers. These are illustrated in Figure A.1 [1].

The temperature gradients, a, used in the model for each of the layers where temperature is not constant is presented in Table A.2, together with the altitude range of each. All the units are of Km[1]. Its important to note that contrary to what the figure might illustrate, both the stratosphere and the mesosphere is divided into two segments with slightly different values for the temperature gradient.

Table A.2: Temperature gradients at the different layers of the atmosphere.

$a_{troposphere}$	-0.0065	$0 \leqslant h \leqslant 11000m$
$a_{stratosphere}$	0.001	$20000 < h \leqslant 32000m$
$a_{stratosphere_2}$	0.0028	$32000 < h \leqslant 47000m$
$a_{mesosphere}$	-0.0028	$51000 < h \leqslant 71000m$
$a_{mesosphere_2}$	-0.002	$71000 < h \leqslant 84852m$

Three simple equations, A.1, A.2 and A.3 are used to compute P, T and ρ respectively at any altitude within a non-zero temperature gradient layer. In these equations the subscript 0 is used to refer to first value of that parameter on that layer. As an example, to compute T at 15000m, Equation A.1 is used, where T_0 is the temperature at 11000m.

$$T = T_0 + (ah) \tag{A.1}$$

[1] `https://www.eoas.ubc.ca/courses/atsc113/flying/met_concepts/03-met_concepts/03a-std_atmos/index.html`, 22-01-2018

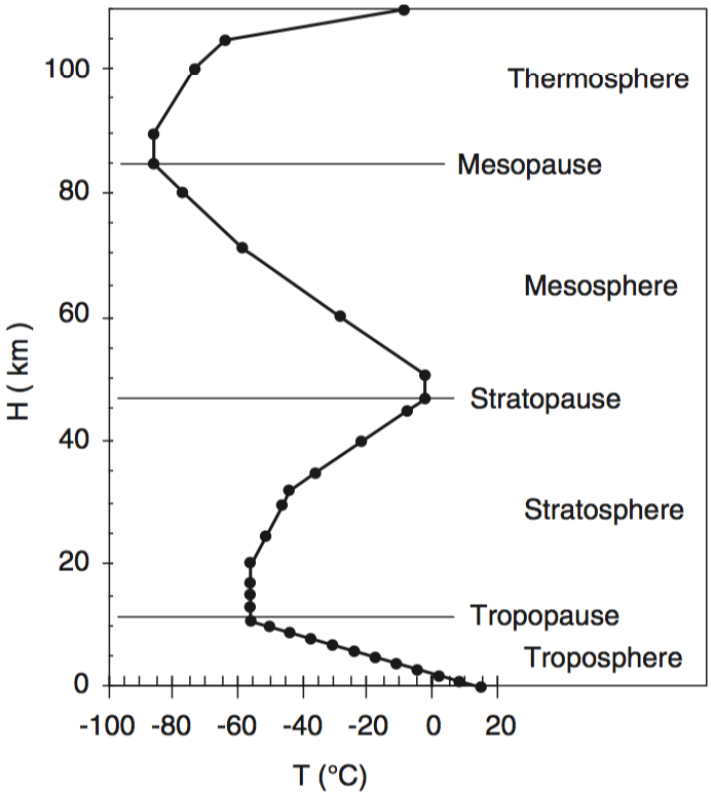

Figure A.1: ISA Standard Atmosphere Layers

$$P = P_0(\frac{T}{T_0})^{(\frac{g_0}{aR})} \tag{A.2}$$

$$\rho = \rho_0 \frac{T}{T_0}^{(-(\frac{g_0}{aR})-1)} \tag{A.3}$$

For zero valued temperature gradients equations A.1, A.2 and A.3 are slightly modified to Equations A.4, A.5 and A.6 respectively.

$$T = T_0 \tag{A.4}$$

$$P = P_0 e^{(-(\frac{g_0}{RT})} \tag{A.5}$$

$$\rho = \rho_0 e^{-(\frac{g_0}{RT})} \tag{A.6}$$

The model was ran from h $0 \leqslant h \leqslant 80000m$. The result is depicted in Figure A.2.

For altitudes higher than 84852m the value of P, T and ρ are set to:

– P = 0.373 Pa
– T = 186.95 K
– ρ = 0 kg m^3

As can be seen from the plot, the results match almost perfectly what is depicted in Figure A.1. The model is hence verified.

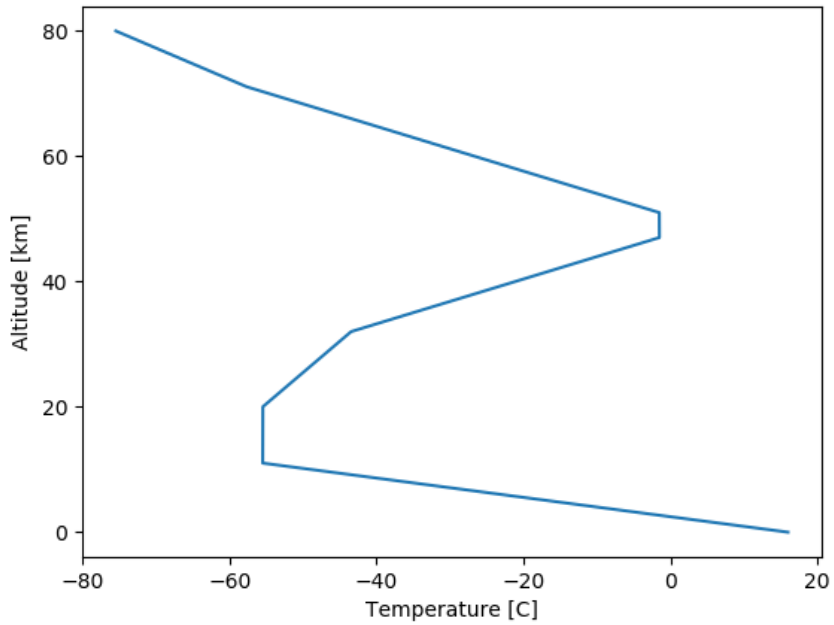

Figure A.2: Atmosphere model simulation results